The mechanical significance of anatomically modern human and Neanderthal mandibular morphology. A study using voxel-based finite element modelling.

Flora Gröning

PhD

University of York
Department of Archaeology

October 2009

Abstract

In this study, finite element analysis (FEA) was used to investigate the mechanical significance of anatomically modern human and Neanderthal mandibular morphology. First, the FEA approach applied here was successfully validated against results of an *in vitro* experiment and the relative importance of different input variables was assessed in a series of sensitivity analyses. Second, masticatory loads were simulated in models of anatomically modern human, Neanderthal and *H. heidelbergensis* mandibles to investigate the mechanical significance of specific aspects of human mandibular morphology and to assess differences in load resistance between these human taxa.

The results are consistent with several previous hypotheses about the relationship between masticatory loads and human mandibular morphology. For example, it is confirmed that the uneven distribution of cortical bone in the human mandible is closely related to masticatory strains and that the unique symphyseal morphology of anatomically modern humans (i.e. the vertical orientation of the symphysis and the presence of a chin) is advantageous to resist certain masticatory loads. It is also shown that the resistance to masticatory loads overall has decreased since the Middle Pleistocene, which is likely to be related to a reduction of masticatory loads due to advances in food processing, and that Neanderthal craniofacial morphology was probably not specifically adapted to resist high anterior dental loads as suggested by some authors.

In general, the results suggest that studying adaptations to masticatory loads is crucial in understanding the evolution and development of human craniofacial morphology. Previous research in this area was difficult because experiments to test certain hypotheses cannot be conducted for ethical or practical reasons. This study shows how virtual modelling techniques like FEA now provide tools to investigate mechanical adaptation even when experiments are not possible, as in the case of fossil taxa.

Table of contents

List of tables

List of figures

List of figures

Chapter 6

Chapter 7

Chapter 10

Acknowledgements

First, I would like to thank my supervisor, Prof. Paul O'Higgins for his guidance, support and his motivating enthusiasm throughout this project. I would also like to give special thanks to Prof. Michael Fagan and Prof. Ulrich Witzel for all their valuable advice and inspiring discussions.

I wish to thank Dr. Kornelius Kupczik for the software training he provided and his invaluable support during the start phase of this project. I am grateful to Dr. Mehran Moazen for assisting me in an initial strain gauging experiment and to Dr. Jia Liu for improving VOX-FE, the finite element software used here, considerably. Without her, many analyses for this thesis would not have been possible. I would also like to thank the members of my thesis advisory panel, Prof. Geoff Bailey and Dr. Sam Cobb, for advise.

In addition, I wish to thank the following people: Dr. Laura Fitton for many inspiring discussions, Prof. Charles Oxnard and Prof. John Currey for sharing their knowledge about bone mechanics as well as Hester Baverstock, Jason Dunn, Dr. Menos Lagopoulos, Laurent Puymerail, Garry Robinson, Martin Walters, Rachel Winnard, Simon Witty and Holly Wright for their help.

For providing me with CT scans and specimens for scanning I would like to thank Prof. Roberto Macchiarelli, Jakov Radovčić, Prof. Fred Spoor and Prof. Frans Zonneveld as well as the NESPOS Society, the European Virtual Anthropology Network (EVAN), the University of Leeds and the Peabody Museum of Harvard University. I am grateful to Sue Taft for the CT scanning of numerous specimens and her technical support during my experimental work.

Finally, I wish to thank my friends and family for their support and patience during the last three years.

This research was funded by Marie Curie Action MEST-CT-2005-020601 (PALAEO).

Author's declaration

I hereby declare that the work described in this thesis is all my own work, except where otherwise acknowledged, and has not been submitted previously for a degree at this or any other university.

Flora Gröning

Chapter 1: Introduction

The evolution of the unique craniofacial morphology of anatomically modern humans has been of major interest since the early days of biological anthropology. Compared with their nearest living relatives, the chimpanzees, and other members of the genus *Homo*, anatomically modern humans show, for example, reduced facial prognathism, a high degree of flexion in the cranial base and a well-developed chin (**Fig. 1.1**). Numerous studies have looked at the variation of these features within anatomically modern humans as well as in extinct hominins. Early studies were either qualitative descriptions or applied distance and angle measurements to quantify single features. More recently, geometric morphometrics (GMM) has been applied to quantify 3D craniofacial shape variation (Bookstein et al. 1999, Bastir et al. 2004, Harvati et al. 2004, Rosas et al. 2006).

Although there are abundant data on craniofacial morphology in anatomically modern humans and their closest relatives, the mechanisms that were responsible for the evolution of the distinct human morphology are not well understood. It is likely that the expansion of the brain, particularly the relative increase in size and position of the temporal lobes made a major contribution to the evolution of the facial features typical of modern humans (Spoor et al. 1999, Lieberman et al. 2002, Bastir et al. 2008). Another factor that might have played an important role in the evolution of modern human craniofacial morphology is the technological progress, which is observed in the Pleistocene: more advanced tools and new methods of food processing like cooking. It is commonly assumed that such advances in food processing and tool use led to a reduction of masticatory loads to which the face adapted (Brace 1979). This is supported by experimental studies, showing that softer and more processed foods impact on craniofacial size and shape (Beecher et al. 1983, Kiliaridis et al. 1985, Engström et al. 1986, Lieberman et al. 2004a).

A fossil hominin group, that is highly relevant in this context is the Neanderthals. They are the fossil hominins with the most abundant preserved material and are thus the best documented. Although they are closely related to anatomically modern humans and were also advanced tool makers, they show different craniofacial features, for example, a large prognathic face, lack of a chin

and the presence of a gap behind the third mandibular molar, the so-called retromolar space (**Fig. 1.1**).

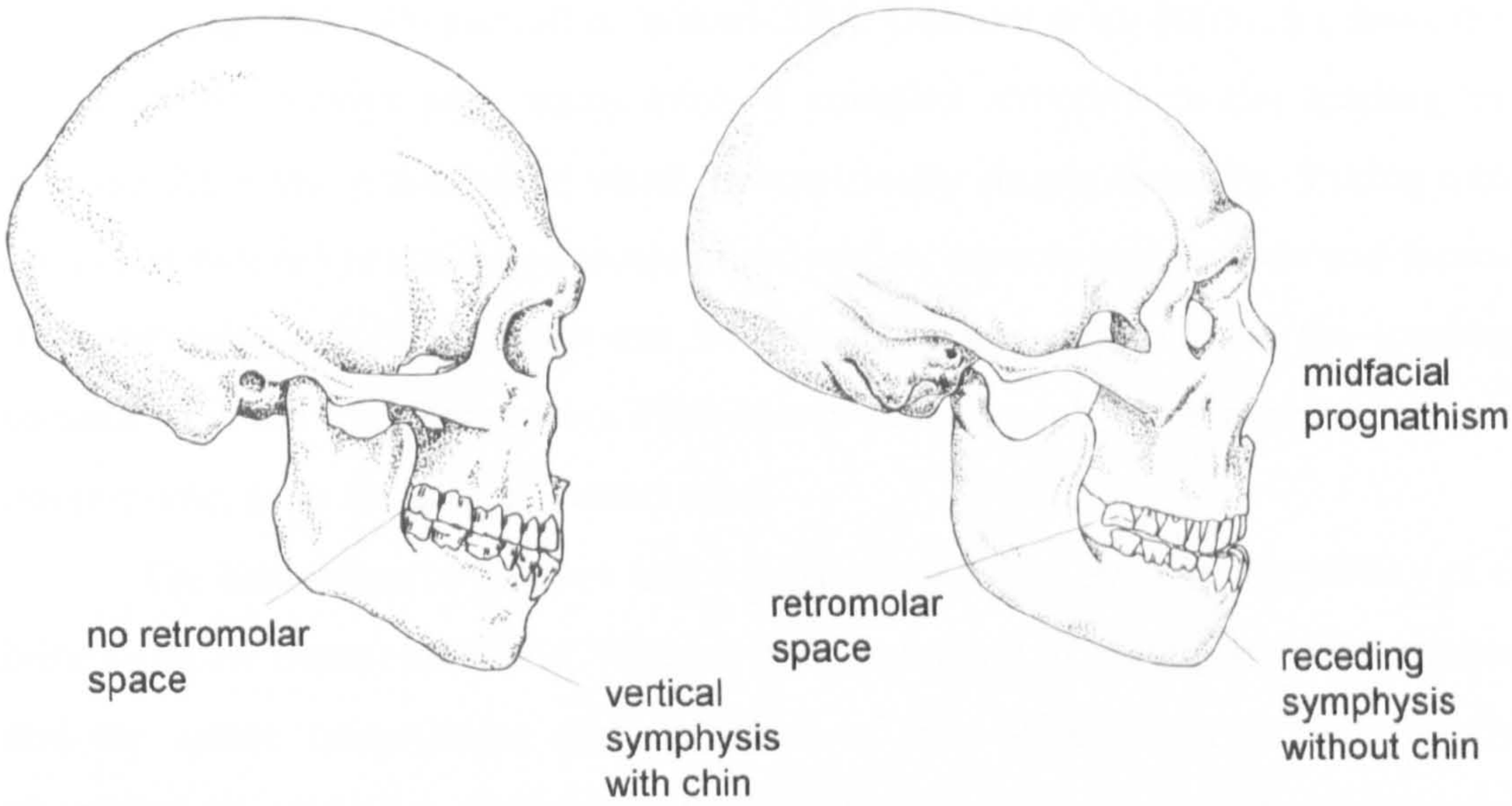

Fig. 1.1. Some of the differences between anatomically modern human (left) and Neanderthal (right) craniofacial morphology (redrawn after Klein 1999: 483, Fig. 6.48).

Some of these are primitive features that also occur in older fossils, but the whole set of features is unique to Neanderthals. As potential explanations for the distinctive Neanderthal craniofacial morphology authors have suggested genetic drift (Coon 1962), an adaptation to cold, arid climate (Sergi 1962, Franciscus & Trinkaus 1988) or a combination of both (Howell 1951, Hublin 1998) as well as integrative effects of changes in the basicranium combined with an adaptation of the respiratory apparatus to specific metabolic demands (Bastir 2008). Some authors have suggested that Neanderthal craniofacial morphology represents an adaptation to certain mechanical loads, specifically to high loads on the incisors due to frequent use of the front teeth for purposes other than food processing (Smith 1983, Rak 1986, Demes 1987, Trinkaus 1987, Spencer & Demes 1993).

It is most likely that the evolution of the modern human and Neanderthal craniofacial morphology is the result of a complex interplay of different factors so that mono-causal explanations cannot be sufficient (see e.g. review in Weaver 2009). However, most of the hypotheses, which are discussed in the literature, are difficult to test due to the lack of data and suitable methods. Those, that have recently become better testable, are mechanical hypotheses thanks to the application of virtual modelling techniques like finite element analysis (FEA).

FEA has been used by engineers for decades, but is now increasingly applied in biology to study form-function relationships (Macho & Spears 1999, Rayfield et al. 2001, Preuschoft & Witzel 2004, Dumont et al. 2005). It allows the estimation of stresses and strains even in complex structures under loading by dividing these into a number of small, geometrically simple elements. Taking into account measured or estimated material properties, muscle orientations and forces in a particular specimen, loads can be simulated that approximate the loading conditions in the living organism. FEA is especially useful, when experiments are not possible, as in the case of extinct taxa.

The estimation of stresses and strains allows us to evaluate the ability of a bone to resist functional loads. When a bone is loaded, it undergoes deformation and the nature (magnitudes and direction) of this deformation is traditionally quantified by strain (ε). Strain is defined as the change in length divided by the original length ($\Delta L/L$). Stress (σ), on the other hand, is a measure for the internal forces in the loaded bone resulting from the deformation (Currey 2002) and is defined as force per unit area (F/A). Depending on how the load is applied, stresses and strains can be classified as compressive, tensile or shear (**Fig. 1.2**). Compression occurs when the bone becomes shorter, tension when it becomes longer and shear when one region of the bone moves parallel to an adjacent region.

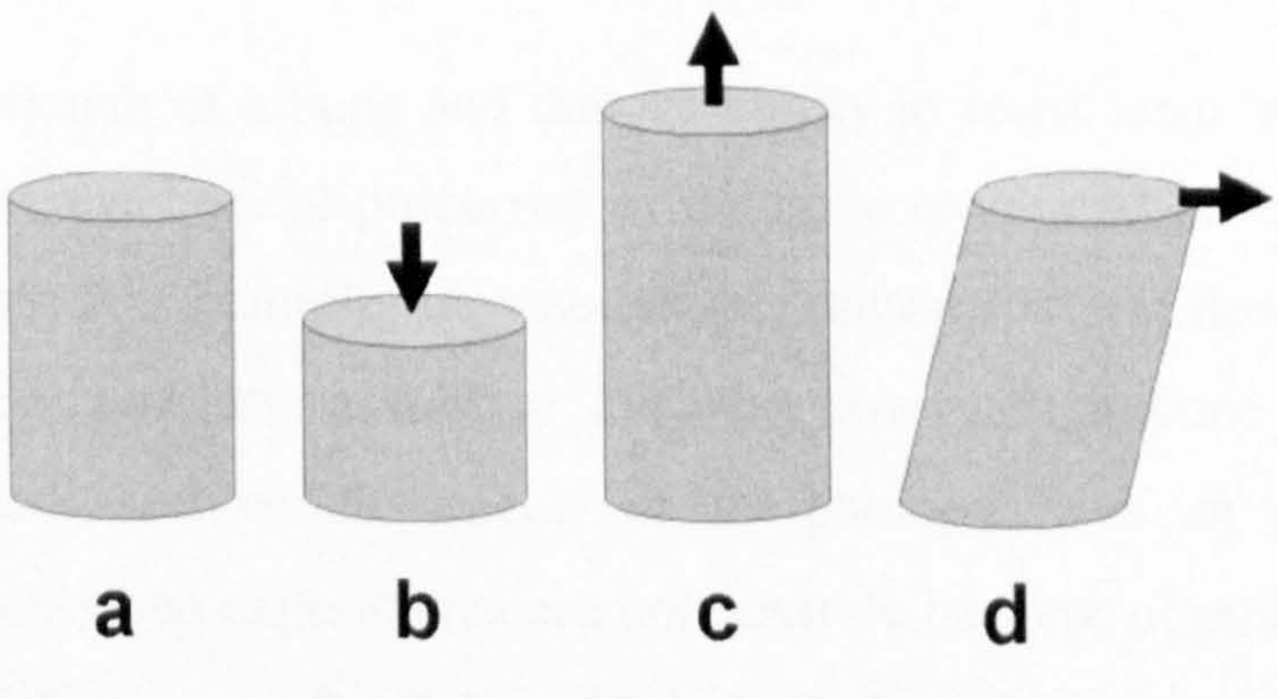

Fig. 1.2. Illustration of the three types of stress and strain: a) undeformed object, b) compression, c) tension, d) shear. By convention, strains which describe a stretching of an object in tension and shear are positive, whereas strains which describe compression and thus a shortening of the object are negative.

The relationship between stress and strain is described by the stress-strain curve (**Fig. 1.3**). When the stresses and strains are within the so-called elastic deformation region, there is a linear relationship between the two and the bone will return to its original condition after releasing the load. However, when the

amount of stress (or strain) increases beyond a certain point, the yield point, damage will be caused to the bone tissue. This second part of the curve above the yield point is the so-called plastic deformation region. If the stress increases further, the point of ultimate strength is eventually reached, which is the amount of stress or strain that the bone can maximally sustain before it breaks.

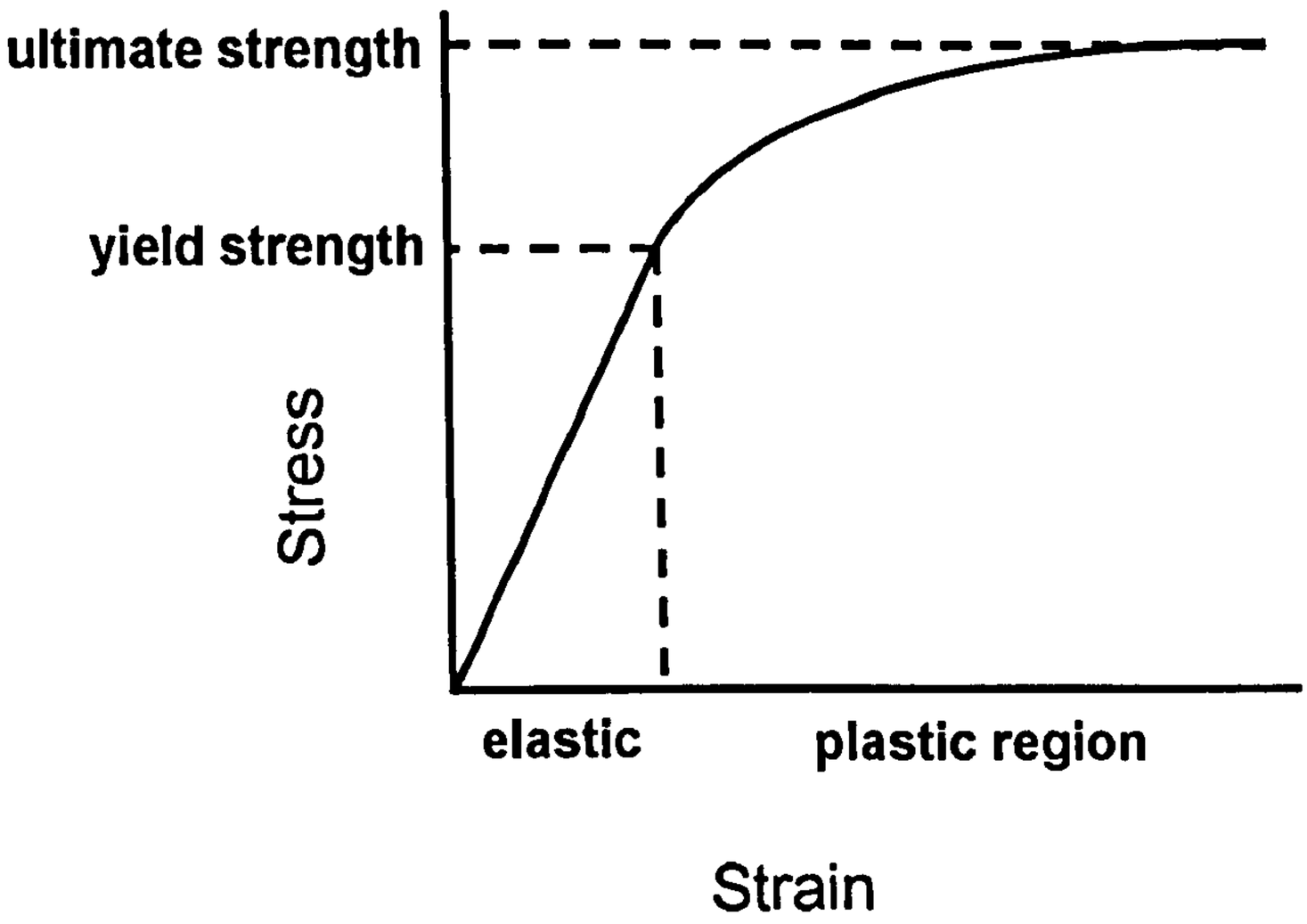

Fig. 1.3. The relationship between stress and strain in a loaded bone. If the amount of stress is within the elastic deformation region, the bone will return to its original condition after the load is released. If the stress rises beyond the yield point and thus enters the plastic deformation region, it causes damage to the bone tissue. The ultimate strength is the stress, which the bone tissue can maximally sustain (redrawn after van Eijden 2000: 124, Fig. 2).

The strength of a bone and thus its ability to resist loads without damage depends on the mechanical properties of the bone tissue and different aspects of its morphology: for example, its size, shape, microstructure, density or cortical thickness. FEA provides a tool to evaluate how well a bone resists certain functional loads and which aspects of morphology have an effect on load resistance, even when experiments are not possible because of ethical or practical reasons, as in humans or fossil taxa. Therefore, it could be a very useful tool to study the role of mechanical adaptations in the evolution of anatomically modern human and Neanderthal craniofacial morphology. However, to date, only few FEA studies have been applied to this area (Ichim et al. 2006a, 2006b, 2007a).

This study uses FEA to investigate the mechanical significance of modern human and Neanderthal mandibular morphology. It aims to 1) quantify the differences in masticatory load resistance between *Homo heidelbergensis*, Neanderthals and modern humans, 2) examine whether some of the

morphological features in modern human and Neanderthal mandibles might represent mechanical adaptations and 3) assess the potential and limitations of FEA for the study of human craniofacial evolution and development.

It focuses on the mandible instead of the whole skull for a number of reasons: finite element (FE) modelling of whole skulls raises some methodological issues, for example, difficult and time-consuming virtual reconstruction because of the complex shape of the cranium and its often fragmentary preservation in fossils, problems in the creation of FE models because of cranial sutures, which can have different mechanical effects depending on their morphology (Rayfield 2005), and difficulties in the interpretation of results because of the diverse non-masticatory functions of the cranium, such as the protection of the brain and sensory organs. By concentrating on the mandible, this study analyses a relatively simple structure. The human mandible is a single bone in the adult and its main functional loadings arise through its role in mastication. Thus, mechanical adaptations to masticatory loads are likely to be more evident in mandibular than in other aspects of craniofacial morphology. In addition, there are numerous examples of very well preserved mandibles in the fossil record and recent comparative studies of modern human and Neanderthal craniofacial morphology have focused on the mandible so that this study can build on abundant data (Rosas & Bastir 2004, Nicholson & Harvati 2006, Rosas et al. 2006, Bastir et al. 2007).

However, before masticatory loads can be simulated in Neanderthal and modern human mandibles, the validity of the modelling approach as well as the effect of altering basic model attributes and input parameters need to be assessed. Therefore, a number of additional analyses have been conducted (Chapters 4-6). Chapter 4 presents a comparison of numerically predicted strains in FE models of a human mandible with the strain measurements from an *in vitro* experiment using the same specimen. It also discusses the importance of model resolution for the accuracy of the FEA results and how to best model internal bone morphology. In Chapter 5 a sensitivity study is described, in which the effects of altering different model attributes and loading conditions are quantified and evaluated. Based on the results of this sensitivity study and their comparison with *in vivo* strain data from animal experiments, it discusses which combination of input variables provides the most realistic FE modelling of the human mandible under masticatory loads.

morphological features in modern human and Neanderthal mandibles might represent mechanical adaptations and 3) assess the potential and limitations of FEA for the study of human craniofacial evolution and development.

It focuses on the mandible instead of the whole skull for a number of reasons: finite element (FE) modelling of whole skulls raises some methodological issues, for example, difficult and time-consuming virtual reconstruction because of the complex shape of the cranium and its often fragmentary preservation in fossils, problems in the creation of FE models because of cranial sutures, which can have different mechanical effects depending on their morphology (Rayfield 2005), and difficulties in the interpretation of results because of the diverse non-masticatory functions of the cranium, such as the protection of the brain and sensory organs. By concentrating on the mandible, this study analyses a relatively simple structure. The human mandible is a single bone in the adult and its main functional loadings arise through its role in mastication. Thus, mechanical adaptations to masticatory loads are likely to be more evident in mandibular than in other aspects of craniofacial morphology. In addition, there are numerous examples of very well preserved mandibles in the fossil record and recent comparative studies of modern human and Neanderthal craniofacial morphology have focused on the mandible so that this study can build on abundant data (Rosas & Bastir 2004, Nicholson & Harvati 2006, Rosas et al. 2006, Bastir et al. 2007).

However, before masticatory loads can be simulated in Neanderthal and modern human mandibles, the validity of the modelling approach as well as the effect of altering basic model attributes and input parameters need to be assessed. Therefore, a number of additional analyses have been conducted (Chapters 4-6). Chapter 4 presents a comparison of numerically predicted strains in FE models of a human mandible with the strain measurements from an *in vitro* experiment using the same specimen. It also discusses the importance of model resolution for the accuracy of the FEA results and how to best model internal bone morphology. In Chapter 5 a sensitivity study is described, in which the effects of altering different model attributes and loading conditions are quantified and evaluated. Based on the results of this sensitivity study and their comparison with *in vivo* strain data from animal experiments, it discusses which combination of input variables provides the most realistic FE modelling of the human mandible under masticatory loads.

Then, it is tested whether the chosen modelling approach is realistic enough to allow the prediction of the internal morphology of the mandible based on strain distributions in models with modified morphology (Chapter 6).

In the subsequent studies, masticatory loads are applied to different FE models in order to investigate the mechanical significance of some characteristic features of modern human and Neanderthal mandibles. Chapter 7 examines the relationship between the presence of a retromolar space, the shape of the anterior mandibular ramus and the internal morphology of the ramus. Chapter 8 describes how the orientation of the temporalis muscle affects different aspects of superior ramus morphology. In Chapter 9, different mechanical hypotheses regarding the evolution of the unique morphology of the human mandibular symphysis are tested. Finally, Chapter 10 compares the load resistance of *H. heidelbergensis*, Neanderthal and modern human mandibles and discusses in which way the observed differences might reflect adaptations to masticatory loads.

In the now following Chapter 2 the literature relevant to this study of the mechanical significance of mandibular morphology in Neanderthals and modern humans is reviewed. It begins with a brief summary of what we know about mechanical adaptation in bone in general. This overview is followed by a description of human mandibular growth with special reference to potential functional adaptations occurring during development. Different theoretical and numerical models of human mandibular biomechanics are then summarised and their advantages and disadvantages are discussed. Finally, major aspects of modern human and Neanderthal mandibular morphology are described and functional hypotheses that try to explain the evolution and development of these morphologies are introduced.

Chapter 2: Literature review

2.1. The mechanical adaptation of bone

The form of a bone is closely related to its function. Since one of the skeleton's main functions is to act as a load-bearing structure, bones need to be strong enough to resist the loads they are commonly exposed to without major tissue damage, but they also have to be light enough to not impair the mobility of an animal. In principal, this can be achieved either by evolutionary or by physiological adaptations. The former result from natural selection and thus genetic modifications (Darwin 1859), the latter imply resorption and deposition of bone tissue during the lifetime of an individual regulated by mechanical stimuli (Wolff 1892) and are thus epigenetic processes. The basic mechanisms of evolutionary adaptation are commonly well known, the mechanical adaptation of bone as a physiological process, however, much less so. This brief review will therefore focus on the latter.

Three terms are especially relevant for the discussion of the physiological adaptation of bone to mechanical stimuli and should be defined at the beginning: growth, modelling and remodelling. Frost (1983) defined "growth" strictly as an increase in size, "modelling" as the shaping of a bone during growth and "remodelling" as the turnover of the bone tissue during the lifetime of an individual (see glossary for more details). Here, the process of bone modelling and how this is related to mechanical stimuli is of special interest, but it should be noted that also bone remodelling is known to be influenced by mechanical stimuli (Lanyon et al. 1982, Currey 1984).

The concept of bone functional adaptation dates back to the late nineteenth century. At that time, an engineer (Culmann 1864-1966) discovered similarities between the orientation of trabeculae in the proximal femur and the lines of principal stress drawn for a crane. Julius Wolff used this apparent link between trabecular architecture and lines of stress to develop a more general concept, known as Wolff's law (Wolff 1892). In brief, it states that every change in the form and function of a bone is followed by certain changes in its internal architecture and secondary alterations in its external conformation in accordance with mathematical laws (Roesler 1981, 1987, Huiskes 2000). This suggests that

bone is internally and externally structured to optimally resist mechanical stresses and thus the forces applied to it.

There is a lot of empirical evidence that mechanical adaptation of the skeleton occurs as a physiological process, but it is so abundant and widespread that the short summary given here can only be selective in nature. In general, it has been shown that the process of bone deposition is associated with higher loads (Jones et al. 1977, Goodship et al. 1979, Lanyon et al. 1982, Rubin & Lanyon 1987), whereas bone resorption is associated with lower loads (Moss & Meehan 1970, Jaworski et al. 1980).

For example, longitudinal studies of animals (Umemura et al. 1997) and humans (Bennell et al. 1997), who started an exercise regime, show that bone mass increases over time. Animal experiments, in which one of two load-bearing bones is surgically removed, show that the cortex of the remaining bone thickens (Jaworski et al. 1980, Lanyon et al. 1982). On the other hand, prolonged space flight and bed rest are known to reduce bone mass (Morey & Baylink 1978, Wronski et al. 1987). When bones that normally bear loads are immobilised in animal experiments, their mass, cortical thickness, and strength decreases (Uhthoff & Jaworski 1978, Jaworski et al. 1980).

Due to this abundant evidence, it is widely accepted that bone is able to adapt to its mechanical environment. The underlying mechanisms and principles are, however, far less clear. Wolff (1892) suggested that the functional adaptation of bone follows mathematical rules, but did not say what these rules might be. Ever since, it has been a major challenge of biomechanical research to find these mathematical laws.

The basis of each algorithm is the mechanical stimulus or parameter that is regarded as relevant for inducing either bone resorption or deposition. Several stimuli have already been suggested by different authors: for example, stress or strain magnitude (Roux 1881, Wolff 1892, Hart et al. 1984, Cowin 1984, Huiskes & Nunamaker 1984, Ruimerman et al. 2005, Tsubota & Adachi 2005), compression versus tension (Jansen 1920, Triepel 1922, Bassett 1965, Oxnard et al. 1994, Hirschberg 2005), strain energy density (Fyhrie & Carter 1986, Huiskes et al. 1987, Harrigan & Hamilton 1992, Weinans et al. 1992), strain gradient with depth (Currey 1968, Frost 1973) or strain rate (Cowin 1984, Lanyon & Rubin 1984).

The simplest algorithms simply use stress or strain magnitudes or the magnitude of strain energy density. Strain energy density (SED) can be defined as the amount of work that could be done by a strained piece of material if it was allowed to relax to the unstrained state. Thus, it includes different kinds of strain (Currey 2002). In general, these theories that regard stress or strain magnitudes as the crucial stimuli assume that bone is deposited where strain magnitudes are large, and decreases, where magnitudes are low.

Probably the most influential theory that is based on strain magnitudes is Frost's "mechanostat" concept (Frost 1987, 2003). According to Frost (1987, 2003), only strains beyond about 1000-1500 με result in bone mass increase. This threshold is called the minimum effective strain. Very low strains below 50-100 με cause bone resorption instead. Between these limits is a zone, where bone mass neither increases nor decreases since bone resorption and formation are in equilibrium. Strains above 3000 με result in damage of the bone tissue which is followed by increased bone apposition to repair this damage (**Fig. 2.1**).

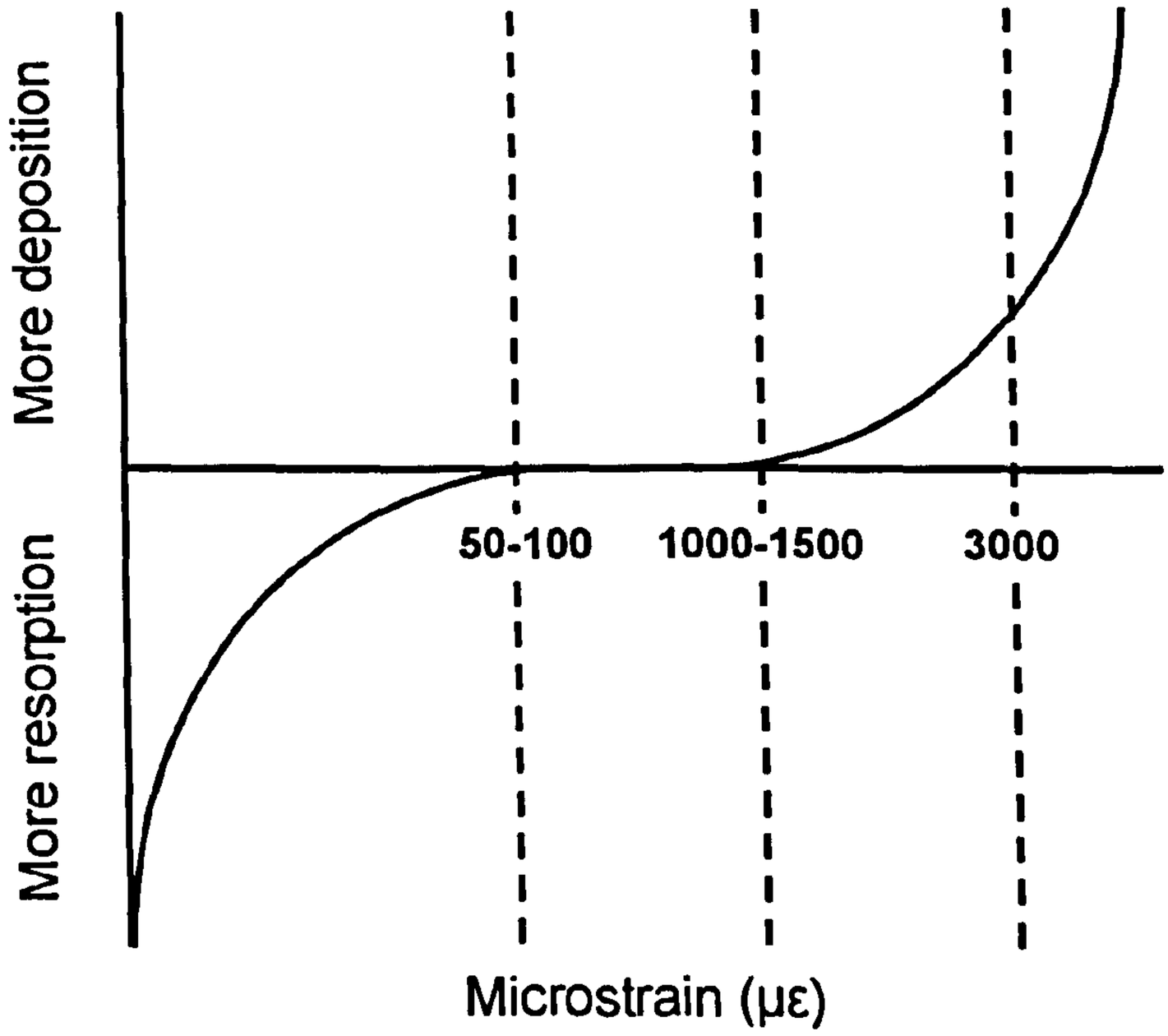

Fig. 2.1. Bone deposition and resorption as a function of strain magnitude based on Frost's (1987) mechanostat theory. The strain range is divided into four zones that differ in the relation between bone formation and resorption. See text for details.

Instead of considering only strain magnitude, some authors have suggested that strain polarity plays a role, which means that bone is deposited in areas under compression and resorbed in areas under tension (Jansen 1920, Triepel 1922,

Bassett 1965, Oxnard et al. 1994, Hirschberg 2005). A common example that illustrates the plausibility of this suggestion is a fractured long bone that has healed at an angle, but then straightens itself over time. Assuming that this long bone is under overall compression during locomotion, the curved bone experiences compression at its concave side, but tension at its convex side. If compression causes bone deposition and tension resorption, the bone will indeed straighten itself. However, although this simple rule works well for the periosteal surface, it would lead to an asymmetric cross-section of the bone (**Fig. 2.2**). As a solution, it has been suggested that bone surfaces which increase their concavity during loading undergo deposition, whereas bone surfaces which increase their convexity undergo resorption (Frost 1964). A simpler concept, but based on the same principle, uses strain gradients instead of the degree of curvature (Currey 1968). According to this, a positive gradient (i.e. stresses and strains become more tensile closer to the surface) leads to resorption, whereas a negative gradient (i.e. increasing compression towards the surface) leads to deposition. Experimental data suggest that there is indeed a high correlation between strain gradients and patterns of bone formation (Gross et al. 1997).

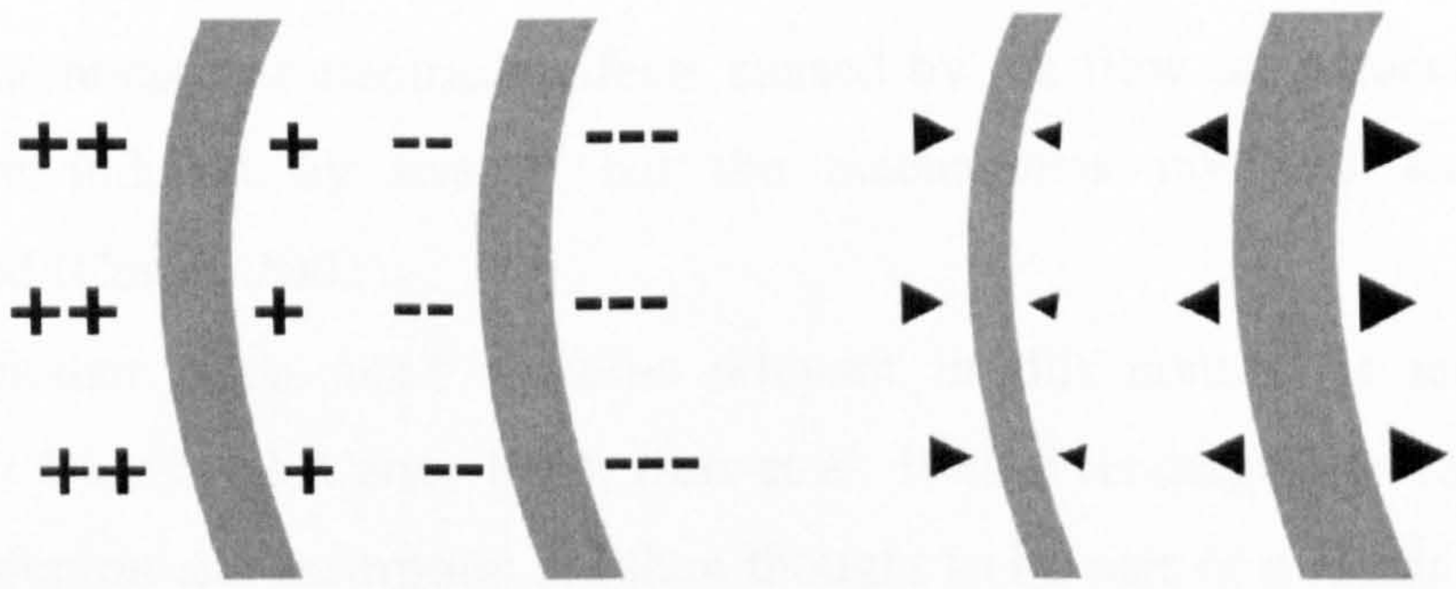

Fig. 2.2. Modelling of a curved long bone when bone is deposited in areas under compression and resorbed in areas under tension. Left image: strains in the bone loaded under compression. Positive signs indicate tension, negative signs compression. The strains are progressively less positive from the convex side to the concave one. Right image: The arrows show the direction of bone modelling, which is more pronounced on the periosteal surfaces than on the endosteal surfaces. This results in an asymmetric thickness of the cortical walls (redrawn after Currey 2002: 350, Fig. 11.4).

However, experimental studies have shown that time-dependent factors also play a role: for example, dynamic loads or in other words changing strains instead of static ones are necessary to affect bone mass (Hert et al. 1971, Lanyon & Rubin 1984, Rubin & Lanyon 1987) and that bone formation increases with higher strain rates (O'Connor et al. 1982, Skerry & Lanyon 1995). Strain rate is

the change of strain divided by the time in which the change occurred. Interestingly, a high strain rate even causes bone formation when magnitudes are relatively low (Rubin et al. 2001).

In addition, there is evidence for a site specifity of strain sensing and responsiveness of bone cells (Skerry 2000). For example, the strains in the skull do not exceed one tenth of those in the long bones even under extreme conditions (Lieberman 1996, Lieberman & Crompton 1998). If the thresholds for bone resorption and deposition were universal, the very low strains in the cranium would lead to dramatic bone loss, which is not the case. A strain-based algorithm, which tries to predict mechanical adaptations in bone will have to take this site specifity into account (Currey 2002).

This brief review shows that the mechanical adaptation of bone does not follow one simple rule. Since each of the mentioned stimuli can explain some aspects of the experimental data, there is probably more than one control system used for regulating mechanical adaptations in bone (Carter et al. 1987). In addition, it has to be considered that parameters like strain magnitudes or strain gradients are not the stimuli to which the bone cells react directly or, in other words, the proximate stimuli. Those proximate stimuli are rather deformations of the cell membrane or electrical effects caused by the flow of extracellular fluid, which are induced by strains, but the mechanisms involved are not well understood (Currey 2002).

Another often cited stimulus relevant in this context is microdamage (Martin & Burr 1982, Carter 1984, Burr et al. 1985, Prendergast & Taylor 1994). Bone formation and resorption are then thought to be part of a repair mechanism targeted to maintain bone strength by resorbing damaged bone and replacing it with new bone (McNamara & Prendergast 2007). Indeed, there is experimental evidence that resorption cavities occur preferentially in regions of microdamage in cortical bone (Burr et al. 1985, Mori & Burr 1993). Thus, microdamage might also be an important proximate stimulus.

Finally, it should be noted that bone modelling as well as remodelling are known to be influenced by a number of non-mechanical factors like nutrition, metabolic rate, hormones or blood supply (Herring 1993). These either have a direct effect on bone formation and re-/modelling or an indirect effect by altering the mechanical adaptation of bone. Testosterone, for example, can directly

activate bone and cartilage-forming cells, thus leading to longer, thicker and denser bones, but also stimulates muscle development, so that the muscle forces acting on the bones increase (Bouvier 1989, Buchanan & Preece 1992, Compston 2001).

Although the mechanism are not yet well understood in detail, there is common agreement that the mechanical environment has an important influence on bone modelling and remodelling. As described above, it seems that especially strain magnitudes and rates are relevant as ultimate stimuli in this context. In addition, strain is relevant for predicting failure of bone (**Fig. 1.3**) and thus is useful for evaluating mechanical adaptations through natural selection. Again, not only the magnitude is important, but also the repetition of the loading, since repeated loading can lead to fatigue fracture. The effect of such time-dependent factors like strain rate is difficult to study with finite element analysis (FEA), but strain magnitudes and their distribution can be evaluated. Most of the analyses in this study will therefore use either absolute or relative strain magnitudes to study mechanical adaptations, even though strain magnitude is certainly not the only relevant parameter.

2.2. Mandibular growth and the role of mechanical stimuli

2.2.1. The "functional matrix" concept of Moss

The studies cited above provide evidence that bone is principally able to respond to its mechanical environment by modelling or remodelling. Since the gross form changes of a bone occur during development, it is especially interesting to study the role of mechanical stimuli during ontogeny. With regard to craniofacial growth, it is widely assumed that mechanical factors play a major role in regulating skeletal growth and development. The theoretical basis for this is provided by the "functional matrix" concept of Moss (Moss 1962, Moss & Rankow 1968, Moss 1969, Moss & Salentijn 1969), which will be briefly described here.

According to Moss (1962, 1969), the skull consists of several functional cranial components, which carry out specific functions. Each of these components is composed of two parts: One is the functional matrix, which actually carries out the function (e.g. a muscle). The other is the skeletal unit, which protects and/or supports its functional matrix. This skeletal unit is not necessarily equivalent to a single bone. It can consist of several single bones (macroskeletal unit), parts of bones (microskeletal unit), cartilage or tendinous tissues. The key idea is that the growth of these skeletal units is determined by their associated functional matrices. As Moss and Salentijn (1969: 566) state, "all growth changes in the size, shape, and spatial position and, indeed, the very maintenance in being, of all skeletal units are always secondary to temporally primary changes in their specific functional matrices".

There are two different ways in which a functional matrix is believed to act upon a skeletal unit. So-called periosteal matrices act upon skeletal units in a direct way, altering the form of the skeletal unit by bone resorption and deposition. These can be soft tissues like muscles and blood vessels, but also teeth. Capsular matrices on the other hand, are volumes that are enclosed and protected by capsules, for example, the brain in the neurocranium. They act upon functional cranial components as a whole by changing the volumes of the capsules, in which the functional matrices are embedded. This results in passive translation of the cranial components. According to Moss' theory, growth results

from a combination of both types of matrices. In other words, growth consists of two processes, translation and changes in form (size and shape).

Figure 2.3 shows how the human mandible can be divided into several functionally and developmentally relevant subunits following Moss' theory (1962, 1969). The growth pattern of each of these subunits is influenced by its respective functional matrix. Major units are the coronoid process, to which the temporalis is attached, the angular unit, to which the masseter and medial pterygoid muscles are attached, the alveolar unit, which provides support for the teeth and the condylar process, which is influenced by the action of the lateral pterygoid (Moss & Salentijn 1969, Sperber 2001).

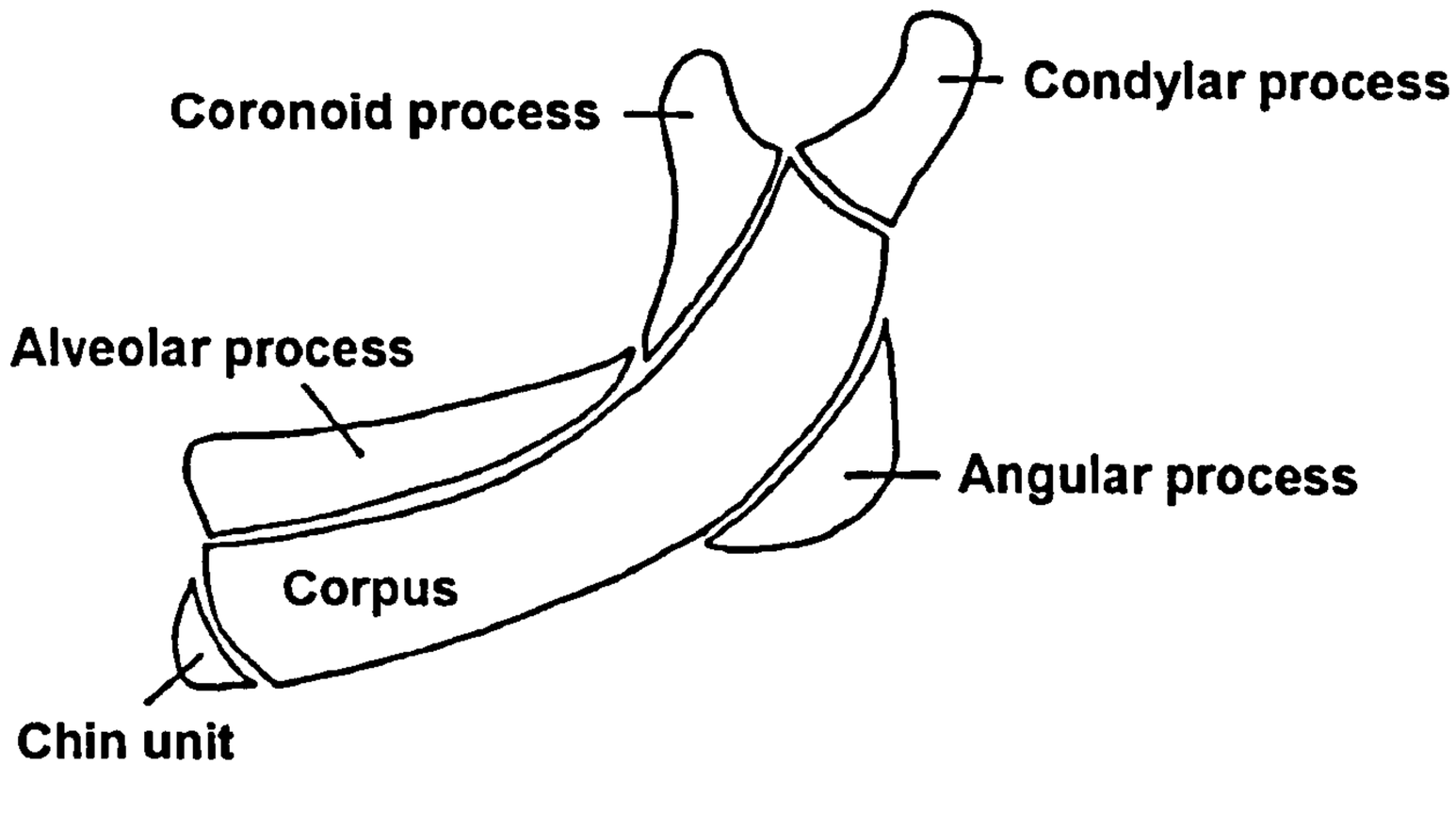

Fig. 2.3. Schema of skeletal units of the mandible (Sperber 2001: 129, Fig. 12-2).

Following Moss' ideas, bone growth is not genetically determined, but regulated by the interaction with functional matrices. In the case of periosteal matrices, the bone changes its size and shape as an adaptation to the mechanical environment, for example, to an increased load produced by a growing muscle. Some authors have criticised Moss' theory, because it relies entirely on such non-genetic interactions (e.g. Ranly. 1988). However, with regard to postnatal mandibular growth, it will be shown below that there is strong evidence for the important role of mechanical influences. The role of mechanical stimuli during prenatal development is much less certain, but some authors have suggested an impact of the mechanical environment also during this part of mandibular development.

2.2.2. Prenatal development

During prenatal development, the mandible is one of the first bones that begins to ossify (Sperber 2001). In the 6th week post conception (p.c.) one ossification centre for each half of the mandible arises lateral to Meckel's cartilage in the first pharyngeal arch (**Fig. 2.4**). Upwards ossification forms a trough and later crypts for the developing teeth, whereas the spread of ossification dorsally and ventrally forms the body and ramus of the mandible (Lee et al. 2001). Meckel's cartilage becomes surrounded and invaded by bone, and since it cannot ossify, disappears by the 24th week p.c.. Between the 10th and 14th weeks p.c., secondary accessory cartilages appear to form the head of the condyle, part of the coronoid process and the chin region. The secondary cartilage of the coronoid process develops within the temporalis muscle and ossifies before birth. The condylar cartilage is replaced by bone by the middle of the fetal development, but its upper part persists into adulthood, acting as both growth and articular cartilage (Sperber 2001). The cartilage at the symphysis menti ossifies at about the 7th month p.c. in the form of variable mental ossicles. These ossicles unite with the adjacent bone, when the symphysis fuses during the first postnatal year (Gray et al. 2005).

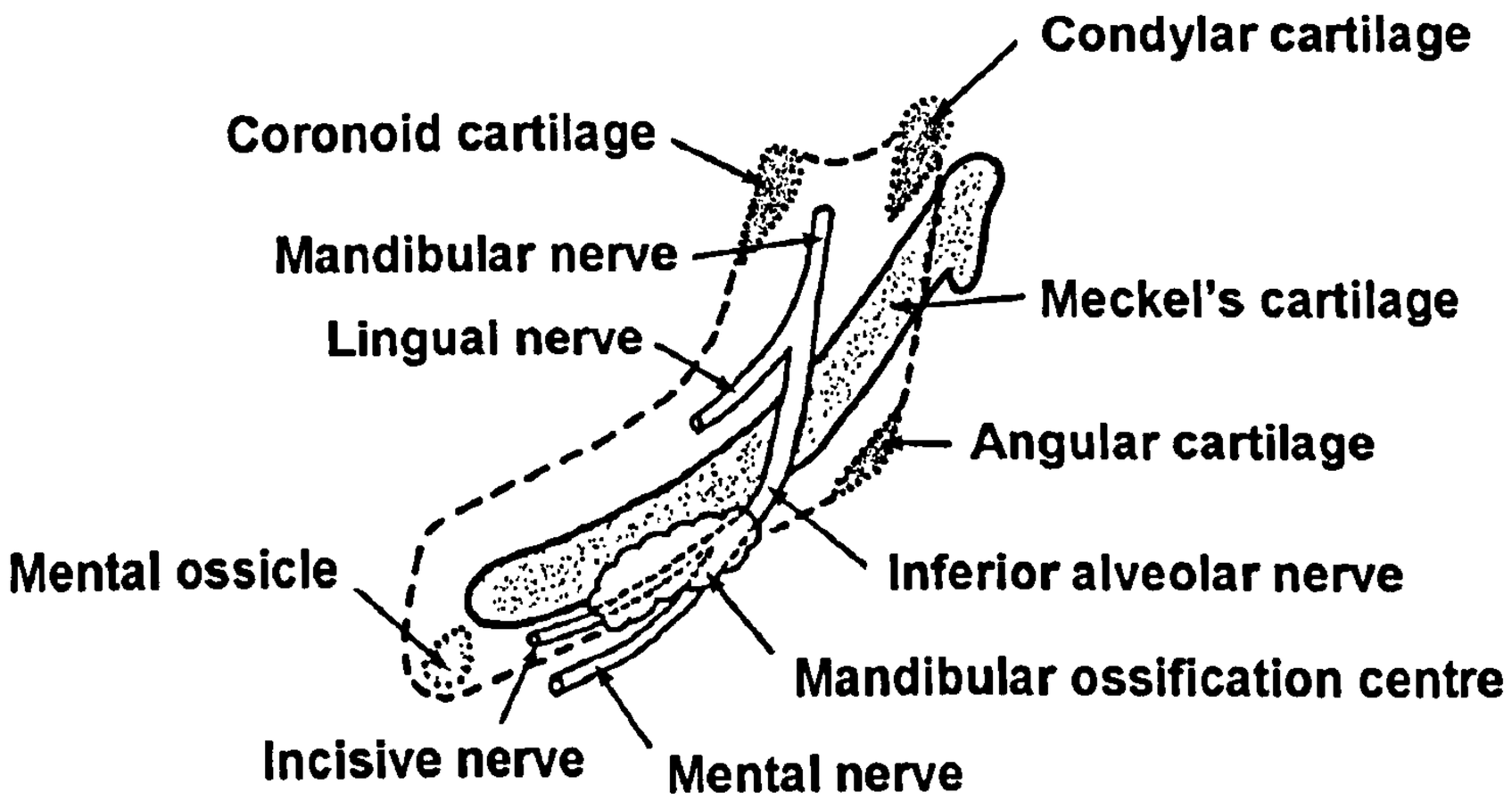

Fig. 2.4. Schema of the origins of the mandible. The centre of ossification is lateral to Meckel's cartilage at the bifurcation of the inferior alveolar nerve (Sperber 2001: 128, Fig. 12-1).

Although several detailed descriptions of prenatal mandibular growth exist, which are mainly based on histological sections and more recently on computed tomography (CT) scans of fetal material (Blechschmidt 1973, Burdi & Spyropoulos 1978, Goret-Nicaise 1981, Goret-Nicaise & Dhem 1984, Radlanski

et al. 1999, Lee et al. 2001, Radlanski & Klarkowski 2001, Radlanski et al. 2003, Möller 2005), little is known about the role of mechanical adaptation during this growth period. It has been suggested that bone is formed when expanding cartilaginous cores slide against surrounding tissue, thus exerting a shearing force (Blechschmidt & Freeman 2004). According to these authors, this process occurs during the formation of mandibular bone next to Meckel's cartilage (**Fig. 2.4**). Another assumption of mechanical adaptation is related to the fact that initial woven bone formed along Meckel's cartilage is soon replaced by lamellar bone and typical Haversian systems are already present at the 5th month p.c.. This bone remodelling occurs earlier than in other bones and has been interpreted as a response to early intense sucking and swallowing, which stress the mandible (Goret-Nicaise & Dhem 1984). Moss and Salentijn (1969) note that the coronoid process arises in the earlier formed anlage of the temporalis muscle, whose contractile abilities are already well developed in prenatal stages and which therefore acts as a functional matrix for the developing coronoid.

2.2.3. Postnatal development

Compared to the available data on prenatal mandibular growth, the postnatal development of the human mandible has been studied much more intensively. This is partly due to its great relevance for orthodontics. Many studies used metallic implants as reference marks in longitudinal radiographic studies (Björk & Skieller 1983, Iseri & Solow 2000). Recently, postnatal growth changes have also been visualised by virtual 3D reconstructions based on CT scans (Krarup et al. 2005). The key references for the postnatal growth of the mandible are the works of Enlow and colleagues (Enlow & Harris 1964, Enlow et al. 1982, Enlow 1992, Enlow & Hans 1996), which are strongly influenced by Moss' concept of functional matrices.

Of all the facial bones, the mandible undergoes the most growth postnatally (Sperber 2001). It does not enlarge by simple symmetrical expansion, but grows predominantly in a posterior and superior direction (**Fig. 2.5**). During this upward and backward modelling, the whole mandible is moved forward and downward (Enlow & Hans 1996). The major sites of postnatal growth are at the condylar cartilages, the posterior borders of the rami, and alveolar ridges (Sperber 2001). Bone deposition in these areas is mainly responsible for the increases in

height, length, and width of the mandible. At the same time bone resorption occurs in order to maintain the shape. The increase in length of the mandible is, for example, achieved by the deposition of bone on the posterior surface of the ramus with compensatory resorption on its anterior surface (Hans et al. 1995). Increase in width of the mandible is accomplished by deposition of bone on the outer surface and resorption on the inner surface (Enlow & Hans 1996). In addition, regional remodelling occurs, which involves selective resorption and displacement of individual mandibular elements (Enlow & Harris 1964).

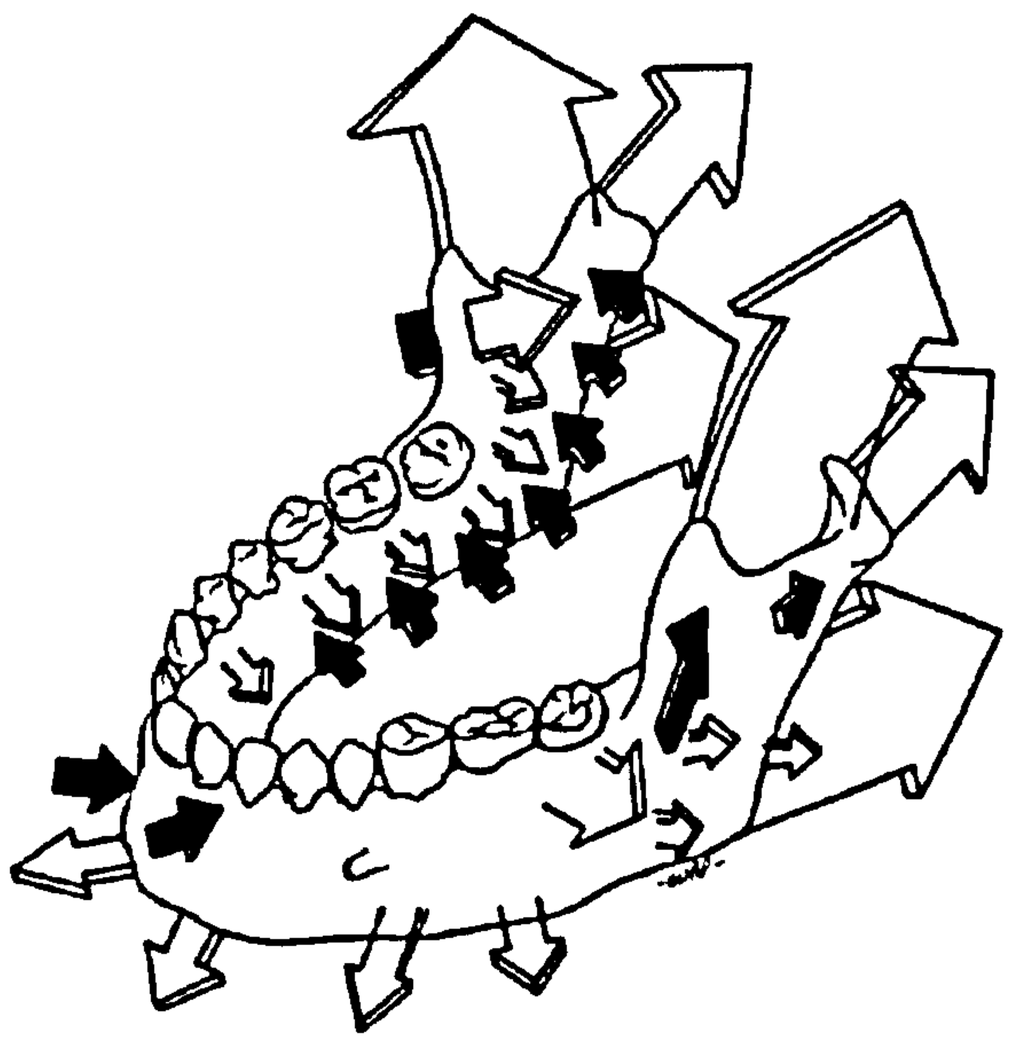

Fig. 2.5. Summary of mandibular growth. Surfaces that are depository are represented by light arrows, resorptive surfaces are shown by black arrows (Enlow 1992: 51, Fig. 4-4).

The significance of mechanical stimuli for postnatal mandibular growth is well supported by clinical studies as well as animal experiments. Healthy and thus functionally intact teeth are necessary for the development and maintenance of the alveolar process: The alveolar bone does not form in individuals with anodontia, the absence of dentition (Gorlin & Pindborg 1964). In cases of oligontia (partial anodontia) as in Ellis van Creveld syndrome, the alveolar bone does not develop in areas where teeth are missing (Biggerstaff & Mazaheri 1968). These clinical data show that alveolar bone forms and resorbs in response to the presence or absence of teeth and, therefore, support the idea that teeth act as a functional matrix for the alveolar process.

Similarly, there is abundant evidence for the necessity of intact masticatory muscles for the development of several mandibular units. Myotonic dystrophy patients, for example, who have lower activity of their masseter

muscles, are characterised by a large angle between the mandibular corpus and ramus as well as by abnormal bone changes (Kiliaridis et al. 1989, Ödman & Kiliaridis 1996, Zanoteli et al. 2002). Increased activity of the masticatory muscles is, on the other hand, associated with an anterior growth rotation of the mandible and well-developed angular, coronoid and condylar processes (Møller 1966, Kiliaridis 1995). In animal experiments, bilateral resection of the jaw-closing muscles causes shortening of the ramal height and elongation of the molars (Fukazawa & Sakamoto 1982). Detachment of the temporalis muscle in rats (Washburn 1947, Moss & Meehan 1970) and cats (Avis 1959) leads to resorption of the coronoid process and marked alterations in its shape. Resection of the masseter muscle results in disappearance of the masseteric ridge, where the masseter attaches at the mandibular angle (Pratt 1943) as well as in an altered shape of the mandibular ramus (Yonemitsu et al. 2007). Removal of the medial pterygoid muscle is similarly followed by resorption of the angular process of the mandible (Moore 1973). Finally, removal of the superficial masseter or the medial pterygoid results in a greatly reduced angular process, but removal of both muscles leads to the complete absence of the angular process (Avis 1961).

Surgical removal of muscles in animal experiments is, however, problematic, because it disrupts the blood supply and causes scarring, which might confound the effects of the altered stresses (Hirschberg 2005), but studies, in which motor neurons or motor nerves were lesioned instead of the muscles yielded similar results. Lesion of the masseteric nerve in rats, for example, stunted bone formation of the angular region and caused elongation of the molars (Kikuchi et al. 1978).

Although there are a lot of empirical data showing that the mechanical environment plays a major role during the development of the mandible, the underlying mechanisms are poorly understood. On the one hand, this is due to the fact that bone modelling does not seem to follow any simple rule. There is, for example, no simple relationship between the location of muscle insertion areas and the general pattern of growth and modelling fields (**Fig. 2.6**). On the other hand, detailed data on the variation of timing and location of bone modelling fields are missing. These data would be necessary to directly compare developmental changes like the eruption or loss of teeth or the growth of the masticatory muscles with responses of the bone tissue.

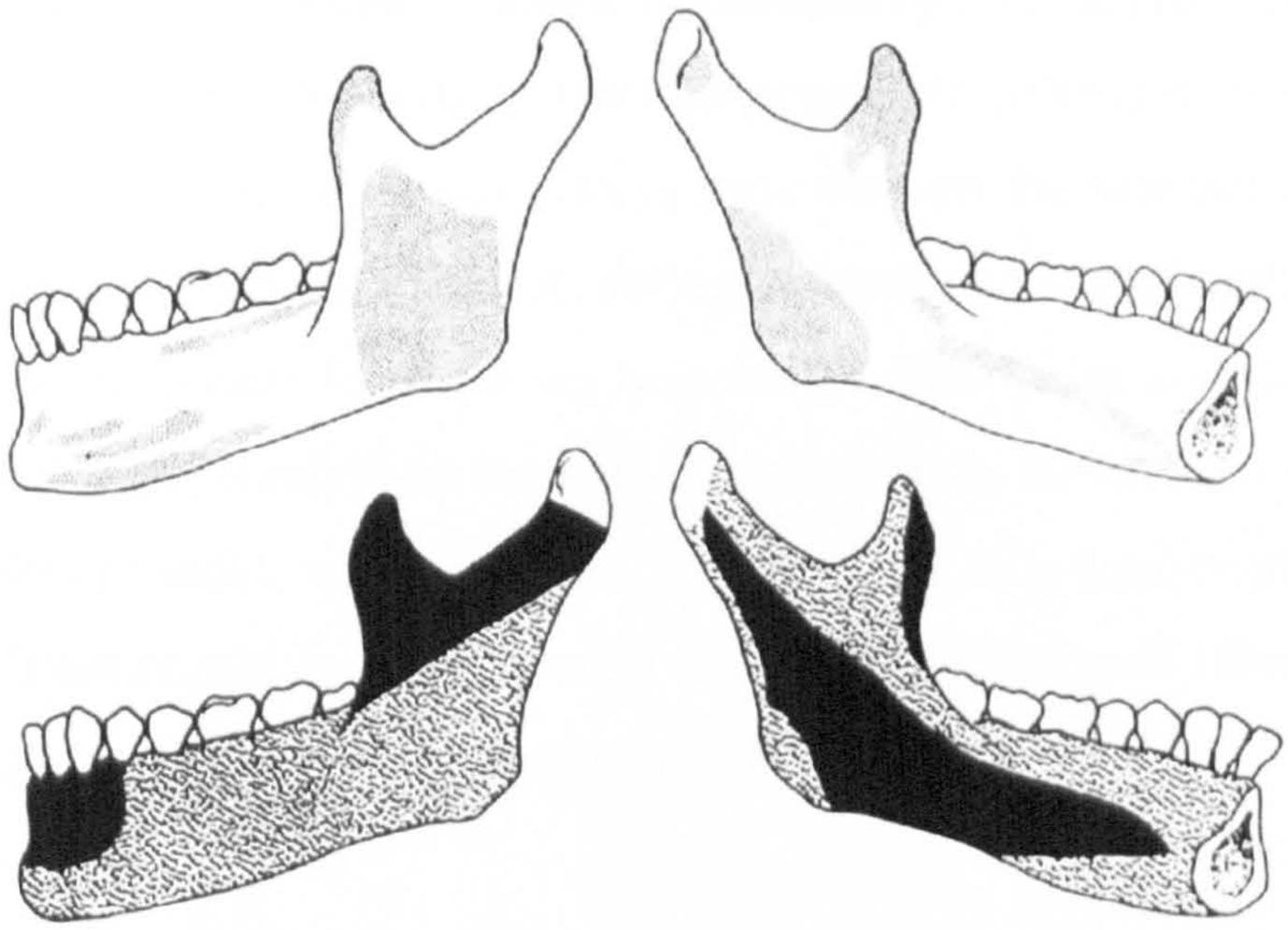

Fig. 2.6. Comparison of muscle insertion areas and surface modelling fields on the buccal (left column) and lingual (right column) sides of the human mandible. Top figures: muscle attachments. Bottom images: generalised pattern of resorptive (dark) and depository (light) fields (Enlow et al. 1982: 235, Fig. 7-1).

2.3. Mechanical models of the human mandible

The human mandible is subjected to a variety of forces during mastication, produced by the masticatory muscles as well as reaction forces at the temporomandibular joints (TMJs) and the teeth. In order to study the nature of these forces as well as the resulting pattern of stresses and strains in mandibular bone, several biomechanical models have been used. These models can be divided into two major types: 1) rigid-body models that treat the masticatory apparatus as a lever system consisting of rigid components and 2) deformation models that are concerned with how the mandible deforms under masticatory loads. Finite element models are an example of the second type.

2.3.1. Rigid-body models

It is commonly thought that the human mandible, like the mammalian mandible in general, functions as a lever during biting, with the condyles as its fulcra (**Fig. 2.7**). In the past, some authors challenged this theory (Robinson 1946, Gingerich 1971, Tattersall 1973). They argued that the resultant of the muscle forces always passes through the bite point and not through the TMJ and that the condylar neck as well as the tissues of the TMJ are not able to withstand reaction forces during biting. Subsequent anatomical studies, however, demonstrated that

the tissues of the TMJ are indeed capable of dissipating considerable joint reaction forces (Hylander 1975). In addition, electromyographic (EMG) data suggest that the resultant muscle force does not always pass through the bite point (Hylander 1975, 1978, Smith 1978), for example, during powerful unilateral molar biting the resultant adductor muscle force passes between the bite point and the balancing condyle, which is the condyle on the side contralateral to the bite point (Hylander 1975). The lever model, which implies that the TMJ is a load-bearing joint, is therefore well supported by experimental data. It is the basis of many principles commonly used in clinical and non-clinical functional morphology.

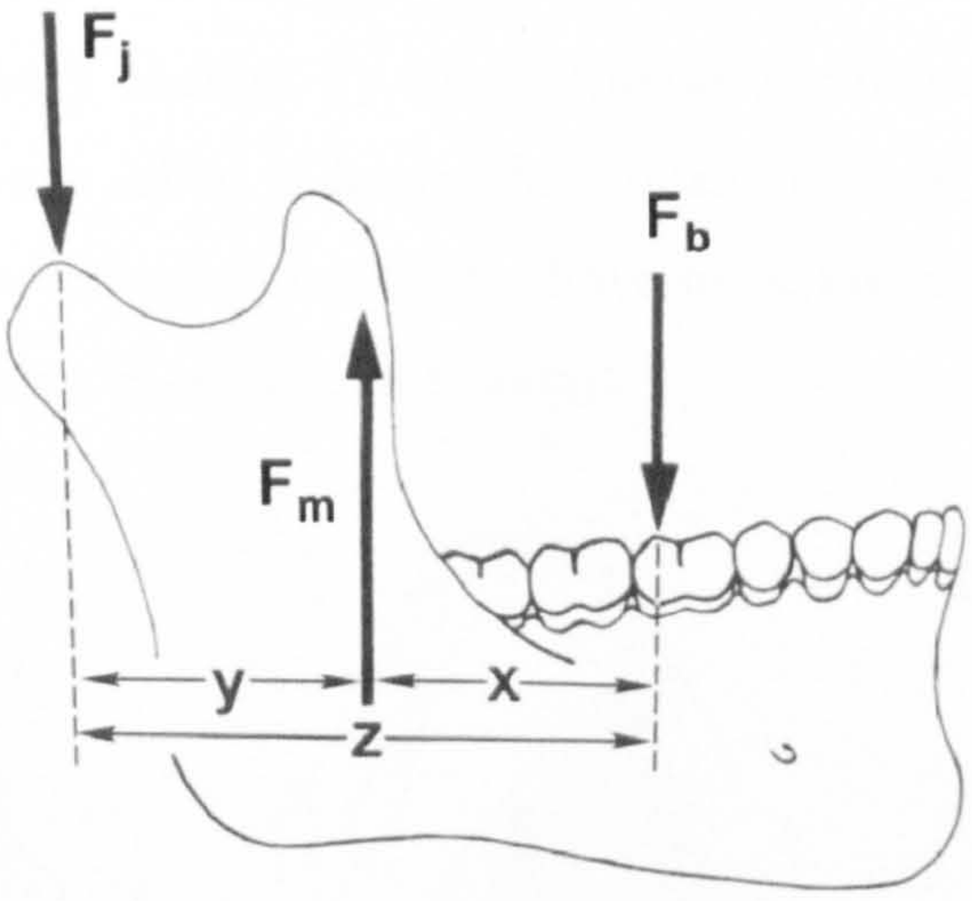

Fig. 2.7. The human mandible functioning as a lever during biting on the first molar. Only the vertical components of the muscle and reaction forces are shown. In order to maintain a static equilibrium, the resultant muscle force (F_m) is divided into reaction force at the bite point (F_b) and reaction force at the two condyles (F_j) (Hylander 1992: 84, Fig. 5-20).

The standard lever model is largely based on Smith (1978). In this model, masticatory force components are represented simply by vertical vectors that are analysed in sagittal as well as frontal projections (**Fig. 2.7**). Thus, it allows estimation of the magnitude of the bite force, combined joint reaction force, and muscle resultant force on the basis of their spatial relationships. Although this simple model has been used in several studies (Hylander 1975, 1992), it does not adequately predict some results of experimental studies. A major problem of this simplistic approach is that it does not imply any restrictions on muscle activity. It assumes that the activity of the masticatory muscles varies little during biting on different teeth, but EMG data suggest that this is not the case (Spencer 1998).

As an alternative to this standard lever model, which Spencer (1998) termed the "unconstrained lever model", Greaves (1978) suggested a "constrained

lever model". In this model, masticatory muscle activity is restricted by the need to maintain compressive forces at both TMJs. Briefly, the model predicts that balancing side muscle activity depends on the position of the bite point. This is based on the concept of the "triangle of support" (Greaves 1978), which is formed by the bite point and the two condyles (**Fig. 2.8**). In order to keep both condyles under compression, the muscle resultant force has to pass through the triangle of support. When the bite point moves posteriorly, this is achieved by decreasing muscle activity on the balancing side. Thus, the muscle resultant force is shifted towards the working side and distraction of the working side TMJ is avoided. An EMG study by Spencer (1998) showed that the relative balancing and working side muscle activities change by bite point as predicted by Greaves' model. However, the results also indicate that other factors, for example, dental morphology and mandibular kinematics, have to be taken into account. Greaves' model is not sufficient to explain all findings.

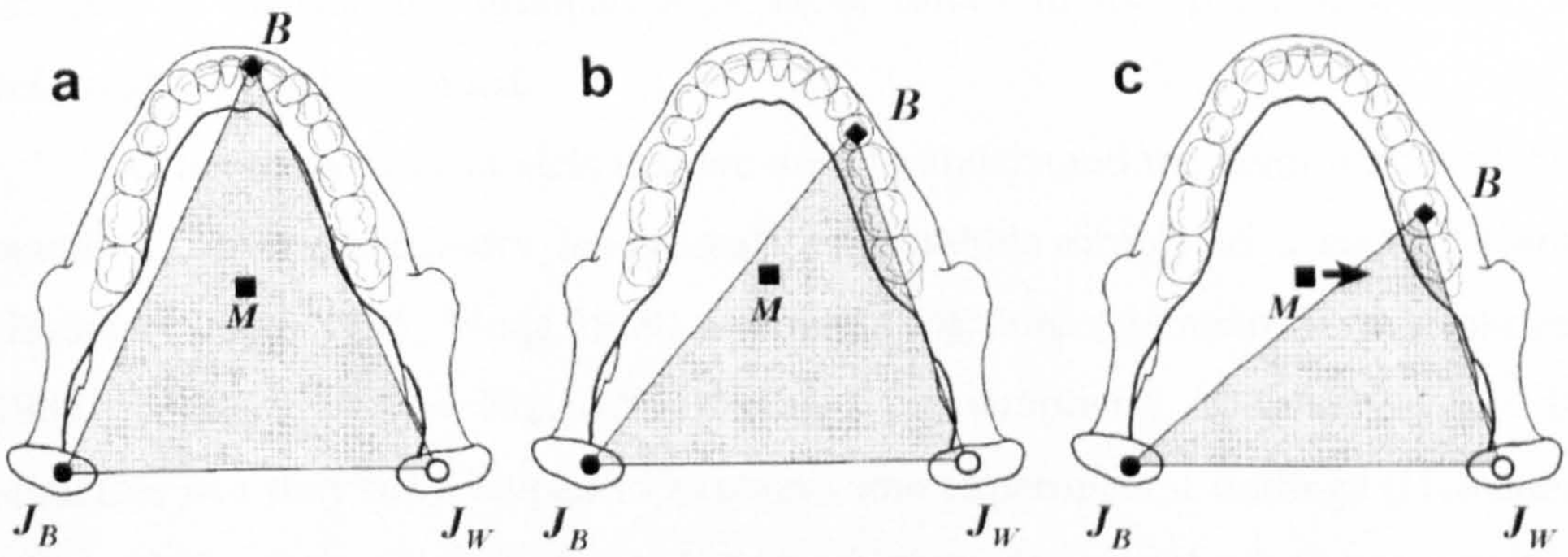

Fig. 2.8. Occlusal view of the human mandible showing the triangle of support (shaded area), as defined by Greaves (1978), during incisor (a), premolar (b) and molar biting (c). During molar biting, the muscle resultant force (M) has to move towards the working side through a reduction in balancing side muscle activity. B – bite force, J_B – balancing side reaction force, J_W – working side joint reaction force (Spencer 1998: 30, Fig. 3).

Most of the early studies that modelled the mandible as a rigid body were limited to the sagittal plane (Robinson 1946, Gingerich 1971, Pruim et al. 1980, Throckmorton 1985). Only few studies projected the forces and reaction forces onto both the frontal and sagittal plane (Hylander 1978, Smith 1978, Antón 1990, 1994). These two projections are, however, still crude representations of the complex masticatory system.

The most appropriate approach to study mandibular biomechanics is a 3D model of the magnitude and direction of all muscle and reaction forces. Thanks to advances in computer technology, the first 3D mathematical models were

introduced in the mid-eighties (Baragar & Osborn 1984, Osborn & Baragar 1985, Smith et al. 1986). In the following years, such models were used to study various aspects of muscle, reaction and bite forces in the human masticatory system (Koolstra et al. 1988, Koolstra & van Eijden 1992, Osborn 1995, 1996). Whereas these early 3D models were only able to simulate static bites, the development of dynamic mathematical models, using multibody dynamic analysis (MDA), nowadays allows the study of the contribution of each masticatory muscle to jaw movements and how the muscles interact with the joints to move the jaw (Koolstra & van Eijden 1995, 1996, 1997, 2001, Sellers & Crompton 2004, Curtis et al. 2008).

2.3.2. Deformation models

All the modelling approaches that have been cited here so far treat the mandible as a rigid body and focus on the study of forces acting on the mandible. In order to analyse the dissipation of these forces in the mandibular bone, a deformable model is needed.

Often theoretical models that are used to understand the deformation of the mandible under masticatory loads treat the mandible simply as a curved beam (Hylander 1984, 1985, Weijs 1989) or a bent long bone (Ashman & van Buskirk 1987), as illustrated in **Fig. 2.9**. Although the simplicity of beam models is attractive and they have helped to explain some experimental findings (Hylander 1984, 1985), they are very limited, because they do not take into account the irregular mandibular shape.

A more accurate representation of mandibular geometry can be achieved with FE models. FEA permits estimation of stresses and strains in a complex or irregular structure by dividing it into a number of small, geometrically simple elements. Forces and constraints (i.e. regions of immobility) can be applied to the model in order to simulate the loading that acts on the structure *in vivo* (Richmond et al. 2005, Rayfield 2007).

Several studies have already applied FE modelling to the human mandible (Gupta et al. 1973, Knoell 1977, Haskell et al. 1986, Hart & Thongpreda 1988, Hart et al. 1992, Korioth et al. 1992, Tanne et al. 1993, Korioth & Hannam 1994a, 1994b, Vollmer et al. 1999, Ichim et al. 2006a, 2006b, 2007a, 2007b). One of the first mandibular FE models was developed by Gupta and colleagues (1973). The

model geometry was derived from measurements of a modern human mandible and provided only a crude representation of a mandibular segment, consisting of the canine and the postcanine dentition. Later, Knoell (1977) generated a model including the full mandibular dentition and the rami, but like Gupta and colleagues (1973), the shape of the model was only based on measurements and, therefore did not represent the shape of a mandible very well.

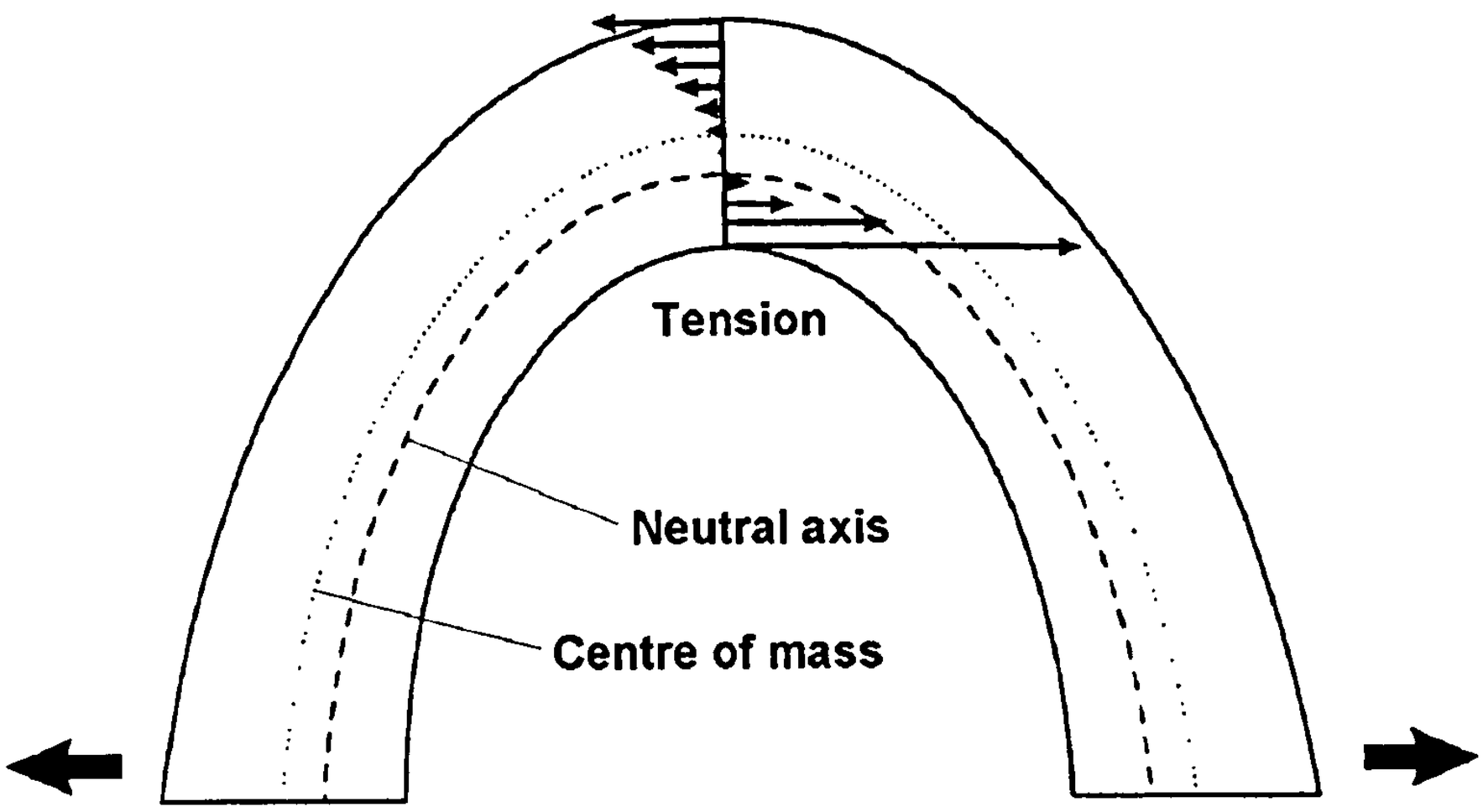

Fig. 2.9. Stress in a curved beam resulting from lateral transverse bending (pulling the two ends of the beam apart as indicated by the two large arrows). The inner surface experiences tension and the outer surface compression. Stress is zero at the neutral axis and reaches greatest values at the inner and outer surfaces, while the stress magnitude increases towards the apex and is highest at the inner surface of the apex region (modified after van Eijden 2000: 131, Fig. 10).

The use of CT to obtain a more accurate model was pioneered by Hart and Thongpreda (1988) and then further improved by higher resolution and more realistic material properties. A very sophisticated model was used by Korioth and colleagues (1992) as well as Korioth and Hannam (1994a, 1994b), who defined for example seven materials with different elastic properties, which included a distinction between enamel and dentin as well as different parts of the periodontal ligament around each tooth root. Nowadays, the use of CT data for building FE models is the standard, so that depending on the resolution of the scan, geometrically very accurate models can be created.

In general, FE modelling is highly useful for the study of the biomechanics of the human mandible, since for practical and ethical reasons it is not possible to directly measure bone strain in the mandibles of living human subjects. The only alternatives to FE modelling are *in vitro* experiments with either fresh or dry human mandibles (Ralph 1975, Ralph & Caputo 1975, Mongini et al. 1979,

Daegling et al. 1992, Daegling & Hylander 1994, Throckmorton & Dechow 1994, Daegling & Hylander 1998, Meyer et al. 2002, DuChesne et al. 2003) or *in vivo* experiments with non-human primates (Hylander 1979a, 1979b, 1984, 1985, Ross & Hylander 1996, Ross 2001). However, mandibular morphology varies tremendously between different primate taxa, so that the application of results to humans has to be done with caution. *In vitro* experiments, on the other hand, do not allow simulation of the actions of the various masticatory muscles due to practical limitations.

The results of FE models of the human mandible are in general qualitatively similar to those of experimental studies. Experimental as well as modelling data indicate that the mandible of humans as well as non-human primates experiences three main types of deformation during static biting and mastication: sagittal bending, rotation (torsion) of the corpora around their long axes and lateral transverse bending (**Fig. 2.10**), which pulls the two rami apart (Hylander 1984, 1985, van Eijden 2000). Chapter 8 will discuss an additional type of deformation that is relevant for the stresses at the symphysis: dorsoventral shear, which results from the action of the balancing side jaw adductors that elevate the balancing side whereas the bite force pushes the working side downward. Sagittal bending occurs as a result of the vertical components of muscle forces, the reaction forces at the condyles and the bite force at the teeth . On the balancing side, it leads to compression at the lower margin of the mandible and tension at the upper margin, while a reverse bending moment occurs on the working side. During incisal biting, sagittal bending on both side of the mandible is equal, but during unilateral biting, the deformations of the working and balancing sides differ. Korioth and colleagues (1992) demonstrated predominant sagittal bending of the balancing side corpus, but sagittal bending and torsion of the working side during unilateral molar biting. This torsion of the mandibular corpora about their long axes, which is caused by the position of the resultant force of the jaw adductors lateral to the long axis of each corpus, results in a narrowing of the dental arch (Korioth & Hannam 1994a). Lateral transverse bending is mainly produced by the laterally directed force components of the temporal and masseter muscles and causes compression at the buccal surface of the mandible and tension at the lingual surface with increasing magnitudes

towards the symphysis, as illustrated in **Fig. 2.9** (Korioth et al. 1992, van Eijden 2000).

Even though FE modelling has provided valuable insights into the stresses and strains in the mandible during biting and mastication, FE models have the disadvantage that they are static and, thus, do not take into account the dynamics of the masticatory system. A very promising approach is, therefore, the combination of FE and rigid-body modelling, which has recently been pioneered by Koolstra and van Eijden (2005, 2006). They modelled the cranium and mandible as dynamic rigid bodies, whereas the TMJ contained two layers of deformable articular cartilage and a freely movable, deformable cartilaginous articular disc in between. These deformable parts were modelled using FEA. The next challenge is to not only apply FE modelling to the TMJ within a dynamic model, but to model the whole mandible as a dynamic as well as deformable structure.

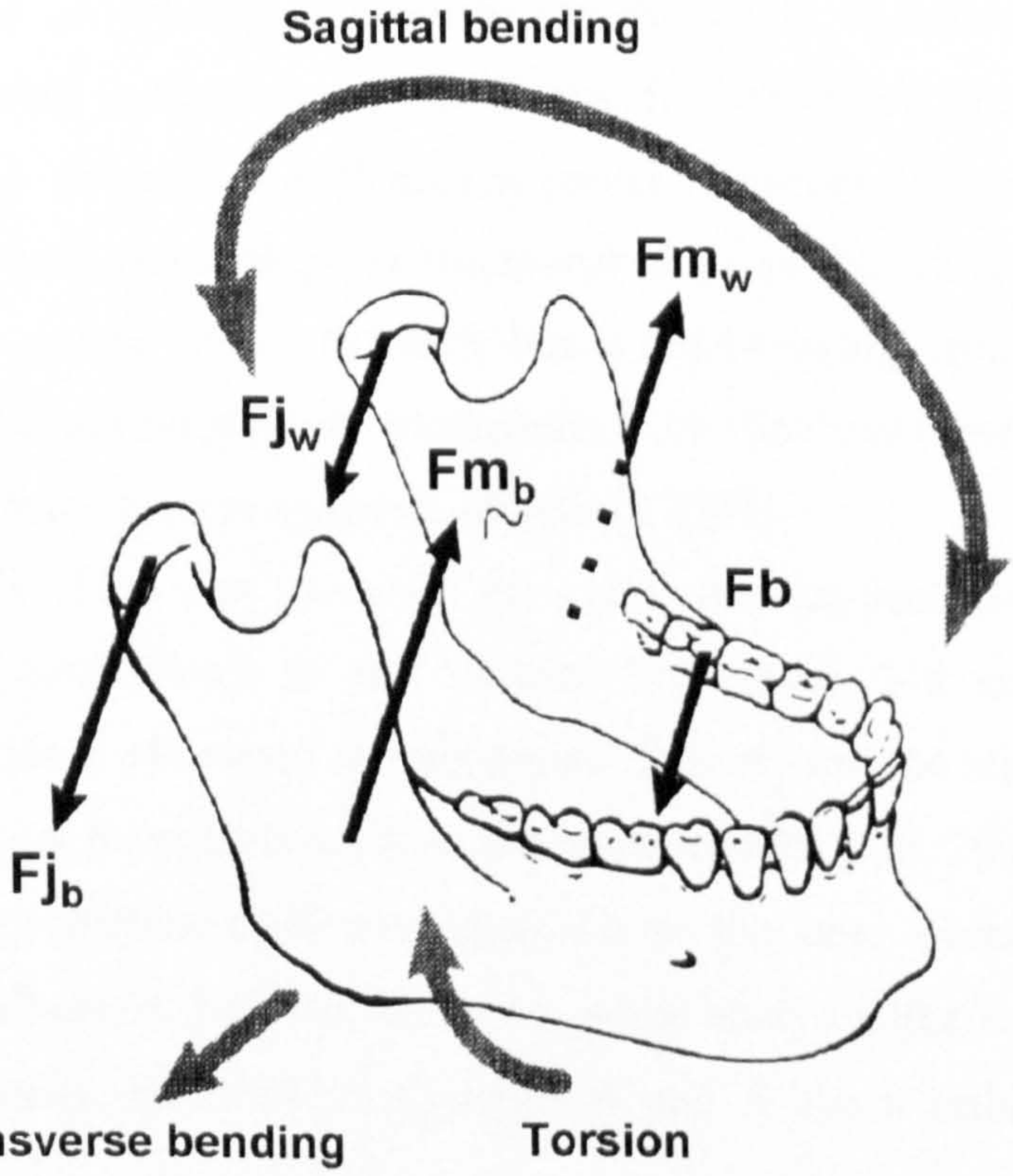

Fig. 2.10. Loading of a mandible during a unilateral molar bite. F_b is the bite force, Fm_b and Fm_w and Fj_b and Fj_w are the muscle and joint forces at the balancing and working sides. The distortion of the corpus can be described as a combination of sagittal bending, torsion, and lateral transverse bending (van Eijden 2000: 130, Fig. 9).

All the FEA studies cited above have in common that they use more or less realistic models of human mandibles in order to study how the human mandible in

general deforms during masticatory function. This approach can be termed inductive and allows to develop general ideas about form-function relationships based on a particular case or to test how a specific structure resists to certain loads (Witzel & Preuschoft 2005, Rayfield 2007).

However, FEA can also be used to synthesize structures applying general mechanical principals like Wolff's (1892) law, which is a rather deductive approach. Pioneering work in this area has been carried out by Witzel and colleagues (Witzel & Preuschoft 2005, Witzel 2006, 2007).

.In their approach, which they termed FESS (finite element structure synthesis), the starting point is a simple homogeneous block to which physiological loadings are applied. Simply by the iterative removal of areas with low compressive stress, they are able to generate crania that resemble the original specimens not only in external but also internal morphology, for example with regard to the position of foramina and sinuses. They argue that such a successful synthesis of the real morphology allows then to deduce *in vivo* loads, which is particularly interesting in the case of fossil taxa, for whom the precise *in vivo* loads are not known (Sverdlova & Witzel in press). However, this builds on the assumption that cranial morphology or the morphology of the whole skeleton is determined almost solely by its function has a load-bearing structure. Other relevant factors like developmental, phylogenetic or functional constraints are mostly ignored in their structure synthesis (Rayfield 2007).

Alternatively, FEA can be used in a hypothetical-deductive way, by altering loads or morphology to test certain hypotheses. For example, the mechanical significance of certain morphological features can be studied by the removal or addition of these features in an FE model (Ichim et al. 2006b, Strait et al. 2007). This hypothetical-deductive approach is the one, which is mainly applied here (e.g. Chapters 7 to 10). However, some analyses like the validation and sensitivity studies described in Chapters 4 and 5 use a rather inductive approach.

2.4. Neanderthal and anatomically modern human mandibular morphology and relevant functional hypotheses

2.4.1. Overview

Neanderthal and anatomically modern humans differ considerably in mandibular morphology. For example, Neanderthal mandibles typically have large anterior teeth relative to the size of their posterior teeth (Brace 1964a, 1979, Trinkaus 1983, 1984, Wolpoff 1999), a gap between the third molar and the ramus, the so-called retromolar space (Coon 1962, de Lumley 1973, Stringer et al. 1984, Condemi 1991, Franciscus & Trinkaus 1995, Arensburg & Belfer-Cohen 1998, Rak 1998, Rosas 2001), and a posteriorly placed coronoid process with a large vertical height often exceeding that of the condylar process and resulting in an asymmetric sigmoid notch (Rak 1998, Rak et al. 2002). Like other archaic members of the genus *Homo*, they also show a receding symphysis, which lacks a well developed *mentum osseum* or chin (**Fig. 2.11**).

The mandibles of anatomically modern humans, on the other hand, have a relatively vertically orientated symphysis with a clearly protruding *mentum osseum*. Normally, there is no gap between the third molar and the ramus and the superior ramus is characterised by a more anteriorly placed coronoid process and a deep, symmetric sigmoid notch (Rak 1998, Rak et al. 2002). In addition, the anterior teeth are relatively smaller, that means to the posterior teeth (Wolpoff 1971, Brace et al. 1981, Bailey & Hublin 2005, 2006).

In the literature, some other features, that differ between Neanderthal and anatomically modern human mandibles have been discussed, for example, the position of the mental foramen relative to the dentition (Stringer et al. 1984, Condemi 1991, Arensburg & Belfer-Cohen 1998, Hublin et al. 1998, Coqueugniot 2000, Rosas 2001, Coqueugniot & Minugh-Purvis 2003). However, this review will only focus on those aspects of morphology that have been linked to masticatory biomechanics. These are 1) the symphyseal morphology, 2) the retromolar space and 3) the superior ramus morphology. Their variation will be described briefly and the relevant functional hypotheses will be introduced. In addition, how differences in tooth size and dental wear patterns have led to more general hypotheses about mechanical adaptations in modern human and Neanderthal craniofacial morphology will be considered.

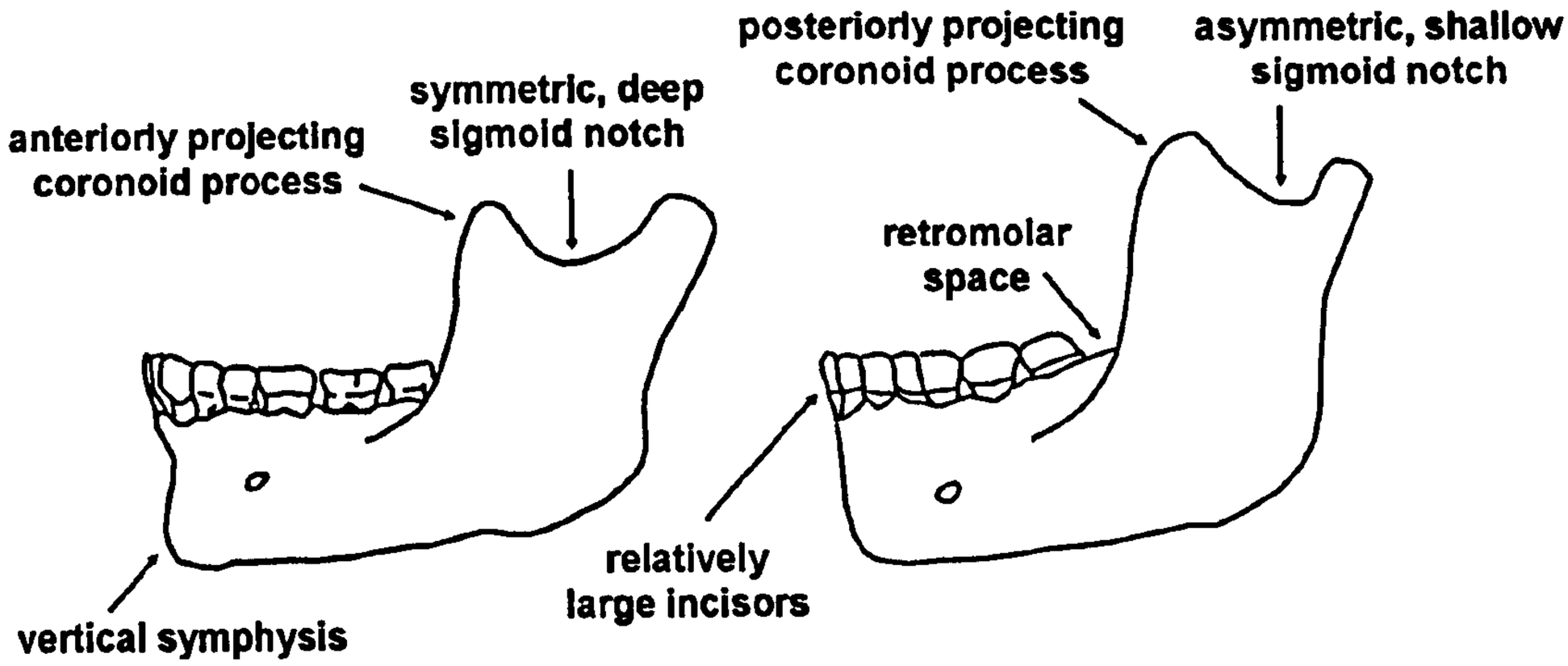

Fig. 2.11. Morphological differences between modern human (left) and Neanderthal (right) mandibles (redrawn after Klein 1999: 381, Fig. 6.8).

2.4.2. Symphyseal morphology

It is generally accepted that a well-developed chin is one of the unique characteristics of anatomically modern humans. Some archaic members of the genus *Homo*, especially some Neanderthal fossils, have been said to show incipient chins or some elements of the *mentum osseum* (McCown & Keith 1939, Ascenzi & Segre 1971, Wolpoff et al. 1981, Smith 1984, Lieberman 1995, Rosas 1995, Lam et al. 1996, Stefan & Trinkaus 1998a, 1998b, Wolpoff 1999), but its consistent presence is found only in early and recent populations of *Homo sapiens* (Schwartz & Tattersall 2000, Dobson & Trinkaus 2002).

However, different definitions of this feature have been used in previous descriptions of its variation in archaic and modern human samples. Sometimes, the human chin has been identified solely on the basis of the general protrusiveness of the symphyseal region (Smith 1984, Lieberman 1995, Lam et al. 1996, Wolpoff 1999), but there are actually more morphological details that are relevant in the description of this feature.

Following the definitions of Weidenreich (1936), three anatomical characteristics should be evaluated in order to judge the extent of chin development (**Fig. 2.12**): the *incurvatio mandibulae*, *mentum osseum*, and *trigonum mentale*. The *incurvatio* is the concavity between the alveolar process margin and the basilar portion of the external symphysis. The *mentum osseum* is the anterior projection of the basilar symphysis. A *mentum osseum* exists when the basilar portion forms an equally rounded swelling across the symphysis. By

contrast, a *trigonum mentale* occurs when the anterior projection of the basal symphysis exhibits a distinctly triangular shape when viewed from the front (Weidenreich 1936). These definitions have been the basis for several comparative studies of archaic and modern humans (Bräuer 1984, Lieberman 1995, Rosas 1995, Rak 1998, Quam & Smith 1998, Dobson & Trinkaus 2002). A study by Schwartz and Tattersall (2000) based the identification of the human chin on the presence of an inverted "T-shaped" structure consisting of a symphyseal keel and a distended inferior mandibular margin.

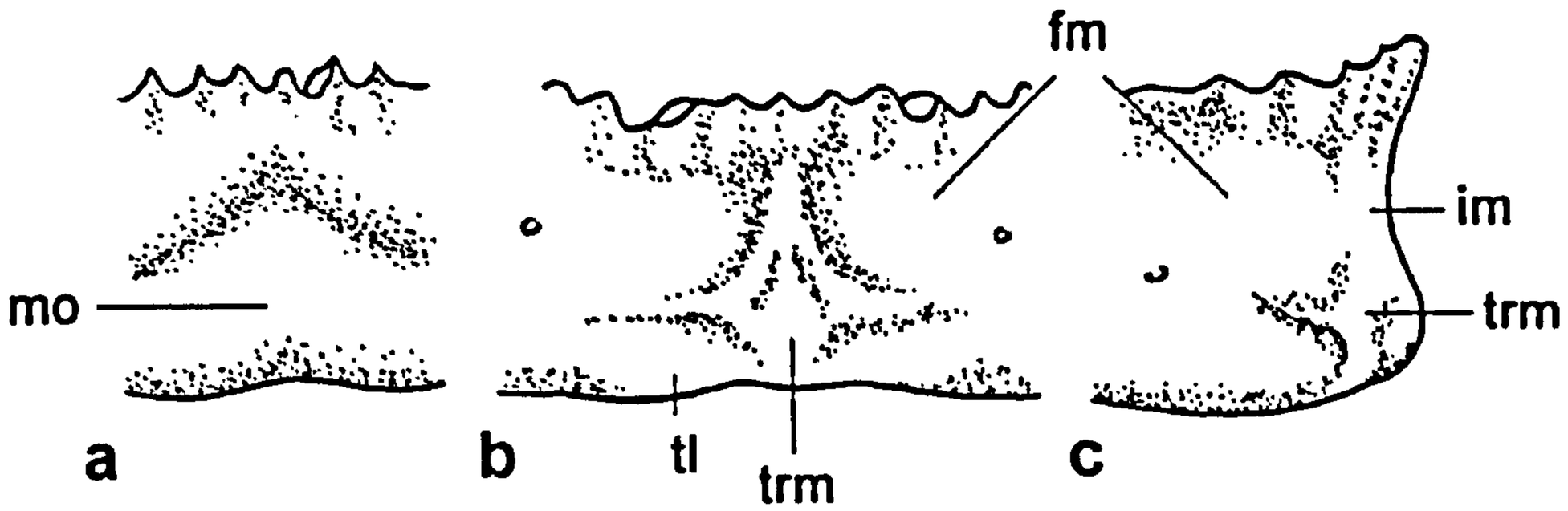

Fig. 2.12. Features of the mandibular symphysis. A: *mentum osseum* (anterior view); B: *trigonum mentale* (anterior view); C: lateral symphyseal view with a *trigonum mentale*. Abbreviations: mo – *mentum osseum*, trm – *trigonum mentale*, tl – *tuberculum laterale*, im – *incurvatio mandibulae*, fm – *fossa mentalis*. (redrawn after Quam & Smith 1998: 412, Fig. 4).

According to these authors (Schwartz & Tattersall 2000), who studied a large sample of modern human and Neanderthal specimens, none of the Neanderthals studied shows this inverted "T-shaped" structure, which is seen in modern *H. sapiens*. This is also the case for juvenile specimens: Although the "T-shaped" structure seems to be already present before birth in modern humans, it is missing in juvenile Neanderthal mandibles (Schwartz & Tattersall 2000). The uniqueness of modern human chin morphology is also supported by the observations of Dobson and Trinkaus (2002). However, their comparison with Mid-Pleistocene specimens indicates that there is a trend through time in which the *mentum osseum* is incomplete to absent in the Middle Pleistocene, but sometimes present in Neanderthals, even though lacking the clear development of a *trigonum mentale*.

Several explanations for the evolution of the human chin have been put forward: Early suggestions included the idea that this feature is a result of the reduction of the dental arch while the length of the inferior corpus was maintained (Hrdlička 1911, Robinson 1913) or the result of a forward shift of the basal

portion of the mandible under the alveolar process during development (Bolk 1924, Biggerstaff 1977). It has also been suggested that it is linked to the evolution of speech (Walkhoff 1904, Ichim et al. 2007a). Later proposals considered the role of masticatory loads: One hypothesis, the so-called "hypofunction" hypothesis stated that the chin evolved because of an overall reduction of the dentition and masticatory musculature in anatomically modern humans (Riesenfeld 1969). DuBrul and Sicher (1954) suggested that the chin serves to buttress the symphysis against medial transverse bending caused by the action of the lateral pterygoid muscles that squeeze the rami together and produce labial tension and lingual compression at the symphysis. White (1977) proposed, in contrast, that the chin provides resistance to lateral transverse bending (wishboning) causing labial compression. More recently, Daegling (Daegling 1990, 1993a) hypothesised that the human chin represents a structural response to resist vertical bending in the coronal plane resulting from torsion of the corpora around their long axes (**Fig. 2.10**).

FEA allows investigation of whether or not the chin has an impact on mandibular load resistance. Therefore this method has recently been used to study the mechanical significance of the human chin (Ichim et al. 2006a, 2006b, 2007a). Interestingly, the results of these studies do not confirm that the presence of a chin is relevant for the resistance to masticatory loads. However, the methodology used in these studies can be further improved with regard to model geometry as well as applied loads and constraints. One aim of this study will therefore be to also apply FEA, but using improved methodology to test the mechanical significance of the human symphyseal morphology (Chapter 9).

2.4.3. The retromolar space

The retromolar space, a gap between the third mandibular molar and the anterior margin of the ascending ramus, is probably one of the most frequently cited Neanderthal characteristics (Coon 1962, Trinkaus 1983, Stringer et al. 1984, Rak 1986, Trinkaus 1987, Condemi 1991, Wolpoff 1999). Often it is considered to be a Neanderthal autapomorphy (Stringer et al. 1984, Condemi 1991), although it is also present in other Pleistocene *Homo* specimens and sometimes in living populations (Franciscus & Trinkaus 1995, Arensburg & Belfer-Cohen 1998, Nicholson & Harvati 2006). Thus, it is not unique to the Neanderthals. However,

it occurs among them at a higher frequency than in most other Pleistocene *Homo* samples (Franciscus & Trinkaus 1995).

By definition, a retromolar space can only be identified after the eruption of the third molar and, thus, only in adult mandibles. In the case of juvenile specimens, where just the deciduous or first two permanent molars are present, it is only possible to make predictions about later adult morphology. Nevertheless, the development of this trait has been discussed by several authors. For example, it has been proposed that the retromolar space develops at the end of the growth period (Tillier 1988). In contrast to this, Ponce de León and Zollikofer (2001) suggested an early rather than late ontogenetic origin of the retromolar space, based on their finding that the mandibular corpus and rami are at a more posterior position relative to the dentition in juvenile Neanderthals compared to modern humans. According to Bastir and colleagues (2007), such an early onset of the retromolar space is, however, unlikely, since facial growth in general terminates rather late in ontogeny. As these conflicting ideas show, it is necessary to conduct further studies on the ontogenetic development of the retromolar space.

Several causes for the high frequency of retromolar spaces in Neanderthals have been suggested: an anterior shift of the dental arcade (Coon 1962, Howells 1974, Wolpoff 1999), a posterior "retreat" of the zygomatic and anterior ramal regions relative to a fixed molar position (Trinkaus 1987), a shortening of the dental arcade either resulting from reduced molar size (Rak 1986), a forward shift of the third molars (Rak & Hylander 2007) or from a combination of anterior migration of the postcanine dentition and posterior migration of the anterior dentition (Spencer & Demes 1993).

A study by Franciscus and Trinkaus (1995) demonstrated that the high frequency of retromolar spaces in Neanderthals might be best seen as a combined result of reduced dental arcade lengths and ramus breadths in the context of little or no reduction in overall mandibular length. A relationship between the retromolar space and mandibular dimensions is supported by the results of Rosas (2001), which show that retromolar space length correlates significantly with the maximum length and height of the corpus in the Simas de los Huesos sample. It is also confirmed by Nicholson and Harvati (2006), who found that retromolar gaps in modern humans are related to increased mandibular size.

In contrast, Rak and Hylander (2007) suggested that the retromolar space is related to larger jaw gape in Neanderthals. According them, the forward shift of the third molars produces a larger vertical distance between the upper and lower third molars than in a mandible with the same gape size, in which the third molars have not shifted anteriorly. However, the potential benefits of this larger gape remain unclear.

The authors that suggested that the retromolar space is linked to mechanical adaptations (Spencer & Demes 1993, Rak & Hylander 2007) generally consider its relevance for bite force production, rather than the effect of the retromolar space on force dissipation in the mandible. However, the region between the third molar and the mandibular ramus is likely to be highly strained during masticatory function, since it lies between the attachment sites of the jaw closing muscles, which pull the mandible upwards, and the high reaction forces that occur at the molar dentition. So, it is interesting to see whether the presence or absence of a retromolar space has an effect on the structural rigidity of this region. This will be tested here with FEA (Chapter 7).

2.4.4. Superior ramus morphology

The superior part of the mandibular ramus of Neanderthals has been characterised by a shallow, asymmetric sigmoid notch and a posteriorly oriented coronoid process, which often exceeds the condylar process in height, while in anatomically modern humans the coronoid process is said to have the same height as the condylar process and both are separated by a deep notch with its deepest point approximately at the midpoint between the two processes, as illustrated in **Fig. 2.11** (Rak 1998, Rak et al. 2002).

Rak and colleagues (2002), who quantified superior ramus morphology by tracing mandibular notch contours and superimposing them, found that Neanderthals differ significantly in this feature from modern humans and other Pleistocene *Homo* fossils. They suggest that this morphology is unique to the Neanderthal lineage. The uniqueness of Neanderthal ramus morphology has, however, recently been questioned by Wolpoff and Frayer (2005). Based on qualitative descriptions of Neanderthal, other Pleistocene archaic human and early modern human mandibles, these authors concluded that a shallow, asymmetric ramal notch is not an exclusive Neanderthal feature, since it also occurs in more

ancient hominins and early modern humans. In addition, they found some Neanderthal mandibles with a rather deep instead of a shallow ramal notch. It is therefore likely that the aspects of superior ramus morphology identified by Rak (1998) and Rak and colleagues (2002) are, as with the retromolar space, not unique to Neanderthals but rather occur among them with a higher frequency than in other hominins (Franciscus & Trinkaus 1995).

Rak (1998) as well as Rak and colleagues (2002) mention that the typical Neanderthal ramal morphology seems to already be present in infant and juvenile specimens like Roc de Marsal, Teshik-Tash, and Krapina 53. Another study (Minugh-Purvis & Lewandowski 1992) showed that a posteriorly oriented coronoid process can also be found in modern children around the time of eruption of the permanent anterior dentition. While this morphology disappears, or is deemphasized in modern humans during development, European Neanderthals usually retained posteriorly oriented coronoid processes into adulthood.

Most propably the variation in superior ramus morphology is closely related to the function of the temporalis, which attaches to the coronoid process (Simon & Moss 1973, Minugh-Purvis & Lewandowski 1992). Indeed, animal experiments support a close link between temporalis function and the size and shape of the coronoid process as well as of the sigmoid notch. The detachment of the temporalis muscle or specific muscle portions in animals (Washburn 1947, Avis 1959, Moss & Meehan 1970) leads to the marked alterations in the shape of the coronoid and the sigmoid notch.

Another functional explanation has been suggested for the relatively low condyle of Neanderthals. Rak and Hylander (2003) suggested that this closer proximity of the condyle to the occlusal plane, in combination with other features of the Neanderthal masticatory system, for example, the retromolar space, increased the maximum jaw gape (but see Wolpoff and Frayer 2005 for a discussion of the variation in condylar height).

The effect of different morphological features on gape size can be studied with rigid-body models. In contrast, the hypothesised relationship between superior ramus morphology and temporalis function can be investigated with FEA, since it relates to bone modelling, which is regulated by strains. This will be the aim of the study presented in Chapter 8.

2.4.5. Dental size and wear patterns

For the study of functional adaptations in the mandible, the morphology and wear of the dentition can provide valuable information. There is abundant literature about tooth morphology and size as well as dental wear in anatomically modern humans and Neanderthals (Brace 1964a, 1967, Wolpoff 1971, Molnar 1972, Wallace 1975, Frayer 1977, Brace 1979, Wolpoff 1979, Trinkaus 1983, 1984, Bailey & Hublin 2005, 2006). Here only some selected findings regarding dental size and wear patterns in relation to functional demands will briefly be described.

From the Middle to Late Pleistocene there is a trend to reduction in size of the permanent posterior dentition, which is linked with reduction of overall mandibular size and robusticity (Brace 1979, Franciscus & Trinkaus 1995, Wolpoff 1999, Nicholson & Harvati 2006, Quam et al. 2009). This decrease in tooth size has been explained as a result of new food preparation techniques, for example, cutting, pounding, grinding and cooking with heated stones (Brace 1979, Wolpoff 1999). Such technological shifts likely decreased the time spent in and power of mastication, thus reducing loads on the postcanine teeth (Franciscus & Trinkaus 1995). Consequently, the selective pressure that had previously maintained tooth size during the Middle Pleistocene was probably reduced so that random changes in the genome leading to a structural reduction were not selected against, which has been termed "probable mutation effect" (Brace 1964b, 1979).

Neanderthals also show such a reduction of postcanine tooth size, as comparisons between early and late Neanderthals have revealed (Brace 1979). Their incisors, however, remained relatively large, so that the incisors became larger in relation to the postcanine dentition (Brace 1964a, 1967, 1979, Trinkaus 1983, 1984, Wolpoff 1999). This increase in relative size of the incisors distinguishes Neanderthals from *H. erectus* as well as Upper Palaeolithic modern humans, although the absolute values for anterior and postcanine tooth size show a great deal of overlap (Stefan & Trinkaus 1998a, Bailey & Hublin 2005, 2006). Why Neanderthals maintained relatively large incisors while selective pressures were probably reduced due to advances in food processing, requires explanation.

Whereas the function of the posterior teeth is to crush food during mastication, the function of the anterior teeth is not so evident. Sometimes the

incisors are referred to as "cutting teeth", but it is known from modern hunter-gatherers that the anterior teeth actually serve as a clamp, to hold the objects that are then manipulated by the hands, for example, pulling them in order to tear them or cutting them with a knife (Brace 1975, 1977, 1979). Based on the assumption that there was no major dietary difference between Neanderthals and their predecessors (but see e.g. Pérez-Pérez et al. 2003), it has been suggested that the relatively large incisors might be due to the use of the anterior teeth for more than just food processing (Brace 1967, Wolpoff 1975, Brace 1979, Brace et al. 1981). Thus, their function as a clamp would have been extended to non-edible objects, whose manipulation was important for human survival, while the selective pressures acting on the molar dentition decreased because of advances in food processing.

This hypothesis is consistent with the dental wear pattern found in adult Neanderthals. Neanderthals show a tendency to wear the anterior teeth down more rapidly down than the posterior teeth, resulting in extreme labial rounding of the maxillary teeth in older individuals (Patte 1959, Brace 1964a, Heim 1976, Brace 1979, Wolpoff 1979, Trinkaus 1983, 1984, Wolpoff 1999). However, most descriptions are solely qualitative descriptions based on few fossils (Wallace 1975, Heim 1976, F. H. Smith 1976, Trinkaus 1983). An exception is a study by P. Smith (1976), who compared dental attrition in Neanderthals and early modern humans from Europe and the Near East. According to her results, the wear pattern was similar for all Mousterian specimens, including the presumably early anatomically modern individuals from Skhūl and Qafzeh, but differed from that in the Upper Palaeolithic specimens in showing more severe attrition anteriorly than posteriorly. As in recent humans, the Upper Palaeolithic specimens showed relatively more wear on the posterior teeth (P. Smith 1976). A more recent study provides a detailed analysis of the rate of bevelling (i.e. the bevelling angle) relative to tooth wear in incisors of Neanderthals, Inuits and Puebloan Amerindians (Ungar et al. 1997). Although these authors found similar patterns in the three samples, the Neanderthal specimens had significantly greater bevelling in more worn teeth than either recent human sample. In addition, microwear data show a high density of labiolingual wear striae and enamel chipping on the occlusal surfaces of anterior Neanderthal teeth (Ryan 1980).

However, the use of the anterior teeth for other activities than food processing is not the only potential cause for this distinctive dental wear pattern oberserved in Neanderthals. Alternatively, high levels of abrasives in the diet of Neanderthals have been suggested (Martin 1923, Siffre 1923, Wallace 1975, Puech 1979, 1981), but if abrasives in the diet were the cause, it is difficult to imagine why only the anterior teeth and not the posterior teeth show such a pronounced wear, particularly since Neanderthal molars are characterised by absolutely and relatively thinner enamel compared to modern human molars (Molnar et al. 1993, Smith & Zilberman 1994, Olejniczak et al. 2008). In addition, microwear data indicate that Neanderthals consumed less abrasive food items (such as meat or fruit) and/or processed their food in a more efficient way (e.g. by cooking) than Middle Pleistocene populations, since Neanderthal teeth show fewer striations (Pérez-Pérez et al. 2003). There is also a growing evidence from isotope studies that by far the largest part of Neanderthal diet consisted of relatively non-abrasive meat (Richards et al. 2000, Bocherens et al. 2001, Bocherens et al. 2005, Richards et al. 2008, Richards & Trinkaus 2009). Therefore, it seems unlikely that abrasives in the diet can explain the typical dental wear pattern seen in Neanderthals.

The suggestion that this wear pattern was caused by the regular use of the anterior teeth for activities other than food processing, in contrast (Stewart 1959, Coon 1962, Brace 1962, 1964a, 1967, Brace et al. 1981, Trinkaus 1983), convincingly explains why the anterior teeth are more rapidly and severely worn than the posterior teeth and is consistent with the currently available data on Neanderthal diet. In addition, microwear analyses of labial incisor crowns frequently reveal transverse scratches that have been related to cutting objects held in the teeth with lithic implements (Martin 1923, Koby 1956, Patte 1960, de Lumley 1973, Trinkaus 1983, Lalueza-Fox & Frayer 1997).

Until recently, the use of teeth for manipulating non-edible objects was common in several human populations. This was especially the case for Inuits who used their teeth for a variety of different tasks (Molnar 1972, Cybulski 1974, Merbs 1983, Larsen 1985, Milner & Larsen 1991). The high mechanical demands on the anterior teeth resulting from this tooth use led to a high frequency of severe tooth wear, pulp exposure, resorption of tooth roots and finally tooth loss as well as to a high prevalence of degenerative changes in the TMJ (Merbs 1983). In

addition, it has been shown that the frequent non-masticatory use of teeth in Inuits is linked with aspects of craniofacial morphology and an ability to produce higher bite forces compared to other populations (Hylander 1977). A similar link between non-masticatory use of the teeth and craniofacial morphology has been suggested for Neanderthals.

2.4.6. The anterior dental loading hypothesis

Some of the features described above like the relatively large and heavily worn anterior teeth and the high prevalence of degenerative changes in the TMJ of Neanderthals have been cited as evidence for the regular use of the front teeth for other purposes than food processing (Stewart 1959, Coon 1962, Brace 1962, Brace et al. 1981, Smith 1983, Trinkaus 1983, Smith & Paquette 1989). This provided the basis for the "anterior dental loading hypothesis" (ADLH), which suggests that the typical Neanderthal craniofacial morphology can be partly explained as an adaptation to regular heavy anterior dental loads that resulted from such non-masticatory activities (Smith 1983, Rak 1986, Demes 1987, Trinkaus 1987, Spencer & Demes 1993).

The first author who interpreted Neanderthal facial morphology in terms of biomechanical adaptations was Smith (1983). Based on Hylander's (1977) study of Inuit craniofacial morphology, Smith (1983) suggests that the Neanderthal face was exposed to high bending stresses during anterior dental loading. According to his explanation, these bending stresses occurred, because the bite forces at the maxillary incisors acted on a long moment arm resulting from prognathism and the posterior positioning of the anterior root of the zygomatic arch in the Neanderthal face. In order to resist these bending moments, the midfacial region of Neanderthals increased in height, since this enlarged the second moment of area of cross sections of the face (Smith 1983).

Instead of the sagittal bending proposed by Smith (1983), Rak (1986) suggests that the high loading of the anterior teeth resulted in sagittal rotational stresses or, in other words, around a transverse axis (**Fig. 2.13**). In order to counter these stresses, the infraorbital region changed from a more coronal to a more sagittal orientation as well as to a more triangular shape. Both features constitute the typical mid-facial prognathism of Neanderthals. Thus, Rak (1986)

explains Neanderthal mid-facial projection in terms of an adaptation to rotational stresses.

Another theoretical approach to the biomechanical adaptation of Neanderthals was introduced by Demes (1987). Unlike Smith (1983) and Rak (1986), who each consider only one type of loading, Demes (1987) considers three different loading situations resulting from high loads on the anterior dentition: torsion around a transverse axis, torsion around a sagittal axis and sagittal bending (**Fig. 2.13**). She agrees that the Neanderthal face represents an adaptation to high anterior loads combined with long lever arms, but estimates the stresses and mechanical adaptations differently from Smith (1983) and Rak (1986), for example, in contrast to Smith (1983), who assumes that the increased height of the mid-facial region improves the resistance to sagittal bending, Demes (1987) suggests that resistance to this loading regime is provided by the inflated maxilla, the convex midfacial profile and the straight infrazygomatic contour in the frontal plane. Counter to Rak (1986), she proposes that the sagittal orientation of the infraorbital region in Neanderthals does not improve the resistance to torsional moments around a transverse axis.

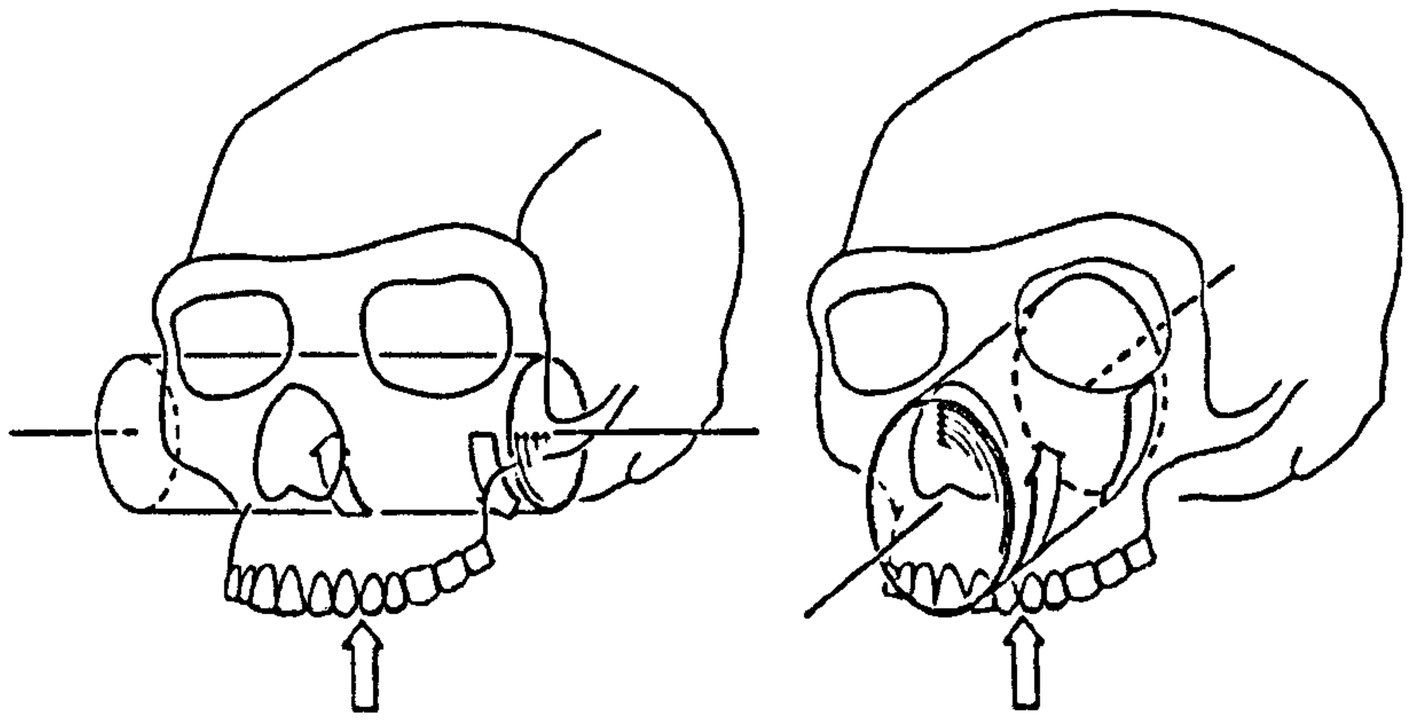

Fig. 2.13. Torsional movements during unilateral incisal biting as suggested by Rak (1986) and Demes (1987). Left figure: torsion around a transverse axis, right figure: torsion around a sagittal axis. Arrows indicate bite force, rotational moments and distribution of torsional stresses in a section (Demes 1987: 298, Fig. 1, 299, Fig. 2a).

In addition to the purely theoretical discussion of Demes (1987), Trinkaus (1987) evaluated Rak's (1986) model based on maxillary and mandibular measurements of fossil specimens. His results indicate that Rak's idea of the Neanderthal mid-facial projection as an adaptation to rotational stresses around a transverse axis does not adequately fit the available data. Therefore, Trinkaus (1987) suggests an alternative model, which he calls the "zygomatic

retreat model". Like Rak (1986) as well as Smith (1983) and Demes (1987), he assumes that the Neanderthal face had to resist elevated levels of biomechanical stress produced by frequent non-masticatory usage of the anterior dentition. However, in contrast to Rak (1986), who considered the reorientation of the infraorbital plate as the dominating and autapomorphic feature of the Neanderthal face, Trinkaus (1987) proposes that the Neanderthal face should be primarily viewed as the product of maintaining the ancestral condition of total facial prognathism combined with the derived condition of posterior migration of the zygomatic root and anterior ramus area relative to the dental arcade. Accordingly, the maintenance of total facial prognathism is a consequence of high anterior dental loading and the selection for large anterior teeth, whereas zygomatic retreat is the result of the general reduction of facial massiveness during the late Middle Pleistocene and early Upper Pleistocene. Trinkaus (1987) assumes that the primary functional effect of zygomatic retreat was reduced mechanical advantage of the primary masticatory muscles and thus a shift towards less powerful mastication, which is also reflected by the reduction of post-canine dentition and mandibular robusticity compared to the Neanderthals' predecessors.

The relationship between zygomatic retreat and a shift to less powerful mastication (Trinkaus 1987) leads to a problem for the ADLH. Although it is suggested that the Neanderthal face is adapted to high anterior dental loading, it is also assumed that the masticatory configuration is rather disadvantageous for producing large bite forces, due to the combination of prognathism and the posterior positioning of the masticatory muscles (Smith 1983, Trinkaus 1987). However, if Neanderthals were adapted to high anterior dental forces, they should also be able to generate these.

Subsequent studies tried, therefore, to estimate the bite force production capability and efficiency of Neanderthals (Antón 1990, Spencer & Demes 1993, Antón 1994, O'Connor et al. 2005). Spencer and Demes (1993) evaluated the position of the masticatory muscles relative to the TMJ and concluded that Neanderthals had increased ability to produce large anterior bite forces compared to anatomically modern humans. Antón (1990, 1994), on the contrary, estimated smaller bite forces in Neanderthals than in modern humans. Finally, the most recent 3D rigid-body modelling study by Connor and colleagues (2005) suggests that Neanderthals and modern humans were equally able to produce anterior bite

forces. The differences in bite force production that these authors found were between large robust individuals and small gracile individuals rather than between anatomically modern humans and Neanderthals. Thus, the results of these previous studies are rather contradictory and further studies should be conducted to test the ADLH.

A recent GMM study of a large sample of modern human and Neanderthal mandibles tried to investigate the general relationship between morphology and non-masticatory tooth use (Nicholson & Harvati 2006). Interestingly, Neanderthal specimens showed a similar mandibular shape to North American Arctic populations, which are known for using their teeth for non-masticatory purposes. The authors of this study suggest, therefore, that at least some features related to non-masticatory functional demands are shared between these two groups. However, since the Upper Palaeolithic and *H. heidelbergensis* specimens also fell close to the Arctic sample, the results are difficult to interpret.

It seems that testing the relationship between anterior dental loading and facial morphology is a task that cannot be fulfilled with morphometric analyses alone and the previous tests of the ADLH have only focused on the bite production capability and efficiency. If Neanderthals were adapted to high anterior dental loads, they should not only show greater ability in producing high forces at the incisors, but also in dissipating these than, for example, modern humans. This prediction will be tested here with FEA (Chapter 10).

2.4.7. Adaptations to reduced masticatory loads due to food processing

As described above, reduction of postcanine tooth size as well as overall mandibular size and robusticity is evident in the human fossil record since the Middle Pleistocene (Brace 1979, Franciscus & Trinkaus 1995, Wolpoff 1999, Nicholson & Harvati 2006, Quam et al. 2009). This gracilisation does not only apply to the lineage that leads to anatomically modern humans, but can be also observed in the Neanderthal lineage, when early Neanderthals that date to the last interglacial are compared with late classic Neanderthals (Franciscus & Trinkaus 1995).

At the same time, there is archaeological evidence for a trend towards more advanced tools and the regular use of fire (e.g. reviewed in Klein 1999) and dental microwear data suggest a major shift towards a less abrasive diet from the

Middle to the late Pleistocene, probably caused by an improvement of food processing techniques (Pérez-Pérez et al. 2003). Some authors have suggested, therefore, that the reduction in craniofacial size and robustictiy since the Middle Pleistocene is the result of new food preparation techniques, for example, cutting, pounding, grinding and especially cooking (Brace 1979, Franciscus & Trinkaus 1995, Wolpoff 1999). Such advances in food processing certainly improved the digestibility of the food and made food softer and smaller in particle size, so that less occlusal force and fewer chewing cycles were required for food breakdown (Lucas & Luke 1984, Lieberman et al. 2004a). This reduction of masticatory loads could have had an impact on mandibular morphology by either reducing the selection pressure for maintaining a large dentition and robust mandibular morphology (Brace 1979), and/or by reducing strains in the bone that stimulate craniofacial growth (Lieberman et al. 2004a).

That the consumption of soft, processed food does indeed have an effect on craniofacial growth is shown by animal experiments. Those animals that are raised on soft, processed food have lower strains in the skull during mastication and show reduced craniofacial growth resulting in smaller skulls of different shape to those of individuals raised on hard, unprocessed food (Beecher et al. 1983, Kiliaridis et al. 1985, Engström et al. 1986, Lieberman et al. 2004a). In humans, those experiments are, of course, not possible, but similar changes in craniofacial morphology have been reported from populations that changed their dietary habits, for example, due to the introduction of agriculture, the industrialisation or colonisation (Carlson 1976, Carlson & van Gerven 1977, Corruccini 1984, 1990, Varrela 1992). For example, in Australian aborigines mandibular and maxillary dimensions have decreased during the last century, which coincides with the transition to a modern, industrially processed diet (Corruccini 1984, 1990).

The same mechanism might be responsible for the gracilisation trend since the Middle Pleistocene. Unfortunately, it is not possible to fully test this hypothesis due to the lack of data and the fact that direct experiments are not possible. However, the prediction can be made that if there was an adaptation to reduced masticatory loads, then the resistance to masticatory load should have decreased over time. With FEA it is possible to test whether load resistance has indeed decreased, which will be described in Chapter 10.

Chapter 3: Material and Methods

3.1. Introduction

This study uses a variety of different techniques for the creation, manipulation and mechanical loading of virtual models as well as for measuring strains in experimentally loaded bones. In order to predict stresses and strains in the bone, the method of finite element analysis (FEA) is applied, which requires a sequence of work steps (**Fig. 3.1**). Based on computed tomography (CT) scans of mandibles, virtual 3D models are created and converted into FE meshes. In the case of fragmentary specimens this 3D reconstruction also includes the reconstruction of missing parts. Additional virtual manipulation can be applied to modify the morphology of specimens, for example, changing one aspect of morphology while keeping all other aspects constant so that the effect of varying particular morphological features can be tested. The final FE models are then loaded and the resulting stresses and strains calculated. In order to make sure that the stresses and strains are predicted accurately, the modelling approach should be validated against strain measurements from an *in vitro* experiment. After the successful validation, the models can be used to simulate the masticatory loads that occur *in vivo*. For this purpose, the muscle forces need to be calculated as accurately as possible. This chapter will provide a general overview of the methods used and will describe those work steps that provide the common basis for the different studies. Those work steps, which are only relevant for specific studies, are described in detail in the respective chapters.

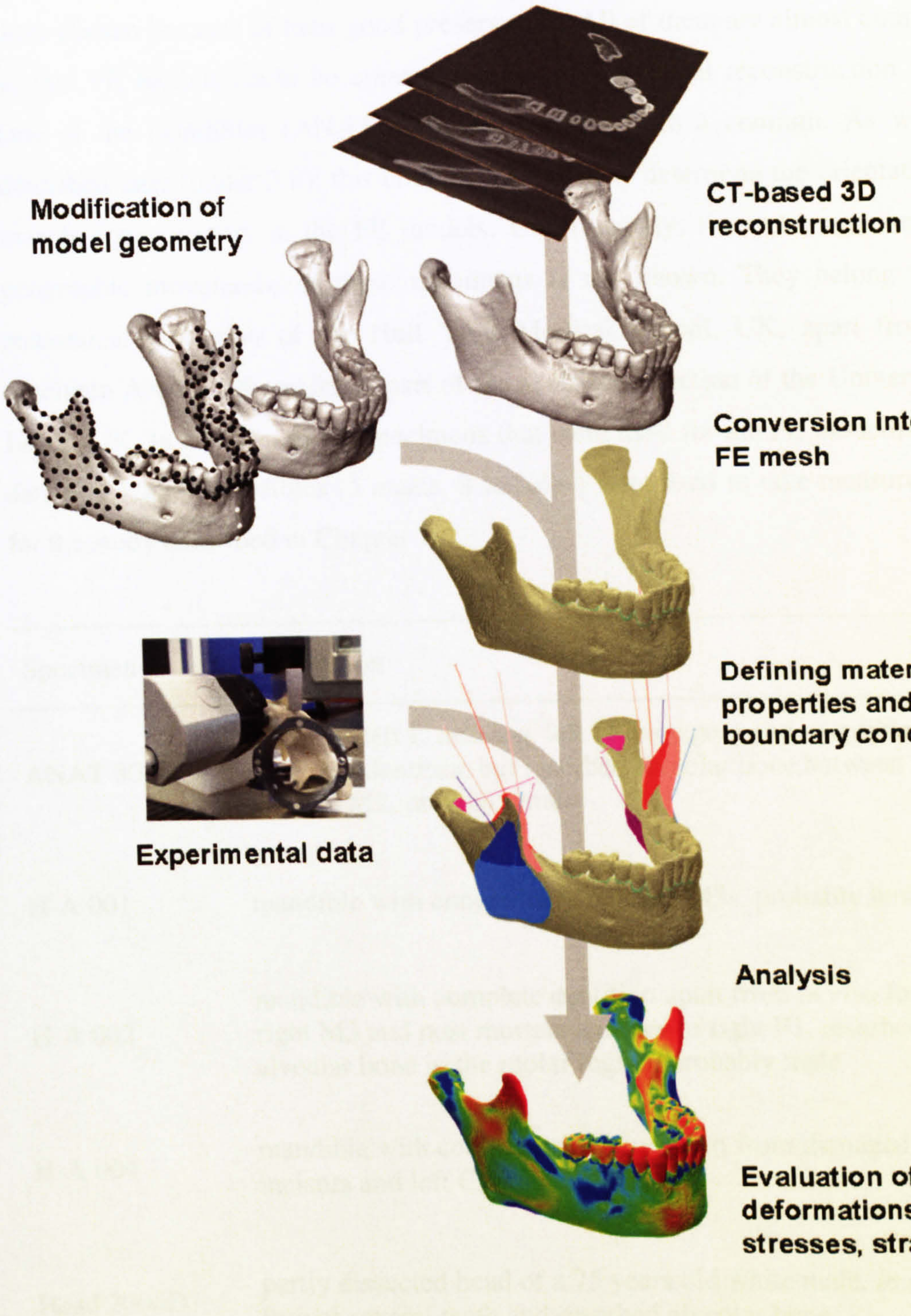

Fig. 3.1. The main steps involved in CT-based FE modelling.

3.2. Modern human specimens

Table 3.1 provides an overview of all the modern human specimens used for FE modelling in this study. This sample consists of four adult mandibles that were chosen because of their good preservation. All of them are almost complete, so that FE models could be created without major virtual reconstruction work. One of the mandibles (ANAT 800) is associated with a cranium. As will be described later (under 3.8); this cranium was used to determine the orientation of muscle force vectors in the FE models. Unfortunately, the exact age, sex and geographic provenance of these specimens is not known. They belong to the anatomical collection of the Hull York Medical School, UK, apart from the specimen ANAT 800, which is part of the skeletal collection of the University of Leeds, UK. In addition to the specimens that were used for the FE modelling, CT data of 13 adult mandibles (5 males, 8 females) were used to take measurements for the study described in Chapter 7.

Specimen	Description
ANAT 800	cranium (left C missing, left I2 damaged) and mandible with complete dentition but resorbed alveolar bone between left M1 and M2, probably male
H-A 001	mandible with congenitally missing M3s, probably female
H-A 002	mandible with complete dentition apart from *in vivo* loss of right M3 and post mortem damage of right P1, resorbed alveolar bone in the molar region, probably male
H-A 004	mandible with complete dentition apart from damaged incisors and left C, probably male
Head 2006D	partly dissected head of a 75 years old white male, *in vivo* loss of several teeth and resorbed alveolar bone

Table 3.1. Modern human specimens used for FE modelling. In addition, measurements were taken on 13 well preserved modern human mandibles (5 males, 8 females) for the study described in Chapter 7.

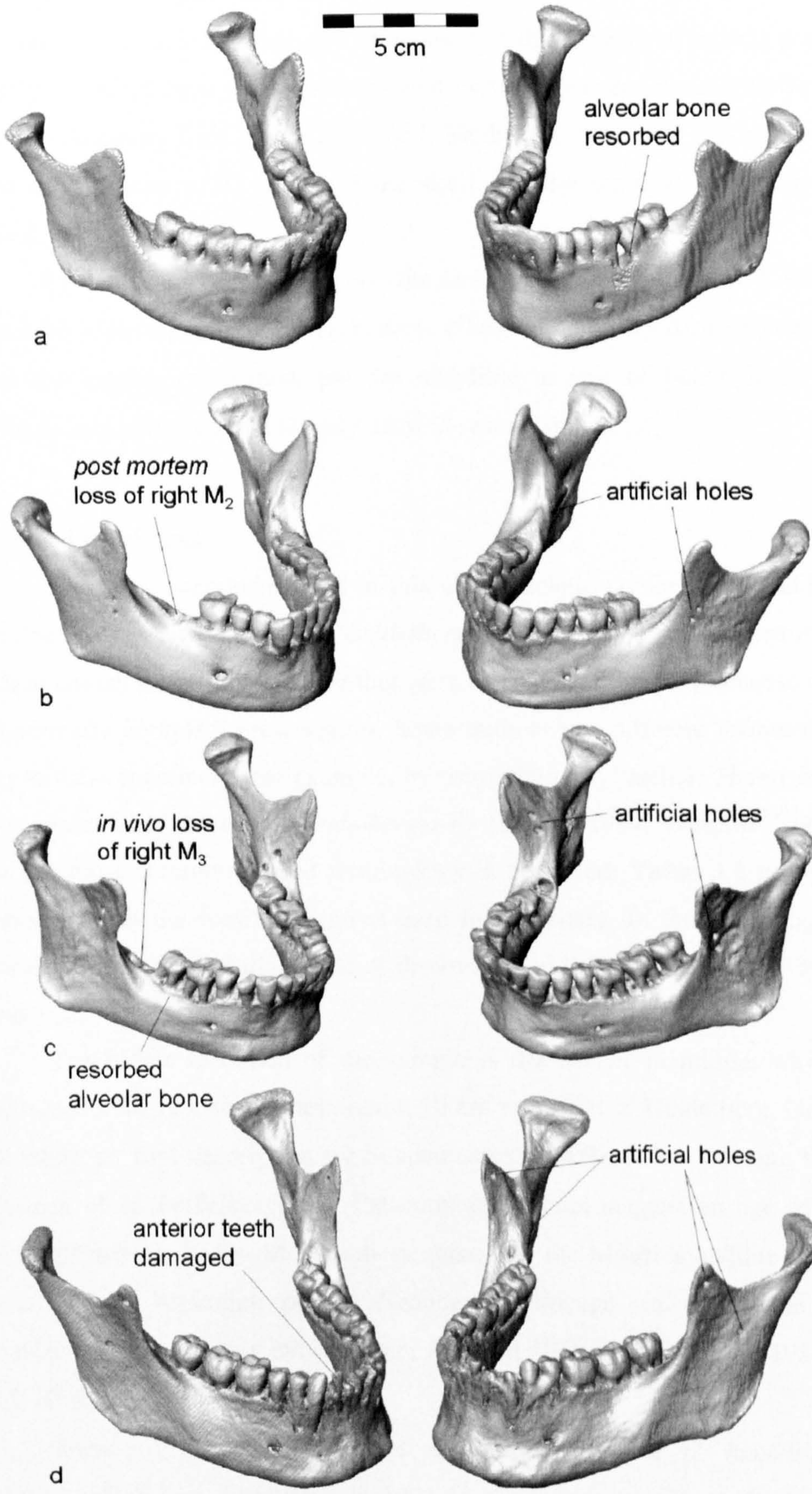

Fig. 3.2. CT-based 3D models of the modern human mandibles used for FE modelling: a) ANAT 800, b) H-A 001, c) H-A 002, d) H-A 004.

In order to gain detailed 3D data about the distribution of the muscle attachment areas and the shape and orientation of the muscles or muscle portions, a partly dissected head from an embalmed human cadaver (Head 2006D) taken from the Anatomy Unit of the Hull York Medical School was CT-scanned and based on this scan a 3D model of the skull and the masticatory muscles was created.

For the validation experiment, the isolated adult mandible H-A 004 was chosen because of good bone preservation, albeit with slightly damaged dentition. Since the loading experiment put the mandible at risk of being destroyed, a specimen was preferred that already showed some damage.

3.3. Fossil specimens

The fossil specimens used in this study include crania and mandibles of European Neanderthals, *Homo heidelbergensis* and one early anatomically modern human from the Near East that were chosen for this study because of their exceptionally complete preservation. Some authors use different terminology to refer to these specimens, for example, by using the term "archaic *Homo sapiens*" for Neanderthals and *Homo heidelbergensis* (Bräuer 1984, Wolpoff 1999), but here the most commonly used terminology is preferred. **Table 3.2** provides an overview of all the fossil specimens used in this study. In the following, basic information like site location, year of discovery and dating will be given for each fossil.

The oldest specimen of the sample is the Mauer mandible, which was discovered 1907 in a sand quarry about 10 km southeast of Heidelberg, Germany. Following its first description by Schoetensack (1908), it has become the type specimen of *H. heidelbergensis*. Palaeomagnetic data suggest an age of 640 to 735 ka (Hambach 1996). Most authors agree that the Mauer mandible should be placed at the beginning of the Neanderthal lineage, in which the typical Neanderthal features only evolved later (Howell 1960, Stringer et al. 1984, Dean et al. 1998).

Kabwe 1 (Broken Hill 1) is an almost complete *H. heidelbergensis* cranium, which was discovered in 1921 in a zinc mine in North Rhodesia, the today's Zambia (Woodward 1921). There are no radiometric dates available for

this specimen, but based on the associated fauna an age of 300 to 600 ka is commonly assumed (Vrba 1982, Klein 1994).

Specimen	Dating	Site location	References
H. heidelbergensis			
Mauer 1 mandible	640-735 ka	Germany	Schoetensack (1908) Czarnetzki et al. (2003) Mounier et al. (2009)
Kabwe 1 cranium	300-600 ka	Zambia	Woodward (1921) Pycraft et al. (1928) Singer (1958)
Ehringsdorf F* mandible	200-250 ka	Germany	Schwalbe (1914) MacCurdy (1915) Vlček (1993)
H. neanderthalensis			
Krapina 59 mandible	120-140 ka	Croatia	Gorjanović-Kramberger (1906) Smith (1976) Radovčić et al. (1988)
Tabun C1* mandible	100-130 ka	Israel	McCown and Keith (1939) Quam and Smith (1998)
Régourdou 1 mandible	65-75 ka	France	Piveteau (1964) Maureille et al. (2001)
La Quina 9* mandible	65-75 ka	France	Martin (1926) Stefan and Trinkaus (1998b) Verna (2006)
Guattari 1 cranium	51-57 ka	Italy	Sergi (1974) Piperno and Scichilone, eds. (1991)
H. sapiens			
Skhūl 5 cranium and mandible	100-130 ka	Israel	McCown and Keith (1939)

Table 3.2. Sample of fossil specimens. See **Figures 3.3** and **3.4** for the preservation of these specimens. *Specimens not used for FE modelling, only for the measurements described in Chapter 7.

The cranium Guattari 1 (Circeo 1) was discovered in a coastal cave at Monte Circeo about 100 km southeast of Rome, Italy, in 1939 (Sergi 1974, Sergi 1991). The associated glacial fauna as well as radiometric dating suggest an age between 51 and 57 ka (Grün & Stringer 1991, Schwarcz et al. 1991).

The almost complete adult mandible Krapina 59 (or Krapina mandible J) comes from the Croatian site Krapina, which yielded more than 800 Neanderthal remains, belonging to more than 80 individuals (Radovčić et al. 1988). These fossils were found in a collapsed cave about 40 km northwest of Zagreb at the beginning of the 20th century. According to electron-spin resonance data, the Krapina material has an estimated age between 120 and 140 ka (Rink et al. 1995).

The young adult skeleton Régourdou 1 was discovered 1957 in a collapsed cave near Lascaux in the Dordogne, France (Piveteau 1964). Based on the sedimentology, the associated fauna and artefacts, it has been suggested that this partial skeleton has an age of 65 to 75 ka (Bonifay 1964, Vandermeersch 1965). The FEA sample thus consists of two very different Neanderthal specimens: the large and robust early Neanderthal mandible Krapina 59 and the smaller, less robust and much younger mandible Régourdou 1, which is, in addition, characterised by unusually small teeth compared to other Neanderthals (Maureille et al. 2001).

Skhūl 5 is an almost complete skull, which was found 1932 together with the remains of nine other individuals at the rock shelter Mugharet es-Skhūl of Mount Carmel 19 km south of Haifa, Israel (Garrod & Bate 1937, McCown & Keith 1939). Thermoluminescence, uranium-series and electron-spin resonance dating suggest an age of 100 to 130 ka (Stringer et al. 1989, Grün et al. 2005). Commonly the Skhūl remains are regarded as an archaic type of *H. sapiens* (Trinkaus 1984, Stringer et al. 1989).

All these fossil mandibles that were used for FE modelling, are not only very well preserved, but also show relatively few pathologies: some arthritic flattening of the condyles of Krapina 59 and Skhūl 5 (McCown & Keith 1939, Wolpoff & Frayer 2005) as well as osteophytes and a depression on the left condyle of Mauer 1, probably resulting from a trauma (Czarnetzki et al. 2003). However, these pathologic changes do not cause a problem for the FEA, since the stresses and strains in the condyles and the condylar necks are not of interest here.

In addition to the specimens used for FE modelling, three more fossil mandibles were measured for the study described in Chapter 7: the *H. heidelbergensis* specimen Ehringsdorf F (Schwalbe 1914, MacCurdy 1915, Vlček 1993) with an estimated age of 200 to 250 ka (Mallick & Frank 2002), the early Neanderthal specimen Tabun C1 (McCown & Keith 1939, Quam & Smith

1998) dating between 100 and 130 ka (Grün & Stringer 2000, Mercier & Valladas 2003) and the Neanderthal mandible La Quina 9 (Martin 1926, Stefan & Trinkaus 1998b) with an estimated age of 65 to 75 ka (Mercier 1992, Debénath & Jelinek 1998). These specimens were too fragmentary to be included in the FEA sample.

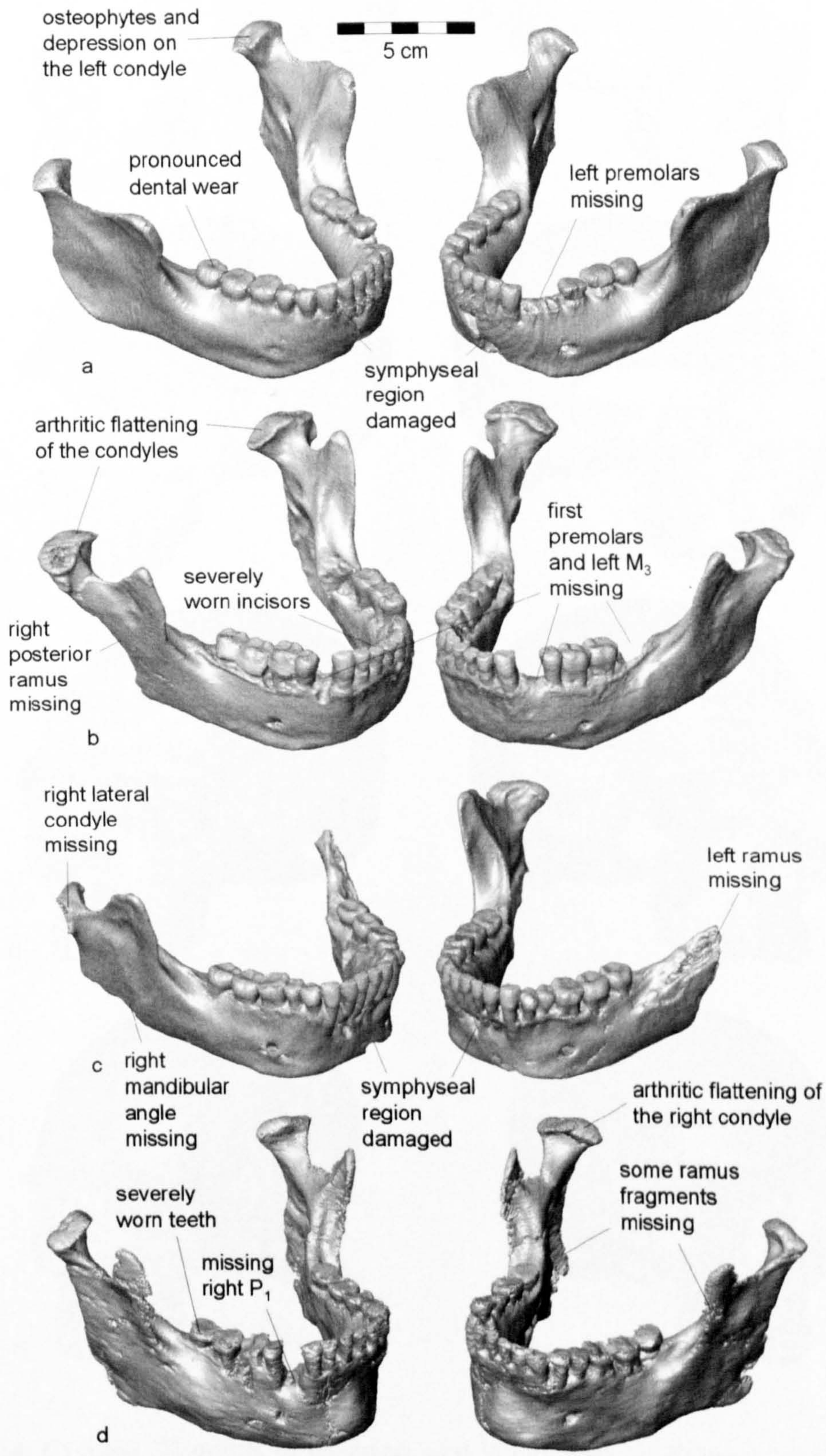

Fig. 3.3. CT-based 3D models of the fossil mandibles: a) Mauer 1, b) Krapina 59, c) Régourdou 1, d) Skhūl 5.

Fig. 3.4. CT-based 3D models of the crania used in this study: a) Kabwe 1, b) Guattari 1, c) Skhūl 5, d) ANAT 800.

3.4. Data acquisition with computed tomography

Computed tomography (CT) is a method for creating cross-sectional images of an object with the use of X-rays. The X-rays, which are attenuated by the object, are detected by sensors, converted into electrical signals and digitised. In the next step, computer-based image reconstruction, an attenuation value is assigned to each pixel. Since each cross-section is scanned from different angles, it is possible to calculate the spatial distribution of these attenuation values. In order to obtain an image, the values are converted into grey levels. Thus, an image of the cross-section is created, which displays the densities of the sectioned structures with different shades of grey (Thurn & Bücheler 1992, Wegener 1992, Grumme et al. 1998).

The stack of all slices of a CT scan can be regarded as a data volume, which can be used to create a 3D model of the scanned object. At the level of the single slice, this means that each scanned cross-section actually represents a volume due to the slice thickness. Thus, each pixel corresponds to a volume element (voxel), whose dimensions are determined by the edge lengths of the pixel and the slice thickness (**Fig. 3.5**). Consequently, the attenuation value (i.e. CT number), which is calculated for each pixel, expresses the average attenuation of the X-rays by the tissue included in the voxel (Thurn & Bücheler 1992, Wegener 1992).

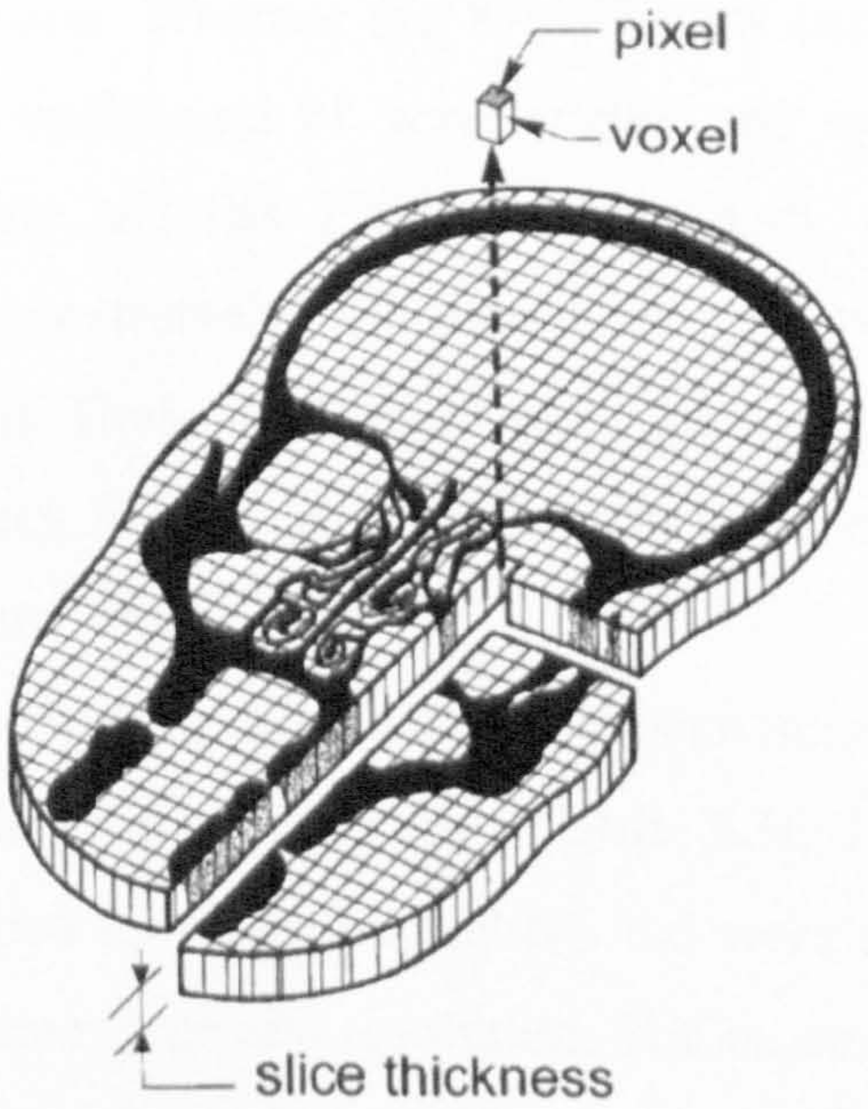

Fig. 3.5. Diagram of a CT slice showing the relationship between pixel size, slice thickness and voxel dimensions (Spoor et al. 2000: 128, Fig. 2).

For scanning *ex vivo* bone tissue, three types of CT are available: medical CT, microCT (μCT) and synchrotron tomography, which differ significantly in their technical principles as well as in the resolution of the scans they produce. In medical CT scanners an X-ray source as well as an array of detectors rotate around the specimen. Modern scanners use the principle of spiral or helical CT, in which the specimen is continuously moved forward during the scan. The measurements are thus taken in a spiral trajectory. This allows reconstruction of cross-sectional images at any position by means of interpolation from the spiral measurements (Buzug 2008).

μCT scanners differ from medical CT scanners in that the specimen itself is rotated during the scan, rather than the source/detector system. In addition, this method can provide image data with a much higher spatial resolution than medical CT scanners. Depending on the size of the scanned objects or the field of view, which is chosen, a spatial resolution of single-digit micrometer values can be achieved (Spoor et al. 2000). Another advantage is that μCT scanners usually produce isotropic voxels (i.e. pixel size and slice thickness are identical). In medical CT scans, the slice thickness is usually larger than the pixel size, which results in anisotropic voxels.

Even better scans in terms of resolution can be achieved with synchrotron tomography. This technique uses the electromagnetic high energy radiation produced by a synchrotron. Whereas the X-ray beams used in medical and μCT scanning consist of a continuum of wavelengths, the synchrotron radiation is typically monochromatic and has a short wave length, which produces cross-sectional images with an extremely high spatial and contrast resolution (Zollikofer & Ponce de León 2005). Thus, synchrotron tomography even allows visualisation of dental microstructures like the Retzius lines in tooth enamel (Mazurier et al. 2006, Tafforeau & Smith 2008).

The specimens used in this study have been scanned with medical CT, μCT as well as synchrotron tomography (**Table 3.3**). The CT scans of fossil specimens were provided by other researchers and were therefore rather diverse with respect to the scanner type and resolution. The modern human specimens, in contrast, were scanned by our research group using two different scanners, depending on the size of the respective specimen.

Specimen	Scanner	Resolution (mm)		Source of scan
		x, y	z	
H-A 001	X-Tek HMX 160 µCT	0.146	0.146	1
H-A 002 left	X-Tek HMX 160 µCT	0.120	0.120	1
H-A 002 right*	X-Tek HMX 160 µCT	0.121	0.122	1
H-A 004	GE Medical Systems BrightSpeed	0.488	0.625	1
H-A 004 left	X-Tek HMX 160 µCT	0.135	0.135	1
H-A 004 right	X-Tek HMX 160 µCT	0.122	0.122	1
ANAT 800	GE Medical Systems BrightSpeed	0.488	0.625	1
Head 2006D	GE Medical Systems BrightSpeed	0.488	0.625	1
Mauer 1	Philips T310	0.437	1.500	2
Kabwe 1	Siemens Somatom Plus 4	0.470	0.500	2
Ehringsdorf F*	BIR ACTIS 225/300 µCT	0.148	0.148	3
Krapina 59	Siemens Sensation 16	0.295	0.400	3
Tabun C1*	Philips T350	0.656	1.500	2
Régourdou 1	ESRF Grenoble	0.350	0.350	3
La Quina 9*	ESRF Grenoble	0.350	0.350	3
Guattari 1	Siemens Somatom HIQ-S	0.490	1.000	3
Skhūl 5	Siemens Multidetector Scanner	0.488	0.500	3

Table 3.3. List of the CT-scanned specimens with the resolutions of the reconstructed image stacks. *Specimens not used for FE modelling, only for measurements described in Chapter 7. In addition, medical CT scans of 13 modern mandibles (pixel size and slice thickness of 0.455-0.533 mm and 0.625-1 mm respectively) were used for Chapter 7. ESRF = European Synchrotron Radiation Facility in Grenoble. Source of each scan: 1 = Hull York Medical School, 2 = F. Zonneveld and F. Spoor, 3 = www.nespos.org.

µCT scanning of the smaller specimens was undertaken with the X-Tek HMX 160 µCT system (X-Tek Systems Ltd., Tring, UK) at the Engineering Department of the University of Hull, using a copper filter. The primary

reconstructions were performed using NGI CT Control Software (X-Tek Systems Ltd., Tring, UK). The resulting data volumes were exported as 16-bit TIFF image stacks.

μCT scans were also obtained of two adult modern human mandibles (H-A 002 and H-A 004), but since these specimens were larger than the maximum field of view of the scanner, each half of the mandibles was scanned separately. For the final 3D model the halves were later put together in Amira 4.1.1 (Mercury Computer Systems, Inc., USA). One of these mandibles, H-A 004, was used in the validation experiment. The same mandible was also scanned with a medical CT-scanner in order to study the effect of the scanning resolution on FEA results.

Medical CT scans were taken with a GE Medical Systems BrightSpeed scanner (General Electric Co., USA) using the helical mode of the machine. Voltage and exposure were set to 120 kV and 11 mA respectively. The "SOFT" convolution kernel of the scanner was chosen because it uses a relatively neutral filter without any edge enhancement, which would have biased the thickness of bone structure. The image stacks were reconstructed with a slice thickness and an interval of 0.625 mm and exported in DICOM format.

Most of the fossil specimens were scanned with different medical CT scanners, but with similar or better resolution than the medical scans of the modern material. Only the CT scans of the Mauer 1 Guattari 1 and Tabun C1 have a considerably larger slice thickness, which results in a lower spatial resolution in the z-direction, the direction in which the specimen was moved through the scanner.

Two Neanderthal specimens, the mandibles Régourdou 1 and La Quina 9, were scanned with synchrotron tomography using the European Synchrotron Radiation Facility in Grenoble, France. Based on the high-resolution raw data, sections were reconstructed and saved as a 32-bit RAW file. The original 32-bit image data was then downsampled and exported as 8-bit TIFF image stacks with a resolution of 0.350 mm in all directions.

3.5. Virtual 3D reconstruction

In order to obtain a 3D representation of a scanned object based on a CT image stack, several work steps are necessary. One major task is to determine the boundaries between adjacent materials. This can be done by defining density

thresholds or by manually separating structures. Incomplete specimens require additional reconstruction work, like mirror imaging or the virtual refitting of fragments. In this study all 3D image processing was performed using the commercial software Amira 4.1.1 (Mercury Computer Systems Inc., USA).

A CT image displays a spectrum of grey scale values that represent the densities of the scanned objects. In order to generate a 3D model, it is necessary to define a threshold value, which separates the structure of interest from surrounding ones. However, finding the optimal threshold is not a trivial problem. Due to the limited resolution, the boundaries between adjacent structures are not clearly defined. At the interface between two materials (e.g. bone and air) there is a gradual decrease of the CT numbers from one tissue to the other rather than an abrupt change (**Fig. 3.6**). Another problem results from the fact that changes in the viewer control settings (window level and width) can severely affect the visual appearance of the CT images, especially along the boundaries of structures. Therefore, threshold values that are just based on the apparent boundaries have been shown to be inaccurate (Koehler et al. 1979, Baxter & Sorenson 1981, Hara et al. 2002, Coleman & Colbert 2007).

The results of phantom studies, in which objects with a simple geometry and known dimensions have been scanned, indicate that the true interface between two adjacent materials is located halfway between the two CT number values of these materials (Ullrich et al. 1980, Eubanks et al. 1985). This position is known as the half-maximum height (HMH). As **Figure 3.6** shows, it can be calculated as the mean of the maximum and minimum density values along a row of pixels that spans the boundary transition (Ullrich et al. 1980). The HMH has proved to produce reliable results when used for measuring human vertebrae (Ullrich et al. 1980), the oval window in primate crania (Coleman & Colbert 2007), the trabecular architecture of long bones (Fajardo et al. 2002) and even fossilised cortical bone and enamel (Spoor et al. 1993).

However, these studies also showed the potential problems in the application of this method. Fajardo and colleagues (2002) found that it is important to sample the appropriate region of interest because bone types of different densities yield different HMH values. In addition, it is advisable to use an elaborated HMH protocol (Fajardo et al. 2002; Coleman & Colbert 2007) for 3D reconstructions. A threshold based on the HMH value of a single slice might

not be accurate for a 3D model, which consists of hundreds of slices. Therefore, this study uses the modified HMH protocol suggested by Fajardo and colleagues (2002), which calculates the mean HMH value for several randomly selected slices.

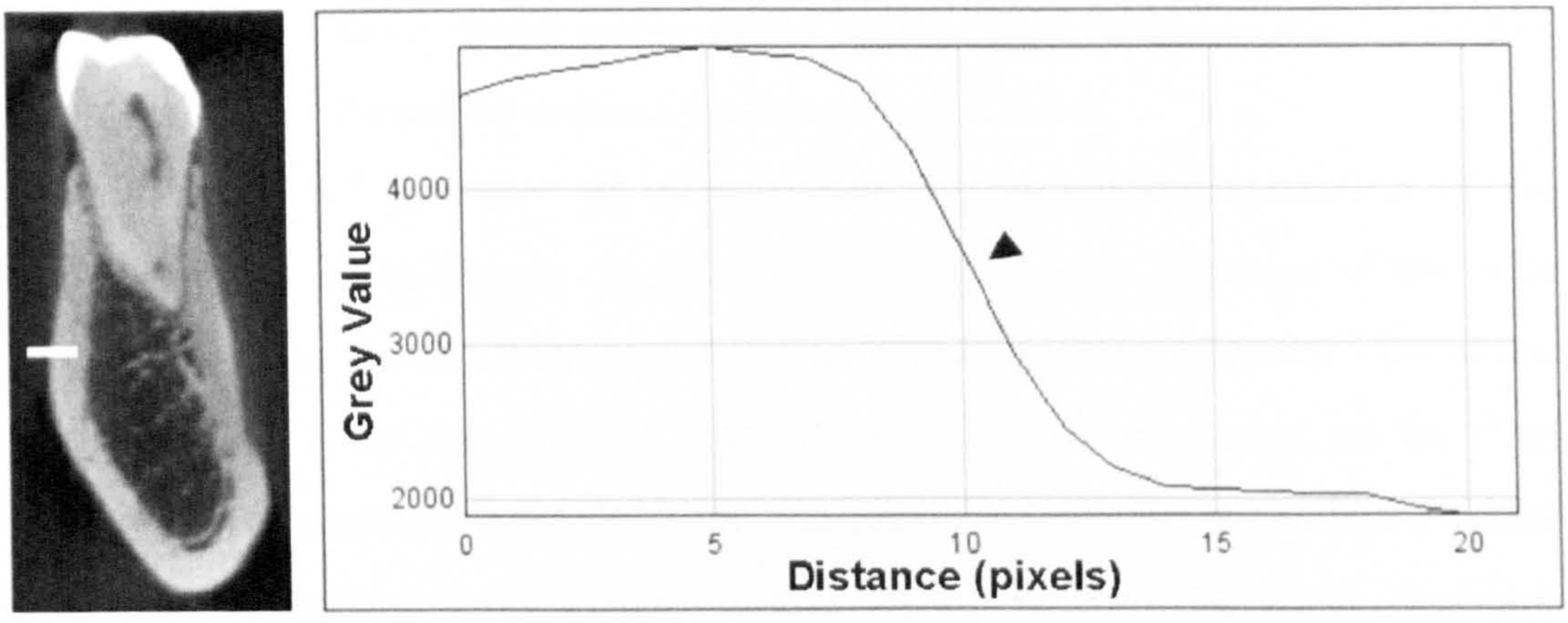

Fig. 3.6. Determining the threshold for separating bone and air. The graph shows grey values along a row of pixels that crosses the boundary between bone and air in a CT slice. The arrow indicates the position of the half-maximum height (HMH).

Sometimes the density ranges of two adjacent materials are too similar to be separated semi-automatically by a threshold value. This is usually the case with fossilised bone vs. sediment or dentine vs. alveolar bone, where only manual separation can be performed. For this purpose, different manual editing tools are used to select or separate structures in the CT slices. In order to ensure that these structures are also separated in the final 3D model, not only the CT slices of the original orientation, but also those of the two orthogonal orientations have to be edited.

Besides separating adjacent structures, manual segmentation is sometimes useful to close artificial holes in the 3D model, which might appear in areas where the bone is very thin. In these areas, due to the limited resolution of CT images, two different materials like bone and air can occupy the same voxel. The CT number of such a voxel thus represents a mixture of two different densities and might therefore be below the minimum threshold chosen for bone. This effect is known as partial volume averaging (Spoor et al. 2000). Since such artificial holes would cause artefacts in the FEA results, they were manually closed during the segmentation work for this study. This procedure was mainly applied to the mandibular condyles, where the cortical bone is typically very thin.

Missing fragments or cracks in the bone would likewise lead to biased FE results and therefore need to be corrected by manual reconstruction. A common

method of virtual reconstruction in palaeoanthropology is mirror imaging (Zollikofer et al. 1995, Thompson & Illerhaus 1998, Zollikofer & Ponce de León 2005). In practical terms, the whole dataset of a specimen is mirrored, the intact counterparts of missing fragments are segmented and finally fitted into the 3D model of the specimen. Small cracks in the bone or gaps between virtually refitted fragments can be closed by manually editing the CT slices.

Figure 3.7 provides an overview of the virtual reconstruction of the specimens used in this study. In Krapina 59, the missing fragment of the right ramus as well as the left third molar and its socket were reconstructed by mirror imaging of the intact contralateral parts. The missing first premolars, on the other hand, were reconstructed by doubling the preserved second premolars on each side. The mandibles of Régourdou and Mauer exhibit complete dentition. However, in the case of Régourdou it was necessary to reconstruct the whole left ramus by mirror imaging and to take the mandibular angles as well as the lateral parts of the condyles from Krapina 59, since these fragments were completely missing. The reconstruction of Mauer did not require the inclusion of fragments from other specimens, but it did require time-consuming manual rebuilding of alveolar bone around the incisors. The mandible of Skhūl 5 is so complete that it only required some manual filling of cracks or the reconstruction of very small fragments of bone and teeth. However, since the specimen is filled with sediment, time-consuming manual segmentation was necessary to segment the internal bone structure. At first, the border between cortical bone and the cancellous network as well as sediment was defined. Then a threshold was applied to separate cancellous bone from the sediment, since the latter has a higher density than the former. In this way, an approximation of the distribution of cancellous bone could be achieved.

In addition to the reconstruction of missing parts in the fossil specimens, some reconstruction work was also necessary in two modern specimens (H-A 002 and ANAT 800). In H-A 002 the right M3 was lost *in vivo* and some *post mortem* damage is present at the right P1. Therefore, the intact left half was mirrored to create a mandible with complete dentition. In specimen ANAT 800, the alveolar bone around the left M1 is damaged so that missing bone was reconstructed by a combination of mirror-imaging and manual editing.

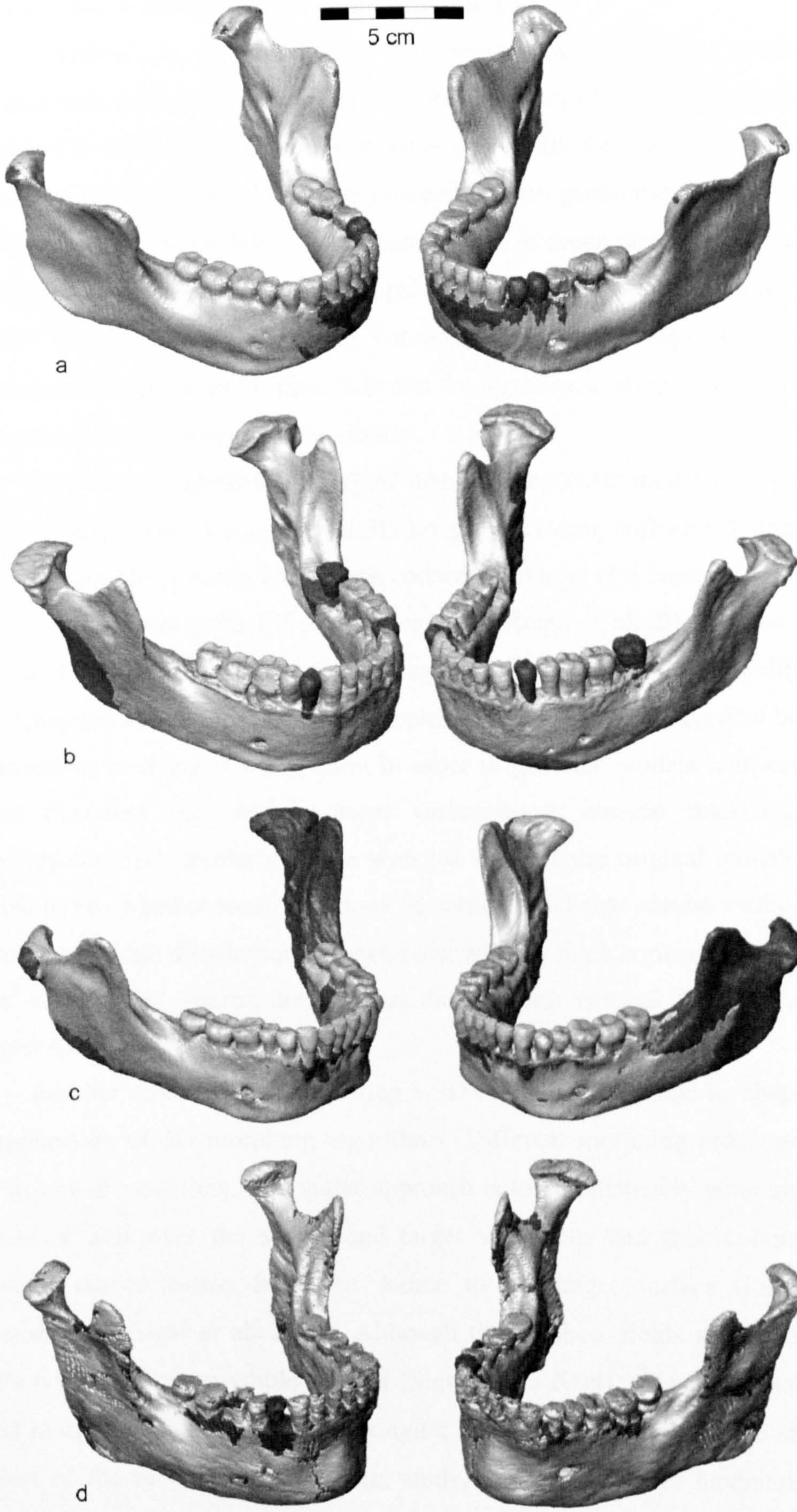

Figure 3.7. Fossil specimens before (left column) and after the reconstruction of missing fragments and teeth (right column): a) Mauer 1, b) Krapina 59, c) Régourdou 1, d) Skūhl 5. Reconstructed parts are shown in dark grey.

3.6. Virtual manipulation of morphological features

In addition to the creation of 3D representations, virtual modelling techniques offer various tools to manipulate the geometry of models. By manually editing the CT slices internal cavities in bones can be filled or trabecular bone can be removed. By combining 3D image processing with geometric morphometrics (GMM), the shape of models can be manipulated or mean shapes of groups of specimens can be generated. These manipulated models can then be used for FEA in order to test hypotheses about form-function relationships. One major advantage of manipulating FE models is that the mechanical effect of the presence or absence of single features can be studied.

The most straightforward way of manipulating a 3D model is to use the standard editing tools of commercial 3D image processing software. Using such tools, it is possible to easily change the cortical thickness of a bone by adding or deleting voxel layers or to fill internal cavities (Reina et al. 2006, Strait et al. 2007). In this study, the internal morphology of the bone is modified in different ways (Chapters 4, 6, 7, 9, 10). For example, the thickness of the cortical bone in the mandibles is changed with Amira in order to generate models with constant cortical thickness (i.e. without local variations in cortical thickness). By comparing the FEA results of these with the ones of the original models, it is possible to see whether local variations in cortical thickness can be predicted by the stress and strain distribution; for example, whether thick cortical bone is found where stresses and strains are high in the constant cortical thickness model (Chapter 6).

Another method of manipulating a 3D model is to change its shape with the application of 3D morphing algorithms. Different morphing procedures are used in virtual modelling. A popular approach is to automatically wrap auxiliary surfaces or nets over the source and target specimens and then compute the necessary transformation from the source to the target surface (Lazarus & Verroust 1998, Sigal et al. 2008). Although this method yields good morphing results when applied to whole objects (Sigal et al. 2008), it is less suitable for partial morphing of structures (i.e. changing one feature but keeping the shape of the rest of the model constant). This study, therefore, applies landmark-based morphing (i.e. warping) for simulating the presence of absence of morphological features (**Fig. 3.8**). Using Amira, landmarks or semilandmarks were manually

placed on the source surface model. The target shape was then defined by placing corresponding landmarks on the CT slices of the same specimen. In order to hold the shape of the rest of the model constant, additional landmarks were placed on the surface of the source model and the coordinates of these were added to the landmark set of the target shape. The warping was then performed by applying the Bookstein thin-plate splines transformation as implemented in Amira, a triplet of thin-plate splines (Bookstein 1989). Thin-plate splines are interpolation functions, which can be used to warp a reference and a target shape. Thin-plate splines are analogous to bending of a thin metal sheet in which bending energy is minimised, resulting in a deformation that is as smooth as possible (Zelditch et al. 2004).

Warping is applied here to study the biomechanical effects of morphological difference in the mandibular symphysis, for example, presence versus absence of the human chin or the orientation of the symphysis (Chapter 9). The target shapes for these warpings were manually defined or taken from landmark data from other specimens.

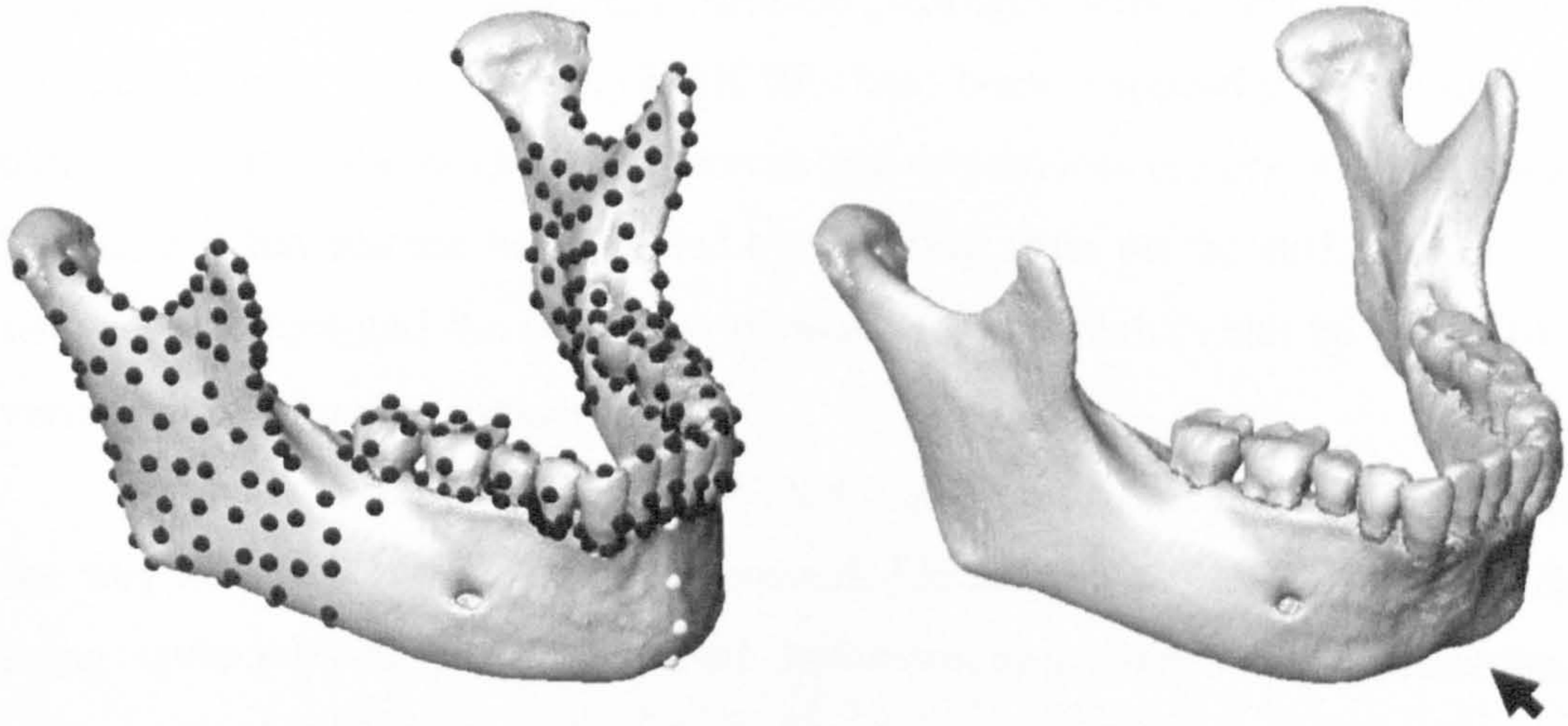

Fig. 3.8. Landmark-based warping in Amira. Upper row: original model on the left, warped model on the right. Bottom row: mid-sagittal sections though the symphysis showing the stages of the warping: a) original symphyseal shape, b) superimposition with target shape and c) target shape after warping. The black landmarks on the original 3D model are anchor landmarks used for keeping the shape of the teeth and the posterior mandible constant.

3.7. Voxel-based finite element modelling

Finite element modelling permits the estimation of stresses and strains in a complex or irregular structure like a bone by dividing it into a number of small, geometrically simple elements, called finite elements. The elements are linked at their corner points, the so-called nodes. Based on the displacements of these nodes during loading, it is possible to calculate the stresses and strains in the whole object. Each of the finite elements possesses user-specified material properties so that the mechanical behaviour of the real object can be simulated. Forces and constraints (i.e. regions of immobility) can then be applied to the model in order to mimic the loadings that act on the structure *in vivo* (Richmond et al. 2005, Rayfield 2007).

In this study, the non-commercial finite element software VOX-FE is used, which has been developed in collaboration between the Functional Morphology and Evolution Unit of the Hull York Medical School and the Departments of Engineering and Computer Sciences of the University of Hull. Unlike standard commercial FEA software packages, which have been designed for engineering applications, VOX-FE has been especially developed for biologists. Thus, the modelling of forces and constraints is very straightforward. Muscle attachments can be modelled by selecting areas on the surface of an area with a brush tool and the directions of muscle force vectors can be interactively varied with the mouse courser.

A major difference between VOX-FE and most other FEA software lies in the way in which the FE model is created. FE models can be generated either using surface-based or voxel-based reconstruction. When the surface-based approach is chosen, the outlines of an object are manually traced in individual CT slices and then linked using computer-automated design (CAD) software (Marinescu et al. 2005, Strait et al. 2007) or the thresholded CT data (i.e. the CT-based surface model), is converted into a 3D wireframe, which is then converted into a FE mesh (e.g. Dumont et al. 2005). Alternatively, 3D surface scans can be converted into FE meshes with this technique, but in this case no information about the internal structure is obtained. In practice, the surface-based approach involves a number of steps using different software applications with different capabilities, including mesh-repairing tools to fix the frequent errors, which occur during the FE meshing of surface models (Rayfield 2007). Thus, model creation

becomes a very time-consuming act. In addition, the accuracy of models can often be relatively low, especially when the models are created by manual outlining and the resulting wireframes have to be reduced because of the common limits of applied FE software.

In contrast, the voxel-based reconstruction technique, which is used for the generation of VOX-FE models, directly converts each voxel of the segmented CT data into a 3D finite element (Vollmer et al. 2000, van Rietbergen et al. 2003, Verhulp et al. 2008). Thus, the fast creation of high-resolution FE models is possible. Since the geometry of the FE mesh is a direct conversion of the voxel structure, the meshing procedure is very straightforward and free from those errors that frequently occur during surfaced-based FE reconstruction. Therefore, subsequent time-consuming mesh repairing procedures are not necessary.

An aspect, which is closely related to the way in which the FE model is generated, is the type of the finite elements. In general, the elements can have a triangular or quadrilateral shape in 2D FE models, and a tetrahedral or cuboidal shape in 3D meshes (**Fig. 3.9**). Referring to the number of nodes per edge, the elements can be either of a linear (i.e. with two nodes per edge) or quadratic (i.e. with three nodes per edge) type (Richmond et al. 2005, Rayfield 2007). Tetrahedral elements are advantageous for meshing complex geometrical shapes with curved surfaces, but they bear the risk that their aspect ratio becomes so high that strains are overestimated (Beaupré & Carter 1992). Cuboidal elements (as in VOX-FE) are in general more accurate, but have the disadvantage that they produce biased results due to the stepped surfaces of the models compared to the more realistic smooth surfaces of FE models made of triangular elements. However, the higher the resolution of model is, the smaller are the element edges and thus the steps that make up the surface are less severe. VOX-FE models are composed of equally sized cubic elements with eight nodes, one on each corner of the element (**Fig. 3.9**). Quadratic elements, which have three nodes per edge, are actually more accurate, since they allow the strains to vary within each element. However, as they have many more nodes than linear elements, the FEA becomes computationally much more expensive (Rayfield 2007). Since voxel-based FE models commonly have more than a million elements, a linear type of element has been chosen for VOX-FE so that computation time stays within reasonable limits. Stepping is dealt with by averaging of adjacent voxel values, although the user

needs to ensure that the FEA results are not over-smoothed, so that resolution is not lost.

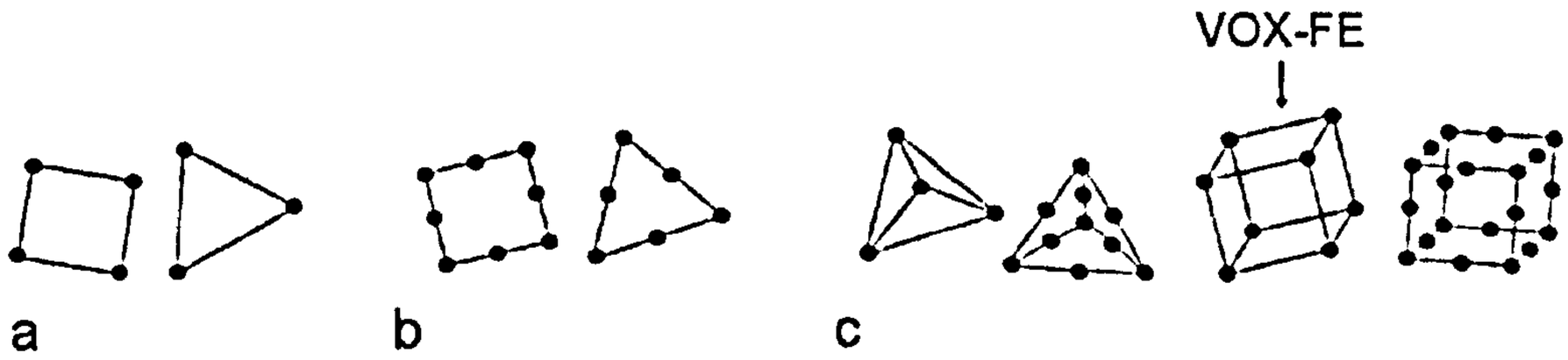

Fig. 3.9. Finite element types. a) 2D linear triangular and quadrilateral, b) 2D quadratic elements, c) 3D linear and quadratic elements. The elements used in VOX-FE are linear and cuboidal (adapted from Rayfield 2007: 550, Fig. 5).

Due to the high resolution of voxel-based FE models, the calculation of FEA results cannot be performed on a common PC within a reasonable time frame. Therefore, only the application of forces, constraints, model properties and the visualisation of the results is done on a PC with VOX-FE, while the actual calculation of the displacements is performed on an EAGLE high-performance cluster (HPC) with 32 processors or nodes (Cisco-Eagle Inc., Dallas, Texas) at the Department of Computer Sciences of the University of Hull. On this HPC, the solution of the FEA is performed with the non-commercial and Linux-based solver PARA-BMU, which is a modified row-by-row iterative solver, similar to that reported by van Rietbergen and colleagues (1996). This solver was developed by the Functional Morphology and Evolution Unit of the Hull York Medical School in collaboration with the Departments of Engineering and Computer Science and Medical Physics of the University of Hull.

Figure 3.10 provides an overview of the tasks performed using VOX-FE and other software applications to conduct an FEA. First, a 3D model, which has been created with Amira and exported as a BMP-image stack is converted into an FE mesh with VoxToVec, a Windows-based application, which was developed together with VOX-FE. After importing the FE model into VOX-FE, material properties, forces and constraints are defined by the user. The values for the mechanical properties, force magnitudes, constraint directions as well as the 3D coordinates of the nodes, to which the forces and constraints have been applied, are then exported as a text file. Together with the model, this script file is sent to the HPC and the PARA-BMU solver is started. Depending on the number of finite elements, the applied loads and the number of used HPC-nodes, the solution of the FEA can take some minutes to several hours. After successful solution, the x-,y- and z-displacements for each node are saved in a text file. Based on this so-

called displacement file VOX-FE calculates the stresses and strains. These can then be either visualised as colour-coded contour maps or stress and strain values from selected locations can be exported as text files.

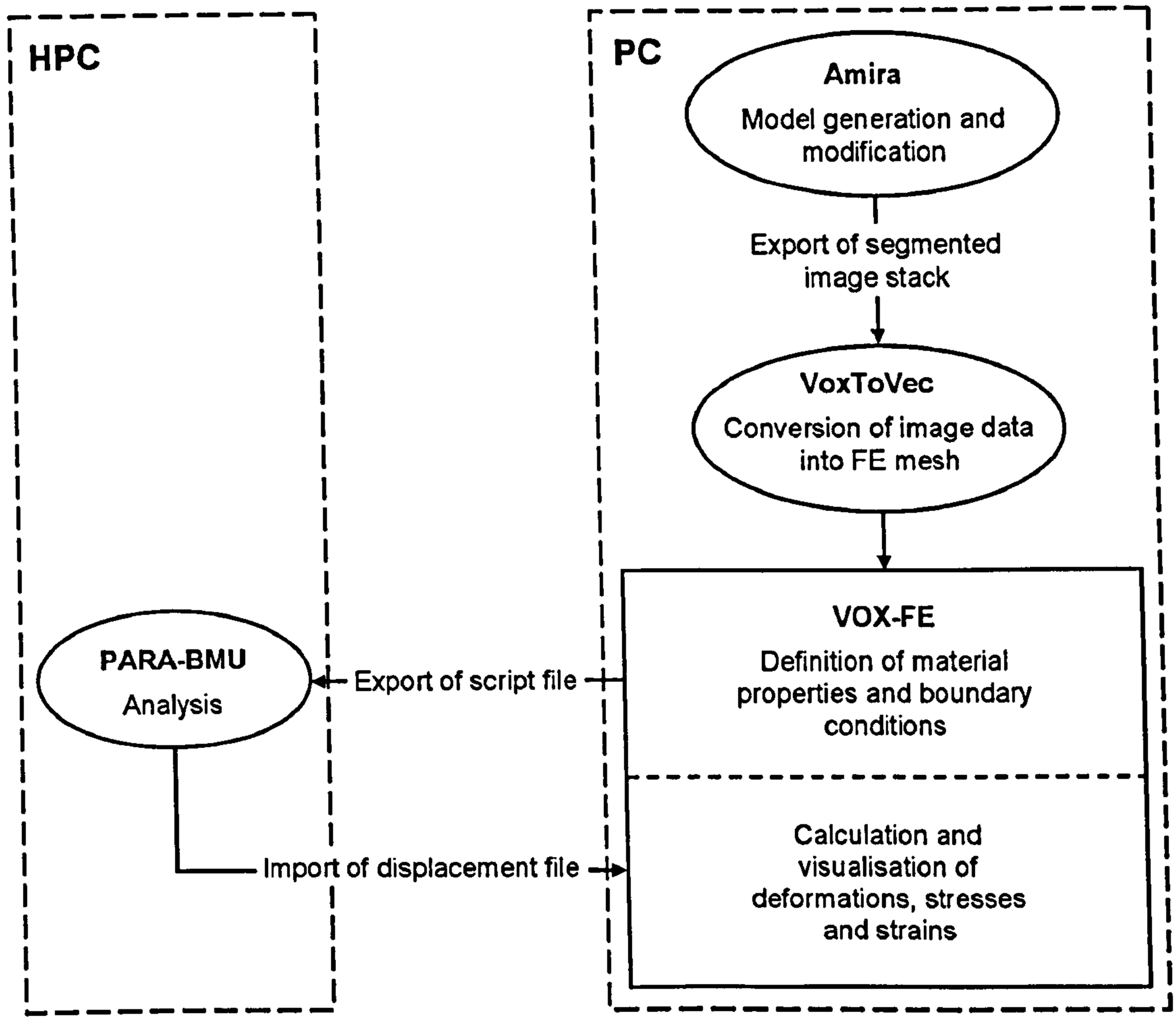

Fig. 3.10. Illustration of the tasks performed by VOX-FE and other software applications used for this study. The actual FEA is performed by a LINUX-based solver (PARA-BMU) running on a high-performance cluster (HPC).

In mathematical terms, FEA aims to find approximate solutions for partial differential equations (Fagan 1992, Zienkiewicz et al. 2005). When the number of elements and thus the number of unknown variables in the system of equations is very high, as in the case of VOX-FE models, a direct solution is not possible. Therefore, an iterative approach is used, in which the solution is stepwise improved until equilibrium is achieved.

The user defines two parameters that are highly important for the successful solution of the FE model: the tolerance value and the maximum number of iterations. The former value determines the difference between the results of two calculation steps that is tolerated. If the difference is below this value, the FEA calculation stops, since it has fulfilled the user-defined criterion of

equilibrium. The latter parameter defines how many iterations the solver can use for its calculation. The maximum number of iterations is only useful in the case where the FE model cannot be solved and prevents infinite attempts at a solution. If the number of maximum iterations is too low, the calculation stops before it reaches a difference smaller than the threshold. Therefore, it is important to use a combination of a high number of maximum iterations and not too small a tolerance value to ensure that the calculation stops because of the threshold and not because of the limited number of iterations.

How severely the FEA results are affected by too low a value of maximum iterations, is shown by a simple example. By creating an artificial CT image stack in Photoshop, a simple tube model was generated. This model is loaded under four-point-bending by pulling the two ends in one direction while the tube is constrained at two points on one side. Due to the simplicity of the model and the loading, it is possible to intuitively predict the resulting strain pattern: a uniform high strain area between the two constraints. However, when the number of maximum iterations is set to 1000, the strain pattern is very heterogeneous (**Fig. 3.11**). Only when the number is increased to at least 4000 is the resulting strain pattern consistent with the predictions. Increasing the number beyond this value does not cause any further changes in the results. Therefore, 1000 iterations are not sufficient to calculate a realistic solution. Instead, the maximum value of 4000 allowed the calculation to reach the user-defined equilibrium.

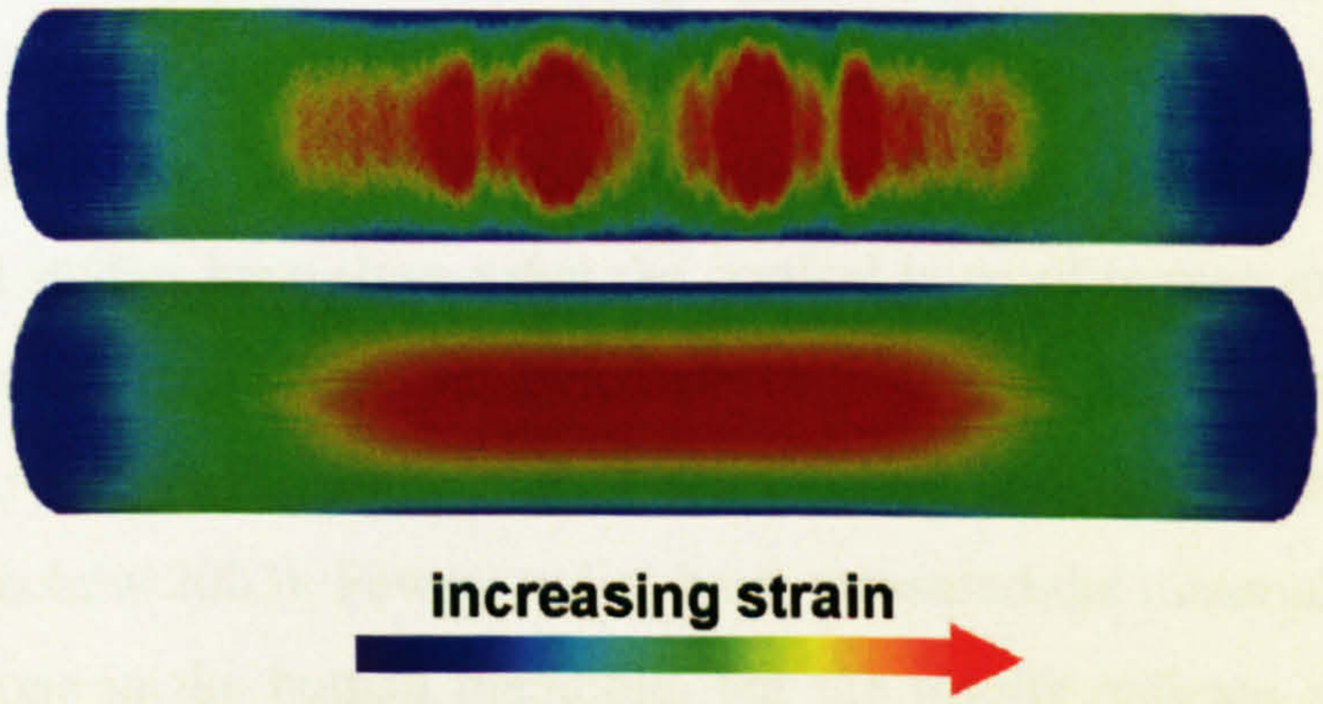

Fig. 3.11. Strain distributions in a tube under four-point-bending to illustrate the effect of an insufficient number of iterations. Upper image: a model in which convergence has not been reached because of a user-defined too low number of iterations (1000), lower image: convergence could be reached thanks to a sufficient maximum of iterations (4000).

This example shows that too low a number of iterations can lead to very misleading results. However, since the required number of iterations depends on

the number of elements as well as the complexity of the model, the value that is sufficient for this simple tube model cannot be generalised. In prior studies of high-resolution FE models, values of 40,000 iterations or more can be found (Verhulp et al. 2008). Similarly high values (20,000-50,000) are therefore used in this study, taking into account the resolution and complexity of the individual models.

In addition to the parameters that control the FEA calculation itself, model parameters are important for the accuracy of the final results. These include the forces, constraints as well as the material properties assigned to the model. When the physiological loading of a bone like the mandible is to be simulated, the forces and constraints have to be consistent with anatomical descriptions of relevant muscles and joints, and physiological data such as bite force measurements, estimates of muscle forces and recorded activation patterns of the muscles. The material properties assigned to the model should ideally be based on measurements of the same specimen or of comparable specimens, for example, other individuals of the same species or in the case of extinct species of closely related extant species.

The material properties of a bone can be either homogeneous (i.e. they do not vary between the different parts of the bone) or heterogeneous (i.e. they vary within the bone). At the level of the single finite element, the material properties can either be isotropic (i.e. the elastic constants have the same values in all directions) or anisotropic (i.e. the elastic properties of the material are not equal in all directions). When the material properties differ in each of three perpendicular directions, they are called orthotropic (van Eijden 2000, Currey 2002). Experimental studies have shown that the cortical bone of human mandibles, like other mammalian mandibles, has heterogeneous as well as orthotropic material properties (Arendts & Sigolotto 1989, 1990, Dechow et al. 1992, 1993, Schwartz-Dabney & Dechow 2003). Fewer studies have measured the material properties of cancellous bone in the human mandible, but the results indicate that properties vary between different regions, for example, in the condyle compared to the corpus (Misch et al. 1999, Giesen et al. 2001). Due to the computational limits of the solver PARA-BMU, the material properties of the models in this study are homogeneous and isotropic. However, the results of prior FE studies suggest that

even such simplistic models are able to provide reasonable stress and strain estimates (Strait et al. 2005, Kupczik et al. 2007).

In order to assure that the FE models in this study are similarly realistic, a validation experiment is performed. For this purpose, a simple, reproducible load is applied to a dry human mandible and the resulting strains are measured. An FE model of the same specimen is then loaded and constrained in the same way and the estimated strains are compared with the experimental results (Chapter 4).

3.8. Estimation of muscle forces

When such a validation against *in vitro* data has been successful and the basic model attributes like model geometry and material properties have proven to be realistic, modelling of *in vivo* loading can be attempted. The biggest challenge is to model the forces of the masticatory muscles accurately. This requires the correct spatial distribution of muscle insertions, orientation of the lines of actions of the muscles as well as correct force magnitudes.

The insertion areas of the human masticatory muscles are published in many anatomy textbooks (Gray et al. 2005). These are, however, generalised and simplified. Actually, there is considerable interindividual variation in the location and distribution of these attachment areas in humans (Goto et al. 1995). Attachment areas defined in the FE model should ideally be estimated based on measurements from the same individual, but for this study only dry human mandibles were available and it is not possible to obtain the exact muscle attachments in the fossil specimens. It was therefore necessary to assume grossly similar spatial distributions of attachment areas in the different individuals, taking into account morphological differences like different ramus breadths. The gross distribution is defined based on published illustrations of the respective insertion areas as well as on a partly dissected head of one human cadaver (Head 2006D). This head was CT-scanned (see 3.2 and 3.4 for more information about the specimen and the scanning parameters) so that a 3D model of the skull and the masticatory muscles could be created (**Fig. 3.12**).

The line of action for each masticatory muscle is required for the accurate orientation of muscle vectors in the FE model. Ideally, it is estimated based on the muscle itself, by cutting the muscle into parallel slices and then connecting the centroids of these successive slices with a curve. This can be done by dissecting

the muscle or estimating these centroids based on CT and magnetic resonance imaging (MRI) scans, which provide virtual slices through the muscle (An et al. 1984, Koolstra et al. 1989, 1990, van Spronsen et al. 1997).

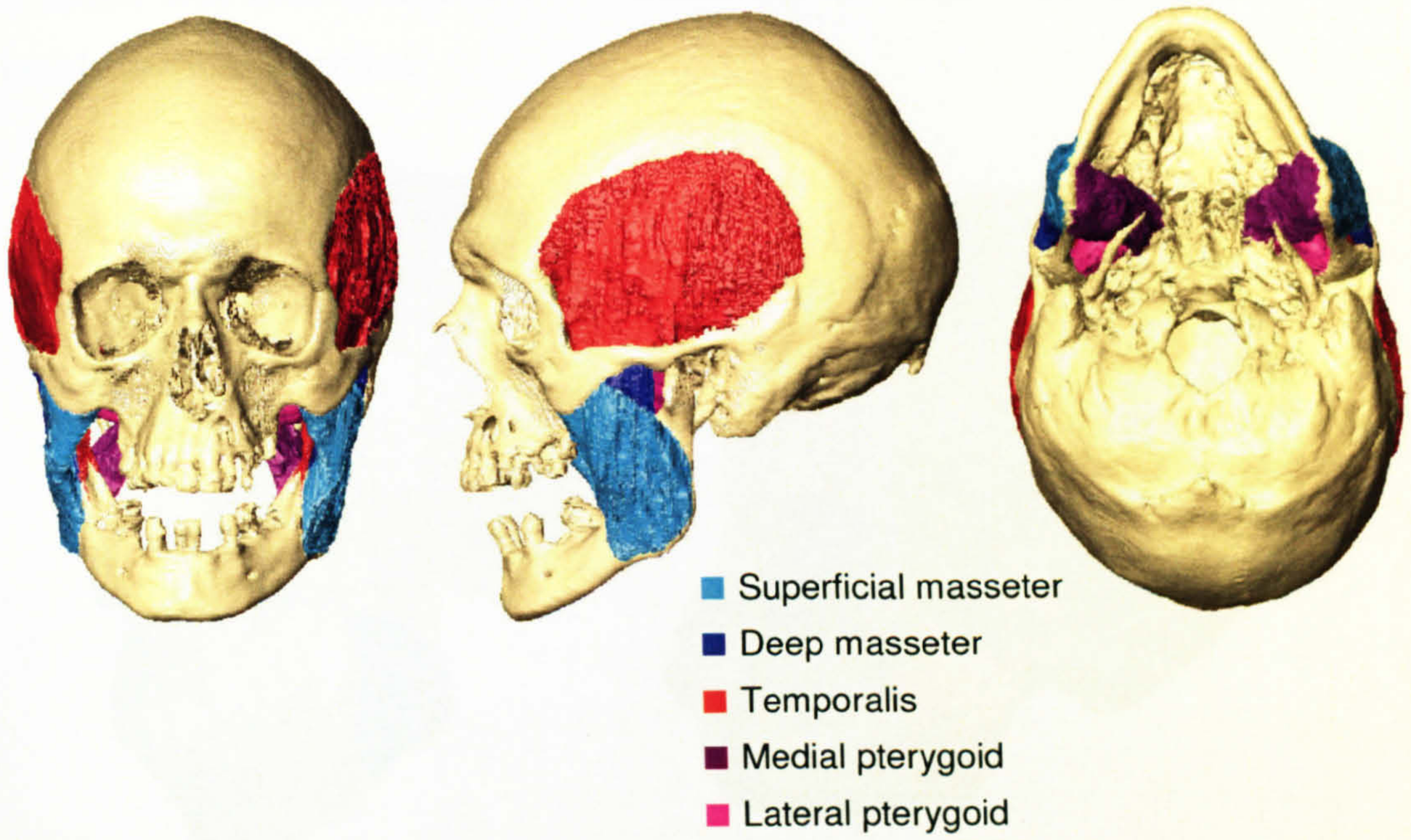

Fig. 3.12. 3D model of the human jaw-closing muscles. The model is based on a CT scan of a cadaveric head (Head 2006D). From left to right: frontal, lateral and inferior views.

Most biomechanical models of the human masticatory apparatus are however based on the so called "straight-line" approach, in which the centres of origin and insertion of muscles or muscle portions are simply connected by straight lines (Pruim et al. 1980, Osborn & Baragar 1985, Antón 1990, 1994, Koolstra & van Eijden 1995, Trainor et al. 1995, Osborn 1996, O'Connor et al. 2005). Although functional units and other aspects of muscle anatomy are ignored by this approach, it seems to provide a reasonable approximation of muscle force direction (O'Connor et al. 2005). A major advantage of this approach is that it can be applied to dry skulls and thus also to fossils. Therefore it has been used here. Two specimens in the sample, one modern human (ANAT 800) and the early anatomically modern human Skhūl 5, were represented by almost complete skulls so that the estimation of the lines of action was straight forward. However, the rest of the sample consisted of isolated mandibles. Therefore, crania from other individuals had to be used: the cranium ANAT 800 for the remaining modern human specimens, Guattari 1 for the two Neanderthal mandibles and Kabwe 1 for the *H. heidelbergensis* mandible (see 3.2 for more information about these specimens). After a simple threshold segmentation and in the case of Guattari 1

and Kabwe 1 a reconstruction of the damaged right halves of the crania by mirror imaging, the 3D models of these crania were fitted to the respective mandibles by rotation, translation and scaling in Amira (**Fig. 3.13**). The orientation of the lines of action was then determined by connecting the origin and insertion of each muscle or muscle portion.

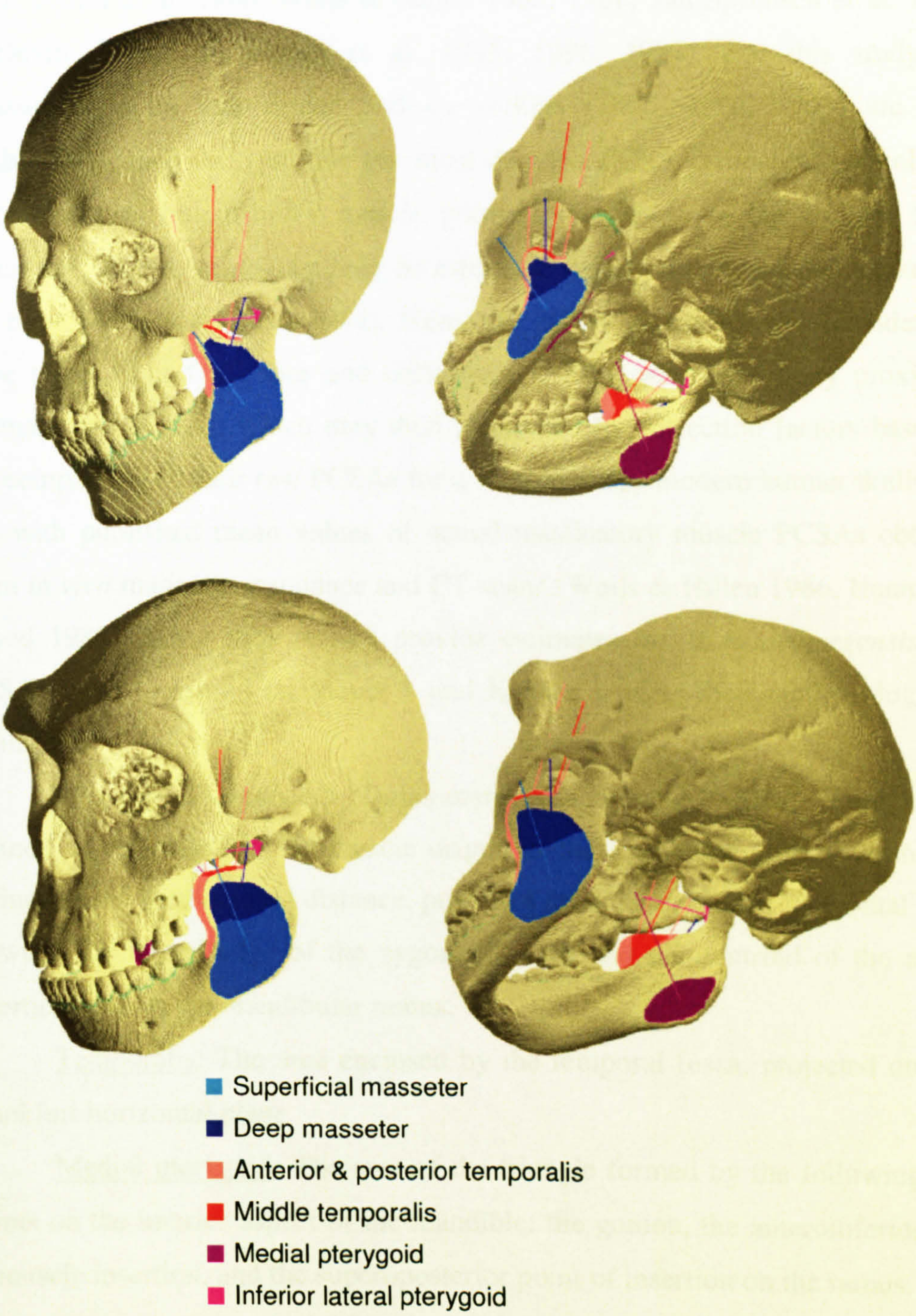

Fig. 3.13. Reconstructed skulls and applied muscle forces. Upper row: the modern human ANAT 800, bottom row: a *H. heidelbergensis* reconstruction using Mauer 1 and Kabwe 1. Not to scale.

The maximum muscle force can be obtained by measuring the physiological cross-sectional area (PCSA) of each muscle, which is the total cross-sectional area of all muscle fibres at a specific length, and multiplying it by the intrinsic strength of skeletal muscle (O'Connor et al. 2005). For human masticatory muscles, several PCSA measurements are available (Schumacher 1961, Pruim et al. 1980, Weijs & Hillen 1985, 1986, van Spronsen et al. 1989, McDevitt 1989, van Eijden et al. 1995, 1996, 1997). For this study the measurements by van Eijden and co-workers (1995, 1996, 1997) are used (**Table 3.4**), since they provide the most detailed PCSA estimates, not only for whole muscles but also for muscle portions. However, in the case of fossil specimens, PCSA values can only be estimated based on measurements taken on the bone (Demes & Creel 1988). Here, the PCSA values for the Neanderthals were taken from O'Connor and colleagues (2005), who used bony proxies to estimate raw PCSAs, which they then multiplied by correction factors based on the comparison of their raw PCSAs for a sample of dry modern human skulls (n = 26) with published mean values of actual masticatory muscle PCSAs obtained from *in vivo* magnetic resonance and CT scans (Weijs & Hillen 1986, Hannam & Wood 1989). Since they do not provide estimates for *H. heidelbergensis*, raw PCSAs were measured on Mauer 1 and Kabwe 1 using their methodology and definitions:

Masseter: The product of masseteric "length" and "width". "Length" was defined as the length of the muscle origin on the zygomatic arch. "Width" was defined as the mediolateral distance, projected onto the Frankfurt horizontal plane, between the lateral edge of the zygomatic arch and the centroid of the muscle insertion area on the mandibular ramus.

Temporalis: The area enclosed by the temporal fossa, projected onto the Frankfurt horizontal plane

Medial pterygoid: The area of the triangle formed by the following three points on the interior aspect of the mandible: the gonion, the anteroinferior point of muscle insertion, and the superoposterior point of insertion on the ramus.

The resulting raw PCSAs were then divided by the correction factors given by O'Connor and co-workers (2005): 0.99, 0.64 and 0.26 for masseter, temporalis and medial pterygoid respectively. The final PCSA values are presented in **Table 3.4** together with the published values for modern humans and

Neanderthals. However, it has to be noted that despite the correction factors, the PCSA values for the fossil specimens can only be regarded as crude estimates due to difficulties in measuring the required dimensions and the unknown relationship between estimated and real PCSA values in extinct taxa.

Muscle	PCSAs (cm^2)		
	H. sapiens[1]	*H. neanderthalensis*[2]	*H. heidelbergensis*[3]
Masseter	10.3	11.9	10.8
Temporalis	13.3	13.3	15.4
Medial pterygoid	6.0	11.9	10.0
Inferior lateral pterygoid	2.8	-	-

[1]van Eijden et al. (1995, 1996, 1997), n = 8
[2]O'Connor et al. (2005), n = 3 (Amud 1, La Chapelle, La Ferrassie 1)
[3]based on measurements of the reconstructed *H. heidelbergensis* skull (Mauer mandible and Kabwe cranium) using the methodology of O'Connor et al. (2005).

Table 3.4. Mean physiological cross-sectional areas (PCSAs) of the masticatory muscles in modern humans, Neanderthals and *H. heidelbergensis*.

In order to obtain the maximum force for each muscle, all PCSA values were multiplied by the intrinsic strength of skeletal muscle. In this study a value of 32 N/cm^2 was used, which is in concordance with published estimates of intrinsic muscle strength (Weijs & Hillen 1985, van Spronsen et al. 1989). **Table 3.5** shows the final values for the maximum forces of the masticatory muscles. In order to model the different portions of masseter and temporalis individually as in modern humans, the maximum masseter and temporalis forces of Neanderthals and *H. heidelbergensis* were divided using the same relationships between the muscle portions as in modern humans (van Eijden et al. 1997). The PCSA and thus the maximum force of the inferior lateral pterygoid could not be estimated in the fossil specimens. In order to include this muscle for a relatively comprehensive modelling of the masticatory forces, the same values as for modern humans were assumed.

Muscle	Muscle forces (N)		
	H. sapiens	*H. neanderthalensis*	*H. heidelbergensis*
Superficial masseter	218	253	229
Deep masseter	112	129	117
Anterior temporalis	168	169	195
Middle temporalis	137	138	159
Posterior temporalis	119	119	138
Medial pterygoid	192	382	315
Inferior lateral pterygoid	90	90	90

Table 3.5. Maximum muscle forces based on PCSA estimates in modern humans, Neanderthals and *H. heidelbergensis*, multiplied by an intrinsic muscle strength of 32 N/cm^2. Due to the lack of PCSA data for the lateral pterygoid in the fossil taxa, the same maximum force as in modern humans is applied.

The final step in the estimation of muscle force magnitudes is the scaling of the calculated maximum force for each muscle or muscle portion according to its activation. This is required since the masticatory muscles generate only a part of their maximum force during masticatory function. The recruitment pattern (i.e. the relative activation of each masticatory muscle and its portions), varies considerably between different masticatory tasks, for example, biting on the left M1 vs. the incisors. This is well documented in humans by abundant electromyographic (EMG) data (Møller 1966, Ahlgren 1966, Pruim et al. 1980, Blanksma & van Eijden 1990, Blanksma et al. 1992, Blanksma & van Eijden 1995, Blanksma et al. 1997, Spencer 1998).

Muscle	Scaling factors[1]					
	Incision		Canine bite		Molar bite	
	Right	Left	Right	Left	Right	Left
Superficial masseter	0.40	0.40	0.46	0.58	0.72	0.60
Deep masseter	0.26	0.26	0.46	0.58	0.72	0.60
Anterior temporalis	0.08	0.08	0.54	0.14	0.73	0.58
Middle temporalis	0.06	0.06	0.48	0.20	0.66	0.67
Posterior temporalis	0.04	0.04	0.42	0.26	0.59	0.39
Medial pterygoid	0.78	0.78	0.55	0.47	0.84	0.60
Inferior lateral pterygoid	0.71	0.71	0.43	0.93	0.30	0.65

[1]Nelson (1986), Korioth et al. (1992), Korioth & Hannam (1994)

Table 3.6. Muscle force scaling factors used for different bites.

Table 3.6 presents the scaling factors used for the different bites that will be modelled here. These scaling factors by Nelson (1986) are the same ones that have already been used in several FEA studies of human mandibles (Korioth et al. 1992, Korioth & Hannam 1994a, Reina et al. 2006, Ichim et al. 2006a, 2007b). In order to obtain the muscle force magnitudes to be applied to the FE model the estimated maximum force of each muscle or muscle portion is multiplied by the respective scaling factor. It is likely that Neanderthals and *H. heidelbergensis* had different activation patterns, since differences in craniofacial morphology can have an influence on the relative activation of the masticatory muscles (Møller 1966), but since the muscle recruitment patterns of these taxa are unknown, the same scaling factors as for modern humans are here applied to them.

3.9. Strain measurements using speckle interferometry

Usually, strain in a bone under loading is measured with strain gauges that are glued to the bone surface. In the literature, numerous examples can be found of studies that successfully measured strains in different bones under *in vitro* as well as *in vivo* loading with strain gauges (Knoell 1977, Mongini et al. 1981, Hylander et al. 1987, Daegling 1993b, Throckmorton & Dechow 1994, Daegling & Hylander 2000, Vollmer et al. 2000, Strait et al. 2005, Kupczik et al. 2007). However, the use of strain gauges involves a number of technical problems. The reliability of the measurements depends, for example, on the quality of the solder connections, the amount of glue used to attach the strain gauges to the bone surface or the temperature and humidity of the environment. In addition, the bone surface needs to be flat to attach gauges, and if it is not, obtaining good adherence to the surface can be problematic. Finally, strain gauges only yield measurements for single points on the surface. As such, when they are used for the validation of an FE model, for which the pattern of strain distribution over the whole surface is relevant, they provide only limited data.

In order to visualise strain distribution patterns, photoelastic material, for example, plastic, instead of strain gauges has been used in some *in vitro* studies. In some of these studies, the external surface of the mandible was coated with a layer of photoelastic material to study surface strains (Mongini et al. 1979, Calderale et al. 1986, Meyer et al. 2002), in other studies, photoelastic material was used to produce replicas of the mandible so that the internal strain distribution

pattern could be visualised (Ralph 1975, Ralph & Caputo 1975, Standlee et al. 1977, 1981). However, a major problem with this approach is that the mechanical properties of plastic are considerably different from those of bone (van Eijden 2000). In addition, this method only visualises the strain distributions, but does not provide measurements of the strain magnitudes, which are also important for the validation of an FE model.

A novel method for measuring surface strains, which is based on the principle of speckle interferometry overcomes these problems. Speckles are granular patterns, which appear when an optically rough surface (i.e. its height variation is in the order of or greater than the wavelength of the light, which applies to most surfaces) is illuminated with coherent light (Yang & Ettemeyer 2003, Basara 2007). These speckles can be used to obtain information about the illuminated surface and have, therefore been applied in various ways, for example, for the measurement of surface roughness (Wykes 1977), contour (Jones & Butters 1975), vibration (Archbold & Ennos 1968), deformation (Archbold et al. 1969, Archbold et al. 1970, Leendertz 1970) or the detection of cracks (Hung et al. 1975).

For measuring surface strains of bones, two of these applications are relevant: the measurement of surface deformation and the measurement of surface contour. **Figure 3.14** illustrates the principle of deformation measurements with speckle interferometry. A laser light is divided into two beams: one beam is used to illuminate the object surface (object beam), the other one is used as a reference beam. Before it reaches the camera, the back-scattered light from the object surface is recombined with the reference beam. The two wave fronts interfere and thus create an interferogram, which is detected by a camera. When the surface is deformed, the phase difference between the object and the reference beams changes. This phase difference is then used to calculate the deformation of the surface. If one reference and one object beam are used, only the displacement in one dimension can be measured, but with at least three light sources and thus three different directions of illumination a 3D displacement measurement of the surface is possible.

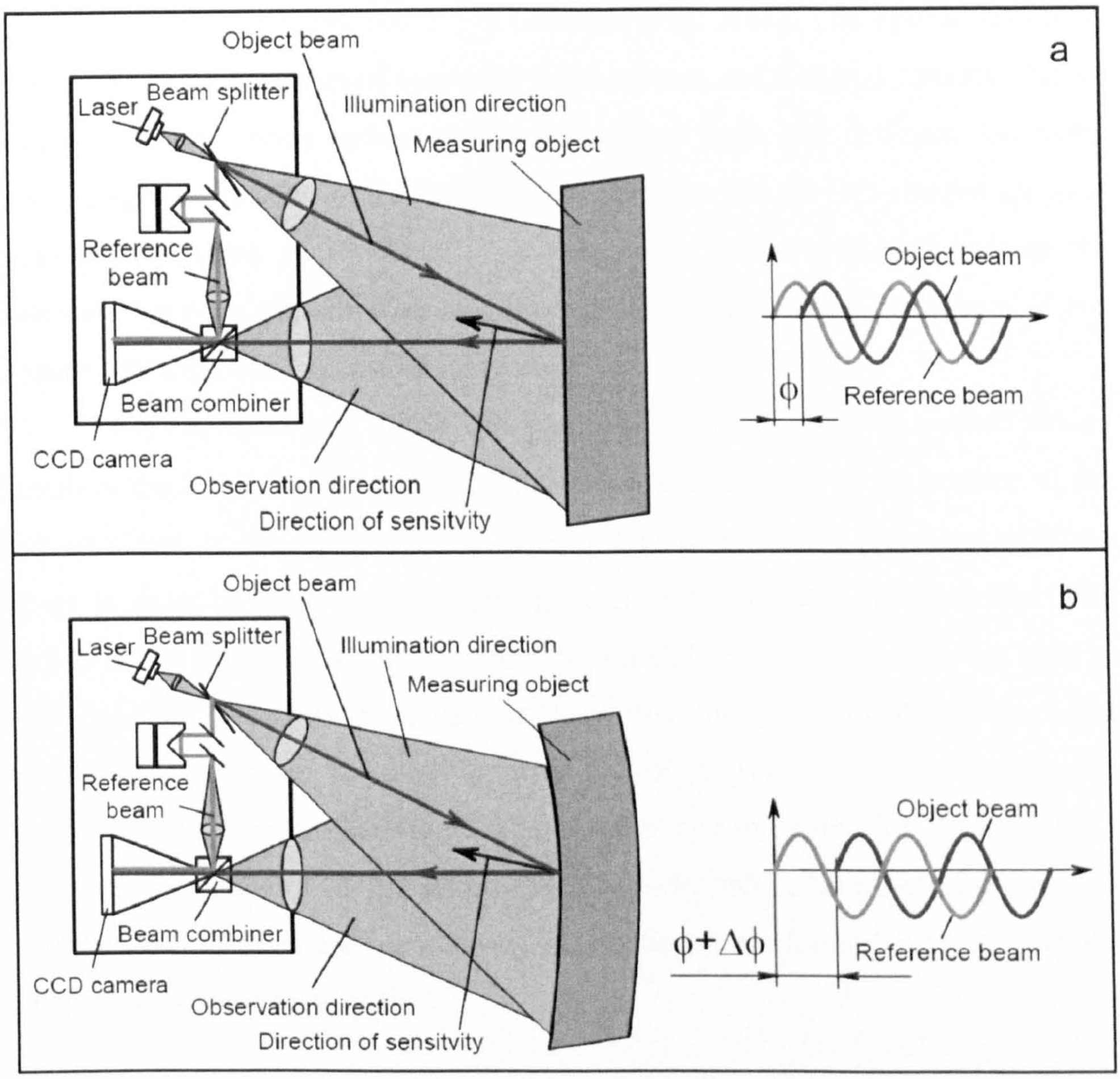

Fig. 3.14. Principle of strain measurements with speckle pattern interferometry: a) undeformed state, b) deformed state. Note the changing phase shift (ϕ) between object and reference beam during the deformation. CCD = charged coupled device, an electronic light sensor used in digital cameras (adapted from Yang & Ettemeyer 2003).

In order to measure stresses and strains in complex surfaces, it is necessary to measure the surface shape. The setup for the shape measurements is similar to that for the measurement of surface deformations, but in this case the beams are slightly shifted over the surface (Zou et al. 1992). Since there is no surface deformation, the phase changes, which result from the shifting of the beams and thus the paths of light, encode information about surface shape. Based on these phase changes, it is possible to calculate the depth of the object surface in the viewing direction.

This study uses a DANTEC Q-100 measuring system (DANTEC Dynamics GmbH, Ulm, Germany), which allows the measurement of stresses and strains as well the 3D shape of a surface. It consists of a laser box, an optical sensor, a control unit and a Windows PC on which the supplementary image

processing software IstraQ100 2.7 is installed (**Fig. 3.15**). The optical sensor of the Q-100 system consists of four laser light sources and a digital camera. During measurement, the bone surface is thus illuminated from four different directions and the speckle images are recorded by the camera. The speckle images are then evaluated with the IstraQ100 2.7 software, while the control unit acts as the interface between the software and the two other hardware components of the system: the laser box and the optical sensor.

The application of the Q-100 DSPI system for measuring surface strains involves the following work steps: First the measuring area on the surface of the test specimen is freed from dust and dirt and covered with a thin layer of white spray in order to create a non-reflecting surface. For reliable measurements, the Q-100 sensor has to be stably mounted onto the object so that it does not shift or tilt during the measurement. This is achieved by gluing a removable adapter ring to the object's surface, to which the front end of the sensor is attached. After the fixation of the sensor and the set-up of the system with the IstraQ100 2.7 software, the shape of the measuring surface is recorded. Loads are then applied and the deformations are recorded by subtracting the reference images from the images of the deformed surface.

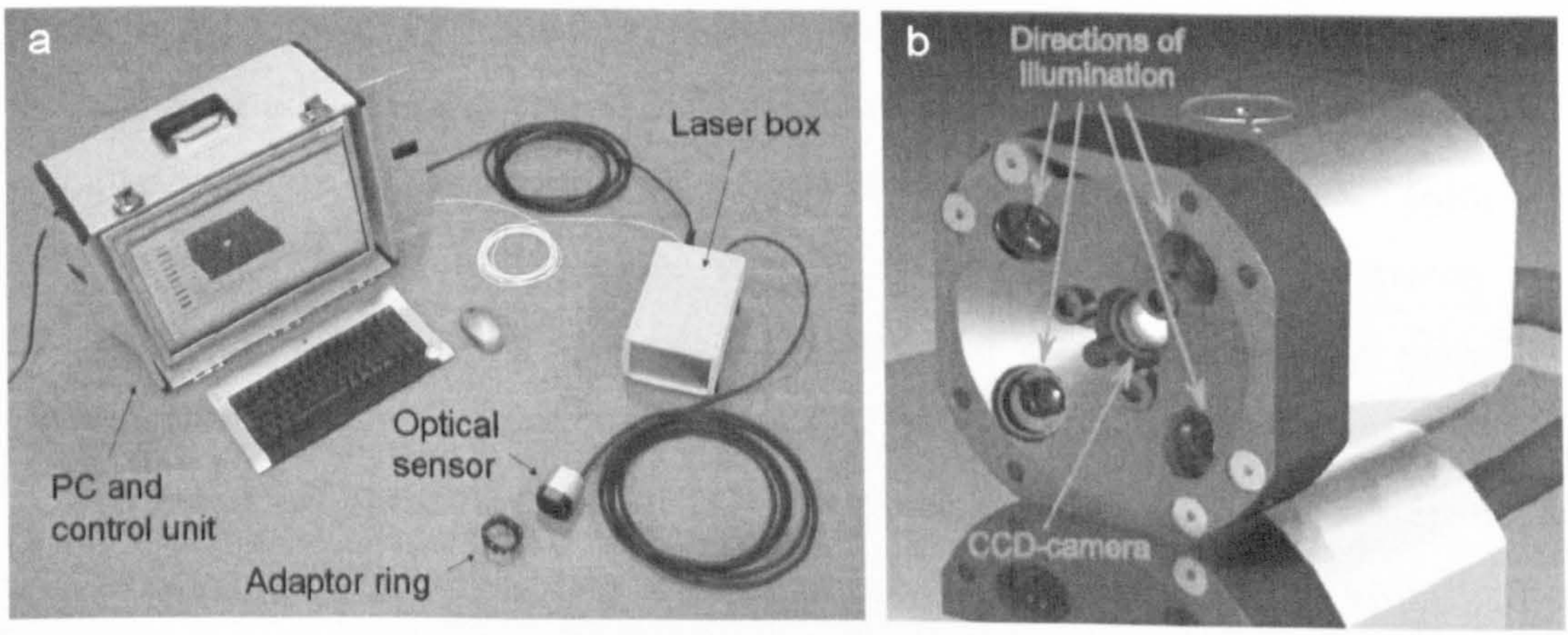

Fig. 3.15. The Q-100 DSPI measuring system: a) its components, b) arrangement of the four laser light sources and the digital camera in its optical sensor (image b from Basara 2007: 62, Fig. 3.12).

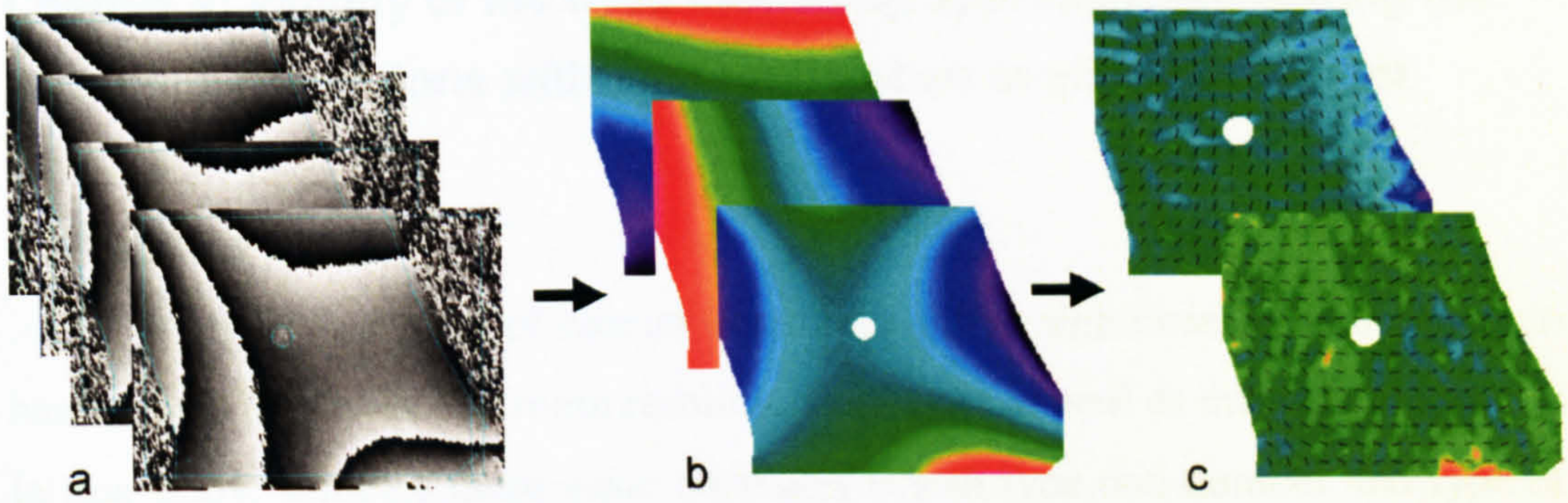

Fig. 3.16. Steps involved in the evaluation of speckle interferometry patterns with the IstraQ100 2.7 software: a) phase maps, each representing the phase differences for one illumination direction, b) visualisation of the x-, y- and z-displacements, c) strain maps.

The image resulting from a deformation of the surface is a speckle pattern with fringes that represent lines of the same deformation. The distance between the fringes equals a displacement of half the wavelength of the light used. It is important to keep the number of fringes per measurement low, since a too high number of fringes affects the accuracy of the measurement. As a guideline, not more than four or five fringes should occur on an image. In order to achieve this, high loads have to be divided into smaller load steps. Thus, the total deformation between the reference and the final load is fragmented into a number of fringe patterns, each including only the recommended number of fringes. In addition, noise in the speckle patterns can occur at the margins of a surface or where the surface is orientated at a steep angle relative to the light sources. For accurate calculation of the displacements, such areas of noise have to be excluded from the measurement. Based on the fringe pattern, the phase differences between the reference and the deformed state are calculated and visualised as phase maps for each direction of the illumination (**Fig. 3.16**). In the following step, the x-, y- and z-components of the deformation for each pixel are calculated. Based on these displacement values, the stresses and strains are finally calculated and visualised.

The stress and strain maps can be visualised in 2D, or in 3D when the contour data are used to generate a 3D surface model. Thus, this technique offers an ideal tool for comparisons with 3D FE models, since the 3D strain maps of the measuring field can be directly superimposed onto the corresponding area of the FE model.

Chapter 4: Validity of the used modelling approach: comparing the numerical predictions with the results of an *in vitro* experiment

4.1. Introduction

Prior FEA studies of human mandibles differ significantly with regard to basic model attributes like mesh resolution and type as well as material properties. In this study, some of these basic attributes (mesh type and number and type of material properties) are predefined by the use of the FE software VOX-FE, but to date its modelling approach has not been validated against experimental data. Other attributes like model resolution and material properties can be varied in VOX-FE, but it is not clear which values are necessary to predict experimental results most accurately. Before attempting to model complex physiological loads, it is therefore necessary to test the validity of basic model attributes against the results of a controlled *in vitro* experiment. In the following, it is reviewed how prior FEA studies of human mandibles differ with regard to these basic attributes and the effects of varying these parameters on the accuracy of FEA results is considered.

In the first FE models of human mandibles, model geometry was derived from manual measurements, which resulted in rather crude representations of mandibular shape (Gupta et al. 1973, Knoell 1977). Later studies used CT data and could thus achieve a much more accurate model geometry (Hart & Thongpreda 1988, Vollmer et al. 2000). Nowadays, the application of μCT data allows the creation of highly detailed FE models, which even include small foramina or the trabecular network within the bone (van Rietbergen et al. 2003, Verhulp et al. 2008). Thus, there has been a clear trend towards more accurate model geometry in FE modelling, but high-resolution models based on μCT data require powerful hardware and/or long processing times. It is therefore worth examing the extent to which high-resolution data are required to address a certain question and how much the model resolution can be reduced without affecting the quality of the results.

The model resolution is closely linked to the meshing approach and the resulting element types. Most published FE models of human mandibles consist of tetrahedral elements, which are typically larger than the voxels in the original CT scans (Ichim et al. 2006b, 2007b). Direct voxel conversion (i.e. each voxel in the

segmented CT image stack is converted into finite elements) has been mainly applied to long bones, particularly to create high-resolution models of the trabecular structure within the femur (van Rietbergen et al. 2003, Verhulp et al. 2006, Chevalier et al. 2007, Verhulp et al. 2008, Tsubota et al. 2009), but has hardly been used in FEA studies of mandibles (Vollmer et al. 2000, van Ruijven et al. 2007). As discussed under 3.7, direct voxel conversion allows a fast and error-free creation of FE meshes, but the resulting models have stepped surfaces in contrast to the smooth surface of tedrahedral meshes, which might affect the accuracy of the results depending on the element size (Yeni et al. 2005).

Another aspect closely linked to model resolution is the way in which the internal structure, particularly the geometry and the material properties of the cancellous bone are modelled. Unless extremely high-resolution μCT data is available, it is not possible to model the geometry of the trabecular network accurately. The spatial resolution needs to be so high that the diameter of a single trabecula is at least depicted by two voxels (Scherf & Tilgner 2009). Otherwise partial volume averaging (see 3.5) does not allow accurate segmentation, since the attenuation values of bone and air get mixed within the voxels. In addition, the scanning parameters have to be optimised in order to reduce image blurring and soft tissue, which can cause major problems for the correct identification of bone boundaries, should be removed completely prior to scanning. Since most CT datasets used for the FEA of mandibles do not fulfil these requirements, many FE studies have modelled the cancellous bone as a homogeneous bulk tissue using different material properties (Korioth et al. 1992, Tanne et al. 1993, Korioth & Hannam 1994a, Ichim et al. 2006b). A major problem with this approach, however, is that it does not account for the large variations in density of the trabecular network between as well as within specimens. It is therefore worth examining whether modelling cancellous as bulk material really can produce more realistic results than simple threshold segmentation.

The material properties assigned to models also differ substantially between prior studies. The simplest approach is to assign homogeneous and isotropic elastic properties to the model (Gupta et al. 1973, Knoell 1977, Ichim et al. 2006b), which is also the approach used in this study. However, studies that measured the material properties of fresh and dry human mandibles have shown that material properties are actually heterogeneous and orthotropic (Arendts &

Sigolotto 1989, 1990, Dechow et al. 1992, 1993, Schwartz-Dabney & Dechow 2003). Most FE studies of human mandibles have therefore tried to account for either the heterogeneity, orthotropy or both (Korioth et al. 1992, Korioth & Hannam 1994a, Vollmer et al. 2000). In order to model the heterogeneous distribution of material properties, some voxel-based FEA studies assigned the elastic modulus of each finite element automatically, based on the attenuation value of the corresponding voxel in the original CT dataset (Vollmer et al. 2000). The elastic properties assigned by this method are however isotropic, so that orthotropy is not accounted for. Other studies have used heterogeneous as well as orthotropic or at least transverse isotropic material properties based on experimental measurements (Korioth et al. 1992, Hart et al. 1992, Korioth & Hannam 1994a). Validation studies have shown that the predicted strain magnitudes of such orthotropic heterogeneous models come closest to experimental results, but that nonetheless isotropic homogeneous models are well able to predict overall strain distributions (Marinescu et al. 2005, Strait et al. 2005, Kupczik et al. 2007).

However, as has been described in the previous chapter (3.9), traditionally bone strains in such experiments have been measured with strain gauges, which only provide single point measurements on the surface. The spatial distribution of strain magnitudes is thus measured with very limited resolution. The optical full-field and non-contact strain measurement technique of electronic or digital speckle pattern interferometry (ESPI or DSPI) overcomes this problem (Jones & Wykes 1989, Yang & Ettemeyer 2003). To date, few studies have applied DSPI to bone, either for measuring strains (Tyrer et al. 1995, Su et al. 2005, Kessler et al. 2006, Yang et al. 2007, Yang & Yokota 2007) or elastic properties of loaded bones (Zhang et al. 2001, Zaslansky et al. 2005, Shahar et al. 2007, Barak et al. 2009). The results of these studies confirm the high reliability and practicality of this technique compared to strain gauges. However, the use of DSPI as a tool for validating FE models of bones has not yet been explored, except for a study that is part of this work (Gröning et al. 2009).

In this study, DSPI is used to measure surface strains in a dry human mandible under simple loading in the laboratory and the results are compared to FE models of the same specimen. The major aims of this validation study are: 1) to test the accuracy of the used voxel-based FE modelling approach with isotropic

homogeneous material properties, 2) to evaluate to what degree different scan and model resolutions as well as different ways of modelling the internal geometry of the bone affect the validity of the FEA results and finally 3) to assess the potential and limitations of this novel technique for the validation of FE models in the field of bone mechanics.

4.2. Material and methods

The experimental strain analysis was performed on a dry adult human mandible (H-A 004), which is complete apart from some damage to the anterior dentition and two holes in each ramus, since this specimen was attached to a cranium with metal springs.

During the experiment, loads were applied to this mandible with a Lloyd's EZ50 tensile testing machine (Ametek-Lloyd Instruments Inc., UK). The mandible was placed upside down in the machine so that it rested on the two condyles and the anterior teeth (**Fig. 4.1**). Compressive loads were then applied to the mandibular angles on both sides of the mandible. In total, eight load series were conducted, in which the loads were increased in 50 N steps from 0 to 250 N.

Deformations were measured using a Q-100 DSPI measuring system (see 3.9 for technical details). Two measuring areas on the right side of the mandible were selected, each ca. 25 x 33 mm in size, which is the maximum field of view of the Q-100 DSPI system. **Figures 4.1** and **4.2** show the location of the measuring fields on the mandible. Prior to loading of the specimen, the bone surface in the respective areas was covered with a thin layer of white spray (DIFFU-THERM developer BAB-BCB, Technische Chemie KG, Herten, Germany) in order to create a non-reflecting surface and the three-legged adaptor rings for the Q-100 sensor were glued onto the bone surface using X60 two component adhesive (HBM Inc., Darmstadt, Germany). After the mandible was placed in the tensile testing machine, the sensor was fixed to one of the adaptor rings.

First, the 3D surface topography was measured in each illuminated area prior to loading. This topographic measurement allows the accurate calculation of the strains even on objects with complex surface contours (Yang & Yokota 2007). Next, the loads were applied and the resulting speckle patterns were used to estimate x-, y- and z-displacements for each load step using IstraQ100 2.7

software (DANTEC Dynamics GmbH, Ulm, Germany). From these, maximum (ε_1) and minimum principal strain (ε_3) were computed and exported as 2D and 3D colour-coded maps and text data files.

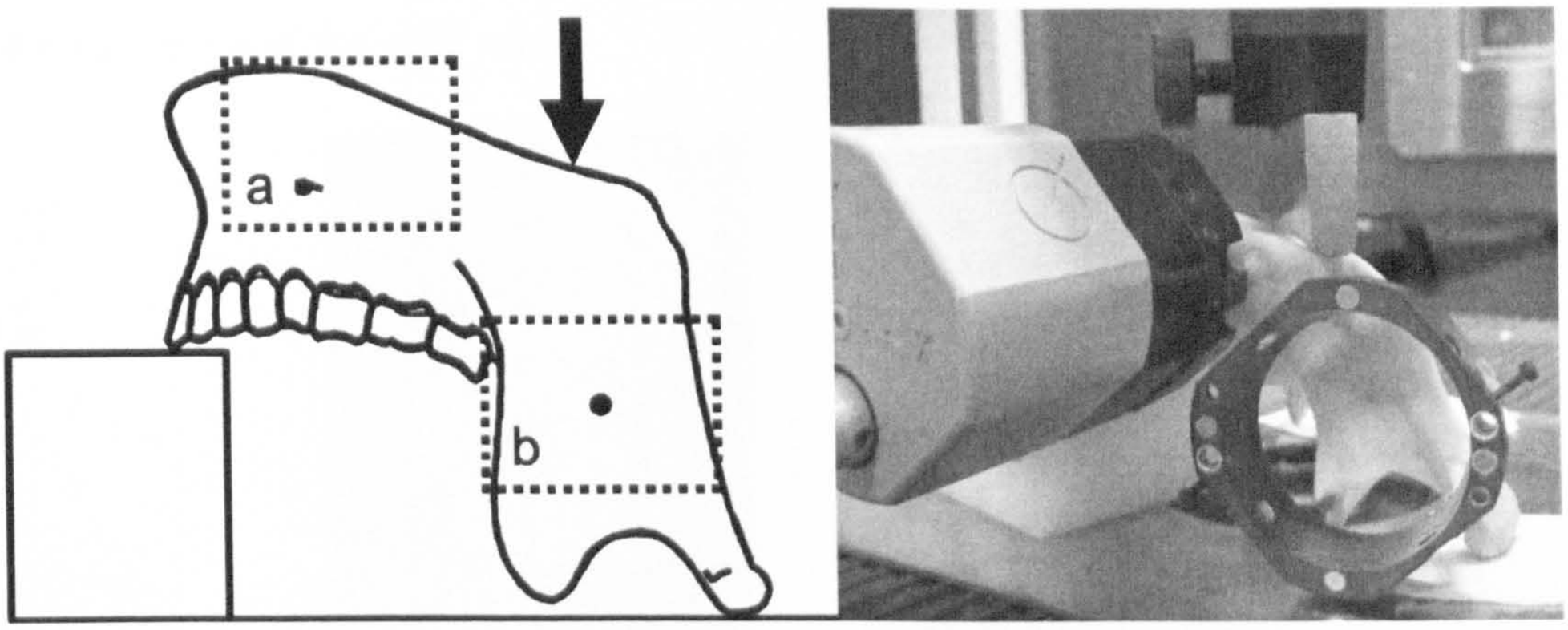

Fig. 4.1. Drawing and photo of the experimental setup. The arrow in the drawing indicates the position and orientation of the applied force, which acts symmetrically on both sides of the mandible (H-A 004). The dashed rectangles highlight the two measurement areas (a) and (b). The photo shows the mandible in the mechanical testing machine, with the two adaptor rings and the Q-100 DSPI sensor attached to the upper ring on the mandibular corpus.

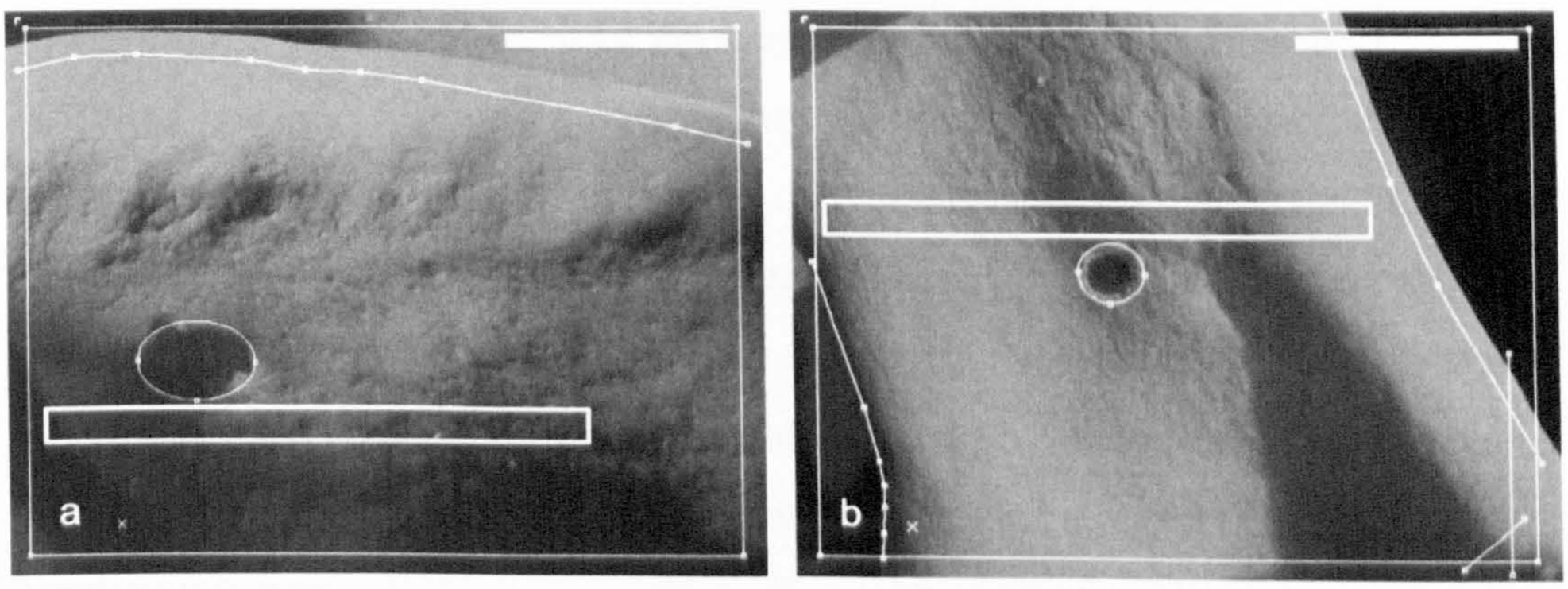

Fig. 4.2. Photos of the two illuminated areas of the bone surface: a) area on the mandibular corpus around the mental foramen and b) central area of the mandibular ramus around an artificial hole. The thin white lines indicate the boundaries of the measurement areas, whereas the white rectangles show the linear areas from which strain profiles were extracted. Scale bars = 1cm.

In order to create FE models of the test mandible, the specimen was CT-scanned prior to mechanical testing (see 3.4 for additional details). High-resolution μCT data were obtained using an X-Tek HMX 160 μCT system. Since the mandible was slightly above the size limit for this scanner, the two halves of the specimen were scanned separately. The primary reconstruction resulted in 16-bit TIFF image stacks with a voxel size of 0.122 mm for the right half and 0.135 mm for the left half.

In addition, medical CT scans were taken of the specimen with a GE Medical Systems BrightSpeed scanner. The image stacks were reconstructed with a pixel size of 0.488 mm and a slice interval of 0.625 mm and exported as DICOM image stacks. **Figure 4.3** illustrates the difference in resolution between the medical and the μCT scan.

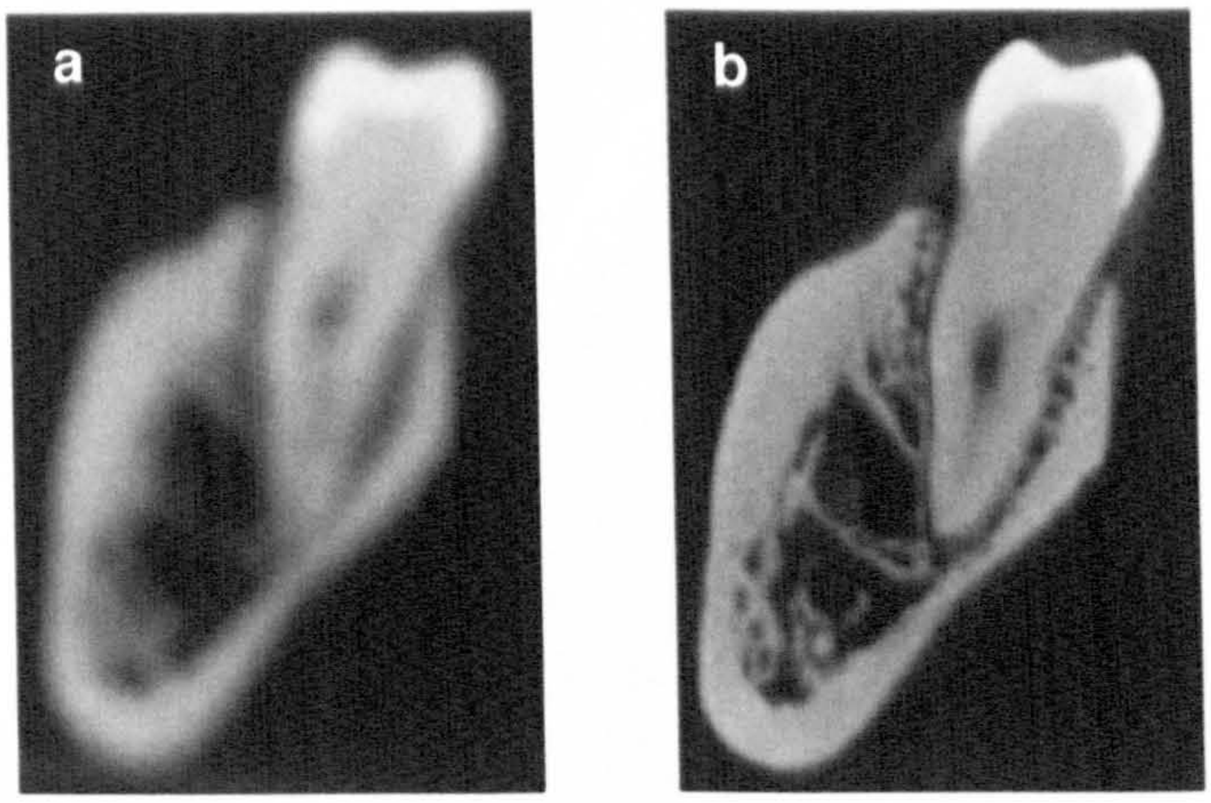

Fig. 4.3. Coronal CT slices through the right second molar: a) medical CT scan with a voxel size of 0.488 x 0.488 x 0.625 mm, b) μCT scan with a voxel size of 0.122 mm in all directions.

Image segmentation was performed using Amira. Bone and teeth were separated from the surrounding air by a user-defined density threshold. The voxels of the segmented medical CT scan were converted into an isotropic data set with a resolution of 0.488 mm in all three axes. The μCT data already consisted of isotropic voxels, but since the two sides of the mandible were scanned individually with the μCT scanner, the segmented data volumes of the two halves were reconnected in Amira by landmark-guided superimposition of the overlapping areas.

In order to distinguish between the effects of scan resolution and model resolution (i.e. element size), the 3D model based on the μCT dataset was downsampled to the voxel size of the low-resolution model (0.488 mm in all axes) and thus an additional model was created (**Fig. 4.4**). This model was also used to test the effect of modelling the cancellous tissue in two different ways. For this purpose, the whole volume encapsulated by the cortical shell was filled and defined as an extra material using the segmentation tools of Amira (**Fig. 4.5**).

The resulting 3D volume datasets were exported as BMP image stacks and converted into finite element meshes by direct voxel conversion resulting in element numbers and sizes of ca. 450,000 (ca. 600,000 for the models including

cancellous tissue as an extra material) and 0.488 mm respectively for the low-resolution models and 19.6 million elements with a size of 0.135 mm for the high-resolution µCT model.

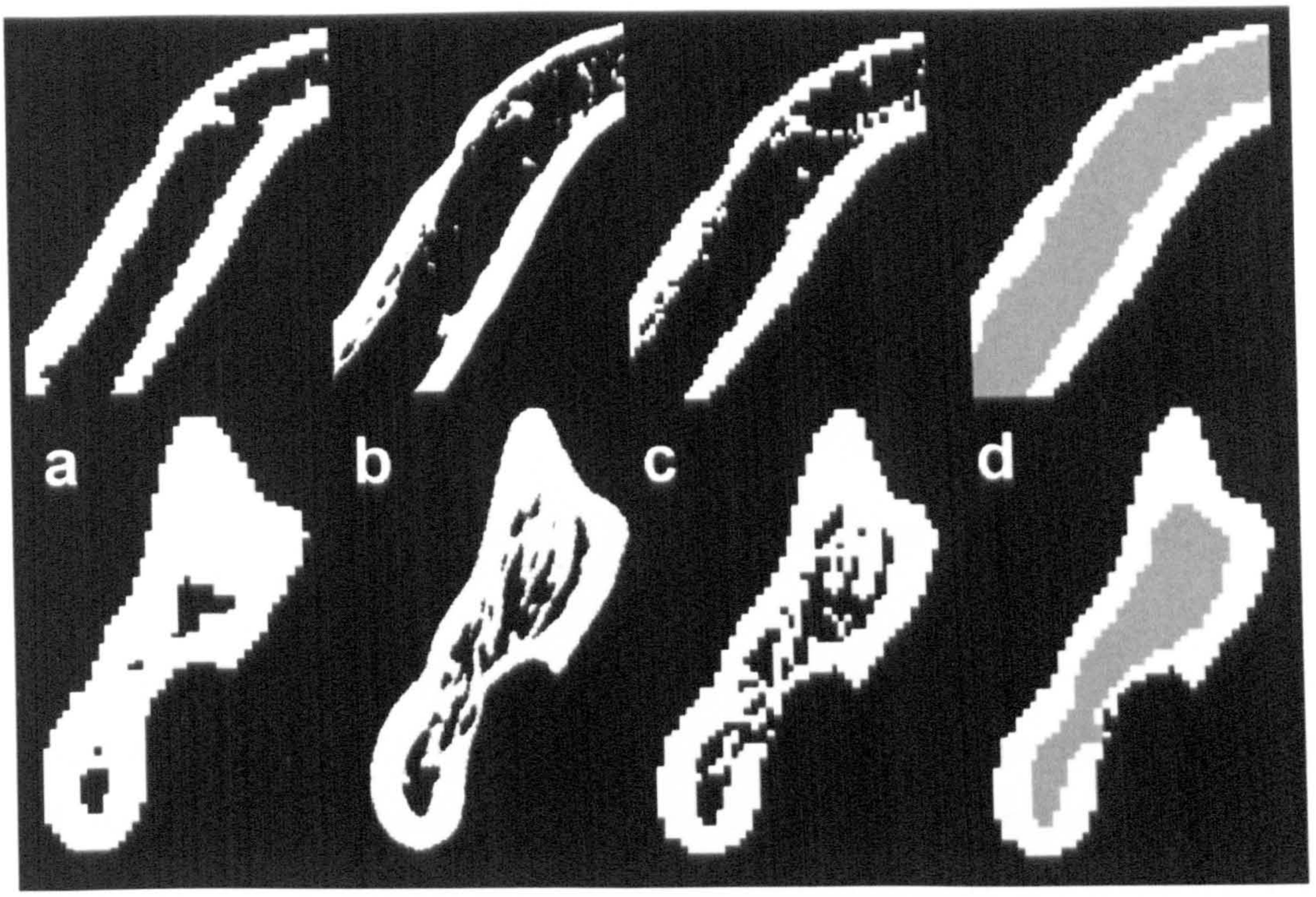

Fig. 4.4. Transverse sections through the models at the height of the linear areas from which strain profiles were extracted (see Fig. 4.2). Upper row: sections through the mandibular corpus, bottom row: sections though the mandibular ramus. a) medical CT model, b) µCT model, c) downsampled µCT model, d) downsampled µCT model with cancellous tissue as bulk material (grey).

The FEA was performed using VOX-FE (Fagan et al. 2007). Isotropic material properties of 17 GPa for Young's modulus (E) and 0.3 for Poisson's ratio (v) were assigned to both bone and teeth, which are values that lie within the range of published values for human mandibles (Ashman & van Buskirk 1987, Arendts & Sigolotto 1989, 1990, Dechow et al. 1993, Schwartz-Dabney & Dechow 2003). In the model, in which cancellous tissue was included as a bulk material, cortical bone was assigned the same material properties as above, but different Young's moduli were defined for the cancellous bone tissue: E = 0.056 GPa based on measurements of cancellous bone tissue in the human mandibular corpus (Misch et al. 1999), E = 0.431 GPa based on measurements of the cancellous tissue in the human mandibular condyle (Giesen et al. 2001), and E = 1.5 GPa, which is the highest value found in recently published FEA studies of human mandibles (Field et al. 2008). In all cases the same Poisson's ratio as for cortical bone was applied (v = 0.3), which is consistent with prior FEA studies

that modelled cancellous bone as a bulk tissue (Korioth et al. 1992, Korioth & Hannam 1994a, Choi et al. 2005, Ichim et al. 2006b, Field et al. 2008)

Fig. 4.5. Material representing cancellous bone tissue within the downsampled μCT model. Cortical bone and teeth have been made transparent.

To summarise, 6 different models were analysed: 1) the high-resolution model based on the μCT scan, 2) the low-resolution model based on the medical CT scan, 3) the downsampled μCT model, 4) the downsampled model with cancellous tissue as an extra material with E = 0.056 GPa, 5) with E = 0.431 GPa and 6) E = 1.5 GPa.

In order to simulate the experimental loading conditions, the FE models were constrained in the vertical axis at the tips of the anterior teeth and the condyles, with vertical compressive forces applied to a small region of the mandibular angle on each ramus (**Fig. 4.6**). The number of constrained or loaded nodes was chosen to be inversely proportional to the resolution of the FE models, in order to ensure that the loaded surface areas were of similar size in the different models. Solution of the FE models was carried out on a 32 processor Eagle HPC (high-performance cluster) with ca. 10,000 iterations for the low-resolution model and ca. 50,000 for the high-resolution model.

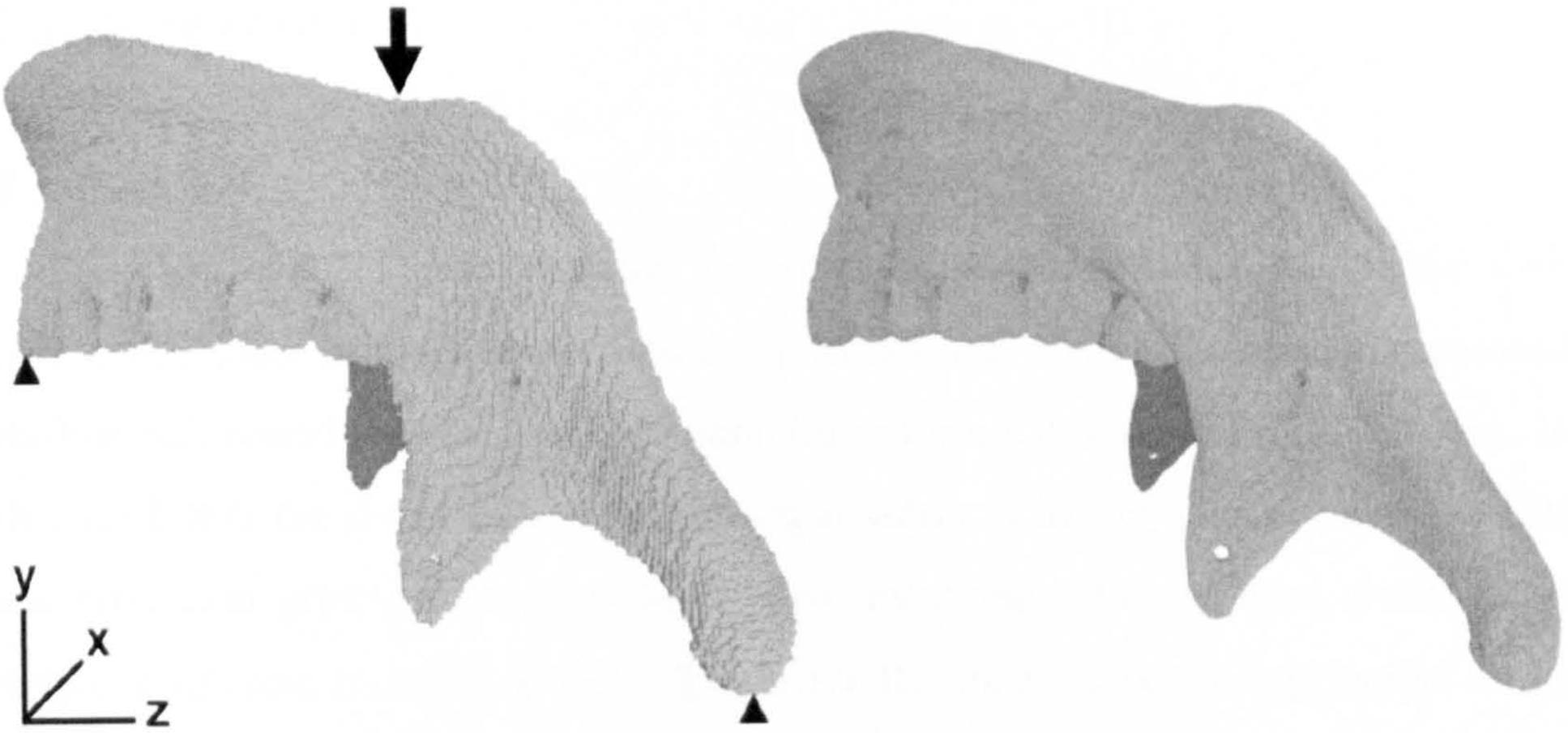

Fig. 4.6. Low- and high-resolution FE models and the illustration of the boundary conditions. Left: low-resolution model based on the medical CT scan (element size = 0.488 mm). The arrow points at the nodes where the vertical force (maximum = 250 N) was applied. The two triangles indicate the constrained nodes. At these nodes only displacements in the y-axis were prevented. Right: high-resolution model based on the µCT scan (element size = 0.135 mm).

In order to quantify the changes in the experimentally measured strain magnitudes with increasing load, the mean maximum (ε_1) and minimum principal strains (ε_3) were calculated for each load step and load series, considering the values for every eighth point in the measurement area, which were approximately 1.1 mm apart. These average strain values were then used to compute the mean for each load step for all series. The reliability of these overall means was evaluated by calculating standard errors. To compare the experimental and FEA results, 3D surface models based on the DSPI shape measurement were created and superimposed on the CT-based 3D models in Amira using its automatic surface alignment tool. Thus, the measuring areas could be matched between the experiment and the FE models. Corresponding profiles of maximum and minimum principal strain values were then exported from the FEA results and the measured strain maps. Since the spatial resolution of the Q-100 DSPI measuring system is limited to typically 0.5 mm (Basara 2007), several parallel profile measurements were taken per measuring field, covering an area of ca. 1.5 mm width × 25 mm length (**Fig. 4.2**). Based on these parallel profiles, a mean strain profile for each sampled area was calculated. For consistency with the profiles from the DSPI strain maps, which represent a 2D projection, the FEA profiles were scaled according to the projected distance between start and end point of each profile. The variance of the DSPI strain profiles was quantified by

computing the standard deviations of the corresponding strain values from the different recordings.

4.3. Results

Figure 4.7 shows that the recorded strain magnitudes are linear with increasing load in both areas under investigation. Only the strains measured during the second load step on the mandibular ramus deviate from this pattern. In this load step the mean maximum principal strain is higher than expected, while the minimum principal strain is lower than expected. The standard errors differ between the two measuring areas. Those for the mean maximum principal strain are considerably larger than the ones for minimum principal strain in the ramus, and *vice versa* in the corpus. However, for the maximum load of 250 N, which is used here for the comparison between measured and predicted strains, the standard error is only ±8 με (9% of the mean) for maximum principal strain in the ramus and ±4 με (~5% of the means) or below for the other three mean strain values. In addition, the DSPI colour-coded strain maps yielded a very consistent strain pattern across the load series as well as across the load steps within each series.

When the experimental and FEA results are compared, the contour maps for the maximum load of 250 N show very good concordance with regard to the spatial distribution of low and high strain areas as well as principal strain directions (**Fig. 4.8**). **Figures 4.9** and **4.10** show the variations of the measured and predicted maximum and minimum strains through the two sample areas. The similarity between the experimental and predicted curves is striking: most predicted values lie within two standard deviations of the mean experimental values.

Interestingly, the two original FE models based on the medical and μCT scans yield largely similar results despite the significant difference in resolution. The greatest difference occurs in the right (posterior) half of the mandibular ramus region, where the minimum principal strain values predicted by the low-resolution medical CT model fall outside the range of two standard deviations of the mean experimental values, while the predictions of the high-resolution model lie within this range. A more locally restricted difference between the two models is found in the area directly below the mental foramen. Here the medical CT model

predicts the minimum principal strain distribution very accurately, but the magnitudes are lower than the ones measured in the experiment. The strain magnitudes predicted by the high-resolution model are, in contrast, very close to the experimental means.

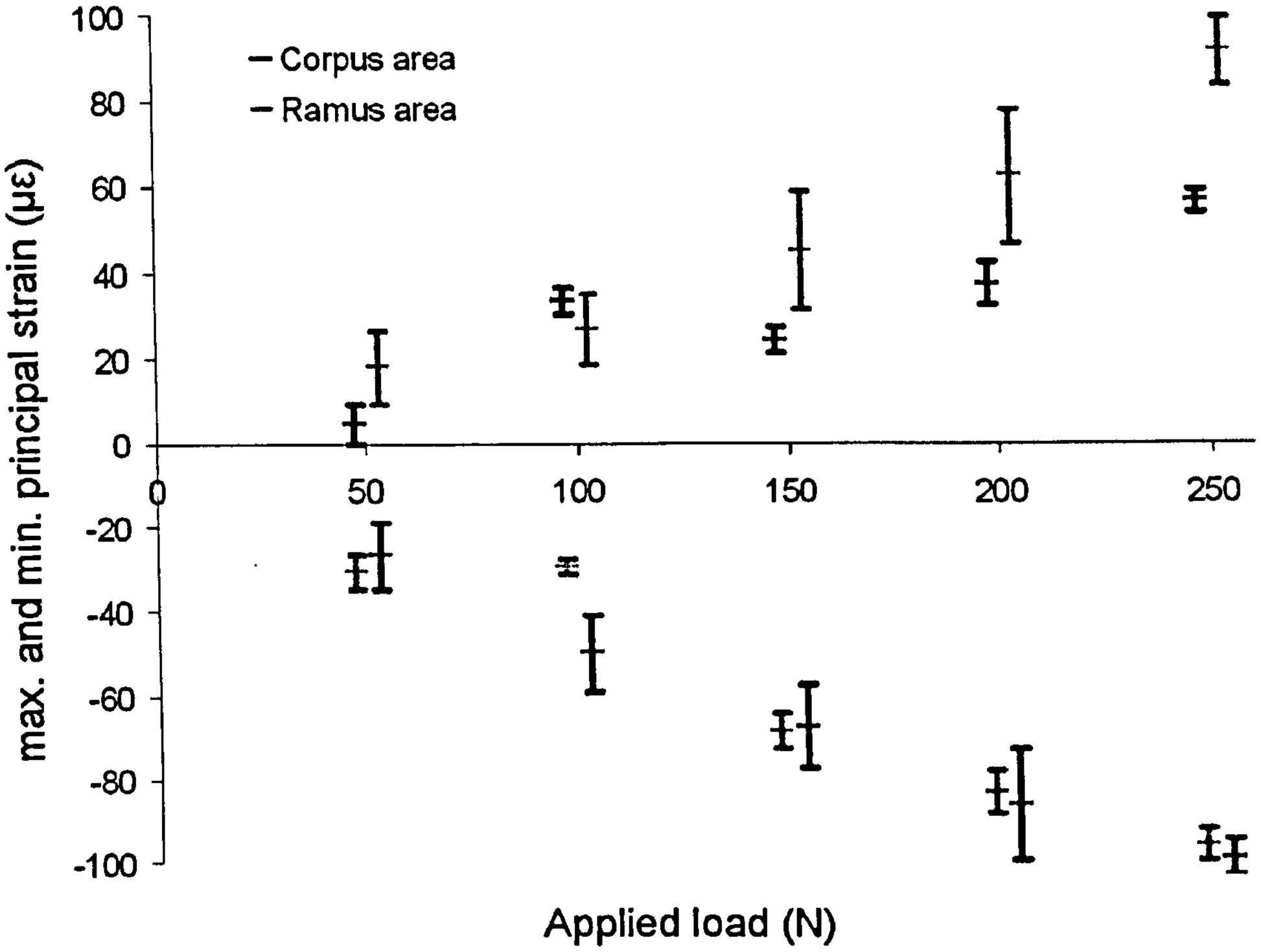

Fig. 4.7. Measured mean maximum and minimum principal strain values against the applied load for the two measurement areas. The bars represent the standard error for each load step.

The model that was created by downsampling the high-resolution μCT model to the element size of the medical CT model, yields strain profiles that are very similar to those of the two original models. However, in the two areas, where the original models differ, directly below the mental foramen and in the posterior half of the mandibular ramus, the strain magnitudes predicted by the downsampled model lie between the two original models, but fall a bit closer to the values of the high-resolution model and thus also to the experimental mean values.

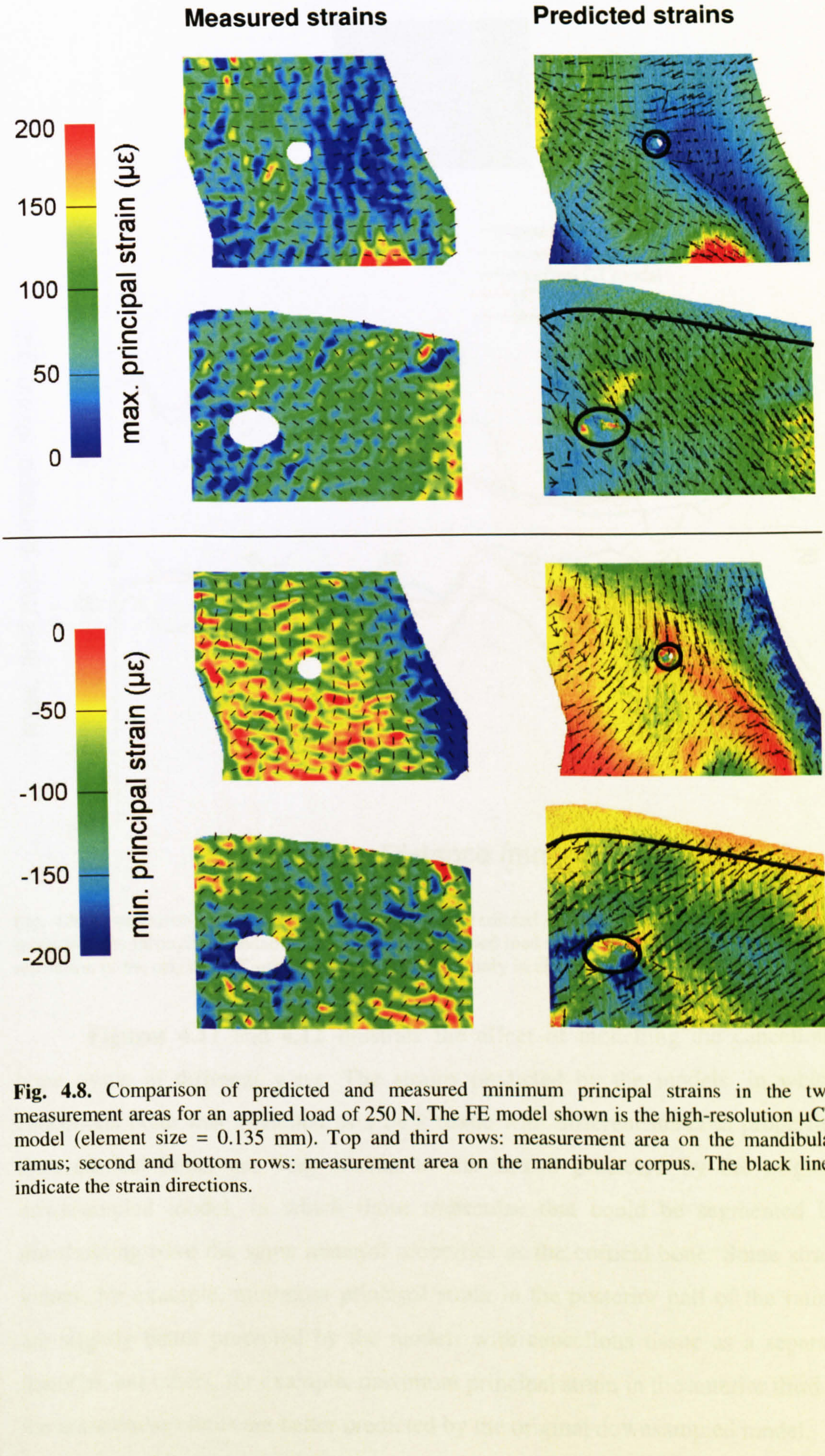

Fig. 4.8. Comparison of predicted and measured minimum principal strains in the two measurement areas for an applied load of 250 N. The FE model shown is the high-resolution μCT model (element size = 0.135 mm). Top and third rows: measurement area on the mandibular ramus; second and bottom rows: measurement area on the mandibular corpus. The black lines indicate the strain directions.

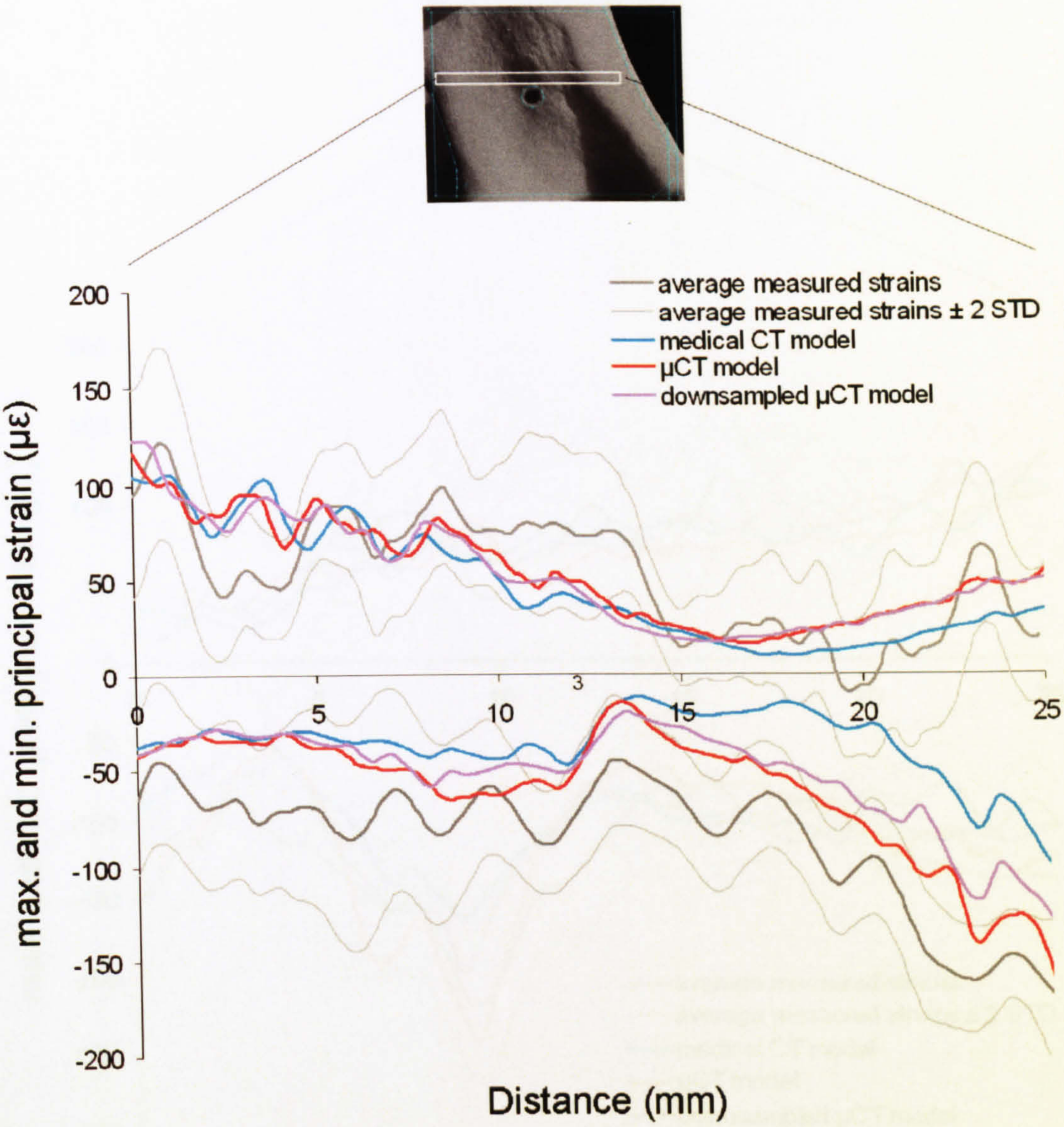

Fig. 4.9. Comparison of the mean experimental and predicted maximum and minimum principal strain profiles through the mandibular ramus area (applied load = 250 N). The models differ in the resolution of the original CT scans and element size or only in element size.

Figures 4.11 and **4.12** illustrate the effect of modelling the cancellous bone tissue in different ways. The strains predicted by the models, in which cancellous bone was modelled as a bulk tissue with different material properties than cortical bone, are very similar to the strains predicted by the original downsampled model, in which those trabeculae that could be segmented by thresholding have the same material properties as the cortical bone. Some strain values, for example, minimum principal strain in the posterior half of the ramus are slightly better predicted by the models with cancellous tissue as a separate material, but others, for example, maximum principal strain in the anterior third of the mandibular ramus are better predicted by the original downsampled model.

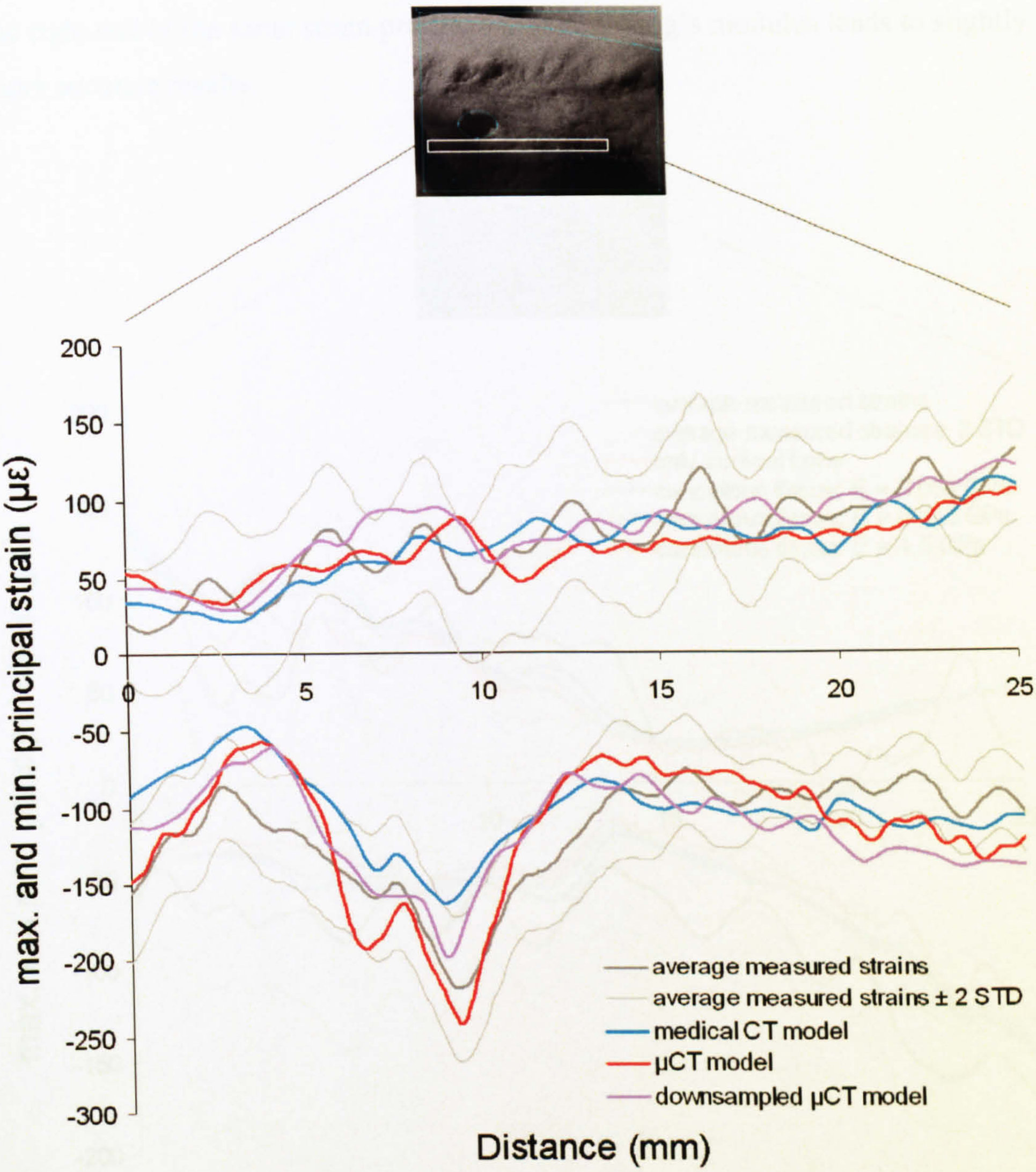

Fig. 4.10. Comparison of the mean experimental and predicted maximum and minimum principal strain profiles through the mandibular corpus area (applied load = 250 N). The models differ in the resolution of the original CT scans and in element size or only in element size.

Changing the Young's modulus of the cancellous tissue results in only minor strain differences. The smaller the values for Young's modulus, the higher are the strain magnitudes, but this is an increase of less than 10 με in most areas. The increase is a bit larger locally for minimum principal strain in the corpus, but still only of ca. 20 με. Like the original downsampled model, the predicted strain values of the different cancellous tissue models lie mainly within two standard deviations from the experimental means. None of the models predicts the experimental values consistently better than the others. A lower Young's modulus results in slightly more realistic strain values in one area, for example, for

minimum principal strain below the mental foramen, but in another, for example, the right end of the same strain profile, a higher Young's modulus leads to slightly more accurate results.

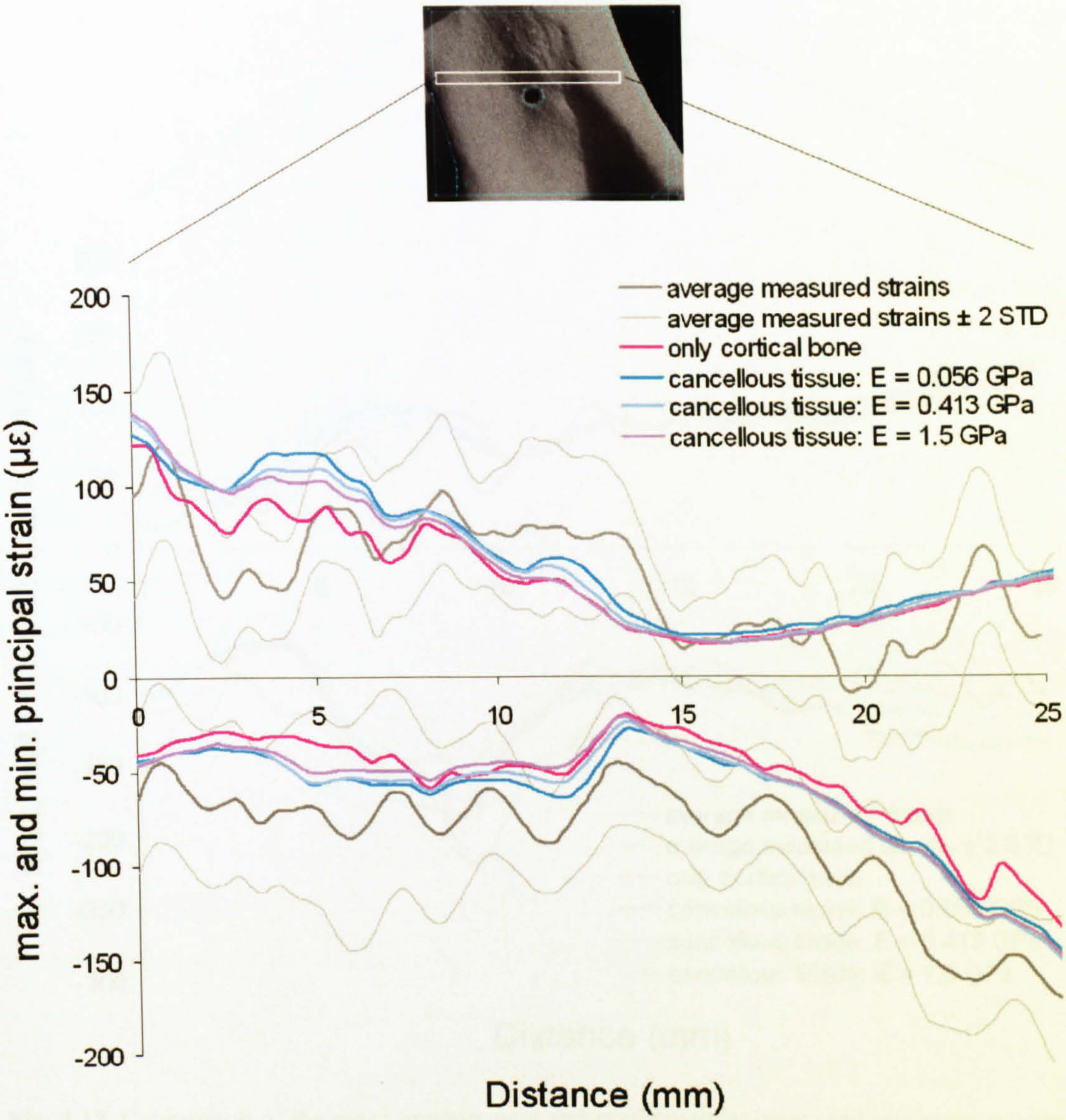

Fig. 4.11. Comparison of the mean experimental and predicted maximum and minimum principal strain profiles through the mandibular ramus area (applied load = 250 N). The models differ with regard to the geometry and the material properties of the cancellous bone tissue.

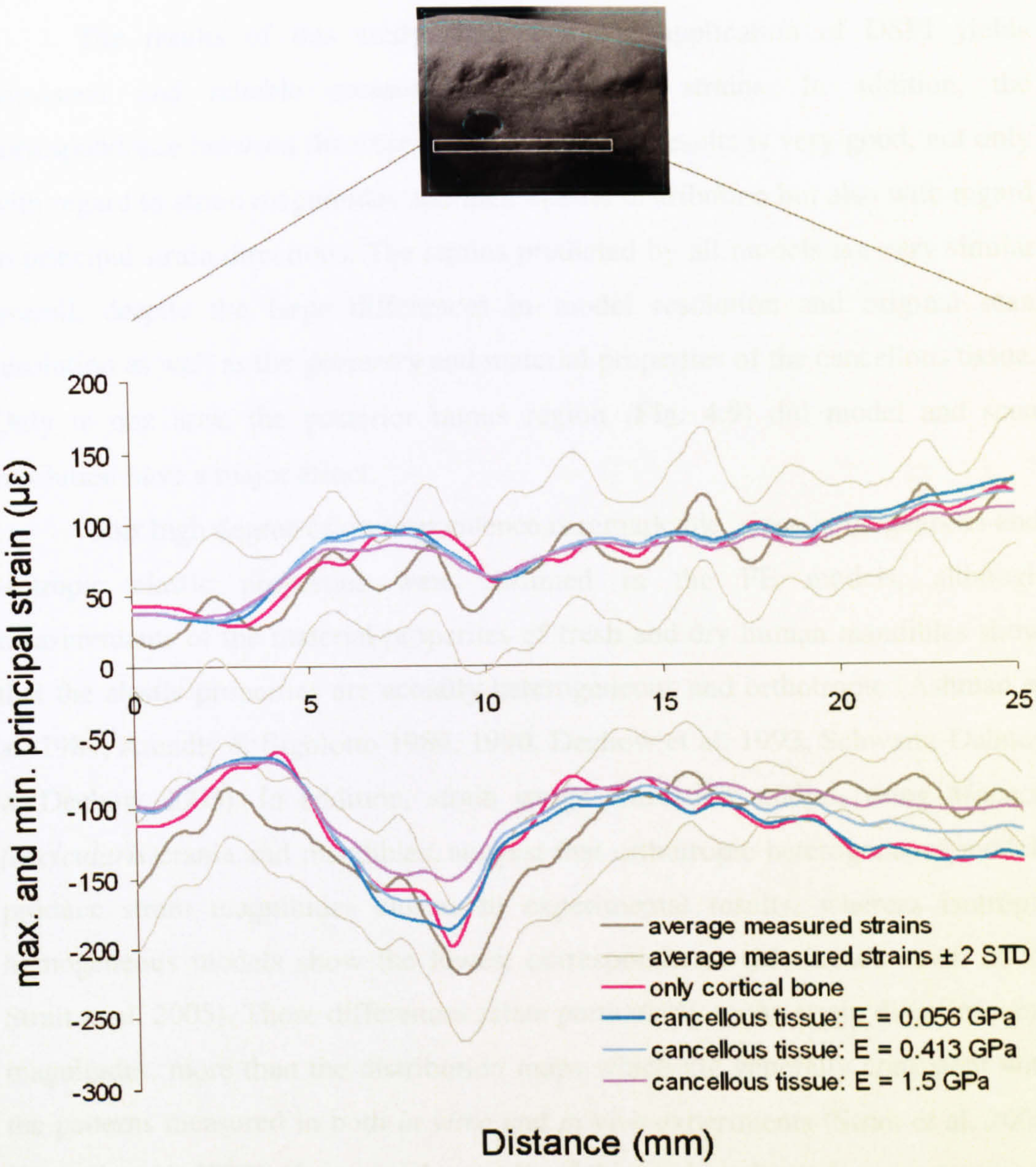

Fig. 4.12. Comparison of the mean experimental and predicted maximum and minimum principal strain profiles through the mandibular corpus (applied load = 250 N). The models differ with regard to the geometry and the material properties of the cancellous bone tissue.

4.4. Discussion

The results of this study show that the application of DSPI yields consistent and reliable measurements of bone strains. In addition, the correspondence between the experimental and FEA results is very good, not only with regard to strain magnitudes and their spatial distribution but also with regard to principal strain directions. The strains predicted by all models are very similar overall, despite the large differences in model resolution and original scan resolution as well as the geometry and material properties of the cancellous tissue. Only in one area, the posterior ramus region (**Fig. 4.9**) did model and scan resolution have a major effect.

This high degree of correspondence is remarkable, since homogeneous and isotropic elastic properties were assumed in the FE models, although measurements of the material properties of fresh and dry human mandibles show that the elastic properties are actually heterogeneous and orthotropic (Ashman et al. 1984, Arendts & Sigolotto 1989, 1990, Dechow et al. 1993, Schwartz-Dabney & Dechow 2003). In addition, strain gauge validation studies, using *Macaca fascicularis* crania and mandibles, suggest that orthotropic heterogeneous models produce strain magnitudes closest to experimental results, whereas isotropic homogeneous models show the lowest correspondence (Marinescu et al. 2005, Strait et al. 2005). These differences relate particularly to the strain directions and magnitudes, more than the distribution maps which are generally consistent with the patterns measured in both *in vitro* and *in vivo* experiments (Strait et al. 2005, Kupczik et al. 2007). However, the results of this study indicate homogeneous and isotropic elastic properties are sufficient, at least in this experimental setup, to accurately predict strain distribution, strain magnitudes as well as strain directions. It is possible that varying values for the elastic properties might improve the fit between our measured and predicted strains, but given the quality of correspondence between the experimental and modelling estimates the gains are likely to be small.

The results also have implications regarding model creation. Unlike most FEA studies, which use tetrahedra or polyhedra of varying shape resulting in smooth model surfaces (Rayfield et al. 2001, Strait et al. 2005), the FE models in this study have been created by the direct conversion of voxels into brick elements (Fagan et al. 2007). Although this meshing approach is very straightforward and

fast, the use of brick elements creates an artificially stepped model surface. However, the comparison between the FEA results and the DSPI measurements indicates that the surface strains can still be predicted accurately by brick element models with a sufficient number of elements. The predictions of the high-resolution μCT model come very close to the experimental results and downsampling the model to a much larger element size has only a small effect on the accuracy. This indicates that a brick element size of 0.488 mm in all directions is already sufficient to model surface strains accurately.

The model based on the low-resolution medical CT scan also produced realistic results. Only in one region, the posterior half of the ramus, did it fail to adequately predict the strain field. Nowadays, the application of μCT scanning allows the creation of highly detailed FE models (van Rietbergen et al. 2003, Verhulp et al. 2008), but the large data sets require significant computing power and processing time. The finding that the two models based on a high-resolution μCT scan and a low-resolution medical CT scan predict similar strains, indicates that FE models based on relatively low resolution CT scans can be sufficient, especially if only the relative strain distribution across the bone surface is of interest, but the model resolution needs to be increased, when strain gradients in small areas are to be assessed accurately.

By comparing the results of the medical CT scan model with those of the downsampled μCT scan model, which both have the same element size of 0.488 mm in all directions, the effect of the scan resolution can be evaluated in isolation from element size. As expected, in those areas where the medical and original high-resolution μCT models differ, particularly in the posterior ramus region, the downsampled μCT model predicts strain values that come closer to the measured strains. **Figures 4.4** illustrates the most likely reason for this. At the height of the profile measurements, the ramus is filled with a relatively dense trabecular network. Due to the low spatial resolution and the blurriness of the images of the medical CT scan (**Fig. 4.3**), thresholding based on the half-maximum height protocol results in a model with an artificially solid cross-section in this region, since the attenuation values of bone and air are averaged within voxels (**Fig. 4.4**). The transverse sections though the corpus at the border of the mental foramen show little differences between the segmentation results based on the medical and the μCT scan. Accordingly, the strain profiles from the same location are very

similar between the models. These results show that scan resolution does not necessarily have a global effect on the strains, but that the effects can vary between different regions within the same specimen, so that the strain pattern across the surface might be altered slightly. FEA studies that compare the results from models based on scans with varying resolution need to take this into account as a potential source of error. Ideally, all specimens of a sample are scanned with the same scanner and identical scanning parameters to achieve maximum comparability.

Interestingly, modelling the cancellous bone in different ways has only a small effect on the strains and none of the respective models is consistently better in predicting the experimental strains. This is surprising, since the range of Young's modulus values assigned to the cancellous tissue as an extra material cover the relatively large range of published values from measurements of human mandibular cancellous tissue (Misch et al. 1999, Giesen et al. 2001). The highest value of 1.5 GPa, which was taken from an FE study (Field et al. 2008), is even above this range as well as above the range of Young's moduli for cancellous tissue in other human bones, which spreads from 0.004 to 0.350 GPa (Hodgskinson & Currey 1992). Nonetheless, the model with this high Young's modulus predicts the experimental strains as well as the other models. The strain differences between the models with cancellous tissue as an extra material and the original downsampled μCT model, in which large trabeculae were segmented by threshold segmentation, are slightly larger, but it cannot be stated that any of these models is better in predicting the measured strains. It seems that a semi-automatic threshold segmentation can yield results that are as good as those from a time-consuming manual segmentation of cortical bone and cancellous tissue.

Again, this is surprising since the resolution of the μCT scan did not allow to extract the whole trabecular network by one threshold, so that only large trabecular struts are present in the model. In addition, the downsampling of the model resulted in a further reduction of the network (**Fig. 4.4**). However, a major advantage of this approach is that it takes the gross geometry of the trabecular network into account and thus the variation in its density within the bone. When the cancellous bone tissue as a whole, including the trabeculae as well as the holes between them, is modelled as one material, such density variations can be simulated by heterogeneous material properties, but this requires time-consuming

manual image processing or an algorithm that automatically converts the attenuation value for each voxel into a Young's modulus value. If heterogeneous properties are assigned manually, then there is the problem that published data on the mechanical properties of cancellous tissue in the human mandible are insufficient for modelling the variation within the whole bone (Misch et al. 1999, Giesen et al. 2001). Modelling the gross geometry of the trabecular network and applying the same mechanical properties to cortical bone and to the cancellous bone material (i.e. the bone within each trabecular) appears to be more straightforward. Experimental measurements and FEA studies have shown that the Young's modulus of human cancellous bone material is indeed very similar to that of cortical bone (see Currey 2002:149 for an overview of published values). These measurements refer to cancellous bone in long bones, but it can be assumed that the values are also similar for cancellous bone in the mandible. The FE models in the subsequent studies (Chapters 5 to 10) will, therefore, follow the same approach: trabeculae will be segmented by thresholding and the same mechanical properties as for cortical bone will be applied to them.

Finally, this study shows that the application of DSPI to the evaluation of bone strains is very promising. Only two potential drawbacks of this method can be reported. Firstly, the load applied during measurement must be small since there is an upper limit to the number of displacement fringes that can be recorded (Archbold et al. 1970). Therefore, larger loads have to be divided into smaller, incremental loads and the experimental setup needs to be adjusted accordingly. Secondly, DSPI is a highly sensitive measurement technique, thus mechanical vibrations or any motion caused by inappropriate fixture of the specimen can result in uninterpretable data (Yang & Ettemeyer 2003, Yang et al. 2007). Consequently, very stable and controlled loading is required, which induces some practical limitations for experimental studies. It is likely that the variance of our observed strain values can be partly explained by instabilities in our experimental setup, for example, some minor movements might have occurred at the condyles and at the points of contact between the tooth roots and the alveolar sockets during loading.

However, the advantages of DSPI compared to strain gauges outweigh the few drawbacks of this technique. The DSPI equipment is easy to handle, the application non-destructive and the measured strain distribution over the surface

can be visualised and directly compared with equivalent strain contour plots in FE models. In addition, the method can measure the strain on curved surfaces and around features, such as in the mandible presented here. Since DSPI is a full-field measurement technique, many data points are generated with each measurement, so that statistical methods can be applied to test hypotheses. In this study, only one-dimensional data from profiles across the surfaces have been used for a quantitative comparison between experimental and FEA results. For future validation studies however, the application of DSPI offers the opportunity to apply statistical methods that compare the complete 3D strain or displacement pattern of the DSPI maps with the FEA results.

Chapter 5: Modelling the human mandible under masticatory loads. Which input variables are important?

5.1. Introduction

The validity of an FE model depends on several factors: its geometry, the material properties assigned to the model as well as the external forces and constraints, which are applied. The relative importance of these for the results of the FEA can be estimated by sensitivity analyses (Dar et al. 2002, Marinescu et al. 2005, Ross et al. 2005, Strait et al. 2005). During a sensitivity study, one or more input parameters are varied and the effect on the resulting stresses and strains is quantified. Such an estimate of the relative importance of the different input parameters is particularly required when decisions have to be made as to how best to simplify the model, for example, in order to save computing time or because of limitations of the software used, without severely compromising the accuracy of the results. Ideally, sensitivity studies are combined with validation studies in order to estimate not only how large the effect of changing one variable is, but also to assess which combination of parameters leads to the most accurate results.

If the function of a bone in the living organism is to be simulated, model geometry and material properties can be validated against data from *in vitro* experiments (Chapter 4). However, the forces and constraints depend on attributes of the system, which cannot be simulated with *in vitro* experimental setups. In the case of mandibles, these are, for example, the orientation, forces and activation patterns of the masticatory muscles and how movements of the mandibles are guided and restricted by the intact temporomandibular joints (TMJs). In order to test whether the forces and constraints applied in the model are realistic, the predicted strains would therefore have to be compared against the bone strains measured *in vivo*. *In vivo* strain data have been collected for mandibles of a number of different mammals including, for example, bovids and camelids (Williams et al. 2009), sheep (Thomason et al. 2001), hyraxes (Lieberman et al. 2004a), pigs (Marks et al. 1997, Liu & Herring 2000), opposums (Crompton 1995) and non-human primates (Hylander 1979b, 1984, Hylander & Crompton 1986, Hylander et al. 1987, Ross 1993, Ross & Hylander 1996, Hylander et al. 1998). For ethical reasons it is not possible to measure *in vivo* strains in the human mandible. This study is therefore restricted to the comparisons of the overall strain

distributions and ranges of strain magnitudes known from animal experiments, in order to test the validity of the used modelling approaches.

Prior FEA studies that have tried to simulate masticatory loads, differ significantly with regard to input variables: for example, whether periodontal ligament (PDL) and the soft tissue in the TMJs is modelled or whether forces or constraints are applied to bite points and joint facets. These differences regarding basic input variables might have a major influence on the results, but often published FEA results are not accompanied by sensitivity studies, which have assessed the consequences of changing input parameters. In the following, it is reviewed how prior FEA studies vary with regard to some of these input variables and briefly described why these variables are relevant.

Whether PDL should be modelled as an extra material with specific material properties in order to obtain realistic bone strains, is of major importance for the model creation process. In general, FE models of whole mandibles or crania are created based on CT scans of dry specimens, where PDL is no longer present, or in the case of fresh specimens the resolution of the scan is not sufficient enough to allow automatic threshold segmentation. Therefore, the inclusion of PDL as an extra material requires time-consuming manual segmentation: painting with a virtual brush around each tooth root in the CT slices. Most FEA studies of non-human crania and mandibles do not include a layer of PDL with specific material properties (Rayfield et al. 2001, Strait et al. 2007), but FEA studies of human mandibles commonly include it (Korioth et al. 1992, Korioth & Hannam 1994a, Vollmer et al. 1999, Reina et al. 2006, Ichim et al. 2007b). FEA studies, which model the PDL differ significantly in the material properties they assign to it, ranging from different types (e.g. homogeneous vs. heterogeneous) of linear elastic material properties (Andersen et al. 1991, Korioth et al. 1992, Korioth & Hannam 1994a, Reina et al. 2006, Ichim et al. 2007b), to bilinear and nonlinear elastic material properties (Vollmer et al. 1999, Cattaneo et al. 2005, Kober et al. 2006b, Cattaneo et al. 2009). Only a few studies have validated the chosen material properties against experimental data or included sensitivity analyses (Andersen et al. 1991, Rees & Jacobsen 1997, Cattaneo et al. 2005, Ichim et al. 2007b). A sensitivity study using a human mandible found that including the PDL as a bilinear elastic material results in lower strains in the alveolar bone and that the PDL thus functions as a force absorbing structure

(Kober et al. 2006b). However, the effect on other regions of the mandible has not yet been investigated with FEA, so that further sensitivity studies need to be conducted.

How the reaction forces at the TMJ are modelled in FEA studies is also highly variable. Some authors model these as forces, which they apply either to the mandibular condyles or the glenoid fossae (Rayfield et al. 2001, Rayfield 2005), whereas in FEA studies of human mandibles constraints are usually applied to the joints (Haskell et al. 1986, Korioth et al. 1992, Korioth & Hannam 1994a, Reina et al. 2006, Ichim et al. 2006a, 2007b). The latter is either done by constraining the mandibular condyles directly (Haskell et al. 1986, Reina et al. 2006), or indirectly by creating layers of soft material around the condyles to mimic the buffering effect of the cartilage in the TMJ (Korioth et al. 1992, Tanne et al. 1993, Korioth & Hannam 1994a, Tanaka et al. 1994, Kober et al. 2004, 2006a, 2006b, Ichim et al. 2007b). As with the PDL, the creation of such additional layers around the condyles or of a simplified TMJ requires time-consuming manual image processing. It is therefore worth testing, whether this additional work really results in more realistic loading conditions. To date, only one sensitivity study seems to have tested the effect of including TMJ soft tissue in an FE model of a human mandible, with the conclusion that it has a major effect on the strains in the mandible (Kober et al. 2004).

Prior FEA studies also differ in how they model the bite force acting on the dentition. Some authors apply a force to the respective teeth (Hart et al. 1992, Rayfield et al. 2001, Rayfield 2005, Witzel & Preuschoft 2005, Pierce et al. 2008), but in most FEA studies the occlusal surface of the teeth is constrained and the bite force is thus modelled as a reaction force (Haskell et al. 1986, Korioth et al. 1992, Korioth & Hannam 1994a, Dumont et al. 2005, Reina et al. 2006, Ichim et al. 2006a, 2007b, Strait et al. 2007). Both modelling approaches can be biologically justified. Applying a force to a tooth makes sense as the force acting on the tooth does not only depend on the action of the masticatory muscles, but also on the material properties of the respective food item. On the other hand, one can argue that during mastication no external force is applied to teeth, only when the teeth are used as a clamp in combination with the hands in order to, for example, break very large objects. The forces that enter the system are thus only the muscle forces, which result in reaction forces at the joint surfaces and the bite

point. Although it is likely that the two different approaches to the modelling of bite forces in FEA will result in different findings, there are no published data that allow an assessment of this.

In addition, there is no consensus about the direction of constraints in FE models of crania and mandibles when masticatory loads are to be modelled. With regard to the constraints at the bite point, two different approaches are used in the literature: constraints in all three axes (Dumont et al. 2005, Strait et al. 2007) or only in the axis perpendicular to the occlusal plane (Haskell et al. 1986, Korioth et al. 1992, Korioth & Hannam 1994a, Reina et al. 2006, Ichim et al. 2006a, 2007b). Theoretically, both can be justified from a biological point of view. In the case of perfect occlusion of all teeth, there should be no transverse movements during the powerstroke of mastication after the breakdown of a food item or during clenching. However, in the case of animals specialised on grinding, or in malocclusion or when teeth are highly worn, substantial transverse movements should occur. The constraints used at the TMJ also differ between studies. In many FEA studies models are constrained at the TMJ in all three axes (Korioth et al. 1992, Korioth & Hannam 1994a, Dumont et al. 2005, Strait et al. 2007), but in some studies the constraints are limited to the vertical axis alone or the vertical axis and one horizontal axis (Witzel & Preuschoft 2005). In general, each of these FEA studies uses only one set of constraints and the effects of altering the directions of the constraints are not examined.

Finally, it is important to know whether a change in the orientation of muscle vectors has a large effect on the FEA results. The orientation of the muscle lines of action can be obtained from measurements on dissected cadavers or from CT and MRI scans of cadavers or living animals and humans (Koolstra et al. 1990, van Spronsen et al. 1997). It is also possible to estimate the lines of action by connecting origin and insertion of the masticatory muscles in dry skulls (O'Connor et al. 2005). Many FEA studies use muscle vector orientations that have been obtained from sources other than measurements from the same individual (Reina et al. 2006, Strait et al. 2009). This procedure is necessary, when only isolated mandibles or crania are available, which is particularly the case with fossil specimens. However, because of interindividual variation in cranial morphology, the lines of action between different individuals can have different orientations, because the spatial relationship between origin and insertion

depends on cranial morphology. Consequently, there is a need to assess the effects of changes in the orientation of muscle vectors. A prior sensitivity study on a macaque mandible showed that the orientation of external forces has a significant effect on FEA results (Marinescu et al. 2005).

This sensitivity study aims to estimate the relative importance of the input variables described above. By using an FE model of a dry human mandible, it will quantify and evaluate the effects of:

1) adding PDL as an extra material with specific mechanical properties
2) adding simplified TMJs with layers of soft tissue material
3) modelling the bite force as an external force vs. as a constraint
4) altering the directions of constraints
5) changing the orientations of muscle force vectors

In addition, the resulting strain magnitudes are compared with *in vivo* data from animal experiments. Based on these comparisons, and by including published data about strain thresholds for bone remodelling and fracture, it will be discussed how to create realistic FEA models of a human mandible under masticatory loads within the limits of the used FEA software.

5.2. Material and methods

The FE models for this study were created based on a µCT scan of a dry human mandible (H-A 002) obtained with an X-Tek HMX 160 µCT system. The two halves of the specimen were scanned separately, since the mandible was slightly above the size limit for this µCT scanner. Because of pre-mortem loss of the right third molar, only the CT scan of the intact left half was then used for further image processing. The primary reconstruction resulted in a 16-bit TIFF image stack with a voxel size of 0.12 mm in all three directions, but in order to save computing time, the stack was downsampled, so that the voxel size was increased to 0.24 mm in all three directions.

Image segmentation was performed with Amira. Bone and teeth were separated from the surrounding air by a user-defined density threshold based on the HMH protocol (Ullrich et al. 1980, Spoor et al. 1993, Fajardo et al. 2002, Coleman & Colbert 2007). After the threshold segmentation a ca. one to two

voxel thick (= 0.24-0.48 mm) layer of periodontal ligament was created by painting around each tooth root (**Fig. 5.1**). This was easily performed since the borders of the tooth roots and of the surrounding alveolar bone were clearly visible in the CT slices. The resulting 3D model of the left hemimandible was then mirror-imaged in order to create a model of an intact mandible with complete dentition. An additional model with simplified TMJs was created by adding two blocks (ca. 20 x 15 x 15 mm) including the articular surfaces of glenoid fossae, which had been segmented based on a medical CT scan of a human cranium. These blocks were positioned above the condyles using measurements taken from a magnetic resonance scan of a human head. On each side the space between the glenoid fossa and the articular surface of the condyle was then manually filled so that a layer of ca. 3 mm (**Fig. 5.2**) was created, which comes close to thickness measurements of the TMJ soft tissue in human cadavers (Hansson et al. 1977).

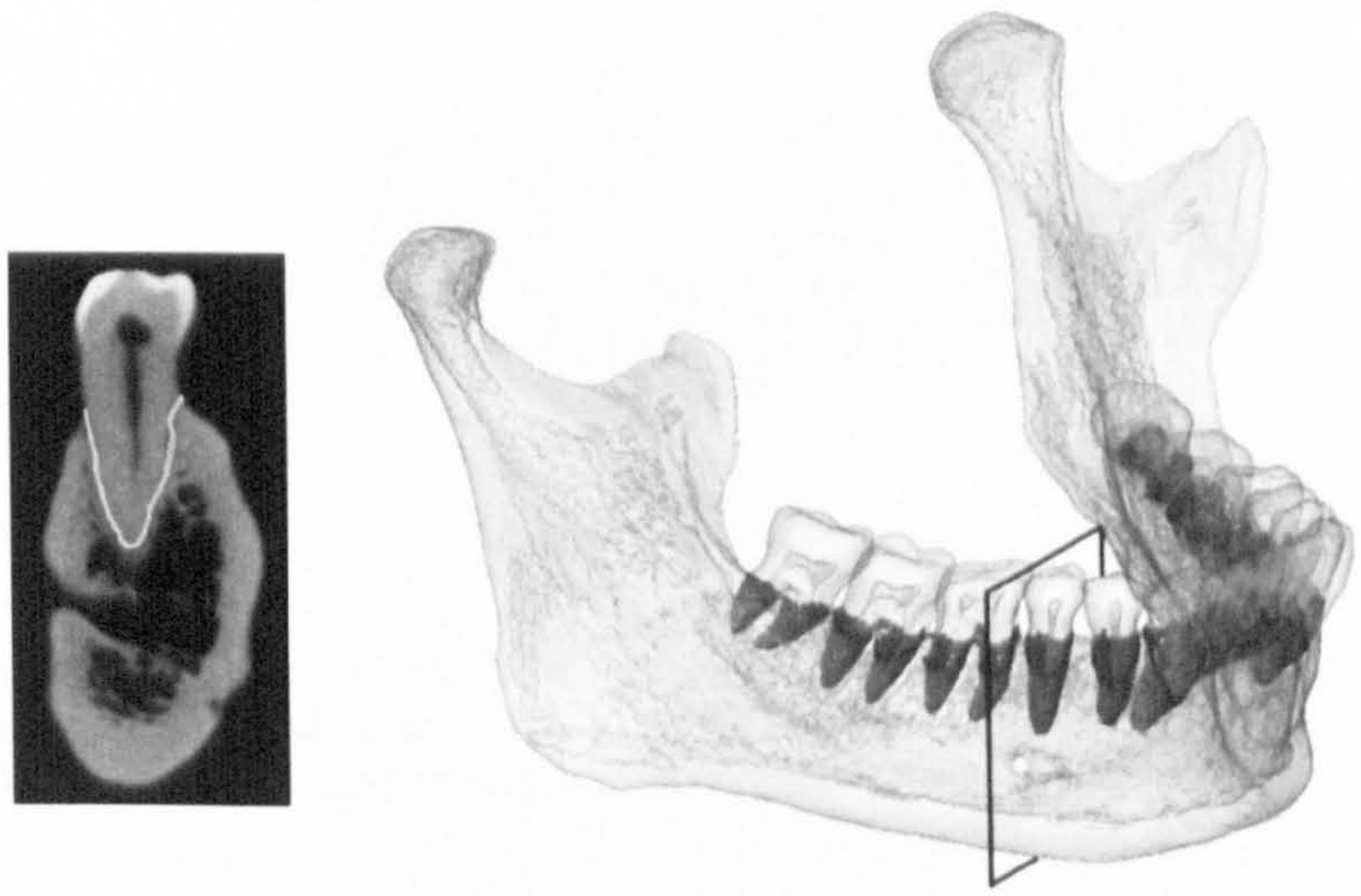

Fig. 5.1. Creation of periodontal ligament (PDL) in a CT-based 3D model of the mandible H-A 002. Left image: coronal CT slice with manually selected PDL (white line). Right image: 3D model with completed PDL (dark grey) within the transparent mandible.

The final models were transformed into FE meshes with element numbers of ca. 2.8 (no TMJs) and 4.4 million (with TMJs). Isotropic material properties of 17 GPa for Young's modulus and 0.3 for Poisson's ratio were assigned to bone and teeth, including the blocks representing cranial bone at the TMJs, whereas a Young's modulus of 0.003 GPa and a Poisson's ratio of 0.45 were chosen for the periodontal ligament as well as the soft tissue layers in the TMJs. These are values that lie within the published range for the cortical bone of human mandibles (Ashman & van Buskirk 1987, Arendts & Sigolotto 1989, 1990, Dechow et al. 1993, Schwartz-Dabney & Dechow 2003), PDL (Tanne et al. 1987, Andersen et

al. 1991, Jones et al. 2001, Poppe et al. 2002, Dorow et al. 2003) and the soft tissue of the TMJ (Tanne et al. 1991, Chen et al. 1998, Beek et al. 2000, Koolstra & van Eijden 2005).

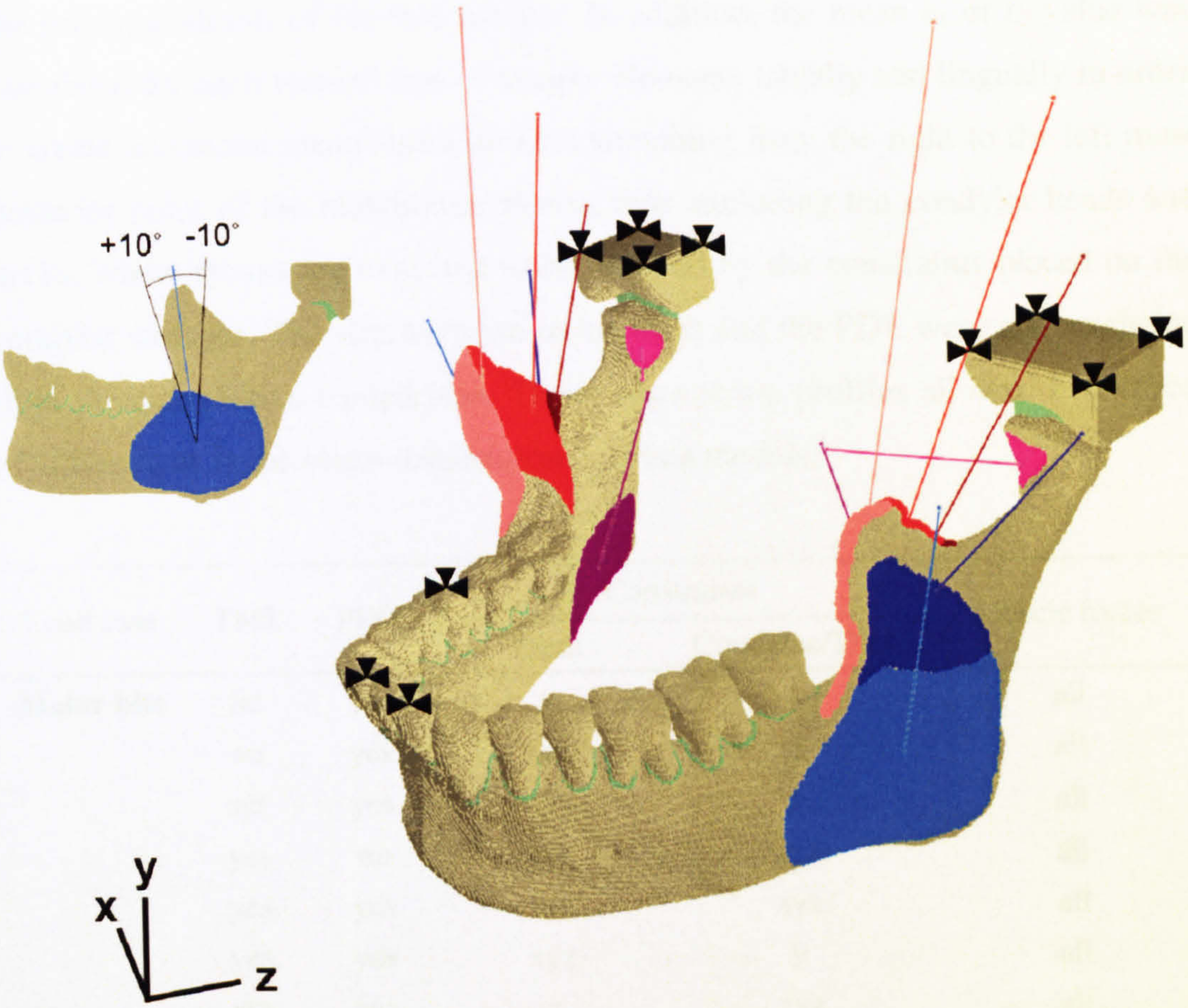

Fig. 5.2. FE model of the mandible H-A 002 including PDL and simplified TMJs. The small triangles indicate constrained nodes. Small image: rotation of the vector for the superficial masseter by 10° anteriorly and posteriorly.

Two bites were simulated: a bite on the right first molar and in addition an incisal bite using the muscle force estimates listed under 3.8. For each bite the model attributes and boundary conditions were varied, resulting in 14 different load cases overall (**Table 5.1**). These load cases do not represent all potential combinations of the varied input variables. Some theoretically possible combinations of constraint axes at the teeth and joints would be insufficient for the successful solution of the model and were thus not tested. In addition, the effect of altering each input variable was in general only tested for one combination of constraint directions in order to limit processing time.

After the solution, element strain values were calculated based on the nodal displacements and the maximum (ε_1) and minimum principal strains (ε_3) were extracted from ca. 1200 evenly distributed elements on the periosteal bone

surface (**Fig. 5.3**). The overall difference in strain values between models was quantified by calculating the Euclidean distance between each pair of models. This was computed as the square root of the sum of squared differences between the principal strains of the two models. In addition, the mean ε_1 or ε_3 value was calculated for each vertical row of sample elements labially and lingually in order to create horizontal mean strain profiles stretching from the right to the left most posterior point of the mandibular ramus, thus excluding the condylar heads and necks, where strains are expected to be affected by the constraints placed on the condylar surfaces. The strains in the in the teeth and the PDL were also excluded from the quantitative comparison. These mean strain profiles allowed evaluation of differences in the strain distribution between models.

Load case	TMJ	PDL	Constraints		Muscle forces
			Teeth	Condyles/TMJ	
Molar bite	no	yes	y	xyz	all
	no	yes	xyz	yz	all
	no	yes	xyz	y	all
	yes	no	xyz	xyz	all
	yes	yes	xyz	xyz	all
	yes	yes	xyz	y	all
	yes	yes	y	xyz	all
	yes	yes	50 N	xyz	all
	yes	yes	xyz	xyz	sup. mass.
	yes	yes	xyz	xyz	sup. mass. +10°
	yes	yes	xyz	xyz	sup. mass. –10°
Incision	no	yes	y	xyz	all
	yes	yes	y	xyz	all
	yes	yes	xyz	xyz	all

Table 5.1. Varied model attributes and boundary conditions. The axes have the following orientations: x = medio-lateral axis, y = axis perpendicular to the occlusal plane, z = axial axis. In order to test the effect of changing muscle vector orientation, the angle of the line of action of the superficial masseter (sup. mass.) with the z-axis was increased by 10° (point of origin moved posteriorly) and decreased by 10° (point of origin moved anteriorly).

Additionally, differences in strain patterns between two models with identical geometry were compared by subtracting the strain value for each element of one model from the value for the same element in the second model with a simple Windows-based application that complements VOX-FE and visualising the differences between all element strain values of the two models as a colour-coded

map in VOX-FE. Differences in the strain orientations were evaluated by comparing the orientations of the maximum principal strain eigenvectors for the selected surface elements.

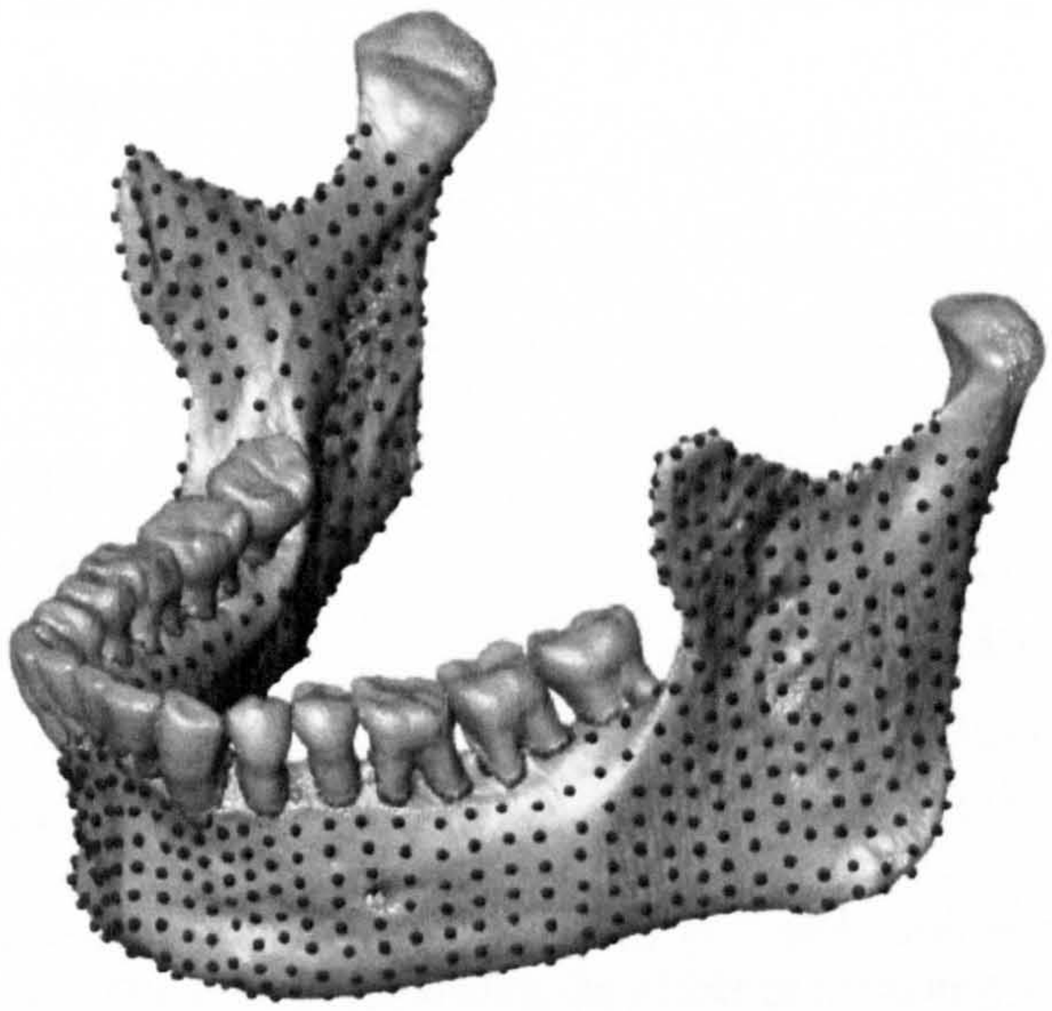

Fig. 5.3. Selected points for the extraction of surface element strains.

5.3. Results

Tables 5.2 to **5.4** show the Euclidean distances between the models. They indicate that the by far largest effect on the strains is measured when an external force is applied to the bite point instead of a constraint vertical to the occlusal axis, followed by the effect of including simplified TMJs and varying some directions of the constraints. Smaller effects are measured, when the orientation of the force vector for the superficial masseter is varied and PDL is included as an extra material.

The strain profiles (**Figures 5.5-5.10**) reveal that for most models the mean tensile and compressive strains are within the range of ±100 to 1000 με. Only the model, in which a force was applied to the bite point shows higher strains, and in the model without TMJ during an incisal bite, magnitudes below 100 με occur. In addition, magnitudes above 1000 με are observed at the posterior margins of the mandibular rami of several models.

As **Figure 5.5** shows, the presence of a PDL does not change the surface strains at the mandibular rami, but increases tensile and compressive surface strains on the mandibular corpus. The 3D visualisation of the strain differences (**Figure 5.4**) reveals that the increase in strains is largest (≥200 με) around the

alveolar sockets and in some areas of the anterior mandible. Tensile strains are increased at the base of the anterior mandible and compressive strains are increased in the region of the chin. In addition, a decrease of maximum and minimum principal strains occurs lingually below the working side premolars and the constrained M1 respectively.

Load cases	EDs for ε_1	EDs for ε_3
no PDL/PDL	2234	2696
no TMJ/TMJ (incisal bite)	7798	9460
no TMJ/TMJ (molar bite)	8524	11709
bite force/constraint at bite point	51400	55903
sup. mass. vector minus 10°	1190	1216
sup. mass. vector plus 10°	1458	1332

Table 5.2. Euclidean distances (ED) for maximum (ε_1) and minimum principal strains (ε_3) between different models. The models for testing the effect of including TMJs were constrained at the bite point in the y-axis and at the joints in all three axes. See **Table 5.1** for details of the boundary conditions in the other models.

	xyz-y-y	xyz-yz-yz	y-xyz-xyz
xyz-y-y		8658	8706
xyz-yz-yz	8159		2246
y-xyz-xyz	8130	2629	

Table 5.3. Euclidean distances for different constraints applied to the model without TMJs. The constraint directions are given in the following order: bite point - left condyle - right condyle. Values in the upper right half of the matrix represent distances for maximum principal strain. Values in the lower left half are the distances for minimum principal strain.

	xyz-xyz-xyz	xyz-y-y	y-xyz-xyz
xyz-xyz-xyz		6384	6158
xyz-y-y	8942		6992
y-xyz-xyz	7267	10643	

Table 5.4. Euclidean distances for different constraints applied to the model with TMJs Labelling and arrangement of the values as in **Table 5.3.**

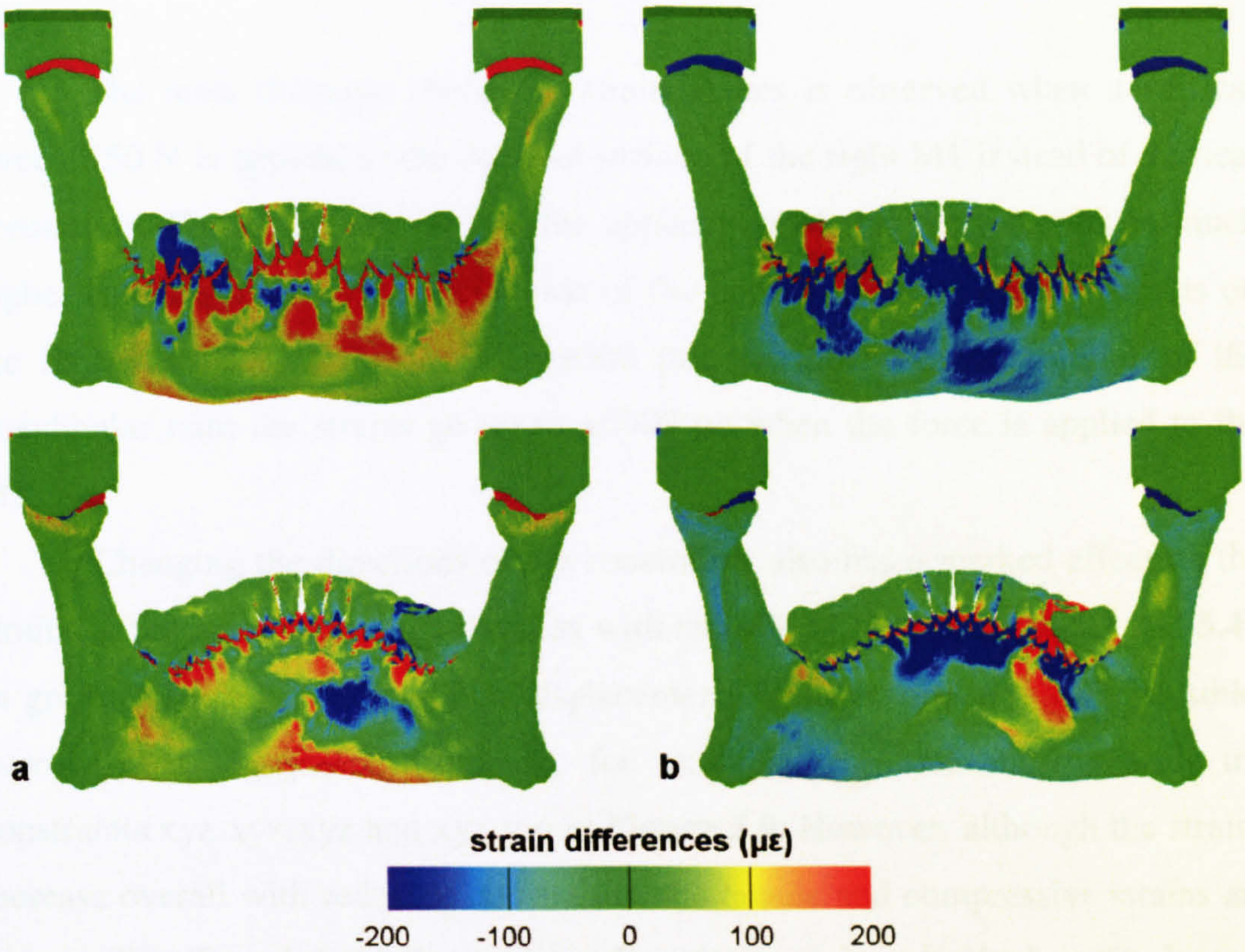

Fig. 5.4. Difference plots for the absence vs. presence of a PDL as an extra material: a) maximum principal strain, b) minimum principal strain. The upper row shows the labial and buccal surface, the bottom row the lingual surface.

Including simplified models of the TMJs has a much larger overall effect on the strains than including the PDL. Tensile and compressive surface strains are increased in almost the whole corpus and the balancing side ramus for both biting tasks when TMJs are included (**Figures 5.6** and **5.7**). The difference is especially pronounced during incisal biting. When nodes on the condyles are fixed during simulated incision, mean strain magnitudes in the corpus hardly exceed 200 με and very low strain magnitudes (≤100 με) are found below the constrained incisors. Constraining the condyles indirectly via simplified TMJs results in much higher tensile strains on the buccal side of the corpus (≥400 με) as well as higher compressive strains at the lingual symphysis (>1000 με). During the molar bite the largest increase in strains (by up to 400 με) is observed below the working side premolars and at the posterior margin of the balancing side ramus. This is especially true of compressive strains on the lingual side of the ramus, where mean magnitudes of ca. -2200 με are reached in the model with a TMJ. The strain differences over the right working side ramus during molar bite, are relatively small, unlike the large differences see in the corpus, apart from a decrease in

compressive strains on the lingual side of the posterior ramus margin (by ca. 700 με).

The most dramatic change in strain values is observed when a vertical force of 50 N is applied to the occlusal surface of the right M1 instead of vertical constraints. **Figure 5.8** shows that the application of this force results in much higher tensile strains on the labial side of the corpus and compressive strains on the lingual side (≤ ±1000 με vs. ~±500 με). At the posterior margins of the mandibular rami the strains go up to ±6000 με when the force is applied to the M1.

Changing the directions of the constraints also has a marked effect on the strains in the model without as well as with simplified TMJ (**Tables 5.3** and **5.4**). In general, strains increase when displacements in more directions are possible, especially at the joints. Compare, for example, the two models with the constraints xyz-xyz-xyz and xyz-y-y in **Figure 5.9**. However, although the strains increase overall with reducing constraints, the tensile and compressive strains are not equally affected. Labially and buccally, tension is increased when the degrees of freedom are reduced, whereas compressive strains stay relatively constant apart from the posterior part of the working side ramus. This increase in labial tension is especially pronounced around the constrained M1. Lingually, the effect on tensile and compressive strains is more similar, with compressive strains tending to increase more than tensile strains. In addition to this general pattern, the chosen constraints at the bite point have a local effect on the strains below the constrained M1. Constraining the occlusal surface of the M1 in all directions instead of only in the vertical axis results in an increase of tensile strains in this area.

Finally, varying the orientation of the vector for the superficial masseter on both sides of the mandible has a noticeable effect on the strains in the mandibular corpus (**Figure 5.10**). A more oblique orientation of the vectors (+10°) results in lower principal strains, whereas a more vertical orientation (-10°) of the vectors leads to higher strains. The latter increase is especially pronounced for labial compressive strains and for lingual tensile strains below the working side canine. **Figure 5.11** shows that unlike the magnitudes, the orientations of the principal strains change only slightly when the orientation of the superficial masseter is altered.

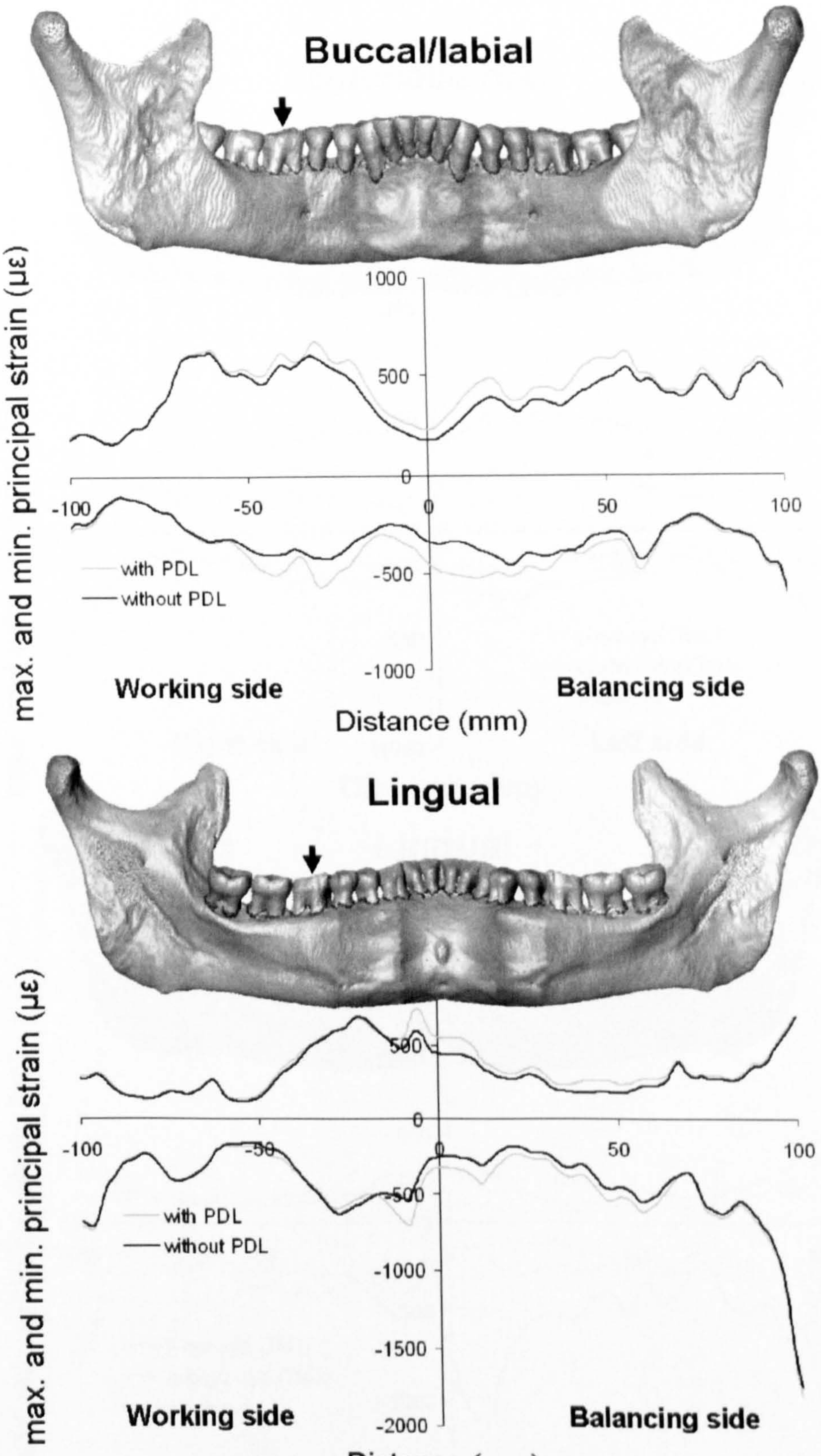

Fig. 5.5. Mean strain profiles showing the effect of including PDL as an extra material on the maximum and minimum principal strains. The models were constrained in all three axes at the TMJs and the occlusal surface of the right M1 (small arrow).

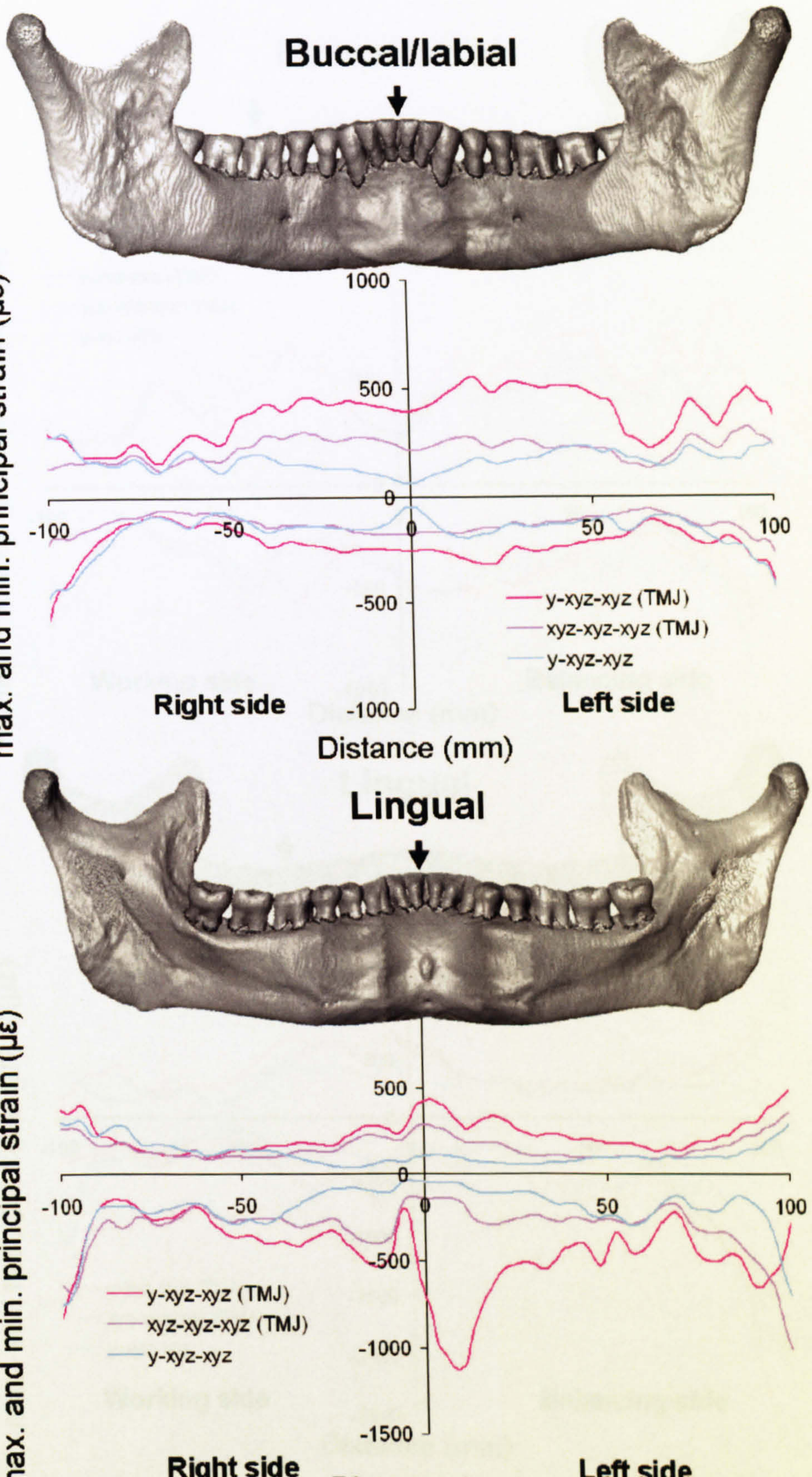

Fig. 5.6. Mean strain profiles for an incisal bite showing the effect of including simplified TMJs and constraining the bite point in two different ways (in all three axes vs. only in the y-axis). The TMJs or condylar surfaces are constrained in all three axes.

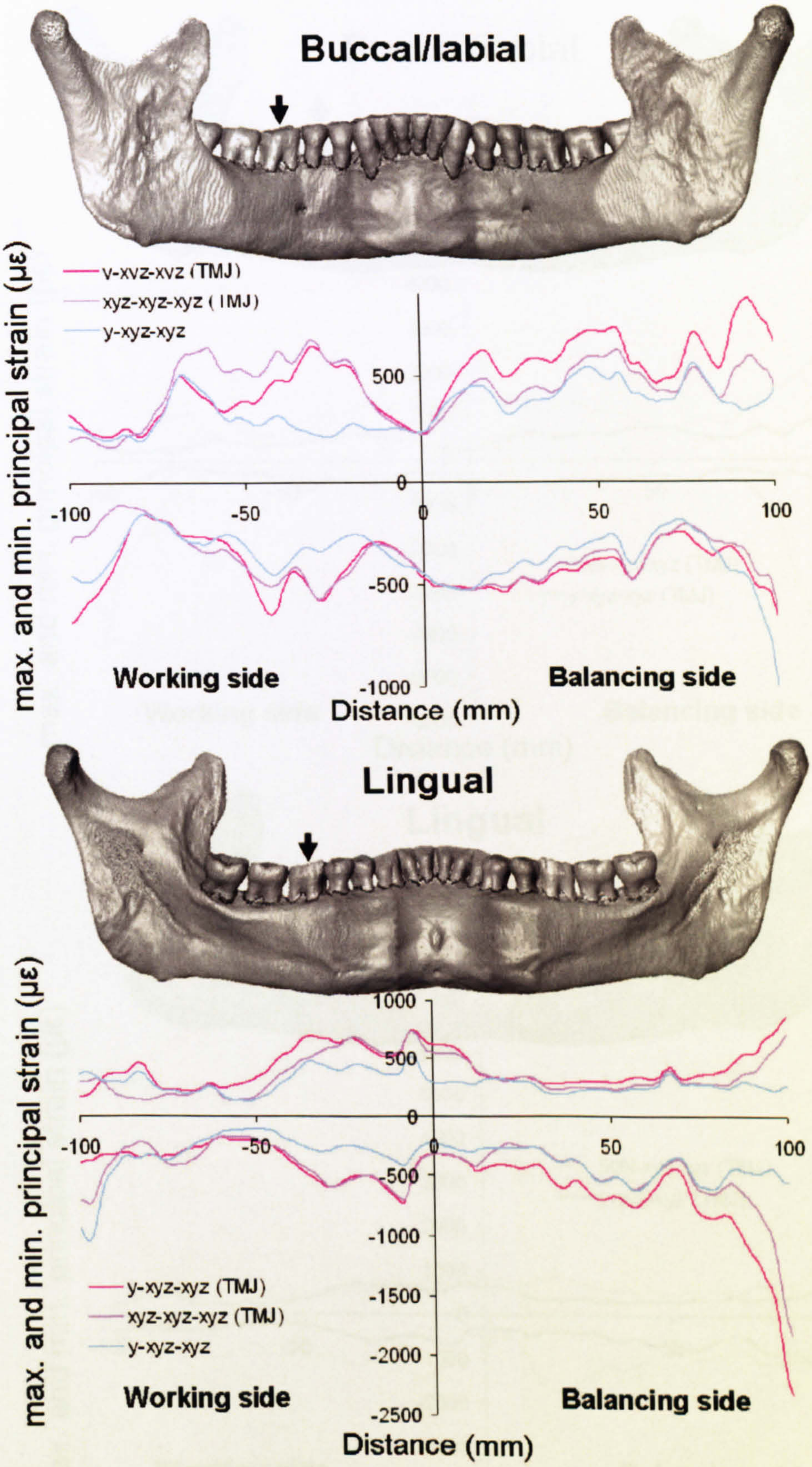

Fig. 5.7. Mean strain profiles showing the effect of including simplified TMJs and constraining the bite point in two different ways (in all three axes vs. only in the y-axis). The TMJs or condylar surfaces are constrained in all three axes as well as the occlusal surface of the right M1.

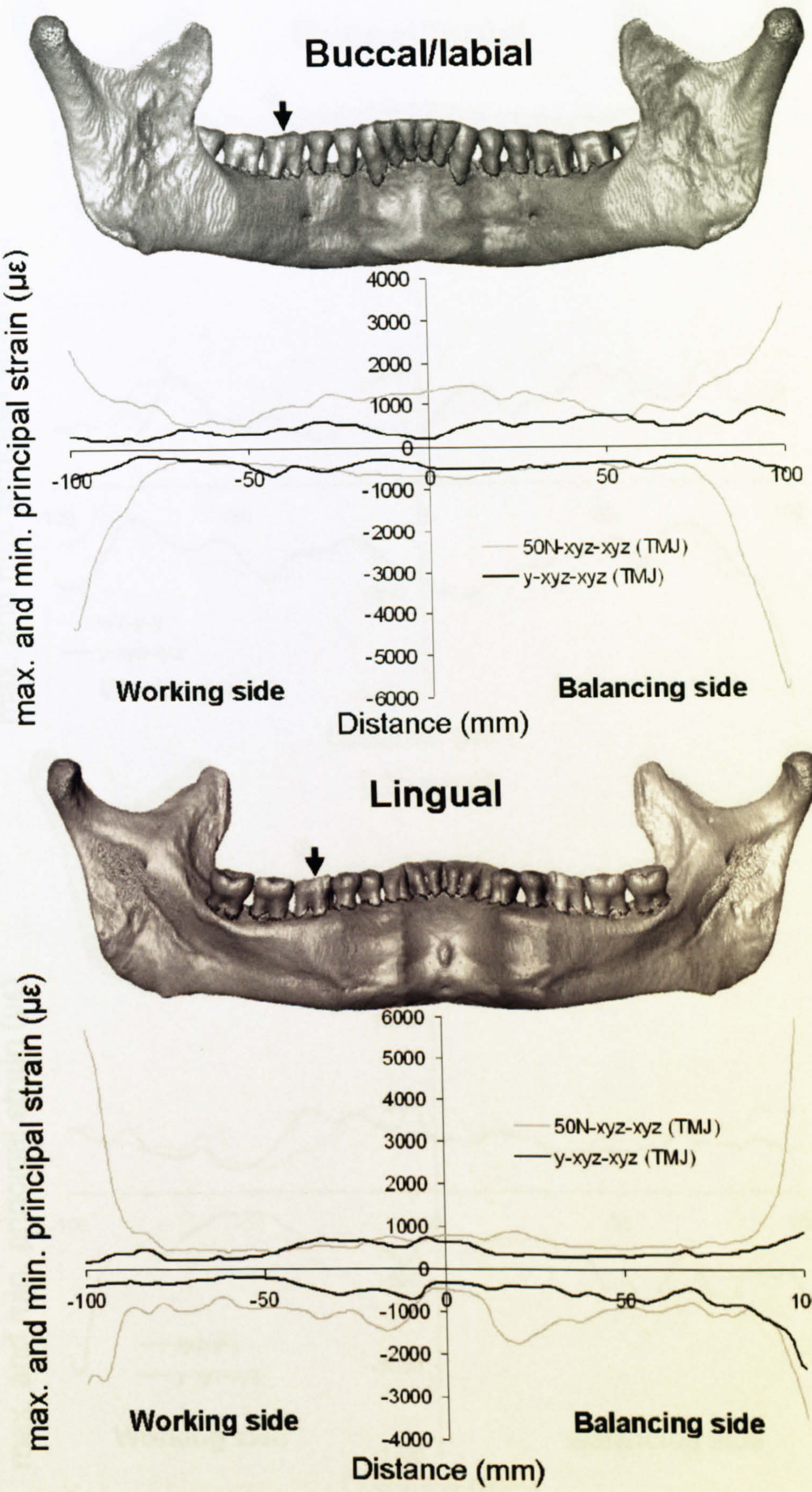

Fig 5.8. Mean strain profiles showing the effect of applying a vertical force of 50 N to the occlusal plane of the right M1 instead of a vertical constraint.

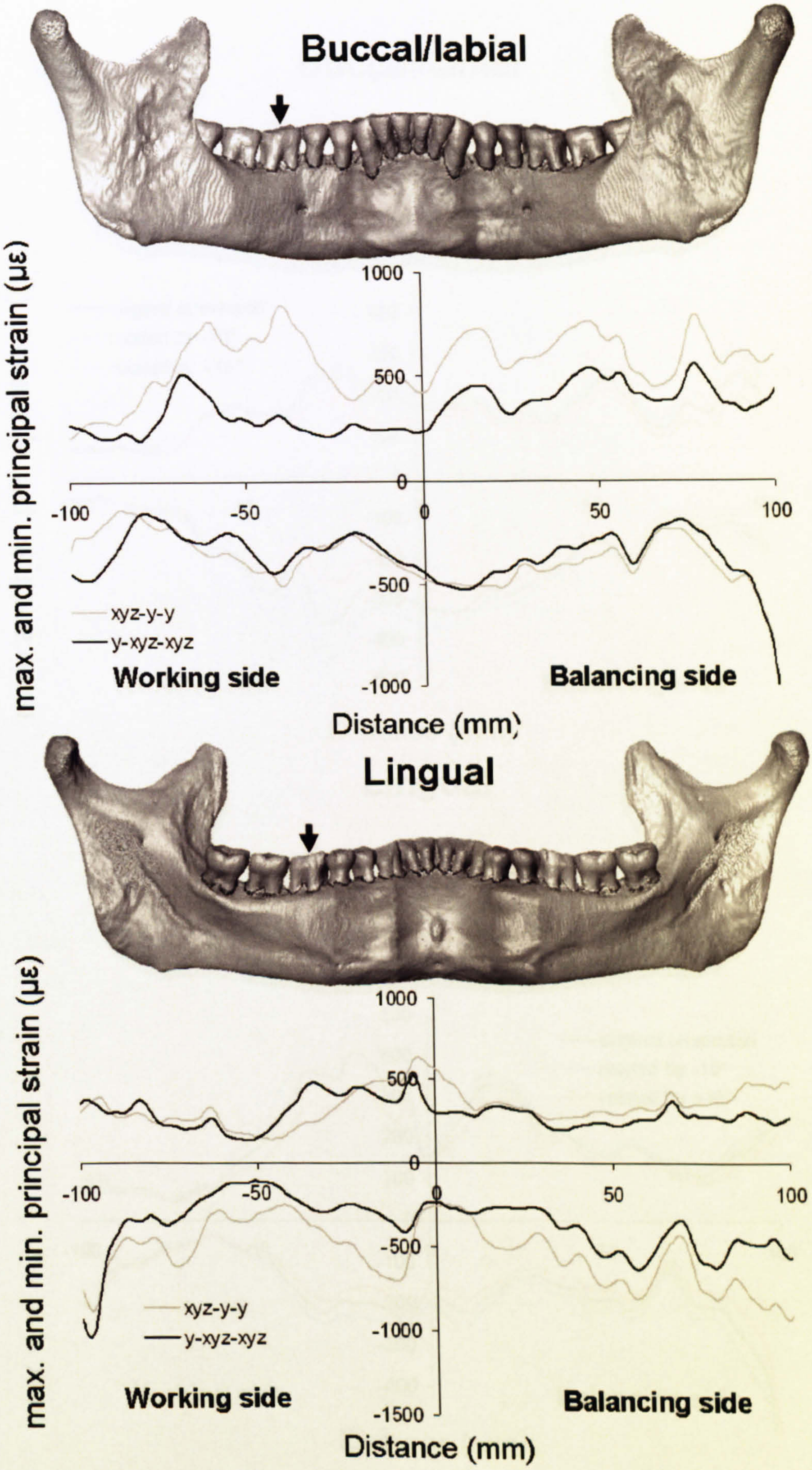

Fig. 5.9. Mean strain profiles showing the effect of altering the constraints at the bite point (right M1) and the condylar surfaces.

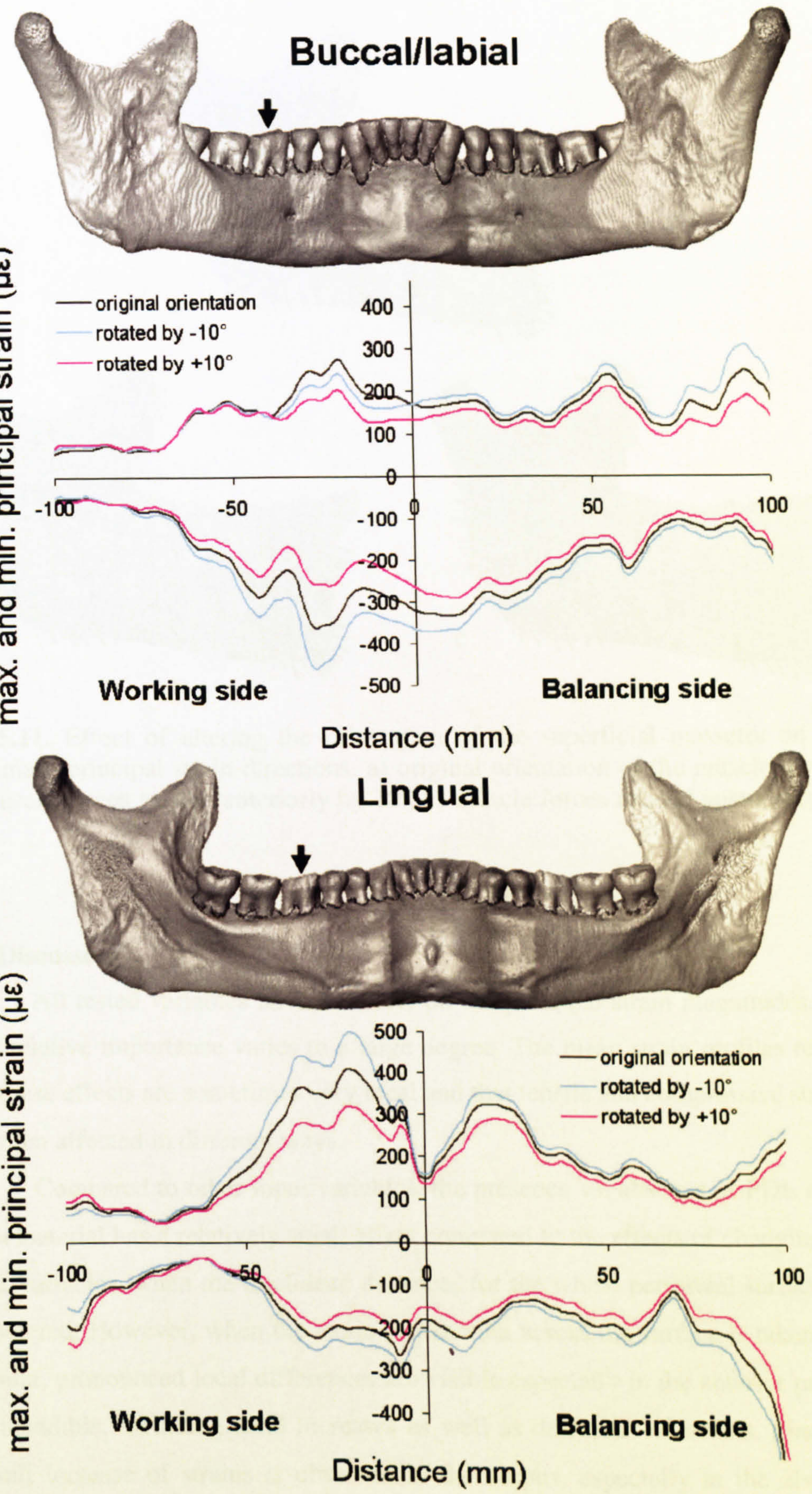

Fig. 5.10. Mean strain profiles showing the effect of rotating the vectors for the superficial masseter anteriorly and posteriorly by 10°.

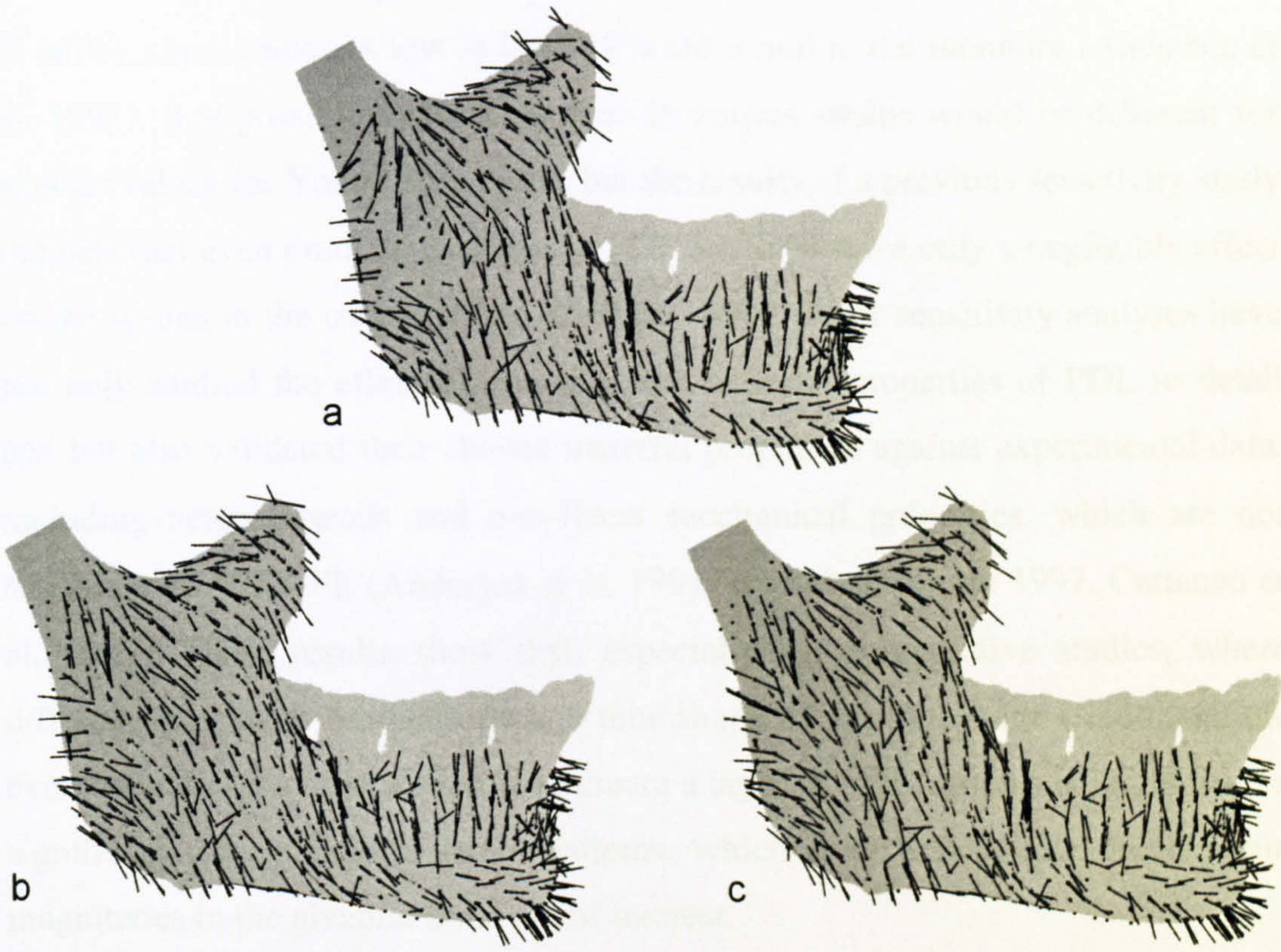

Fig 5.11. Effect of altering the orientation of the superficial masseter on the maximum principal strain directions. a) original orientation of the muscle forces, b) muscle forces rotated anteriorly by 10°, c) muscle forces rotated posteriorly by 10°.

5.4. Discussion

All tested variables have an effect on the principal strain magnitudes, but their relative importance varies to a large degree. The mean strain profiles reveal that these effects are sometimes very local and that tensile and compressive strains are often affected in different ways.

Compared to other input variables, the presence vs. absence of PDL as an extra material has a relatively small effect compared to the effects of changing the other variables, when the Euclidean distances for the whole periosteal surface are considered. However, when the strain distribution across the surface is taken into account, pronounced local differences are visible especially in the anterior part of the mandible, including local increases as well as decreases of strains. Since an overall increase of strains is observed in the corpus, especially in the alveolar region, a force absorbing function of the PDL as suggested by Kober and co-workers (2006b) cannot be confirmed, at least with the material properties chosen

for this study. The Young's modulus used for PDL is relatively high at 0.003 GPa (3 MPa), since values as low as 0.07 MPa are found in the literature (Andersen et al. 1991). It is possible that the increase in corpus strains would be different for smaller values for Young's modulus, but the results of a previous sensitivity study indicate that even dramatic changes in PDL stiffness have only a negligible effect on the strains in the corpus (Chen & Chen 1998). Other sensitivity analyses have not only studied the effect of changing the material properties of PDL in detail and but also validated their chosen material properties against experimental data, including heterogeneous and non-linear mechanical properties, which are not testable with VOX-FE (Andersen et al. 1991, Rees & Jacobsen 1997, Cattaneo et al. 2005). These results show that, especially for comparative studies, where differences in tooth morphology and thus shape of the PDL within the mandible exist between taxa, it is advisable to create a layer of PDL, since this might have a significant effect on local strain patterns, which is especially relevant if strain magnitudes in the alveolar bone are of interest.

Whether the mandibular condyles are constrained directly or indirectly via simplified models of the TMJs has a big effect on strain magnitudes (**Fig. 5.6-7**): strains increase considerably, particularly during incisal biting, when simplified TMJs are included. The extremely low strains below the incisors as well as the low overall values in the mandibular corpus suggest that the model is overconstrained when the surface of the condyles is constrained directly. One would not expect that strains are smallest in the bone below the teeth which are loaded, and as such this model appears to be less realistic than the one with TMJs. During unilateral molar biting, the effect of including TMJs is not as extreme as during incisal biting, but it is still pronounced, particularly below the constrained M1 and at the posterior border of the balancing side ramus. Again, the model with directly constrained condyles shows relatively low strains below the constrained tooth, whereas the model with TMJs exhibits a peak of higher strains in that area and thus appears more realistic in this regard. The results of this sensitivity study therefore confirm previous results, which have shown that including TMJ joint capsules allows the FE model to deform more and thus helps to avoid overconstraining the model (Kober et al. 2004). However, the soft tissue within the TMJ could only be modelled very crudely. Thus, the model cannot, for example, account for the differences in the mechanical properties of the articular

cartilage layers and the articular disc or their viscoelastic properties (Beek et al. 2001, Koolstra & van Eijden 2005, 2006). A more accurate representation of TMJ morphology and mechanical properties could have an effect on the strains in the mandible, which needs to be tested in future sensitivity studies.

The largest impact on the strains is found when an external force is applied to the biting tooth instead of a vertical constraint, the former leading to extremely high strains in the posterior ramus. As the deformations reveal, these high strains close to the constraints at the joints are caused by deformation of the mandible around the medio-lateral axis through the joints. Although constraining the joints in all three axes is sufficient for the solution of the FEA, it does not keep the model stable enough. Other authors have successfully applied external forces to bite points in their FE models (Rayfield et al. 2001, Rayfield 2005, Witzel & Preuschoft 2005, Pierce et al. 2008). However, these studies model the cranium. A cranium can be sufficiently constrained by fixing the area of the occiput, where the neck muscles attach, and the artefacts resulting from the constraints are far enough away from the region of interest, which is typically the face. As the results of this study show, a mandibular model cannot be sufficiently stabilised by constraining the joints alone. If the bite force is to be modelled as an external force, it is necessary to apply additional constraints, as has been done, for example, by Hart and co-workers (1992). However, these additional constraints are difficult to justify if the aim is to model masticatory loads realistically. Therefore, it seems more feasible for FE models of mandibles to constrain the respective bite points and only simulate the muscle forces as external forces. Another alternative is to import boundary conditions from multibody dynamic analyses. Since those forces are in equilibrium, the strain artefacts around the constrained nodes are negligible.

The directions of the applied constraints also have a major impact on the results. Overall, strains decrease as the model is increasingly constrained. Interestingly, when displacements in the transverse or x-axis are possible, tensile strains increase more on the labial/buccal surface than compressive ones and the opposite is the case on the lingual surface. This pattern is consistent with medial transverse bending (i.e. the bending that occurs when the mandibular rami are squeezed together), if the mandible is assumed to behave in principle like a curved beam (**Fig. 2.9**).

The fact that constraining the biting teeth in all three axes as opposed to only one axis results in higher local strains during a molar bite, but in much lower strains during incision can be probably explained by the spatial distribution of the constrained nodes. When the occlusal surfaces of all four incisors are fixed, this stabilises the whole symphyseal region, whereas the constraints applied during molar biting only apply to one tooth, so that they only very locally prevent displacements.

It is not straightforward to decide upon the best combination of constraints. In general, the aim should be to constrain the model as little as possible, since artefacts appear at the constrained nodes and the adjacent areas and the deformation of the whole model is limited by the constraints. Following this principle, the most favourable combination would be to constrain the bite point in all three axes, but the joints only in the vertical axis, since this is the minimum number of constraints necessary to keep the model stable. In the case of molars it could be further argued that constraints in all three axes at the occlusal surface simulate idealised occlusion with the corresponding upper molar most realistically, since the intertwining cusps prevent horizontal movements. Constraining the condylar surfaces only in the vertical axis makes sense from a functional point of view, since this is the major direction of the joint reaction force and the freely movable articular discs within the TMJs allow principally horizontal movements of the condyles. Thus, using this set of constraints should have a similar effect to including simplified TMJs. Indeed, the strain patterns are very similar, except for the posterior part of the balancing side ramus, which are larger in the model with TMJs, especially on the lingual side (**Figures 5.7** and **5.9**).

During incision, however, the situation is different. Horizontal movements at the occlusal surfaces should be possible, since they are not prevented by intertwining cusps, but constraining the teeth as well as the joints only in the vertical axis would not stabilise the model sufficiently for a solution of the FEA. Including simplified TMJs provides a solution, since the model can be constrained in all three axes at the joints without overconstraining it.

The observation that a 10° rotation of the force vector of the superficial masseter has a relatively large effect on the strain in the corpus, especially on the working side corpus, indicates how important the muscle vector orientations are

for the accuracy of the results. This is also supported by the observed asymmetry in the strains during the simulated incisal bite, which is most probably due to minor differences in vector orientations between the left and right side (**Fig. 5.6**). The results confirm those of a previous sensitivity study, which showed that even small changes in the direction of external forces result in significant changes in the predicted strains (Marinescu et al. 2005). The lines of action of the masticatory muscle should be, therefore, estimated as carefully as possible, ideally based on the measurements of the same individual. Unexpectedly, the strain orientations are remarkably stable, which suggests that only a change of the overall load type and thus type of deformation will have an effect on the strain directions.

Due to the lack of *in vivo* strain data for human mandibles, no direct validation is possible. Differences in mandibular morphology, muscle forces and muscle recruitment patterns between species are likely to have a significant influence on the bone strains. However, it is interesting to compare the results with the general strain patterns known from animal experiments, especially from non-human primates.

It seems to be a general pattern of mammalian mandibular function that tensile and compressive strains are higher on the mandibular corpus of the working side than on the balancing side, although this working side/balancing side ratio differs between species (Hylander 1979b, Hylander & Johnson 1994, Williams et al. 2009). These *in vivo* strains have been typically measured on the buccal side of the corpus below the molar dentition. If this pattern is generalisable to humans, those of our models seem to be most realistic, where the biting M1 is constrained in all three axes, because such constraints result in higher tensile strains below the molar dentition.

While strains in the working side corpus are commonly higher than on the balancing side, the opposite is the case, when the buccal sides of the condylar processes and the adjacent areas on the rami are considered (Hylander 1979a). All models, those with, as well as without TMJ, show the same pattern.

Another general pattern, observed in non-human primates, is that strains are higher on the lingual side than on the labial side of the symphysis due to the higher curvature on the lingual surface (Hylander 1984, 1985, Hylander & Johnson 1994). Since human mandibles are short anteroposteriorly and wide

mediolaterally and thus have a less pronounced curvature than, for example, cercopithecine mandibles, the differences between labial and lingual strains should be smaller, but still measurable. This is the case in all models with TMJs during a molar bite and for the model with TMJ, in which the teeth were only constrained in the vertical axis during an incisor. The other models show relatively equal strains on the labial and lingual side of the symphysis.

Strain measurements in macaques also show that the strains on the buccal side of the working side corpus are much higher than on the labial symphysis during mastication (Hylander & Johnson 1994). The models that best fit this prediction are the models with TMJs and in which the bite point is constrained in all three axes. In contrast, the model, in which the condylar surfaces are constrained in all three axes does not show this pattern.

Unfortunately, *in vivo* strain data from incision are scarce. Based on a few experiments in macaques, it appears that the maximum principal strains on the labial symphysis are typically much higher during incision than during unilateral molar biting, whereas the difference in minimum principal strains is less consistent (Hylander 1984), and that the maximum and minimum principal strains on the buccal side of the mandibular corpus below the molars are very similar to the balancing side strains at the same location during unilateral molar biting (Hylander 1979b). The models with TMJs, in which the incisors are only constrained in the vertical axis seem to come closest to this pattern. The model, in which the condylar surfaces are fixed, on the other hand, shows symphyseal strains that are much lower than the ones during a unilateral molar bite, which is probably due to the fact that the model is overconstrained.

In addition to comparing the results with the general strain patterns known from *in vivo* experiments, it is worthwhile to compare the predicted maximum strain magnitudes with those measured in *in vivo* experiments. In galago and macaque mandibles compressive strains up to -2100 με and -1500 με respectively have been measured during molar biting on the buccal surface below the molar dentition (Hylander 1979b). Maximum tensile strains between 2000 and 2500 με have been reported for the lingual side of the symphysis (Hylander 1984). In the mandibles of some other mammals lower maximum strain values (below ±1000 με) were measured (Williams et al. 2009). However, these are measurements from single points and differences in gauge location might explain

some part of the observed variation of strain magnitudes. In general, maximum and minimum strain magnitudes between 2000 and 3000 με seem to be close to the upper limit of functional strains occurring in adult load bearing bones during routine behaviours like swimming, running, flying and biting (Rubin 1984, Lanyon & Rubin 1985). All those models, in which the bite points were constrained, produced strain values that are below this measured physiological maximum: The strains rarely exceed ±1000 με and the highest observed strains are around -2000 με at the posterior balancing side ramus of the models with TMJs. Only in the model, in which a force was applied to the bite point, strains up to ±6000 με occur at the ramus. Most bone materials yield in tension at about 2000 με (Currey 2002). In a living individual, these extremely high strains would cause damage to the bone tissue and are thus unlikely to be realistic.

So far, only the strain magnitudes have been considered for the comparison with experimental data, but in order to obtain a complete picture, strain directions should also be evaluated. As with strain magnitudes, direct validation is not possible because of the lack of *in vivo* strain data from human mandibles. However, alternatively, the predicted strain directions can be compared with the directional differences in mechanical properties, since the latter are likely to be linked with functional strains. **Figure 5.12** shows the axes of maximum stiffness in human mandibular cortical bone (Schwartz-Dabney & Dechow 2003) and the predicted maximum and minimum principal strain directions during a unilateral molar bite in a model including PDL and TMJs which are constrained in all three axes. Interestingly, some correspondences can be found. Overall, the maximum principal strain directions on the buccal side are very similar to the measured axes of maximum stiffness, but in the two areas with the highest magnitudes of minimum principal strain, the posterior margin of the mandibular ramus and below the constrained M1, it is the minimum principal strain directions, which correspond well with the axes of maximum stiffness. On the lingual side, there is good correspondence between these axes and the minimum principal strain directions in most areas of the ramus and the posterior corpus, but a better fit of the maximum principal strain directions where maximum principal strain magnitudes are very high, at the base of the anterior corpus and the anterior margin of the ramus. These results suggest that there is no simple relationship between the axes of maximum stiffness and the directions of

one of the principal strains, but that the strain magnitudes or maximum/minimum principal strain ratios need to be considered as well. The comparison presented here is only preliminary and based on a single load case only, but further studies should explore these relationships. Eventually, such comparisons might provide an additional indirect validation for FE models when *in vivo* strain data are not available.

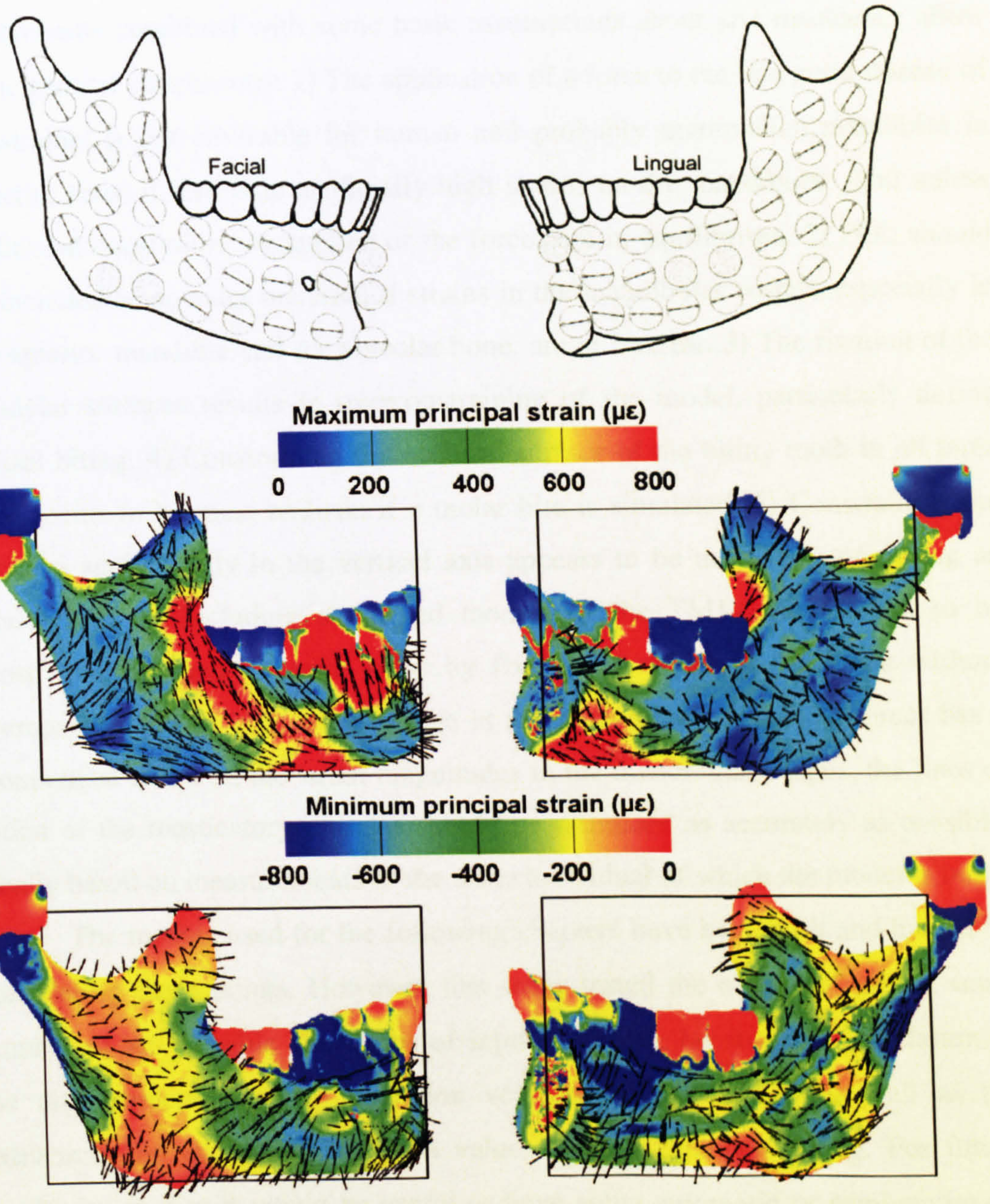

Fig. 5.12. Comparison of maximum and minimum principal strain directions with the measured axes of maximum stiffness of the mandibular cortical bone by Schwartz-Dabney and Dechow (2003: 258, Fig. 3). The strain directions (black lines) have been taken from a simulated molar bite. The TMJs and the occlusal surface of the right M1 are constrained in all three axes.

To summarise, it can be stated that the alteration of each variable has an effect on the strains. While varying in degree, the effects are all large enough to be relevant for the biological interpretation of the strains. Therefore, caution is required in the definition of these input variables. Due to the lack of *in vivo* strain data from human mandibles, it is difficult to decide on the most realistic combination of these variables. However, the comparison of results with the general strain patterns and the maximum strain magnitudes measured in animal experiments combined with some basic assumptions about jaw mechanics allow some general conclusions: 1) The application of a force to the bite point instead of constraints is not advisable for human and probably mammalian mandibles in general, since it results in artificially high strains on the mandibular rami unless additional constraints are applied or the forces are in equilibrium. 2) PDL should be included as an extra material, if strains in the mandibular corpus, especially in the anterior mandible and the alveolar bone, are of interest. 3) The fixation of the condylar surfaces results in overconstraining of the model, particularly during incisal biting. 4) Constraining the occlusal surface of the biting tooth in all three axes seems to be most realistic if a molar bite is simulated. 5) Constraining the occlusal surface only in the vertical axis appears to be most realistic during an incisal bite. 6) Including simplified models of the TMJs allows teeth to be constrained in such different ways by fixing the model at the joints without overconstraining it. 7) Since a change in the orientations of muscle forces has a pronounced effect on the strain magnitudes in the mandibular corpus, the lines of action of the masticatory muscles should be estimated as accurately as possible, ideally based on measurements of the same individual of which the model is built.

The models used for the following chapters have been built and loaded by considering these points. However, this study tested the effects of only a small number of the possible alterations of input variables, because the calculation of the displacements in high-resolution voxel-based FE models as well as the extraction and evaluation of strain values is very time-consuming. For future sensitivity studies it would be useful to have some automatic or semi-automatic technique to alter variables and extract results.

Chapter 6: Comparison of predicted strain patterns and the distribution of cortical bone in a human mandible

6.1. Introduction

There is abundant evidence for a close relationship between bone mass and functional loads. For example, cortical bone thickness decreases when bones that normally bear loads are immobilised (Uhthoff & Jaworski 1978, Jaworski et al. 1980), or increases when bones are exposed to higher loads (Jones et al. 1977, Lanyon et al. 1982). This relationship is relevant for understanding variation in cortical bone thickness between species, individuals or bones on the left and right sides of the same individual (Ruff et al. 1993, Trinkaus et al. 1994, Ruff et al. 1994, Trinkaus 1997, Lieberman et al. 2004b). In addition, it has been suggested that variation of cortical thickness within a bone can be explained by this relationship: that unevenly distributed cortical bone is associated with unevenly distributed stress in the bone during functional loads (Demes et al. 1984, Daegling & Hotzman 2003).

Most studies that have investigated the relationship between stress distribution and the distribution of cortical bone, have been conducted on long bones, particularly on the femur (Ohman et al. 1997, Demes et al. 2000, Lovejoy et al. 2002), but some studies have also applied the principle to the mandible (Demes et al. 1984, Daegling 1989, Daegling & Grine 1991, Daegling 2002, Fukase 2007, Fukase & Suwa 2008). For example, it has been shown that the distribution of cortical bone in the human mandibular symphysis corresponds with expected load patterns: Bone is particularly concentrated at the lower lingual aspect of the symphysis, which is assumed to experience high tensile stress during mastication (Fukase 2007, Fukase & Suwa 2008).

In the posterior corpora of anthropoid mandibles, cortical bone is thicker buccally than lingually, which has been explained as a result of the combined effects of the vertically directed bite force and the torsion of the mandibular corpora around the anteroposterior axis (Demes et al. 1984). *In vitro* experiments with human mandibles (Daegling & Hotzman 2003) have shown that this combination of loads does indeed lead to the strain pattern predicted by Demes and colleagues (1984). In contrast, the results of a recent FEA study suggest that

the asymmetric distribution of cortical bone in the human mandible is not related to masticatory strains (Ichim et al. 2007b).

Studying the relationship between stress or strain distribution and the distribution of cortical bone with FEA is not straightforward. Healthy adult bones can be expected to be more or less optimally adapted to the loads they experience during normal function. Where stresses are high, more bone should be deposited, which results in a better load resistance of the bone in that area reflected by a decrease in strain. The stress and strain distribution observed in an adult bone cannot be expected to reflect the distribution prior to adaptation, for example, at earlier ontogenetic stages, since cortical thickness will vary as a result of adaptation, thus altering the distribution of stresses and strains under load. When stresses and strains are low in one area, this can be either due to the particular load and the overall shape of the bone or because the bone has successfully adapted to the load by, for example, increasing its density or cortical thickness.

Ideally, FEA studies intended to test the relationship between stress and strain distribution and the distribution of cortical bone should therefore use models, which represent the bone before it adapted to functional loads. In this way predictions about mechanical adaptation can be tested. Using juvenile specimens would be one option, but is problematic, in part because the required data (e.g. material properties, EMG, muscle force magnitudes) is often not sufficiently known to build and load FE models accurately. More importantly, it is questionable whether there is ever a stage during ontogeny, in which the bone is not adapted to the functional loads it experiences. Rather, through constant modelling and remodelling, it is likely that a growing bone is always more or less adapted to the current mechanical environment. A more fruitful approach is to create and load models with a hypothetical internal morphology that is not adapted, that are, for example, completely solid or have an equal cortical thickness throughout. Recently, this approach has been applied to a human mandible (Reina et al. 2006). By applying an internal bone remodelling algorithm to an FE model, in which all internal cavities had been filled, Reina and co-workers (2006) were able to generate a distribution of bone density and elastic properties similar to that in the real specimen.

The present study will adopt a similar approach in using models with hypothetical "unadapted" internal morphology in order to test whether an

association exists between the strain pattern resulting from simulated masticatory loads and the distribution of cortical bone. If such a relationship can be confirmed, this will potentially not only support prior functional hypotheses about the distribution of cortical bone in the human mandible, but also indicate that the chosen model attributes and loading conditions are probably realistic. In addition, different strain parameters are used for the comparison, in order to investigate which show the closest relationships with the distribution of cortical bone.

6.2. Material and methods

The human mandible that was chosen for this study (H-A 002), is the same that has been used for the sensitivity study (Chapter 5). The virtual reconstruction of this specimen is therefore described in detail in Chapters 5, as are the steps in creation of PDL and simplified models of the TMJs. Based on this original model, two hypothetical models were created using the automatic and manual segmentation tools available in Amira: one model, in which all internal cavities were filled and a second, in which an arbitrary equal cortical bone thickness of ca. 1.7 mm (= 7 voxel layers, each 0.24 mm thick) was created (**Fig. 6.1**).

The two hypothetical models were converted into VOX-FE meshes and material properties were defined as described in Chapter 5. Seven different load cases were simulated for each model: incision with all four incisors, right and left canine bites (including the lateral incisors and the first premolars), bites on the right and left first molars and bites on the right and left second molars) using the muscle forces listed under 3.8. The aim was to simulate a wide spectrum of load cases consistent with the range of normal mandibular loading since adaptation is expected to reflect this range rather than any particular bite. The models were always constrained at the simplified TMJs in all directions. The occlusal surfaces of the teeth were constrained in all directions during unilateral bites and only in the vertical axis during incision.

After the solution of the FEA, for each load case values for the following parameters were calculated: maximum principal strain (ε_1), minimum principal strain (ε_3) and von Mises strain (ε_v). Von Mises strain is a function of all principal strains ($\varepsilon_1, \varepsilon_2, \varepsilon_3$) and can be used to predict failure in a ductile material under load. Thus, it is also assumed to have some biological significance. In order to create summary contour plots representing the peak strain pattern over all load cases

(**Fig. 6.2**), the maximum strain value for each finite element across the different load cases was selected from the exported element strain value files and accumulated in a new cumulative contour plot (Witzel & Preuschoft 2005, Kupczik et al. 2009).

Fig. 6.1. Transverse sections through the original model (left) and the model with equal cortical bone thickness (right).

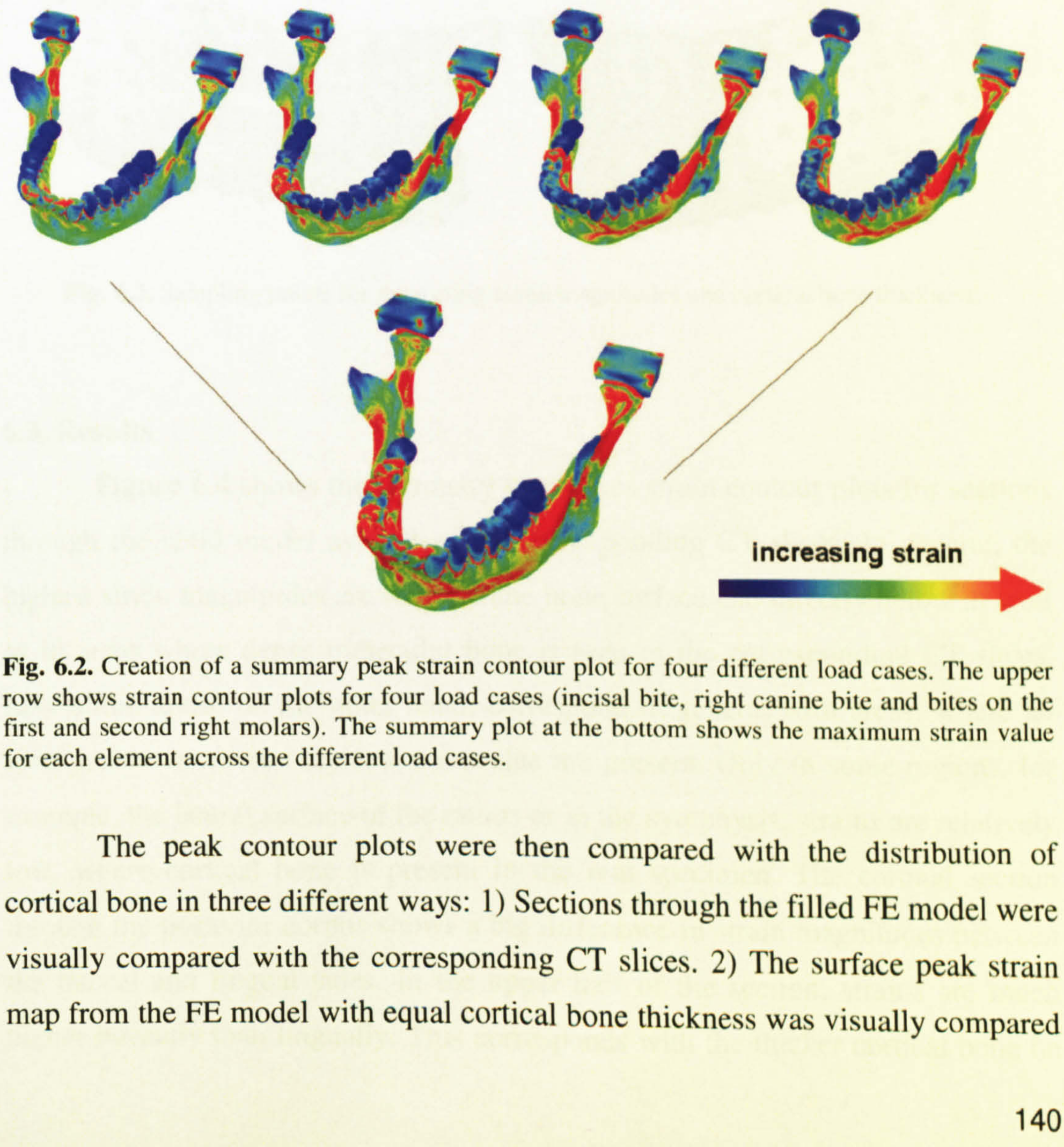

Fig. 6.2. Creation of a summary peak strain contour plot for four different load cases. The upper row shows strain contour plots for four load cases (incisal bite, right canine bite and bites on the first and second right molars). The summary plot at the bottom shows the maximum strain value for each element across the different load cases.

The peak contour plots were then compared with the distribution of cortical bone in three different ways: 1) Sections through the filled FE model were visually compared with the corresponding CT slices. 2) The surface peak strain map from the FE model with equal cortical bone thickness was visually compared

with a 3D map of cortical thickness variation in the same specimen. This 3D cortical thickness map was created by defining the endosteal and periosteal surfaces as two separate surfaces and visualising the minimum distances between the two as a colour-coded map using the "distance module" in Amira. This required some additional manual segmentation like deleting trabecular bone. 3) The correspondence between surface strains in the FE model with equal cortical bone thickness and the cortical thickness variation in the original specimen was quantified by defining 111 evenly distributed points on the bone surface and extracting the strain value as well as the minimum distance to the endosteal surface for each point (**Fig. 6.3**). The association between strain magnitudes and cortical bone thickness was then quantified by calculating correlation coefficients.

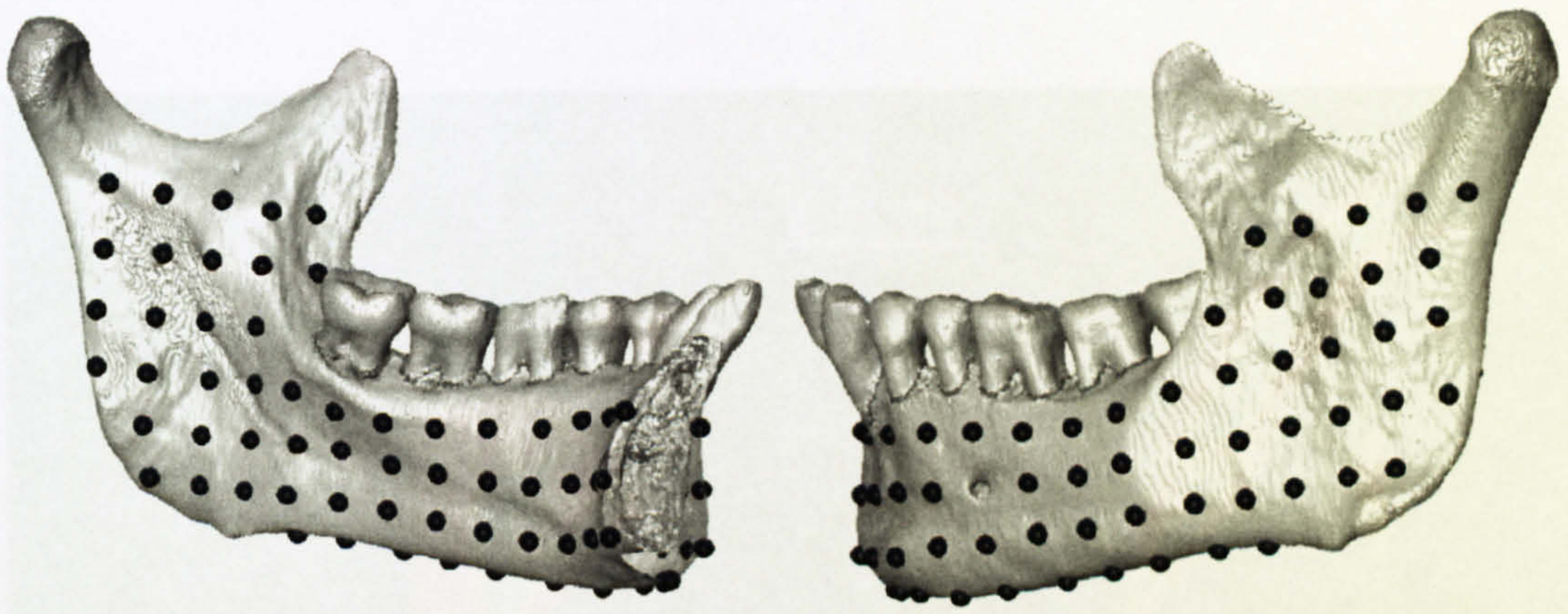

Fig. 6.3. Sampling points for measuring strain magnitudes and cortical bone thickness.

6.3. Results

Figure 6.4 shows the summary von Mises strain contour plots for sections through the solid model as well as the corresponding CT slices. In general, the highest strain magnitudes are found at the bone surface and directly below as well as in areas where dense trabecular bone is seen in the corresponding CT slices. Low strain areas, on the other hand, correspond in general with areas, where no bone exists or where only few trabeculae are present. Only in some regions, for example, the lateral surface of the ramus or in the symphysis, strains are relatively low, where cortical bone is present in the real specimen. The coronal section through the posterior corpus shows a big difference in strain magnitudes between the buccal and lingual sides. In the upper half of the section, strains are much higher buccally than lingually. This corresponds with the thicker cortical bone on

the buccal side compared to the lingual one. In the symphyseal cross-section, strains are higher lingually than labially, which also corresponds with the difference in cortical bone between the labial and the lingual sides of the symphysis.

The spatial distribution of surface strains is shown for the model with equal cortical bone thickness (**Fig. 6.5**). The highest strains are found below the molar dentition labially and lingually, at the anterior margin of the mandibular ramus, the base of the corpus, the sigmoid notch and the posterior margin of the ramus just below the condyles. These are also the areas, where the highest cortical bone thickness is measured. The majority of the ramal surfaces as well as the anterior labial symphysis show relatively low strains, which corresponds with the thin cortical bone that is found in these areas.

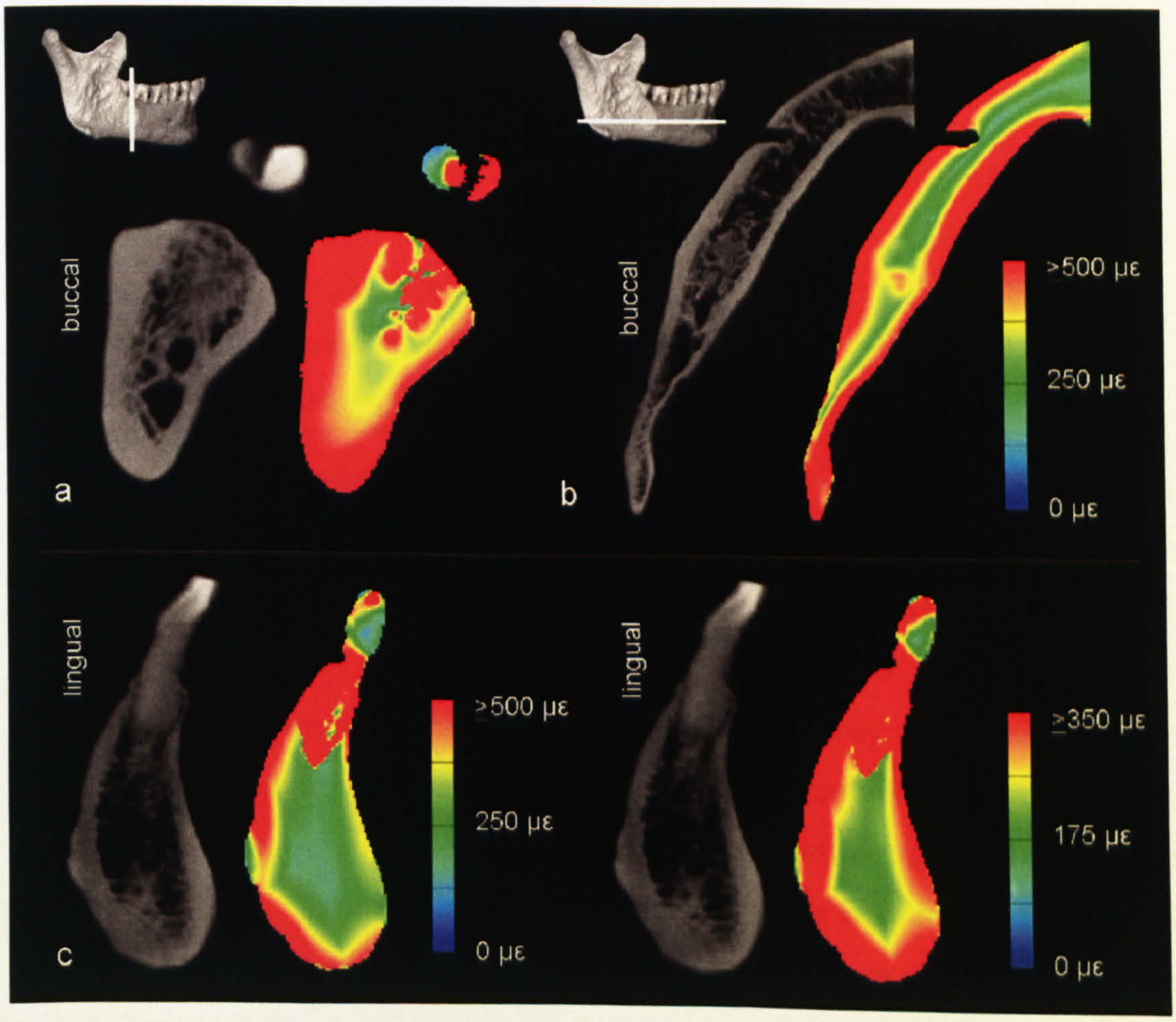

Fig. 6.4. Comparison between CT slices and corresponding slices though the filled FE model with von Mises strain (ε_v) contour plots: a) coronal section through the posterior corpus between M2 and M3, b) transverse section through the mental foramen, c) mid-sagittal sections through the symphysis. Note that two different colour ranges are used to visualise the strain distribution in the symphysis.

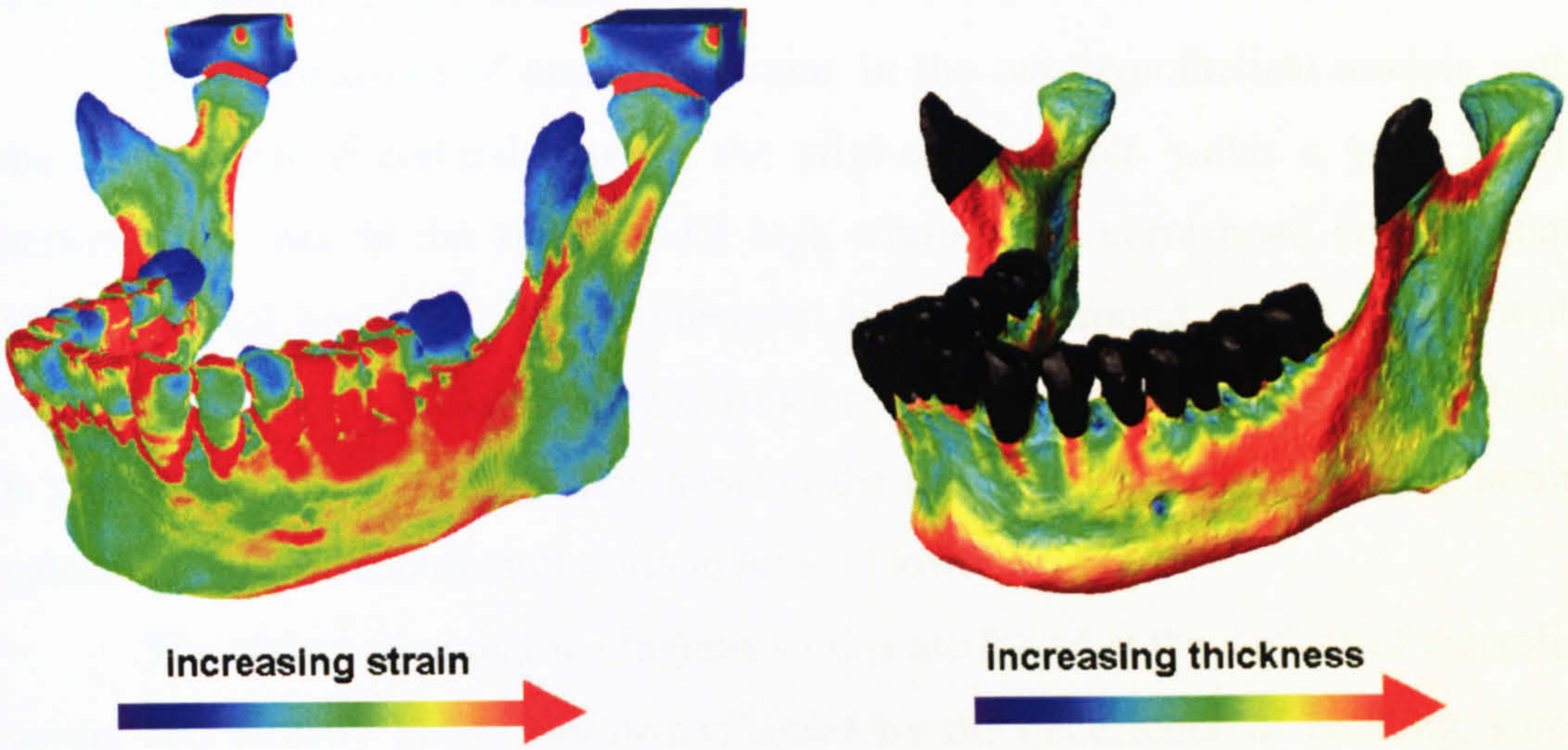

Fig. 6.5. Comparison between predicted von Mises strain (ε_v) distribution in the FE model with equal cortical bone thickness and the cortical bone thickness variation in the original specimen. The black areas in the 3D cortical thickness map are those which cannot be compared with the FEA.

Strain parameter	r	*P*
von Mises strain (ε_v)	0.35	< 0.0005
Maximum principal strain (ε_1)	0.45	< 0.0001
Minimum principal strain (ε_3)	-0.20	< 0.05
Max./min. principal strain ratio ($\varepsilon_1/\varepsilon_3$)	0.13	< 0.5
Maximum shear strain (γ_{max})	0.42	< 0.0001

Table 6.1. Correlation coefficients and *P*-values for cortical thickness and strain distribution using different strain parameters.

The association between strain patterns and variation of cortical bone thickness is quantified by the correlation coefficients listed in **Table 6.1**. In general, the correlation coefficients are quite low, but they differ considerably between the different strain parameters. The highest correlations, which are also highly significant, are found for maximum principal strain (ε_1) and maximum shear strain (γ_{max}). The latter is defined as the difference between maximum and minimum principal strain (ε_1- ε_3). The lowest correlations are given for minimum principal strain (ε_3) and the maximum/minimum principal strain ratio ($\varepsilon_1/\varepsilon_3$).

6.4. Discussion and conclusions

The comparison of predicted strains in the two hypothetical models with the distribution of cortical bone in the original mandible yields a good match between the two. In the solid model high strain areas correspond with regions where cortical bone or a dense trabecular network is found. In the model with equal cortical bone thickness they correspond with areas where the cortical bone is particularly thick. Only in few areas is the correspondence between the strain pattern and the distribution of cortical bone is low.

The observation that the highest strains are found at the surface of the solid model and directly below can be explained by the occurrence of bending, since during bending strain magnitudes increase with the distance from the neutral axis, which runs through the centre of the bone (Currey 2002). This is also illustrated by **Figure 2.9**. The highest strains within the solid model are close to the roots of the molars, where high strains occur because of the constraints applied to the occlusal surfaces of the teeth in order to simulate the effect of the bite force acting on the teeth. The constraints at the molar teeth are certainly also the reason for the high surface strains below the molar dentition in the model with equal cortical thickness.

The good overall correspondence between the strain distribution and the distribution of cortical bone confirms prior studies that have suggested a link between the two in the mandible (Demes et al. 1984, Daegling 1989, Daegling & Grine 1991, Daegling 2002, Fukase 2007, Fukase & Suwa 2008). The strain patterns observed in the solid model are very similar to the distribution of bone density reported by Reina and co-workers (2006), who applied an internal bone remodelling algorithm to a filled FE model of a human mandible and also found a good match between the resulting density maps and the distribution of bone in the original specimen. Their muscle force magnitudes are very similar to the ones used in this study. The constraints at the joints and occlusal surfaces are, however, rather different, which suggests some robusticity of these results. In addition, this study shows that the distribution of bone can be reasonably well predicted by simple summary strain contour plots even without applying a complex time-dependent remodelling algorithm like Reina and co-workers (2006).

The peak von Mises strain map in the solid model also clearly reflects the difference in cortical bone thickness between the buccal and lingual sides of the

posterior corpus, which is typical for anthropoid mandibles (Demes et al. 1984). This suggests that the uneven distribution of cortical bone in the posterior corpus is indeed related to masticatory loads. A prior FEA study by Ichim and colleagues (Ichim et al. 2007b) did not confirm this relationship, most probably because they only looked at the strain distributions from single load cases instead of summary contour plots derived from several load cases and because the internal morphology of the their model was not altered, so that they did not control the variation of cortical thickness within the bone. As discussed above, only the use of hypothetical models, in which this variable is controlled, allows investigating whether the distribution of cortical bone is determined by the strain patterns resulting from functional loads.

In addition, the strains in the symphysis of the filled model correspond well with the general distribution of cortical bone in the human symphysis, which is thicker lingually than labially. The results seem to confirm the suggestion of some authors that this distribution of cortical bone is directly linked to masticatory strains (Fukase 2007, Fukase & Suwa 2008). Although, it needs to be further explored why the strains in the symphyseal region are in general rather low compared to the posterior corpus.

The good correspondence overall between strain patterns and bone distribution indicates that the modelling approach used, particularly the applied forces and constraints, is relatively realistic. The low correspondence between strain patterns and the distribution of cortical bone in some areas could be due to the fact that not all relevant load cases have been modelled, for example, biting on the third molars or the second premolars was not simulated because of the lack of the respective muscle force data.

This might also be the reason, why the correlation coefficients are relatively low. Thus only a small part of the variance in cortical bone thickness can be explained by strain differences. Interestingly, maximum principal strain and maximum shear strain show the highest correlation coefficients, while minimim principal strain and the maximum/minimum principal strain ratio yield poor correlations. This corresponds well with the fact that bone is weaker under tension and shear than under compression (Currey 2002). Thus, it would be advantageous for bone to increase its thickness especially in those areas, where high tensile and shear strains occur. This should be further investigated.

Sensitivity studies could explore the effect of altering input variables, especially the muscle forces, on the summary strain plots. It is possible that the correlation between strain and cortical bone distribution is improved with different, more realistic boundary conditions. However, sensitivity studies of this kind would require the solution of numerous FE models for each input value, since several load cases have to be applied in order to obtain a comprehensive summary contour plot and thus call for supercomputing or massive processing time.

In general, the use of hypothetical models like those in this study might be very useful as a validation tool, where *in vivo* strain data cannot be collected, as in humans or extinct species, assuming that the mechanisms and principles of the mechanical adaptation of bone are universal in vertebrates.

With the models used in this study it has been possible to predict were bone is needed to resist certain loads within an existing external form. By modifying aspects of the external form this approach allows to study how internal and external morphology are related, which will be shown in the following Chapter 7.

Chapter 7: Internal morphology of the mandibular ramus and its relation to the presence or absence of a retromolar space

7.1. Introduction

The retromolar space, a gap between the third mandibular molar and the anterior margin of the ascending ramus, is probably one of the most frequently cited Neanderthal characteristics (Coon 1962, Trinkaus 1983, Stringer et al. 1984, Rak 1986, Trinkaus 1987, Condemi 1991, Wolpoff 1999). Often it is considered as a Neanderthal autapomorphy (Stringer et al. 1984, Condemi 1991), although it is also present in other Pleistocene *Homo* specimens as well as sometimes in living human populations (Franciscus & Trinkaus 1995, Arensburg & Belfer-Cohen 1998, Nicholson & Harvati 2006). Thus, it is not unique to Neanderthals, but occurs among them at a higher frequency than in most other Pleistocene *Homo* populations (Franciscus & Trinkaus 1995).

Different explanations for the high frequency of retromolar spaces in Neanderthals have been put forward: an anterior shift of the dental arcade (Coon 1962, Howells 1974, Wolpoff 1999), a posterior shift of the zygomatic and anterior ramal regions relative to a fixed molar position (Trinkaus 1987) or a shortening of the dental arcade either resulting from reduced molar size (Rak 1986), a forward shift of the third molar (Rak & Hylander 2007) or a combination of anterior migration of the postcanine dentition and posterior migration of the anterior dentition (Spencer & Demes 1993). It has also been suggested that the high frequency of retromolar spaces in Neanderthals is the result of reduced dental arcade length combined with a reduced ramus breadth in the context of little or no reduction in overall mandibular length (Franciscus & Trinkaus 1995).

Whereas the hypotheses above try give a reason for the high frequency of a retromolar space in Neanderthals, one could also ask what the mechanical effect of having or not having a retromolar space is. The region between the third molar and the mandibular ramus is especially interesting from a mechanical point of view, since it lies between the attachment sites of the jaw closing muscles, which pull the mandible upwards, and the high reaction forces that occur at the molar dentition. Thus, it can be expected that this area is exposed to high stresses and strains during masticatory function. Indeed, FEA studies of human mandibles by other authors (Korioth et al. 1992, Choi et al. 2005, Ichim et al. 2006a) as well as

the study described in the previous chapter show that high stresses and strains occur in the bone posterior to the third molar and in the lower half of the anterior ramus, when physiological loads are simulated.

As described in detail in Chapter 2, there are abundant empirical data that confirm the close relationship between bone mass and functional loads, for example, how cortical bone thickness decreases when bones that normally bear loads are immobilised (Uhthoff & Jaworski 1978, Jaworski et al. 1980), or increases when bones are exposed to higher loads (Jones et al. 1977, Lanyon et al. 1982). In addition to these empirical data, the results of the previous chapter show that there is a high correspondence between the strain pattern resulting from simulated physiological loading and the variation in cortical thickness within the human mandible.

This study investigates whether the cortical bone distribution in the anterior ramus is related to the absence/presence of a retromolar space and whether it is possible to predict differences in cortical thickness in the ramus with FEA. Preliminary visual comparisons of CT scans of a number of modern human as well as Neanderthal and *H. heidelbergensis* mandibles suggest that there might be a relationship, but that a third factor needs to be considered, which is the angle of the anterior ramus (**Fig. 7.1**).

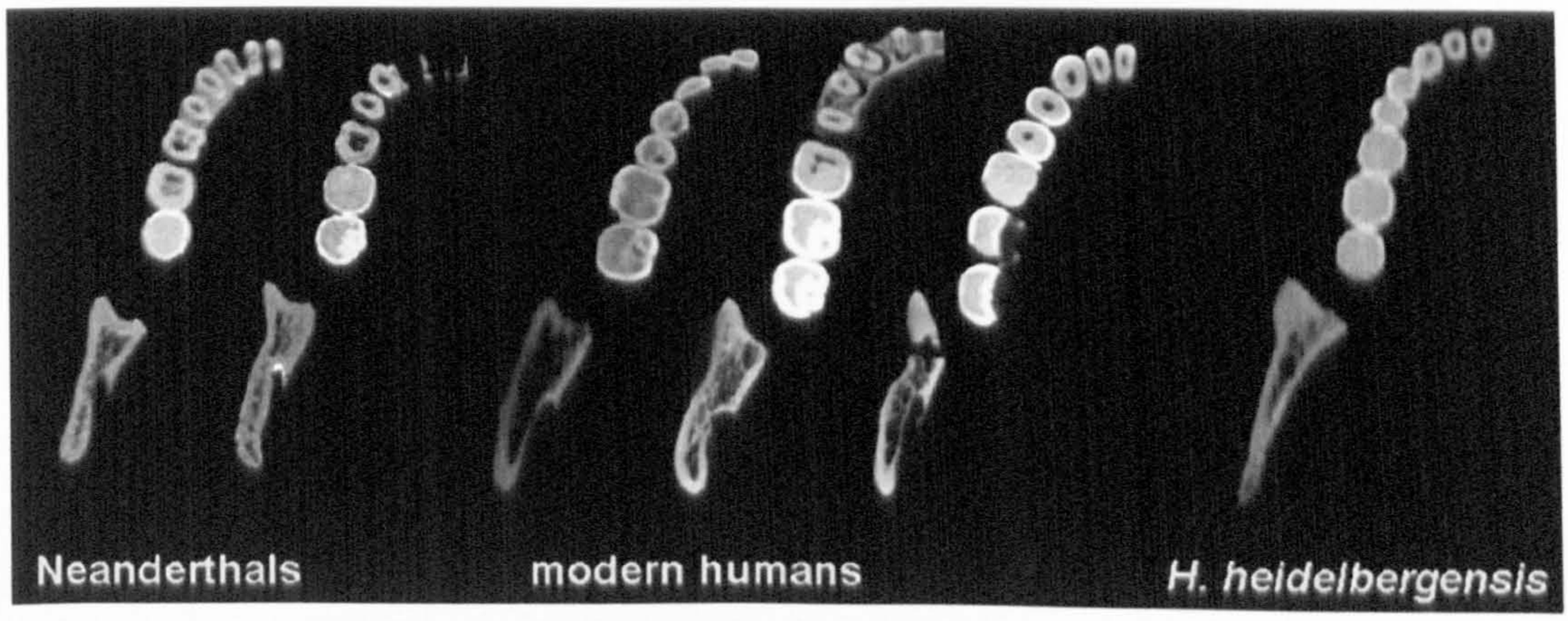

Fig. 7.1. Variation in the distance between molar dentition and ramus, anterior ramus shape and cortical bone distribution within the ramus in modern humans, Neanderthals and *H. heidelbergensis*, as seen in transverse CT slices. Note the more sagittally orientated anterior surface of the ramus in mandibles where the space between molars and ramus is reduced, and the more unequal distribution of cortical bone at the medial and lateral edges of the anterior ramus.

It appears that in mandibles without a retromolar space the basal portion of the anterior ramus tends to have a more sagittal orientation, providing space for the third molar and that in these mandibles a thickening of the cortical bone on the

lateral side of the anterior ramus can be observed. This lateral thickening of the cortical bone might be explained by the simple mechanical principal that higher stresses and strains occur, where surfaces meet at an acute angle (Demes et al. 1984, Demes 1987). If this model is correct, this would be the case in mandibles without a retromolar space (**Fig. 7.2**). Alternatively, the presence/absence of a retromolar space could have a direct effect on the stress and strain distribution in the anterior ramus, since it is likely that the stiffness of the area as well as the loading conditions change with the distance between the molars and the ramus.

Figure 7.3 gives an overview of the three variables of interest and the possible causal relationships. The first part of this study will test whether relationships do exist between the respective variables using a traditional morphometric approach. The second part of this study will test the effect of single variables on the strain pattern in the bone by virtual modification of single features and FEA.

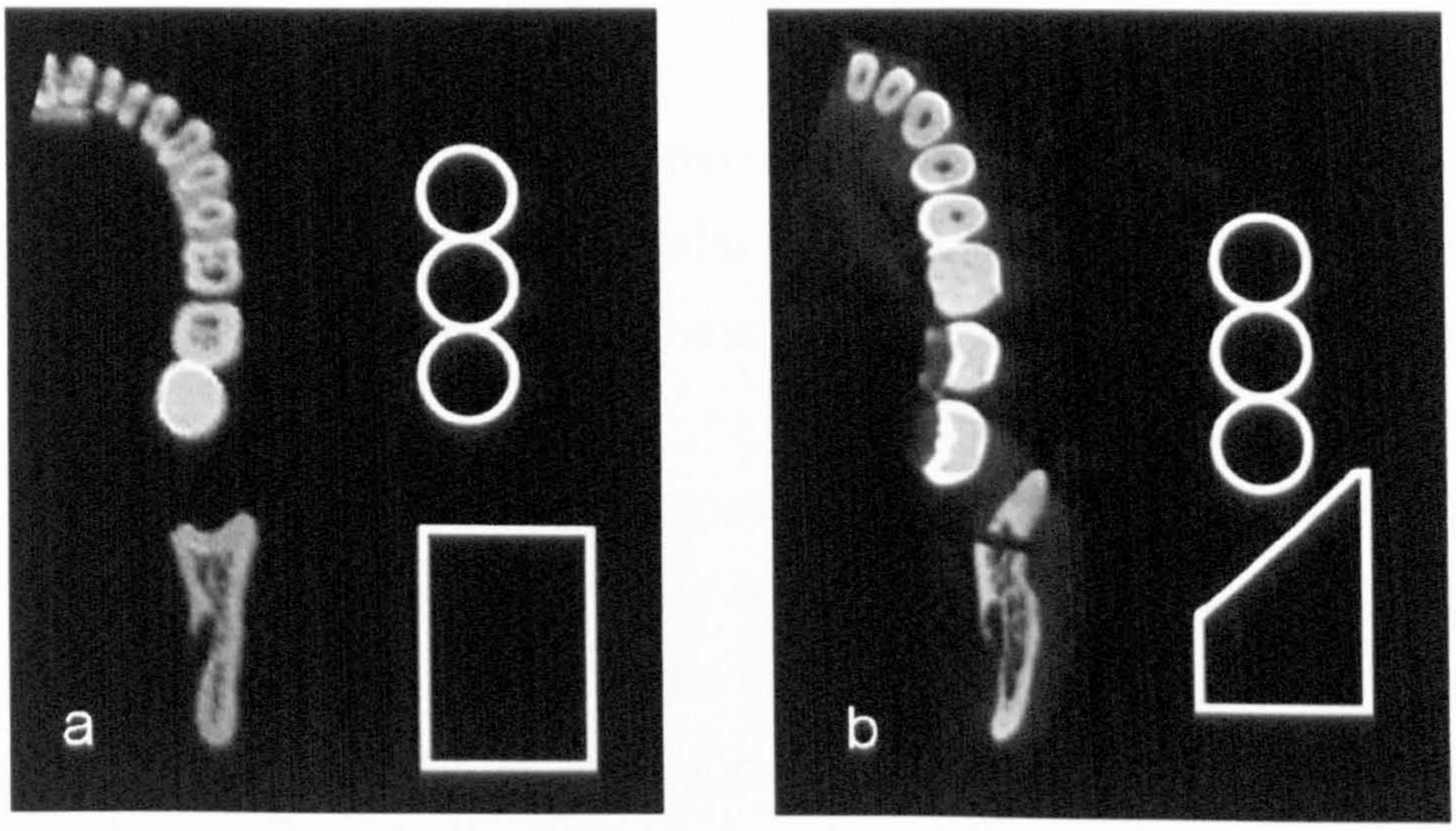

Fig. 7.2. The hypothesised relationship between the presence/absence of a retromolar space and the shape of the anterior ramus: a) retromolar space present, b) retromolar space absent.

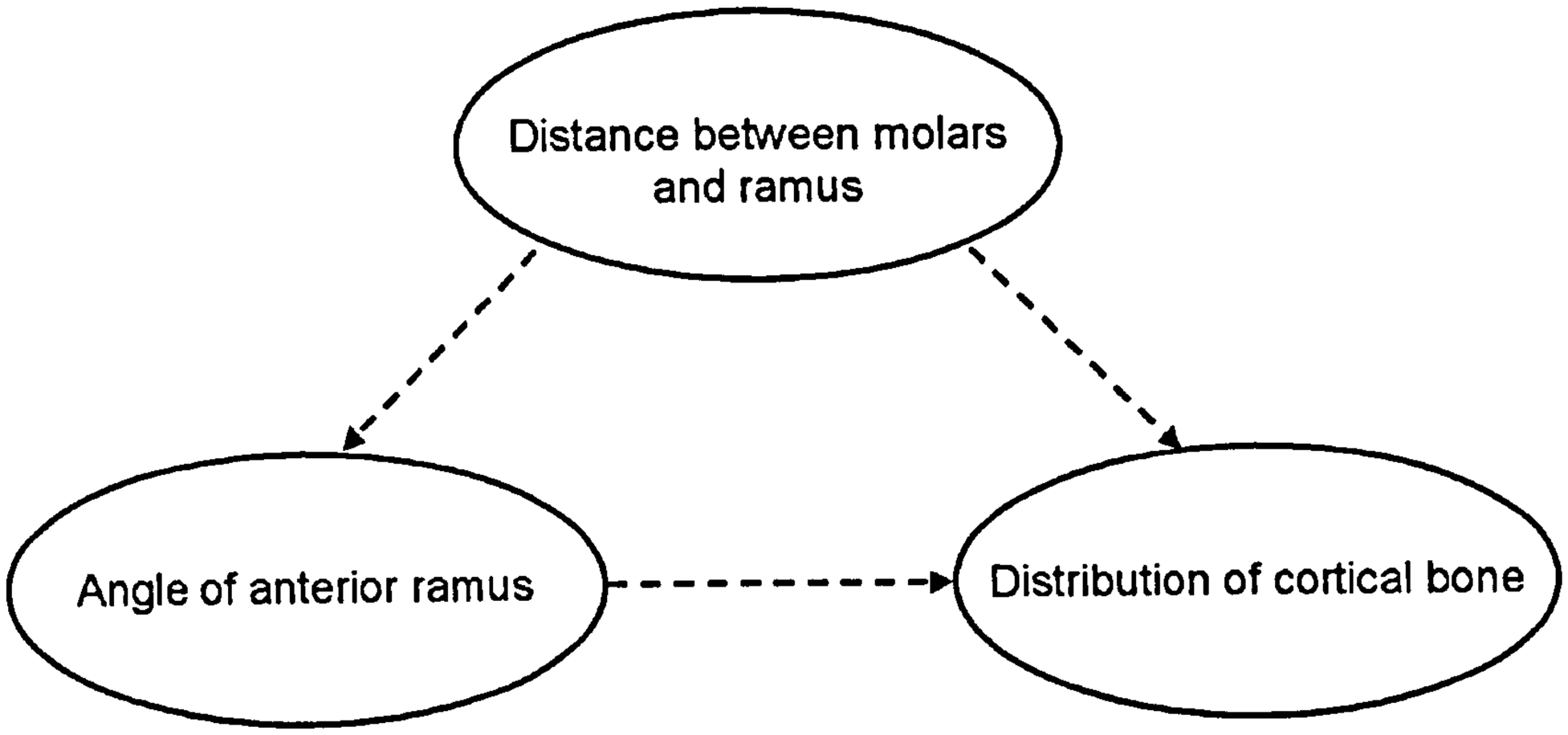

Fig. 7.3. Possible causal relationships between the three variables of interest.

7.2. Material and methods

For the morphometric study, CT scans of 18 adult modern human and 7 fossil mandibles were used. **Table 7.1** gives an overview of the measured specimens.

For each specimen the measurements were taken on a transverse section along the occlusal plane and on both sides of the mandibles, unless one side was too damaged to take measurements. These measurements are defined as follows **(Fig. 7.4)**:

1. Relative position of the most posterior molar: The projected distance between the most posterior point on the margin of the alveolar socket of the most posterior molar (i.e. the third molar if the dentition is complete and the second molar, if third molars were missing *in vivo*) and the most anterior point on the ramus. Positive values are assigned when the most posterior point of the molar is anterior to the most anterior ramus point. Negative values are used, when the molar point is posterior to the ramus point.
2. Angle of the anterior ramus: The angle between the coronal plane and a line connecting the most anterior point of the lateral surface of the ramus and the most anterior point of the medial surface of the ramus.
3. Cortical thickness ratio, which describes the relation between the cortical thickness on the medial side and the cortical thickness on the lateral side of the anterior ramus: The minimum distance between the endosteal

surface and the most anterior and medial point of the ramus divided by the minimum distance between the endosteal surface and the most anterior and lateral point of the ramus.

Based on these measurements bivariate plots were generated and the correlation coefficients for the three possible pairs of the variables were calculated as a measure of association.

Specimen	*Taxon*	Measured sides
Mauer 1	*H. heidelbergensis*	left and right side
Ehringsdorf F	*H. heidelbergensis*	only right side
Krapina 59	*H. neanderthalensis*	left and right side
Tabun C1	*H. neanderthalensis*	only left side
La Quina 9	*H. neanderthalensis*	only left side
Régourdou 1	*H. neanderthalensis*	only right side
Skhūl 5	*H. sapiens*	left and right side
18 modern humans	*H. sapiens*	left and right side, 1 only right side

Table 7.1. List of measured mandibles. See sections 3.2 and 3.3 for more details about the specimens.

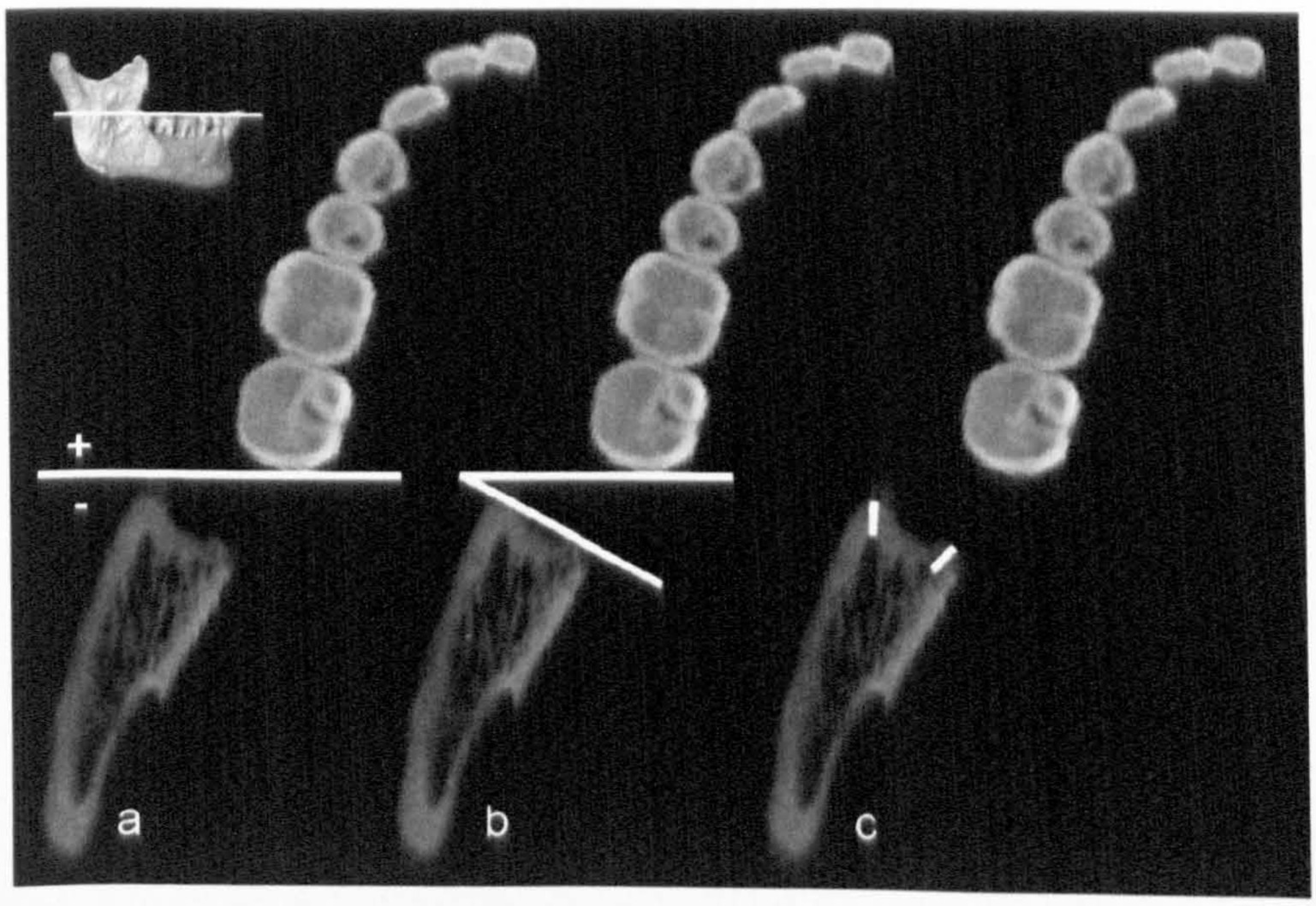

Fig. 7.4. Illustration of the three measurements taken on each mandible (on a transverse section along the occlusal plane): a) distance between the most posterior molar and the most anterior point of the ramus, b) angle between the coronal plane and a tangent along the anterior ramus, c) cortical thickness measurements at the lateral and medial edges of the anterior ramus.

For the FEA, two of the best preserved mandibles were selected to represent the extremes of the range of molar position in relation to the ramus. One

is a modern human mandible (H-A 002) with a ramus clearly overlapping the third molar in lateral view and one a Neanderthal mandible (Régourdou 1) with a characteristic retromolar space. The CT scanning parameters as well as the virtual 3D reconstruction of these two specimens are described in detail in Chapters 3 and 5.

In order to be able to predict where thicker cortical bone is needed to resist higher strains, the existing variation in cortical bone thickness has to be removed. Therefore, an equal cortical bone thickness of ca. 1.7 mm was created in all models as described in Chapter 6.

The effect of the presence/absence of a retromolar space (defined as the distance between the most posterior molar, not necessarily the third molar, and the ramus) as well as the angle of the anterior ramus on the strain magnitudes and distribution, was tested by modifying morphological features in the 3D models with Amira. In order to investigate the effect of the presence/absence of a space behind the most posterior molar, the third molars in the modern human mandible were removed and in the Neanderthal specimens one additional molar on each side was added (**Fig. 7.5**). The mechanical significance of the anterior ramal angle was studied by transplanting the anterior ramus of the Neanderthal specimen into the modern human mandible and *vice versa* (**Fig. 7.6**).

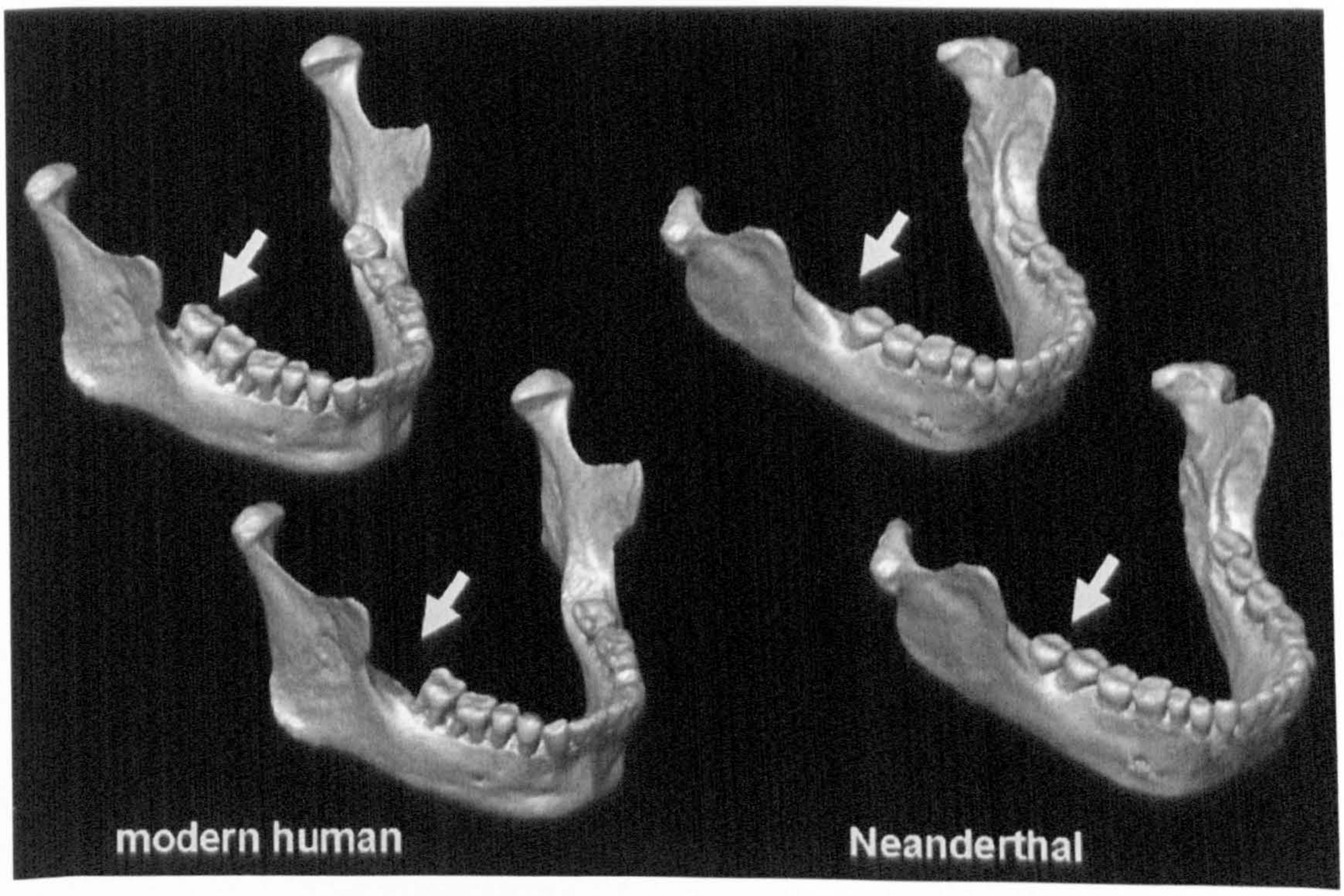

Fig. 7.5. Removal of the third molars in the modern human mandible and addition of two "fourth molars" in the Neanderthal mandible to test the mechanical significance of the presence/absence of a space between molars and ramus.

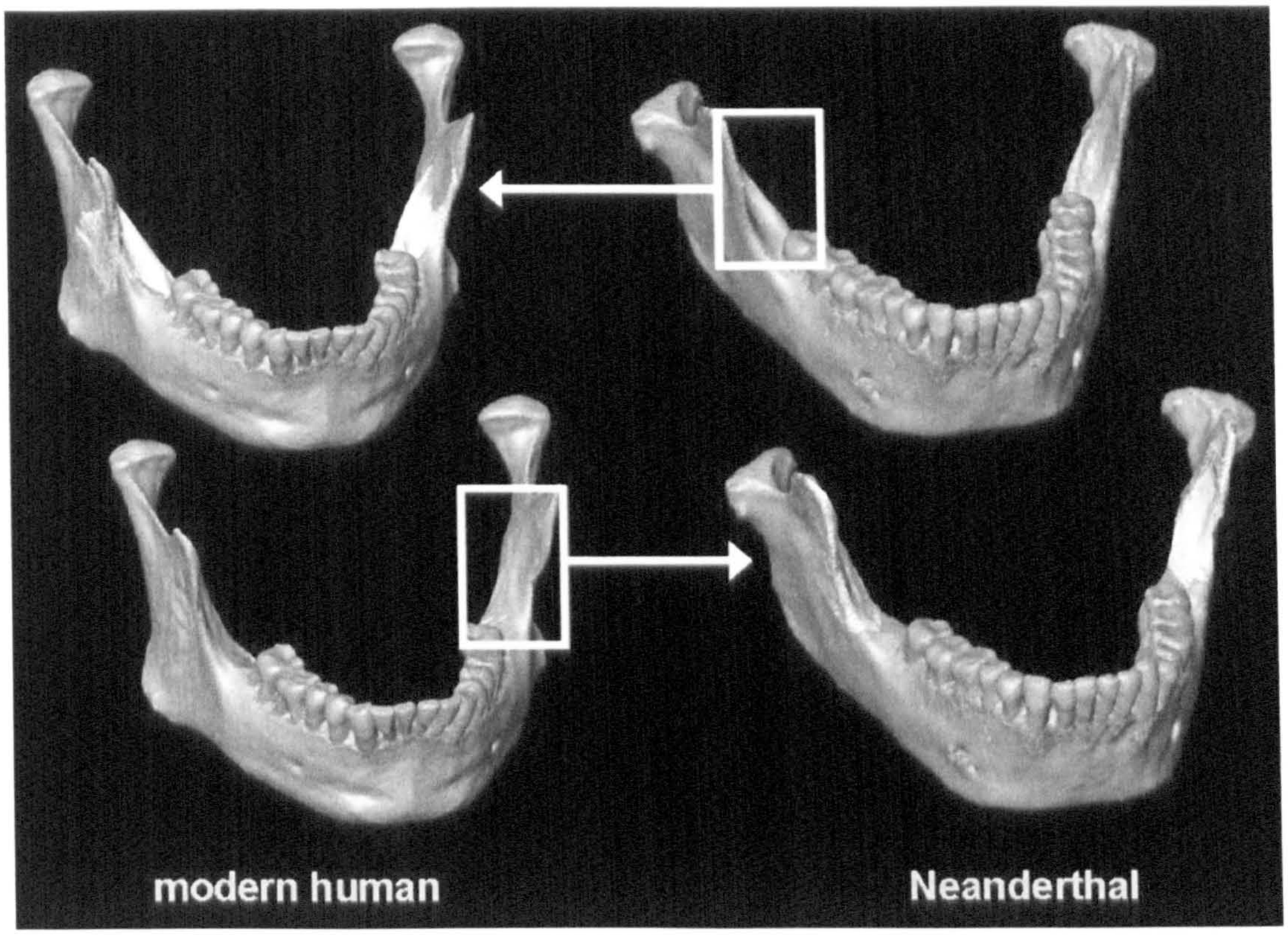

Fig. 7.6. Exchange of the anterior ramus (white) between the modern human and the Neanderthal mandible to test the effect of a different anterior ramus shapes.

The final models were transformed into FE meshes and material properties and boundary conditions as described in Chapter 5 were defined, using modern human muscle forces for the modern human mandible and estimates of Neanderthal muscle forces for the Neanderthal mandible (for values see 3.8). For each model, four load cases were simulated: incision, right canine bite, bite on the right first molar and bite on the right second molar.

The resulting local deformations in the models were quantified using von Mises strains. In order to obtain a summary contour plot for all load cases, the maximum strain value for each finite element across the different load cases was selected, as described in the previous chapter. Based on these summary contour plots, strain values from 50 elements on the periosteal and endosteal surfaces at the most anterior points of the lateral and medial margins of the anterior ramus were exported and the mean strain values for each selected area were calculated. This procedure was applied to the working as well as the balancing side ramus and the maximum values were selected for the analysis.

7.3. Results

Figures 7.7 to **7.9** show the plots for the three possible pairs of the three variables. For all three pairs, strong linear relationships can be observed. In detail, these relationships are 1) a decrease in the angle of the anterior ramus with increasing distance between the most posterior molar and the ramus, 2) an increase of the cortical thickness ratio (i.e. its convergence to one), with decreasing angle of the anterior ramus, 3) an increase of the cortical thickness ratio with increasing distance between the most posterior molar and the ramus. The correlation coefficients for all three pairs of variables are above 0.7 and highly significant (**Table 7.2**) and the graphs do not show any extreme outliers (**Fig. 7.7-7.9**). All specimens fall relatively close to the regression lines.

Variable 1	Variable 2	r	*P*
Relative molar position	Angle of anterior ramus	-0.76	< 0.0001
Cortical thickness ratio	Angle of anterior ramus	-0.81	< 0.0001
Relative molar position	Cortical thickness ratio	0.72	< 0.0001

Table 7.2. Correlation coefficients and *P*-values for the three pairs of variables.

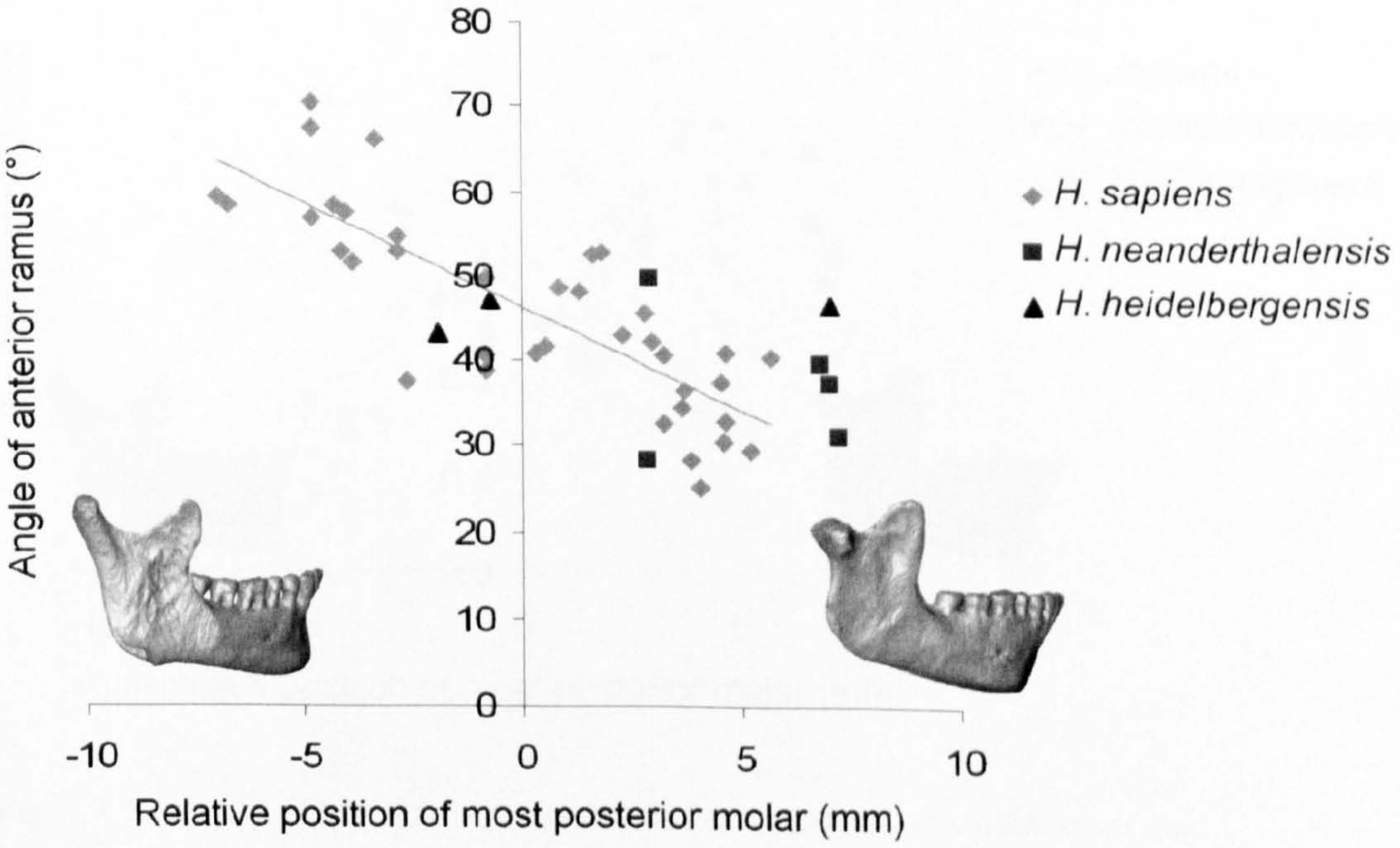

Fig. 7.7. Position of the most posterior molar in relation to the ramus against the angle of the anterior ramus. The regression lines in this and the following figures are based on the whole sample, thus including *H. sapiens*, *H. neanderthalensis* and *H. heidelbergensis*.

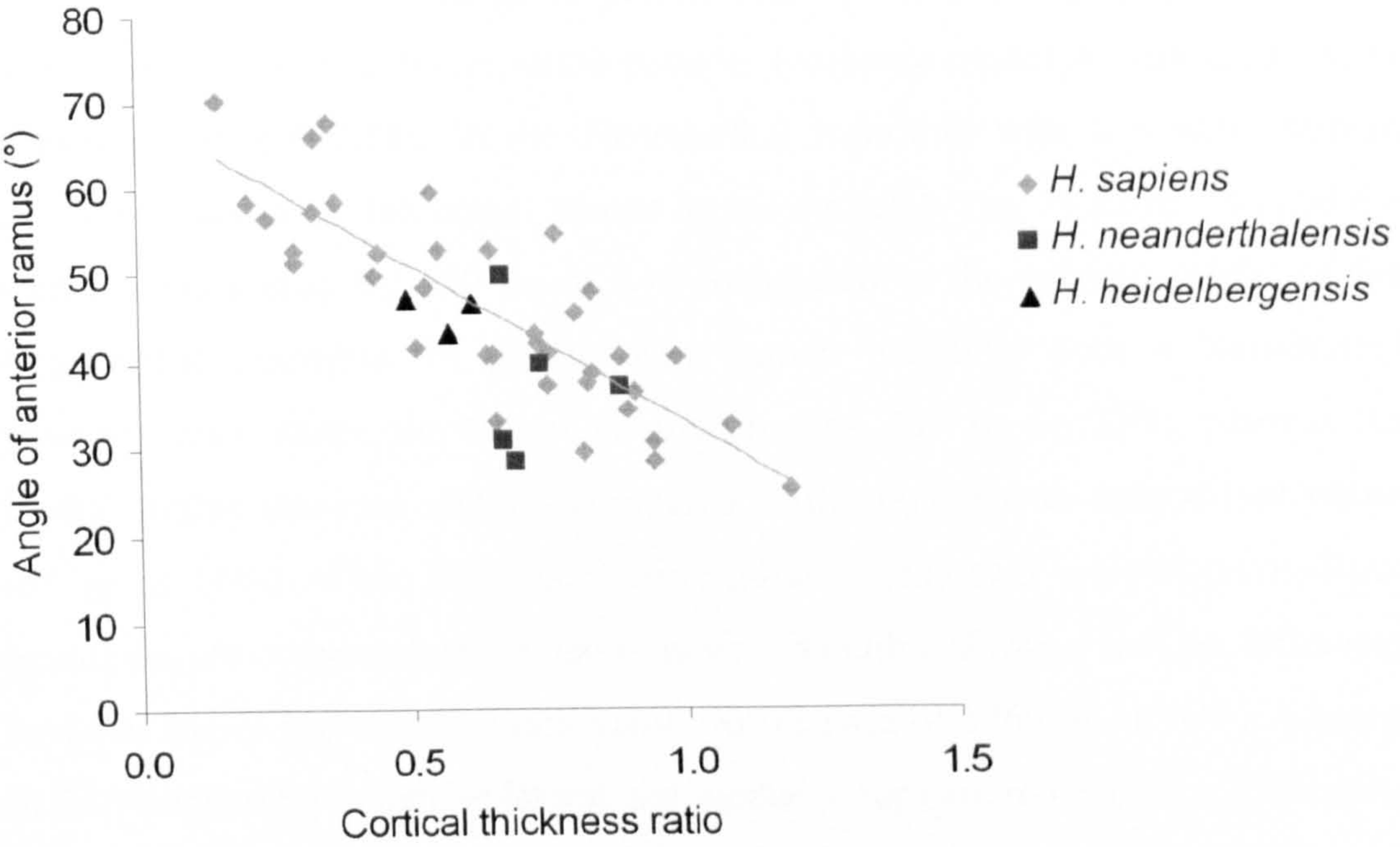

Fig. 7.8. Cortical thickness ratio against the angle of the anterior ramus.

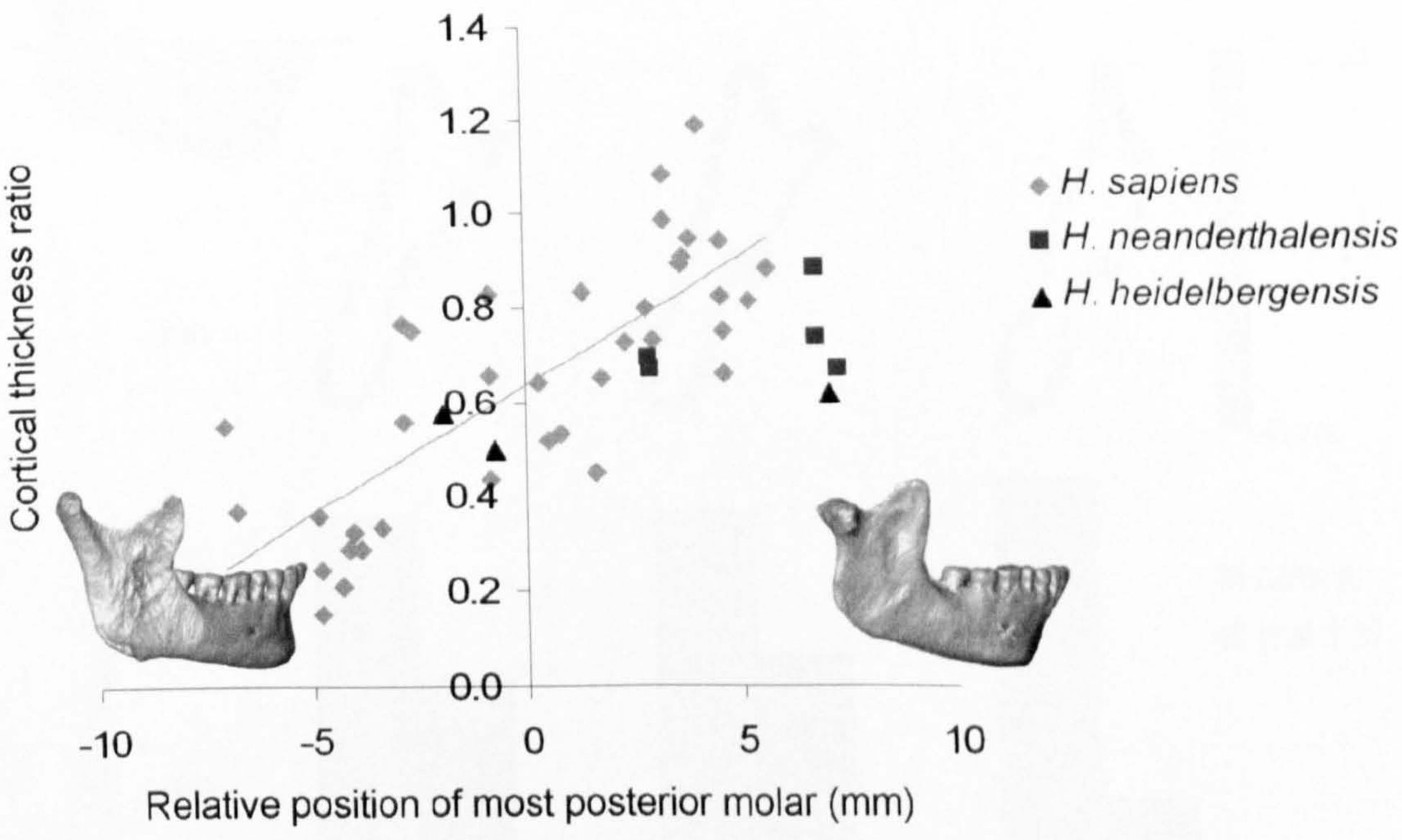

Fig. 7.9. Relative position of the most posterior molar against cortical thickness ratio.

Figures 7.10 and **7.11** summarise the results of the FEA: the von Mises strain values from the medial and lateral corners of the anterior ramus as well as the contour plots of transverse sections through the rami. In both mandibles, the artificial removal or addition of molars has little or no effect on the strain pattern

in the anterior ramus (compare model A with model B in **Figures 7.10** and **7.11**).

However, the exchange of anterior ramus morphology between the two mandibles results in different strain patterns (compare model A with model C in **Figures 7.10** and **7.11**). In the Neanderthal mandible with a modern human anterior ramus shape the lateral strains increase slightly (by 76 με or 7%) and the medial strains drop by 250 με or 34% compared to the original model of the Neanderthal mandible. In the modern human mandible with a Neanderthal anterior ramus shape the lateral strains drop by 443 με or 22%, whereas the medial strains decrease slightly compared to the model with unmodified ramus (67 με or 16%). When the strain distributions in the two original, unmodified mandibles are compared, the modern human mandible shows a striking difference between lateral and medial strain values (difference of 1560 με or 76%), whereas in the Neanderthal mandible lateral and medial values are more similar (difference of 358 με or 33%).

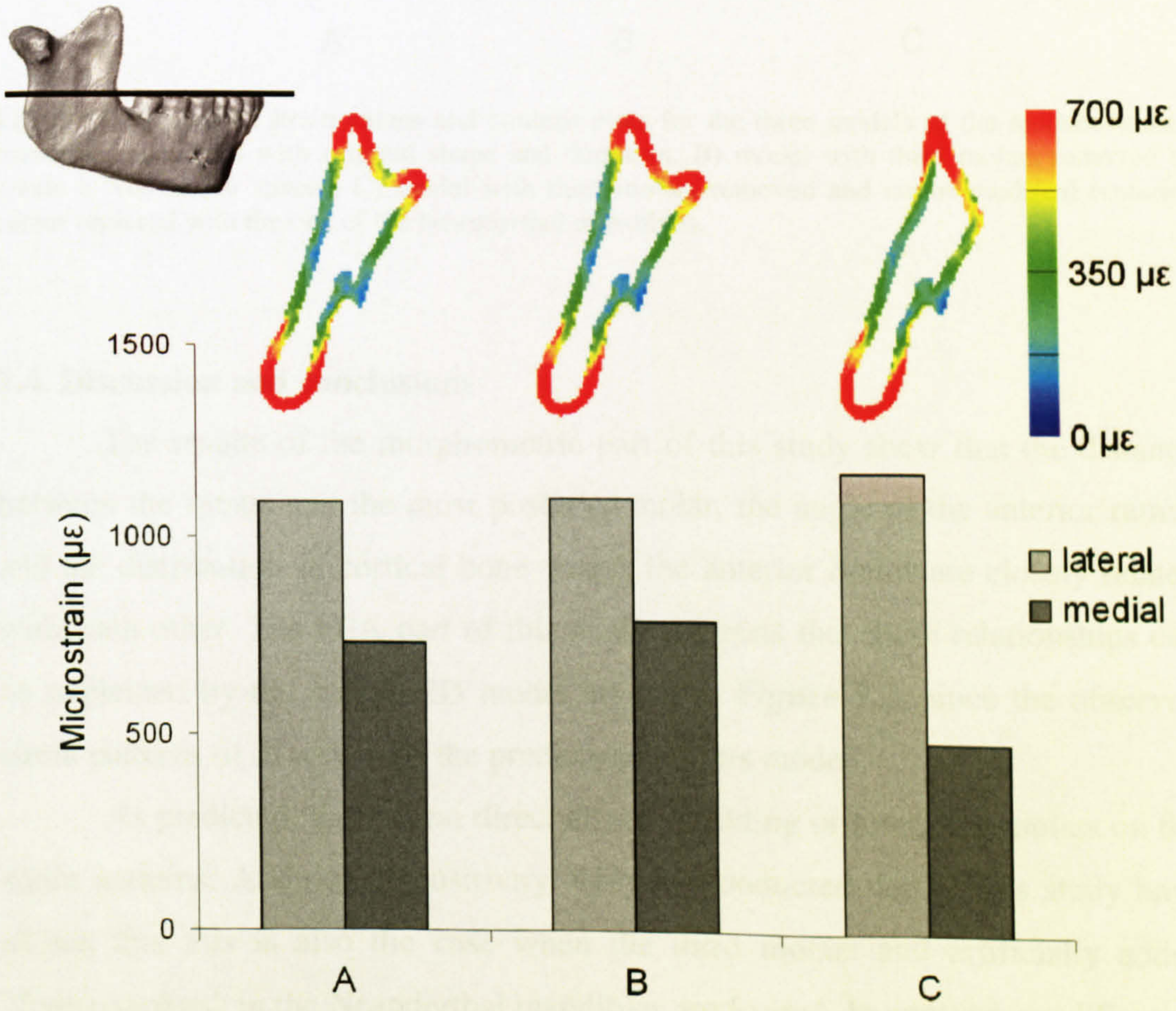

Fig. 7.10. Von Mises strain values and contour plots for the three models of the Neanderthal mandible: A) model with original shape and dentition, B) model with added "fourth molars" and thus lacking a retromolar space, C) model with original dentition but modified ramus (anterior ramus replaced with the one of the modern human mandible).

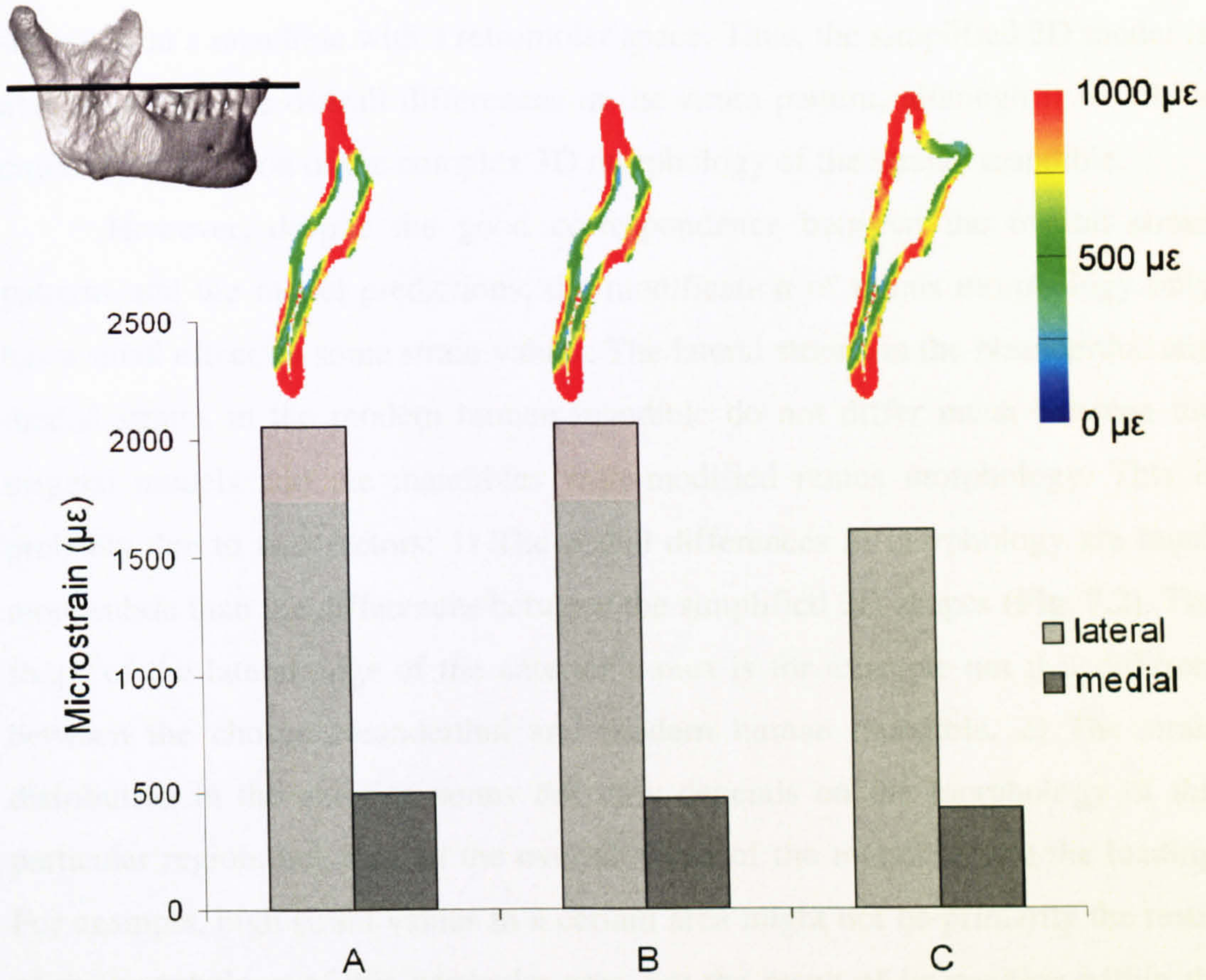

Fig. 7.11. Von Mises strain values and contour plots for the three models of the modern human mandible: A) model with original shape and dentition, B) model with third molars removed to create a "retromolar space", C) model with third molars removed and ramus modified (anterior ramus replaced with the one of the Neanderthal mandible).

7.4. Discussion and conclusions

The results of the morphometric part of this study show that the distance between the ramus and the most posterior molar, the angle of the anterior ramus and the distribution of cortical bone within the anterior ramus are closely related with each other. The FEA part of this study suggests that these relationships can be explained by the simple 2D model shown in **Figure 7.2**, since the observed strain patterns fit in well with the predictions of this model.

As predicted, there is no direct effect of adding or removing molars on the strain patterns. Additional sensitivity analyses conducted during this study have shown that this is also the case when the third molars and artificially added "fourth molars" in the Neanderthal mandibles are loaded. In contrast, modification of anterior ramus morphology results in different strain values. The difference between lateral and medial strains increases when the anterior ramus is shaped as

in a mandible without a retromolar space and decreases when the anterior ramus is shaped as in a mandible with a retromolar space. Thus, the simplified 2D model is able to predict the overall differences in the strain pattern, although it is only a crude representation of the complex 3D morphology of the human mandible.

However, despite the good correspondence between the overall strain patterns and the model predictions, the modification of ramus morphology only has a small effect on some strain values. The lateral strains in the Neanderthal and medial strains in the modern human mandible do not differ much between the original models and the mandibles with modified ramus morphology. This is probably due to two factors: 1) The actual differences in morphology are much more subtle than the differences between the simplified 2D shapes (**Fig. 7.2**). The shape of the lateral edge of the anterior ramus is for example not that different between the chosen Neanderthal and modern human mandible. 2) The strain distribution in the anterior ramus not only depends on the morphology of this particular region, but also on the overall shape of the mandible and the loading. For example, high strain values in a certain area might not be primarily the result of the morphology of this particular area, but the result of its position within the whole structure. In this case, changing the morphology of this particular area would have only a minor or no effect on the stresses and strains.

The combination of 3D FEA with the virtual modification of morphological features allows the effect of local morphological changes within the whole complex structure of a bone to be explored. By controlling potential confounding variables, it offers an almost experimental approach to test theoretical predictions. This approach appears to be especially useful if it is combined with data from traditional or geometric morphometric analyses as in this study. Thus, it is possible to study first whether or not variables are associated and then as a second step to test whether this reflects a causal relationship in a mechanical sense.

As pointed out at the beginning, this study did not attempt to address the question as to why retromolar spaces occur with a higher frequency in Neanderthals than in other Pleistocene *Homo* taxa or modern humans. Instead it aimed to investigate the effect of a retromolar space on the internal bone structure. Nevertheless, the result of this study that strains are unchanged despite the artificial removal or addition of molars, allows the conclusion to be drawn that it

is unlikely that a retromolar space occurred more often in Neanderthals because it improved the resistance to masticatory loads. Having the molar dentition closer or further away from the ramus does not result in a change of the stiffness of that region. However, the results do not rule out the possibility that a retromolar space was mechanically advantageous in a different way or the side effect of mechanical adaptations as has been suggested by some authors (Spencer & Demes 1993, Rak & Hylander 2007). These suggested a forward shift of the molar dentition (resulting in a retromolar space) to keep the molars within the most efficient bite zone (Spencer & Demes 1993) or to create a larger vertical distance between the upper and lower molars for the same gape size (Rak & Hylander 2007).

Finally, the results of this study should be seen within the broader context of interplay between developmental constraints and mechanical adaptations. Here, the spatial requirements of the molar dentition seem to place constraints on the external shape of the anterior ramus. This creates certain mechanical conditions to which the internal structure of the bone adapts. In future studies, it would be interesting to investigate this interplay between developmental constraints and mechanical adaptations in the mandibular ramus during ontogeny.

Chapter 8: Superior ramal morphology and its relation to the orientation of the temporalis' lines of action

8.1. Introduction

The superior part of the mandibular ramus shows considerable morphological variation in Pleistocene as well as modern humans (**Fig. 8.1**). Some authors have suggested that Neanderthals show a unique superior ramal morphology (Rak 1998, Rak et al. 2002): a shallow, asymmetric sigmoid notch and a posteriorly orientated coronoid process, which often exceeds the condylar process in height, while modern humans are said to have a coronoid process of the same height as the condylar process and a deep, symmetric sigmoid notch approximately at the midpoint between the two processes. This distinction has recently been challenged on the basis of the large variation within anatomically modern humans, Neanderthals and *H. heidelbergensis* (Wolpoff & Frayer 2005).

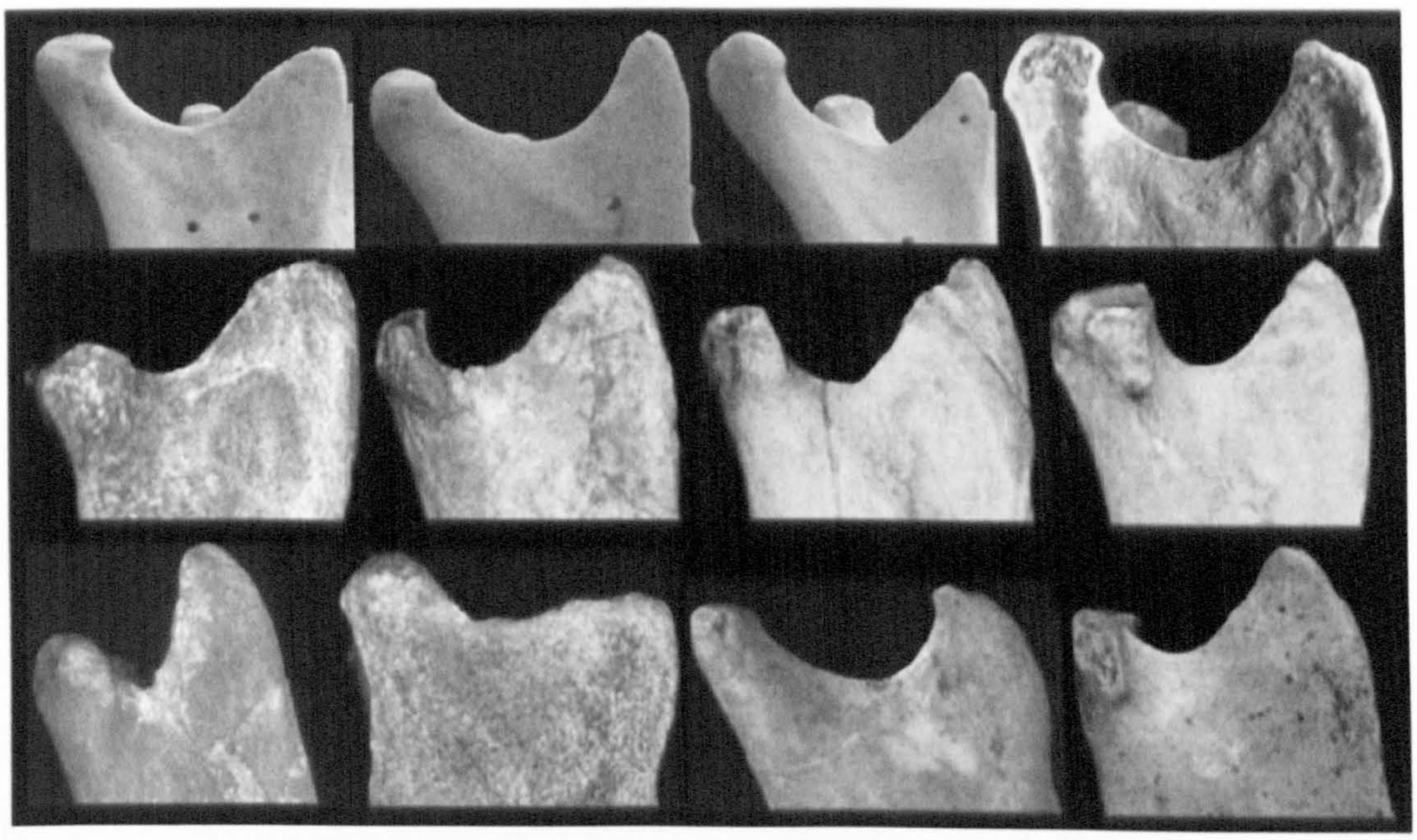

Fig. 8.1. Variation of superior ramus morphology in mandibles of anatomically modern humans (upper row), Neanderthals (middle row) and *H. heidelbergensis* (bottom row). The mandibles are so orientated that the occlusal plane is horizontal. Not to scale.

However, even if these aspects of superior ramal morphology are not unique to Neanderthals, they occur among them with high frequency, which is interesting from a functional perspective. The coronoid process provides the insertion area for the temporalis muscle, which is one of the most powerful muscles of mastication in humans. It is commonly assumed that the temporalis

muscle acts as a part of a functional matrix (see 2.3.1 for a detailed description of the concept) for the coronoid process during growth (Moss 1962, Moss & Rankow 1968, Moss & Salentijn 1969, Moss & Meehan 1970): During masticatory function the contracting temporalis fibres apply forces to the coronoid process that stimulate bone resorption and deposition. Thus, the form of the coronoid process is altered depending on the magnitudes and directions of the muscle forces. In addition, it has been suggested that the form of the sigmoid notch is largely determined by the form of the coronoid process: that an anteriorly oriented coronoid process is associated with a shallow notch, a posteriorly oriented coronoid process with a deep notch (Simon & Moss 1973). Therefore, the form of the sigmoid notch should also be affected by the action of the temporalis.

Indeed, animal experiments support a close link between temporalis function and the size and shape of the coronoid process as well as of the sigmoid notch. The detachment of the temporalis muscle in rats (Washburn 1947, Moore 1959) leads to the resorption of the coronoid process and marked alterations in its shape. The selective removal of the posterior and middle temporalis fibres in rats results in a more anteriorly orientated coronoid process (Avis 1959) and a shallower sigmoid notch (Moss & Meehan 1970).

Simon and Moss (1973) have used the latter observation to explain the morphological variation of the superior ramus in modern human and Pleistocene populations. They hypothesised that when the activity of the anterior, vertically orientated fibres of temporalis dominates this produces an anteriorly oriented coronoid process and a shallow sigmoid notch, whereas high activity of the middle and posterior fibres, which have a more horizontal orientation, generates a posteriorly oriented coronoid process and a deep sigmoid notch. In contrast to this, Neanderthals are said to have a posteriorly oriented coronoid process but shallow sigmoid notch and modern humans an anteriorly oriented coronoid process but a deep sigmoid notch (Minugh-Purvis & Lewandowski 1992, Rak 1998, Rak et al. 2002). It seems likely that these differences between Neanderthals and modern humans are also linked to temporalis function and anatomy, but maybe in a different way than in the cited animal experiments.

Experimental detachment of muscle fibres is not possible in humans but FEA allows "virtual experiments". Muscle forces can be added or deleted and their orientation can be altered arbitrarily. This study will investigate the effect on

the strain distribution in the superior ramus of virtually removing temporalis fibres. It is well known that that alterations of loading and resulting changes in the strain distributions influence bone modelling (e.g. Lanyon & Rubin 1984). In consequence, variations in strain distributions observed during such virtual experiment might be used to infer where bone would be resorbed or deposited in the mandible. While there is still debate about how strains relate to bone modelling in general (see 2.1 for a review) bone deposition usually occurs where peak strains are large and resorption where strains decrease. Additionally, some authors have suggested that strain polarity plays a role: that tension causes bone resorption, and compression bone formation (Jansen 1920, Triepel 1922, Bassett 1965, Oxnard et al. 1994, Hirschberg 2005). Ideally, bone modelling in response to changes in the temporalis should be studied by simulating the actual modelling processes.

This study is, however, limited to the evaluation of the changes in the strains. If bone modelling is directly related to strain magnitude, than Simon and Moss' (1973) hypothesis predicts that the removal of the middle and posterior temporalis fibres (given that total temporalis force is kept constant) should increase strains at the anterior margin of the coronoid process but decrease strains posteriorly, whereas removal of the anterior fibres should decrease strains at the anterior margin and increase strains at the posterior margin. In addition, the effects of virtual removal of temporalis fibres on strains at the deepest point of the sigmoid notch will be examined to see if these decrease as would be predicted by the observations of Simon and Moss (1973). If strain polarity plays an important role, then the same distribution as for low and high magnitudes would be expected for compressive and tensile strains respectively.

8.2. Material and methods

For this study, a modern human mandible with dentition complete apart from congenitally absent third molars was chosen (specimen H-A 001). The initial image processing (i.e. the definition of a density threshold for bone and teeth and the addition of a layer of periodontal ligament around each tooth root) was performed using the original μCT scan of the specimen with a voxel size of 0.15 mm in all directions (see **Table 3.3** for more information about the scan). In order to reduce processing time, the model was then downsampled to a voxel size

of 0.3 mm. Two simplified TMJs were added as described in Chapter 5 and the model was converted into a FE mesh with ca. 2 million elements.

After defining material properties (see Chapter 6 for values), a unilateral molar bite was simulated by constraining the occlusal surface of the right M1 and the corners of the TMJs in all three axes and applying the muscle force magnitudes and orientations as described in section 3.8. In order to assess the effect of removing temporalis fibres, two additional load cases were modelled (**Table 8.1**): 1) by deleting the forces representing the middle and posterior temporalis fibres on both sides of the mandible and adding these forces to the force representing the anterior temporalis, 2) by deleting the force for the anterior temporalis and assigning it to the middle and posterior portions so that the ratio of the force magnitudes between middle and posterior fibres was kept constant (**Fig. 8.2**). The respective muscle forces of removed fibres were thus not simply deleted, but distributed over the remaining muscle portions to allow comparison of the strain distributions when the same force is applied in different ways.

Temporalis portion	Muscle force magnitudes (N)					
	All portions present[1]		Anterior portion removed		Middle and posterior portions removed	
	W	B	W	B	W	B
Anterior	123	97	-	-	284	235
Middle	91	92	161	157	-	-
Posterior	70	46	123	78	-	-

[1]based on PCSA measurements from van Eijden and co-workers (1995, 1996, 1997), n = 8

Table 8.1. Force magnitudes in N applied to the temporalis portions on the working (W) and balancing (B) sides for the three different load cases.

Based on the node displacements of the solved models, maximum (ε_1) and minimum principal strain (ε_3) and von Mises strain (ε_v) were calculated for each finite element. The differences in the strain distributions between the load cases were visualised by difference contour plots: The strain value for each element of one model was subtracted from the value for the same element in the second model with the resulting differences between all elements visualised as a colour-coded contour map.

Additionally, element strain values (ε_1, ε_3, ε_v) were extracted from four locations, each covering an area of 100 finite elements (**Fig. 8.3**): 1) the anterior margin of the coronoid process, 2) the tip of the process, 3) the posterior margin of the process and 4) the area around the deepest point of the sigmoid notch when the mandible is orientated so that the occlusal plane is horizontal. The extracted maximum and minimum principal strain values were used to calculate the minimum/maximum principal strain ($\varepsilon_1/\varepsilon_3$) ratio for each of the locations, so that differences in the ratio between tensile and compressive strains could be evaluated in addition to the comparison of the strain magnitudes.

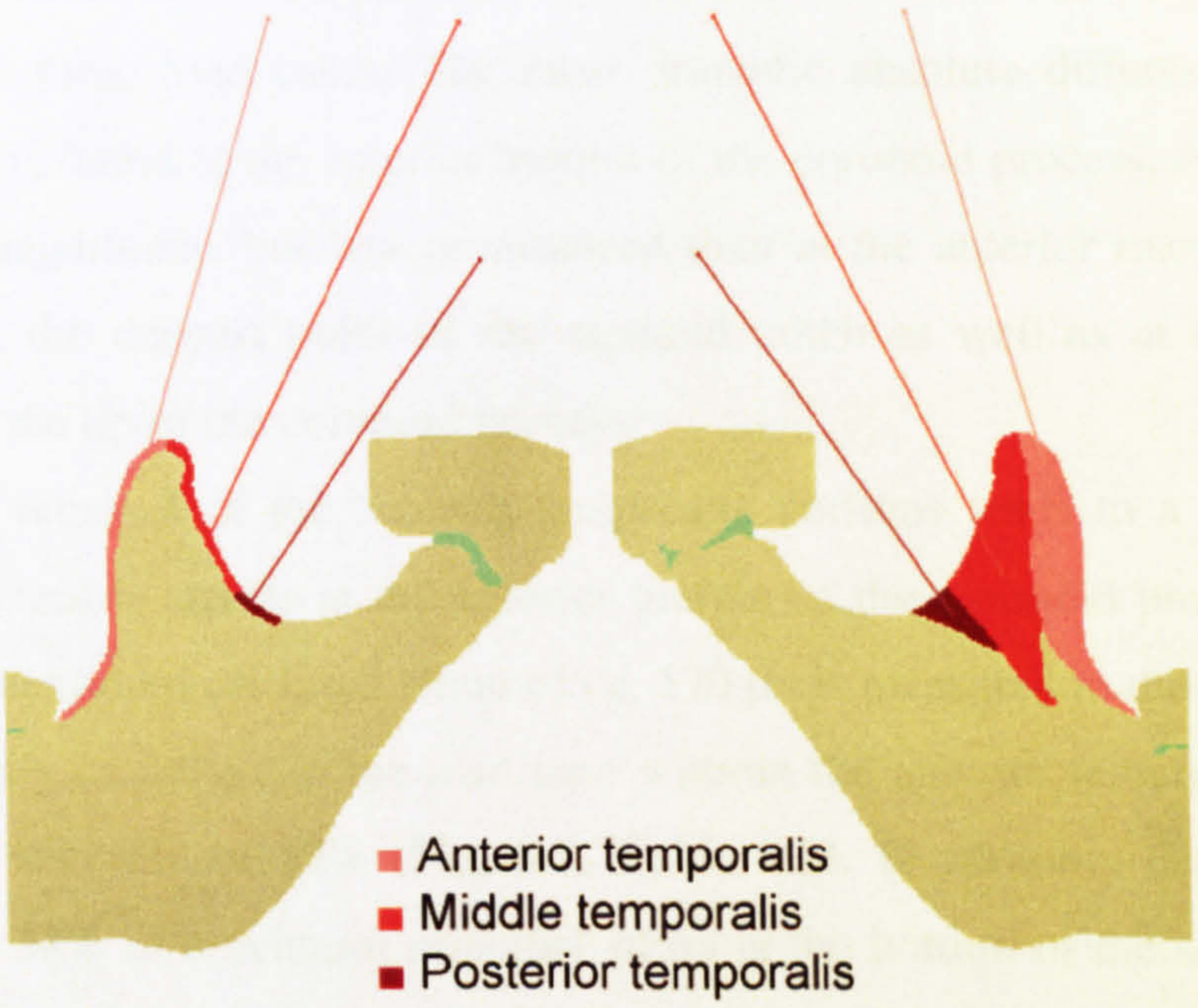

Fig. 8.2. Modelling of the three temporalis portions. Left image: buccal view, right image: lingual view. The mandible used is H-A 001.

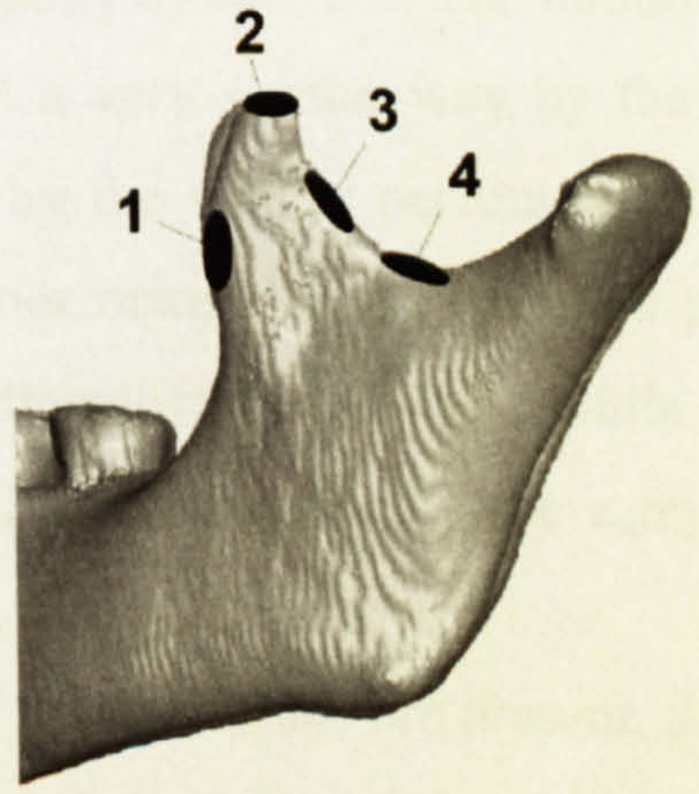

Fig. 8.3. Areas from which surface strain values were extracted: 1) the anterior margin of the coronoid process, 2) the tip of the process, 3) the posterior margin of the process and 4) the area around the deepest point of the sigmoid notch. All the strains were extracted from the working side ramus.

8.3. Results

In general, the strain magnitudes in the coronoid process and the adjacent areas are low compared to other regions of the mandible (see e.g. Chapter 5). At the four sampling locations, maximum and minimum principal strain values do not exceed ±500 με (**Fig. 8.5**). The strain magnitudes at the working side ramus are higher than at the balancing side ramus, but the strain distributions as well as the differences observed between load cases do not differ appreciably between sides. The strain values presented in **Figures 8.4-8.7** and **Table 8.2** are therefore only from the working side ramus.

The strain distributions show considerable local variation (**Figure 8.4**) between the three load cases. The most dramatic absolute difference in strain magnitudes is found at the anterior margin of the coronoid process. Alterations in the strain magnitudes, but less pronounced than at the anterior margin, are also observed at the deepest point of the sigmoid notch as well as at the posterior margin and the tip of the coronoid process.

The removal of the anterior temporalis portions leads to a considerable decrease in tensile strains at the anterior margin of the coronoid process. At this location a maximum principal strain of ca. 170 με is measured in the original load case, but only ca. 20 με in the load case without the anterior temporalis portion, which is a decrease of 89% (**Fig. 8.5, Table 8.2**). In addition, there is a local increase of 37% in maximum principal strain at the bottom of the sigmoid notch as well as some increase at the bottom and the top of the posterior margin. At the centre of the posterior margin and the tip of the coronoid process maximum principal strain decreases slightly by ca. 12%. The minimum principal strain at the four locations is affected in a very similar way by the removal of the anterior temporalis, being reflected by the similar percentage changes (**Table 8.2**). The only exception is the posterior margin of the coronoid process, where minimum principal strain decreases dramatically by 76%, while the maximum principal strain only decreases by 12%. Consequently, the $\varepsilon_1/\varepsilon_3$ ratio at this location is altered (**Fig. 8.6**).

When all portions of the temporalis are present, the posterior margin of the coronoid process is loaded under compression, which is reflected by a $\varepsilon_1/\varepsilon_3$ ratio below one. The $\varepsilon_1/\varepsilon_3$ ratios for the other three locations are above one and therefore tension dominates in these areas. The removal of the anterior temporalis

portion results in a $\varepsilon_1/\varepsilon_3$ ratio, which is above one at all four areas, indicating that they are under net tension.

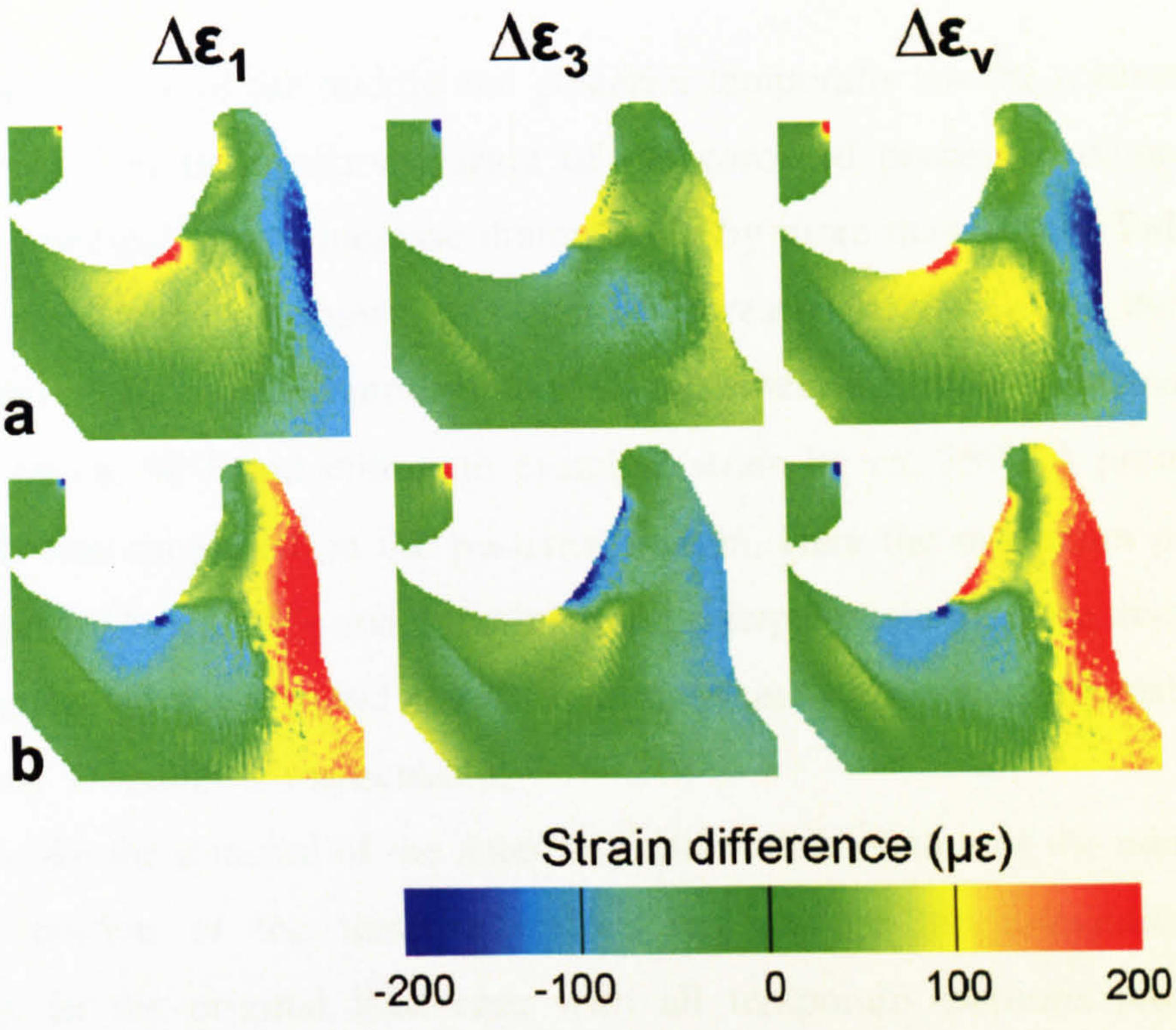

Fig. 8.4. Strain difference maps for the working side ramus showing the differences in strain magnitudes in the two load cases with deleted temporalis portions from those of the original load case with all three temporalis portions: a) effect of deleting the anterior temporalis, b) effect of deleting the middle and posterior temporalis. Differences are shown for maximum principal strain (ε_1), minimum principal strain (ε_3) and von Mises strain (ε_v).

Locations	Percentage changes in strain magnitudes					
	Anterior temporalis removed			Middle and posterior temporalis removed		
	ε_1	ε_3	ε_v	ε_1	ε_3	ε_v
1	-89	-90	-89	118	121	54
2	-13	-14	-12	48	74	39
3	-12	-76	-57	61	115	52
4	37	43	38	-37	-23	-47

Table 8.2. Percentage increase and decrease in strain magnitudes as a result of removing different temporalis portions. Shown are percentage changes for maximum principal strain (ε_1), minimum principal strain (ε_3) and von Mises strain (ε_v). Each percentage value is computed as ((b-a)/a)*100 (a = strain value from the model with all temporalis portions, b = strain value from a model with temporalis portions deleted). Positive values indicate an increase in strain magnitudes, negative values a decrease.

The comparison of the von Mises strain values, which combine principal strains, at the four locations indicates that the removal of the anterior temporalis

leads to a decrease in von Mises strains at all locations on the coronoid process except at the deepest point of the sigmoid notch where strains increase by 38% (**Fig. 8.7**).

The removal of the middle and posterior temporalis has the reverse effect on the strains. At the anterior margin of the coronoid process maximum and minimum principal strains increase dramatically by more than 100% (**Table 8.2, Fig. 8.5**). As **Figure 8.4** shows, this area of increased strains covers the whole anterior part of the coronoid process up to its tip, where maximum principal strain increases by ca. 50% and minimum principal strain by ca. 75%. A pronounced increase is also measured on the posterior margin. Here the maximum principal strain increases by ca. 60% and the minimum principal strain by more than 100%. At the bottom of the sigmoid notch, maximum and minimum principal strains decrease by 37 and 23% respectively.

Unlike the removal of the anterior portion, the deletion of the middle and posterior portion of the temporalis does not change the $\varepsilon_1/\varepsilon_3$ ratios much (**Fig. 8.6**). In the original load case with all temporalis portions present the anterior margin and the tip of the coronoid process as well as the bottom of the sigmoid notch are under net tension, while the posterior margin of the coronoid process is under net compression. The same pattern is observed when the middle and posterior portion are removed.

In keeping with the results for maximum and minimum principal strains, removal of the middle and posterior temporalis portions results in an increase in von Mises strain magnitudes at all locations on the coronoid process, but in a decrease in the sigmoid notch (**Fig. 8.7**).

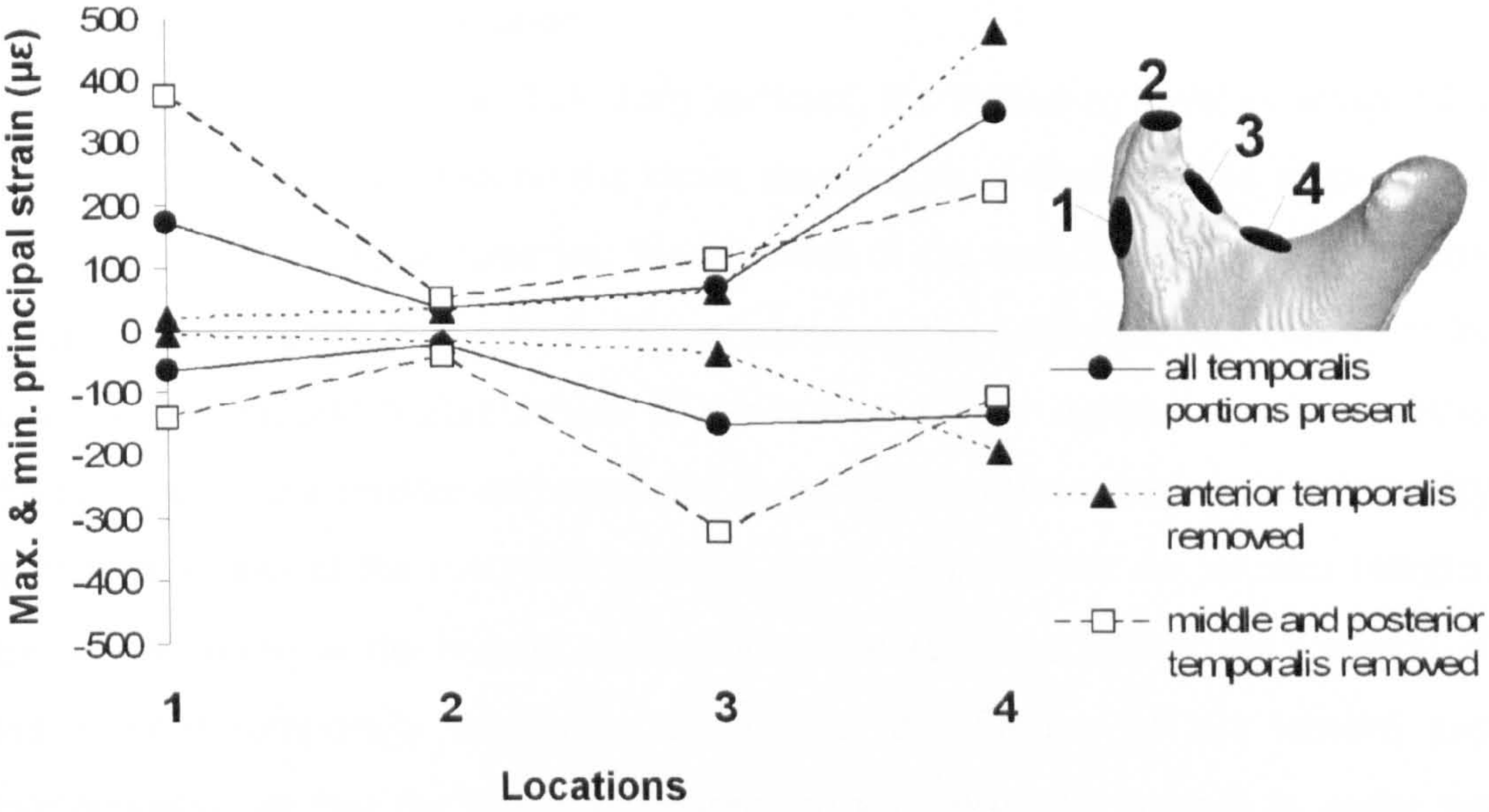

Fig. 8.5. Maximum and minimum principal strain magnitudes at the four sampling locations.

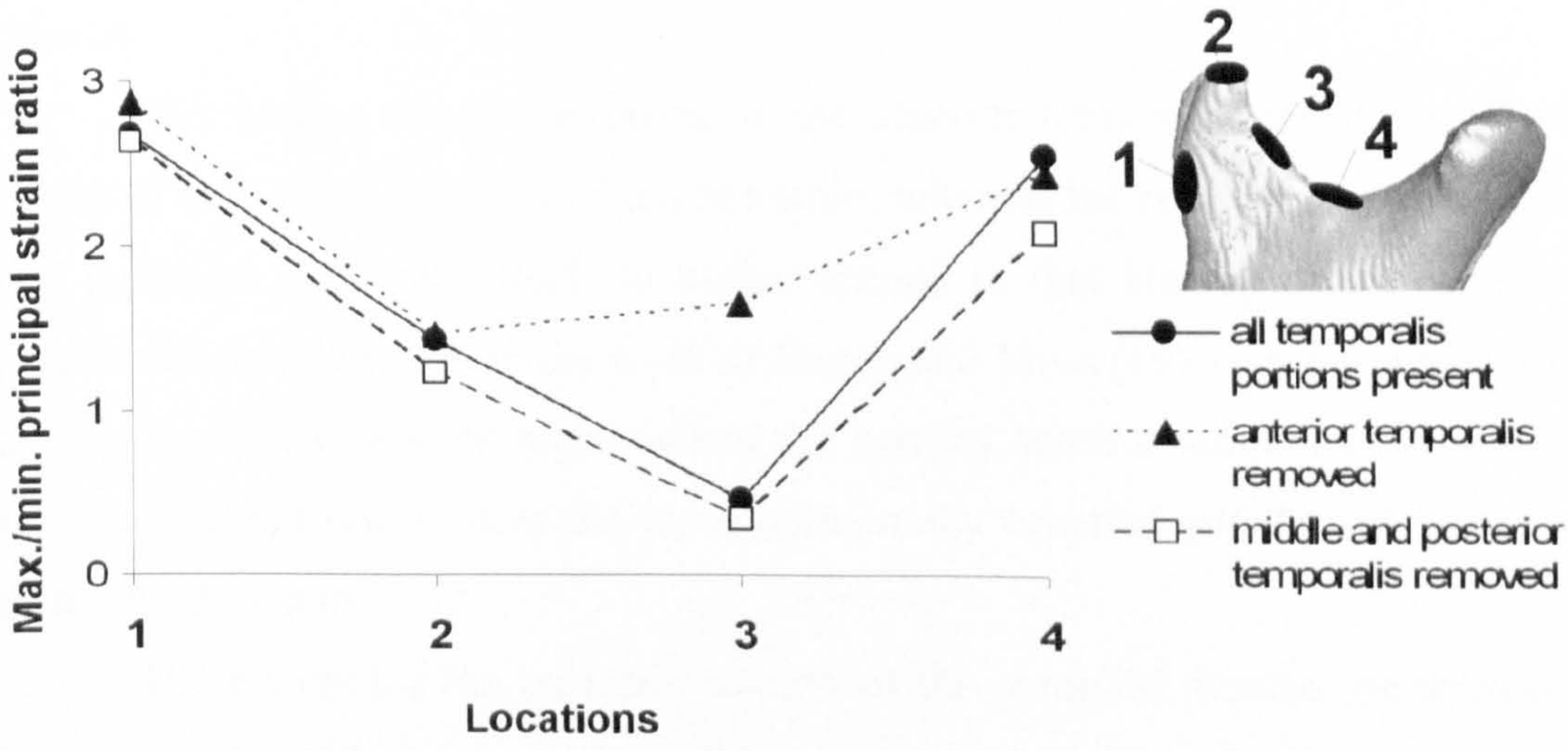

Fig. 8.6. Maximum/minimum principal strain ($\varepsilon_1/\varepsilon_3$) ratio for the four sampling locations.

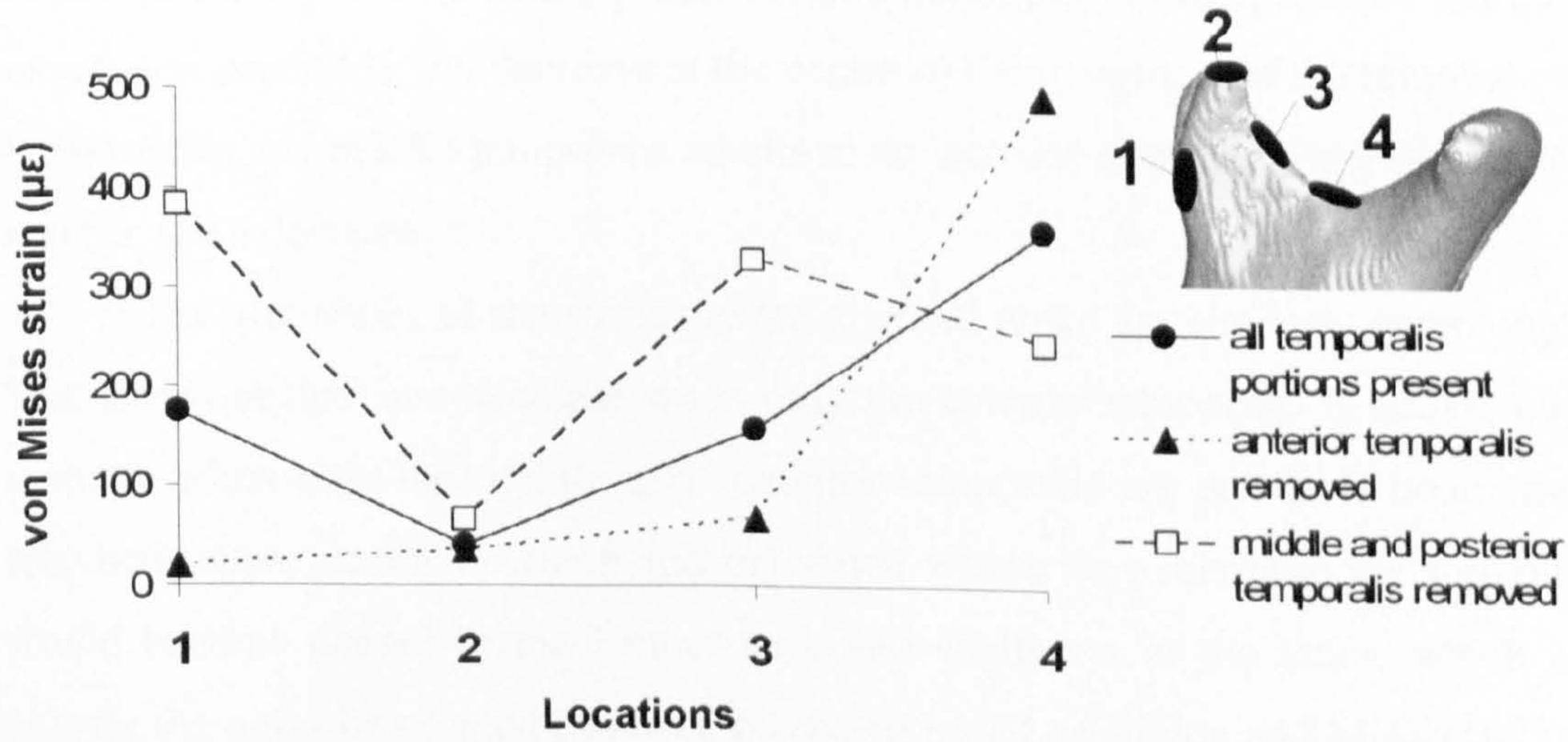

Fig. 8.7. Von Mises strain magnitudes at the four sampling locations.

8.4. Discussion and conclusions

As the results of this FEA study indicate, the virtual removal of temporalis portions has a marked effect on the strain magnitudes at the coronoid process and the sigmoid notch. To summarise, the removal of the anterior temporalis portion results in lower principal and von Mises strains at the coronoid, particularly at its anterior margin, and higher strains at the bottom of the sigmoid notch, whereas the removal of the middle and posterior temporalis portions leads to dramatically increased strains at the coronoid process, again especially at its anterior margin, and lower strains at the bottom of the sigmoid notch. In addition, the removal of the anterior temporalis results in a different distribution of net tension and compression, so that the posterior margin of the coronoid process is under net tension, while it is under net compression when all temporalis portions are present.

The finding that the removal of the anterior temporalis results in lower strains at the anterior margin of the coronoid, whereas the removal of the middle and posterior temporalis leads to higher strains in that area is consistent with predictions that derive from the work of Simon and Moss (1973) that strains at the anterior margin should be higher when the vertical anterior temporalis fibres are more active and lower when the more horizontally oriented middle and posterior fibres are dominant.

The results for the posterior margin of the coronoid process are however less consistent with the predictions. When the anterior temporalis is removed, the strains just below the tip of the process and at the bottom of the posterior margin increase as predicted, but decrease at the centre of the margin. And the removal of the posterior and middle temporalis results in an increase of strain along the whole margin, not a decrease.

The alterations of the strains in the sigmoid notch are similarly surprising. The strains in this area decrease when only the anterior temporalis is active, but increase when only the middle and posterior temporalis are active. If bone was resorbed where strains decrease and deposited where they increase, the sigmoid would become deeper in the former case and shallower in the latter, which is exactly the opposite of what has been predicted based on Simon and Moss (1973). However, these results are consistent with the differences between Neanderthals and modern humans (Rak 1998, Rak et al. 2002), since a deepening of the

sigmoid notch would be associated with a forward shift of the anterior coronoid margin and bone deposition in the notch with a backwards shift.

If the idea of strain polarity as a stimulus for bone modelling is applied (Jansen 1920, Triepel 1922, Bassett 1965, Oxnard et al. 1994, Hirschberg 2005), there is no clear pattern visible. Almost all locations, from which strains were extracted, are under net tension, apart from the posterior margin of the coronoid in two of the load cases. This should lead to resorption of a large part of the coronoid, even if all temporalis fibres are present, which cannot be the case.

However, additional studies are necessary to properly investigate the relationship between temporalis function and specific aspects of the superior ramus morphology. Ideally, more than just one load case should be modelled in order to obtain a more complete image of the strain distribution in this region. In addition, bone adapts to its function by continuous remodelling activity and each alteration of the morphology will alter the strain pattern slightly. It is therefore not possible to predict the change in form due to remodelling based only on the initial strain patterns.

Instead of just quantifying strains and making assumptions about potential bone remodelling activity, it would be better to actually simulate bone modelling by combining FEA with bone modelling algorithms. Moreover, this study virtually removed temporalis fibres in an adult mandible. In the animal experiments discussed by Simon and Moss (1973), the respective fibres were excised in young juveniles (Moss & Meehan 1970). In order to simulate the experiments properly, it would be interesting to use juvenile mandibles and apply bone remodelling algorithms to these. In addition, the attachment of the muscle fibres in the FE could be modelled more realistically. Currently, only nodes on the model surface are selected to apply muscle forces. Histological studies have however shown that the temporalis tendons attach to the mandible in different ways, for example, via a fibrocartilage tissue or by directly inserting into the bone (Hems & Tillmann 2000). If this could be modelled in the FE model accurately, it might change the strain pattern.

Although the simplicity of the present study does not allow the relationship between temporalis function and morphological changes in the superior ramus to be tested directly, it shows that the strains in this region are altered significantly when temporalis portions are removed and the orientation of

the muscle force is thus changed. This supports the idea that variations in superior ramus morphology among Pleistocene and modern humans are indeed closely linked with differences in temporalis anatomy and function.

Theoretically, there are several potential reasons why Neanderthals might have been different in this respect. One reason is the different cranial morphology compared to modern humans. The orientation of the temporalis fibres is defined by the spatial relationship between their origin and insertion, which depends on the ramal height, breadth and angulation as well as the form of the cranium, for example, a low and elongated neurocranium should result in more horizontally oriented temporalis fibres, whereas a high and short neurocranium should lead to a more vertical orientation. In addition, experimental data suggest that the relative activity of the temporalis portions is closely linked with different aspects of cranial and mandibular morphology, particularly with the degree of prognathism (Møller 1966). Therefore, it is likely that Neanderthal temporalis anatomy and function were different to those of modern humans.

Finally, there is abundant experimental data which show that the relative activity of different portions within each masticatory muscle also depends on the task (Møller 1966, Vitti & Basmajian 1977, Blanksma & van Eijden 1990, Blanksma et al. 1992, Blanksma & van Eijden 1995, Murray et al. 1999). For example, the anterior temporalis fibres are especially active during an upwards pull of the mandible whereas the more horizontal posterior fibres are particularly active when the mandible is retracted (Gray et al. 2005).

The differential activation of the temporalis portions has been used to explain the typical Neanderthal superior ramus morphology as an adaptation to frequent paramasticatory use of the front teeth (Minugh-Purvis & Lewandowski 1992). These authors argue that such use of the front teeth led to a frequent stimulation of the posterior temporalis so that a posteriorly oriented coronoid process was retained into adulthood. However, such behavioural interpretations should be treated with caution. Even if a link between a posteriorly oriented coronoid process and the activity of the posterior temporalis could be confirmed, it would not necessarily indicate a behavioural adaptation. As mentioned above, certain fibre orientations or differential activities of muscle portions can be likewise the effect of the overall cranial and mandibular form and the spatial relationship between different aspects of the masticatory apparatus. The

morphological variation in the superior ramus should be therefore not seen in isolation but in the context of the considerable variation of cranial and mandibular form in the Pleistocene as well as in modern human populations.

This study has only provided some first, preliminary results regarding the relationship between temporalis and superior ramus morphology. Future studies should further investigate this link, for example, by altering the orientation of muscle vectors instead of deleting them and modifying the morphology of the superior ramus and studying the effect on the strain distribution. However, eventually, studies should combine FEA with a bone modelling algorithm since the evaluation of strain distributions can only provide limited information.

Chapter 9: The mechanical significance of anatomically modern human symphyseal morphology

9.1. Introduction

It is generally accepted that a clearly protruding *mentum osseum* or chin is a feature unique to anatomically modern humans. Although some archaic members of the genus *Homo*, especially some Neanderthal fossils have been said to show incipient chins or some elements of the *mentum osseum* (McCown & Keith 1939, Ascenzi & Segre 1971, Wolpoff et al. 1981, Smith 1984, Lieberman 1995, Rosas 1995, Lam et al. 1996, Stefan & Trinkaus 1998a, 1998b, Wolpoff 1999), its consistent presence is only found in early and recent populations of *Homo sapiens* (Schwartz & Tattersall 2000, Dobson & Trinkaus 2002).

Closely linked with the emergence of the human chin is a change in the orientation of the mandibular symphysis. In anatomically modern humans, the symphysis is more vertical (**Fig. 9.1**) than in earlier hominins and other primates. This change of symphyseal orientation occurred together with the emergence of the chin during the later Pleistocene (Stefan & Trinkaus 1998b, Dobson & Trinkaus 2002).

The uniqueness of the modern human symphyseal morphology has led to speculation about its functional significance. Some have suggested that the chin is linked to other unique aspects of modern human evolution like the development of speech (Walkhoff 1904, Ichim et al. 2007a), or the reduction of the dentition and masticatory musculature resulting in "hypofunction", and thus a functionally deficient mandible (Riesenfeld 1969). The speech hypothesis is difficult to test and seems unlikely, since stresses and strains during speech can be assumed to be much lower than during incision and mastication. The "hypofunction" hypothesis has been convincingly ruled out by Daegling (1990, 1993a), who questioned the comparability of the experimental basis of this hypothesis and pointed out that there is no convincing evidence for the assumption that human mandibles are structurally weak compared to those of other primates.

Other authors have tried to explain the human chin as a buttress to resist specific loads occurring during masticatory function (DuBrul & Sicher 1954, White 1977, Daegling 1990, 1993a). From *in vivo* strain measurements in non-human primates, especially *Macaca fascicularis*, it is known that the primate

symphysis is primarily loaded in four ways (Hylander 1984, 1985). During incision and the powerstroke of mastication, these are: 1) lateral bending in the transverse plane (LTB or wishboning), 2) dorsoventral shear (DVS), and 3) vertical bending in the coronal plane caused by a twisting of each corpus around its anteroposterior axis (CB). In addition, medial transverse bending (MTB or reverse wishboning) occurs during jaw opening (**Figure 9.2**).

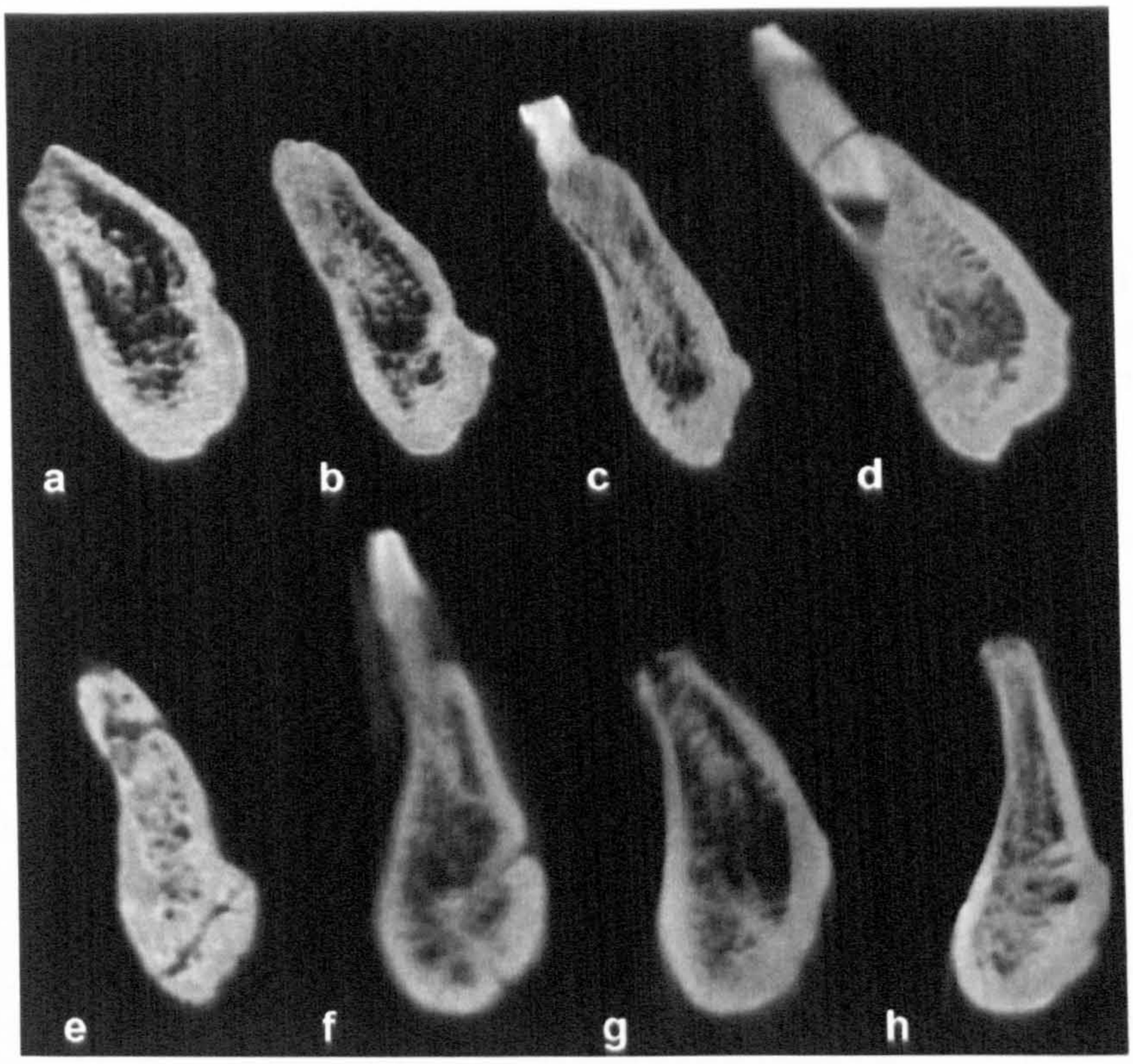

Fig. 9.1. Symphyseal cross-sections of *H. neanderthalensis* and *H. sapiens*: a) Krapina 57, b) Krapina 58, c) Krapina 59, d) Régourdou 1, e) Skhūl 5 and 3 modern humans (f, g, h). Not to scale. Specimens are orientated so that the occlusal plane is horizontal.

The occurrence of these load types is due to the recruitment pattern and orientation of the lines of action of the masticatory muscles. When the jaw is opened, MTB occurs due to the medially directed force component of the lateral pterygoid muscles that squeezes the rami together, resulting in labial tension and lingual compression at the symphysis. During the powerstroke DVS at the symphysis is created by the vertical component of the balancing side jaw adductor muscle force, which elevates the balancing side of the mandible (Hylander 1984, 1985). Wishboning, which occurs at the end of the powerstroke, is associated with late peak activity of the balancing side deep masseter coupled with a residual force from the decreasing activity of the working and balancing side superficial masseters (Hylander et al. 1987, Hylander & Johnson 1994). Since the lines of

action of these muscles are partly horizontal, the two halves of the mandible are pulled apart like a wishbone, causing labial compression and lingual tension. Finally, since the resultant force of the adductor muscles is located lateral to the long axis of each mandibular corpus, the corpora rotate about their long axes, which results in eversion of the lower border and inversion of the postcanine alveolar process. This axial torsion of the corpora causes vertical bending in the coronal plane with compression at the alveolar region and tension at the symphyseal base (Hylander 1984).

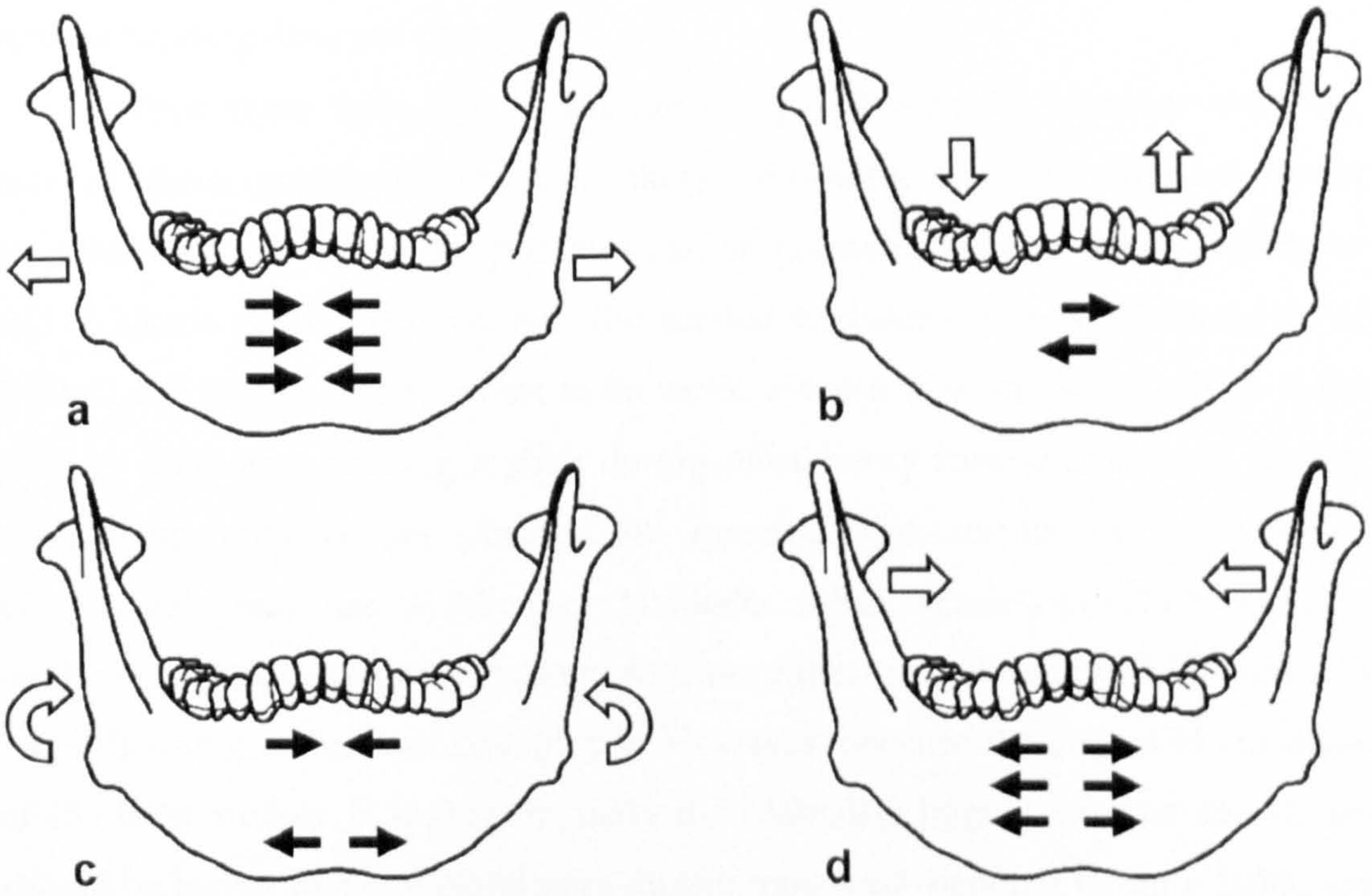

Fig. 9.2. Potential loads at the human symphysis during masticatory function (modified after Fukase 2007: 56, Fig. 1). White arrows indicate the effect of the muscle forces. Black arrows show the stresses on the labial surface of the bone at the symphysis. Tensile stresses are visualised by arrows pointing away from each other, compressive stresses by arrows pointing towards each other, shear stresses by arrows on top of each other pointing in different directions. a) wishboning or lateral transverse bending (LTB), b) dorsoventral shear (DVS), c) vertical bending in the coronal plane due to an axial rotation of the mandibular corpora (CB) and d) reverse wishboning or medial transverse bending (MTB).

According to Hylander (1984, 1985), the mandibular symphysis can adapt to these loads in different ways: for example, by increasing its labio-lingual thickness to counter CB and transverse bending (i.e. MTB and LTB), and increasing its cross-sectional area, especially at the lower aspect of the symphysis to better resist DVS, or increasing its vertical height to counter CB. In addition, an increase of cross-sectional area of the symphysis helps to counter all load types.

Other authors have explained the human chin as an adaptation to some of these particular loads described by Hylander (1984). DuBrul and Sicher (1954)

suggested that the chin serves to buttress the symphysis against MTB, which produces labial tension at the symphysis. White (1977) proposed the contrary, that the chin provides resistance to LTB resulting in labial compression. Finally, Daegling (1990, 1993a) hypothesised that the human chin represents a structural response to resist CB, which leads to tension at the labial symphyseal base. He argues that LTB became less important when the length of the mandible was reduced during the evolution of anatomically modern humans, since in a shorter mandible the masticatory muscles have less leverage, but that the degree of vertical bending does not change.

When these three hypotheses are compared with the experimental data, two of them appear to be less likely, assuming that the *in vivo* strain measurements in non-human primates can be generalised to humans. As Dobson and Trinkaus (2002) pointed out, the medial transverse bending hypothesis of DuBrul and Sicher (1954) seems to be weak, since it is wishboning, which is the primary transverse bending regime during masticatory function, whereas reverse wishboning only occurs during jaw opening and results in much lower symphyseal stress than wishboning (Hylander 1984). White's (1977) hypothesis, on the other hand, is in concordance with the experimental data with its emphasis on wishboning, at least on first glance. However, because the degree of curvature of the bone surface is higher lingually than labially, lingual stresses and strains should be higher than the labial ones during transverse bending (Young 1989, van Eijden 2000). This is confirmed by *in vitro* experiments (Hylander 1984, 1985). It is therefore unclear, why in humans no lingual buttress, such as a superior transverse torus or a simian shelf has evolved, as in other primates. In addition, it has been argued that a stronger inclination of the symphysis is an efficient way to counter wishboning. Like a superior torus it increases the second moment of area about the vertical axis (Hylander 1984, Daegling 1990, Ravosa 1991, Daegling 2001). If wishboning played an important role during the evolution of modern human symphyseal morphology, it is unclear why the human symphysis became more vertically orientated and thus less well adapted to counter wishboning.

Given the experimental evidence, Daegling's (1990, 1993a) hypothesis is most convincing. Recently, Dobson and Trinkaus (2002) tested its predictions by quantitative comparison of symphyseal cross-sections of Middle and Late Pleistocene specimens and anatomically modern humans. Their findings suggest

that there is indeed a trend towards less resistance to wishboning during the later Pleistocene, while CB resistance is maintained. This is as predicted by Daegling (1990, 1993a), but Neanderthals and early modern humans did not differ significantly regarding wishboning resistance, although Neanderthals have significantly longer mandibles. However, in this study bending resistance could only be estimated by linear measurements based on the outer contours of the symphysis. With finite element analysis (FEA), on the other hand, it is possible to simulate the respective bending loads and quantify bending resistance of different symphyseal morphologies more accurately.

The most recent attempts to test the biomechanical significance of the chin and the vertical orientation of the human symphysis have therefore used FEA (Ichim et al. 2006a, 2006b, 2007a). Ichim and co-workers (2006b) created different hypothetical symphyseal shapes in a simplified beam model and in a CT-based model of a human mandible and applied loads that represent the three major symphyseal loads, wishboning, DVS and CB. In a subsequent study they also simulated physiological loading during incision and molar biting (Ichim et al. 2006a). They found very similar strains in all models and concluded that the evolution of modern human symphyseal morphology is therefore unrelated to the mechanical demands placed upon the mandible during masticatory function (Ichim et al. 2006a, 2006b). Instead, they suggested that the chin evolved as an adaptation to the forces generated by the muscles of the tongue and other perioral muscles and is thus closely related to the development of human language (Ichim et al. 2007a).

While Ichim and colleagues (2006a, 2006b, 2007) used a powerful methodological approach to test the mechanical significance of the modern human symphyseal morphology, their study does not allow all relevant questions to be addressed. In particular: 1) Although they created an inclined symphysis or hypothetical simian shelf in their simplified beam model, they did not test the effect of symphyseal inclination in their CT-based model of a human mandible. 2) Their hypothetical flat-symphysis model differs from the original model with a chin not only in the absence of a chin, but also in other aspects of the symphyseal cross-section, such as the shapes of the whole lingual as well upper labial surfaces. Therefore, the mechanical effect of a labial thickening at the lower aspect of the symphysis was not studied in isolation. 3) Finally, the simplified

load cases modelled in their first study (Ichim et al. 2006b) were not physiologically representative, for example, the rami were constrained instead of the condyles and no constraints were placed on the teeth, although these loads (CB, LTB and DVS) occur during the powerstroke of incision and mastication (Hylander 1984, 1985) and the direction of the torsional load used for simulating CB was opposite to that observed in experiments with macaques (Hylander 1984). Thus, the strain patterns observed during these simplified load cases might not be representative of the real strains occurring during masticatory function.

This study will therefore use a similar methodology to Ichim and co-workers (2006a, 2006b), but different hypothetical symphyseal shapes and loading conditions. Thus, it aims to investigate the mechanical significance of modern human symphyseal morphology (i.e. vertical orientation and presence of a chin) more comprehensively. Based on previous discussions in the literature, the following hypotheses are tested:

1) The presence of a chin, as compared to a vertical symphysis without chin, should have the following effects (Hylander 1984, 1985): 1) better resistance to CB, 2) better resistance to transverse bending (LTB and MTB) due to the increase in labio-lingual thickness of the symphysis, and 3) better resistance to DVS due to the increase in cross-sectional area of the lower aspect of the symphysis.
2) A vertically orientated symphysis should show: 1) better resistance to CB, but 2) weaker resistance to transverse bending (LTB and MTB) than an inclined symphysis (Hylander 1984, Daegling 1990, Ravosa 1991, Daegling 2001).
3) When a modern human symphysis is compared with a symphysis of another member of the genus *Homo* without a chin, for example, a Neanderthal, Daegling's hypothesis (1990, 1993a) makes the following predictions: 1) The CB-resistance should be equal between the two, and 2) the resistance to wishboning should be reduced in the modern human symphysis.

In addition, physiological loading during incision and a molar bite will be simulated to test, which symphyseal morphology appears to be most effective in

resisting more complex loads that come closer to the actual conditions during masticatory function.

9.2. Material and methods

For this study, an adult human mandible with complete permanent dentition, apart from the congenitally missing third molars, was chosen (H-A 001), which is the same mandible that has been used for the study described in the previous chapter.

Details about the reconstruction of this specimen are therefore given in Chapter 8. Three models with modified cross-sectional form of the symphysis were then created from this base model using thin-plate splines ("Bookstein warp" in Amira): 1) a vertically orientated symphysis without *mentum osseum*, 2) the same symphysis as in 1) inclined lingually by 20°, and 3) a Neanderthal symphysis (**Figure 9.3**). In all these models the shape of the rest of the mandible was kept constant by ca. 500 anchor landmarks, which were approximately evenly distributed across the surface of the mandible excluding the symphyseal region. In the case of the first two warped models the target shape was completely hypothetical. For the creation of a Neanderthal symphysis, however, the target shape was the cross-sectional symphyseal shape of the Neanderthal mandible of Régourdou 1. Based on a synchrotron CT scan of this specimen with a reduced voxel size of 0.35 mm, a surface model was created, superimposed onto the modern human mandible by matching the two occlusal planes (molars to incisors) and scaled to the same vertical symphyseal height. Finally, the symphyseal cross-sections were superimposed using the alveolar margin.

Potential confounding variables like cross-sectional area, symphyseal height and cortical bone thickness that are likely to have a significant effect on the stress and strain magnitudes and pattern (Hylander 1984, 1985, Daegling 1993a), were controlled by creating: 1) equal cross-sectional areas in the hypothetical chin-less vertical and inclined symphysis, 2) equal symphyseal heights, and 3) equal cortical bone thickness of 1.8 mm in all models. Thus, the effects of changes in cross-sectional symphyseal shape and orientation could be studied systematically. Cancellous bone was not modelled, since its geometry would have been altered by the warping into different symphyseal shapes, which would have affected the comparability of the models.

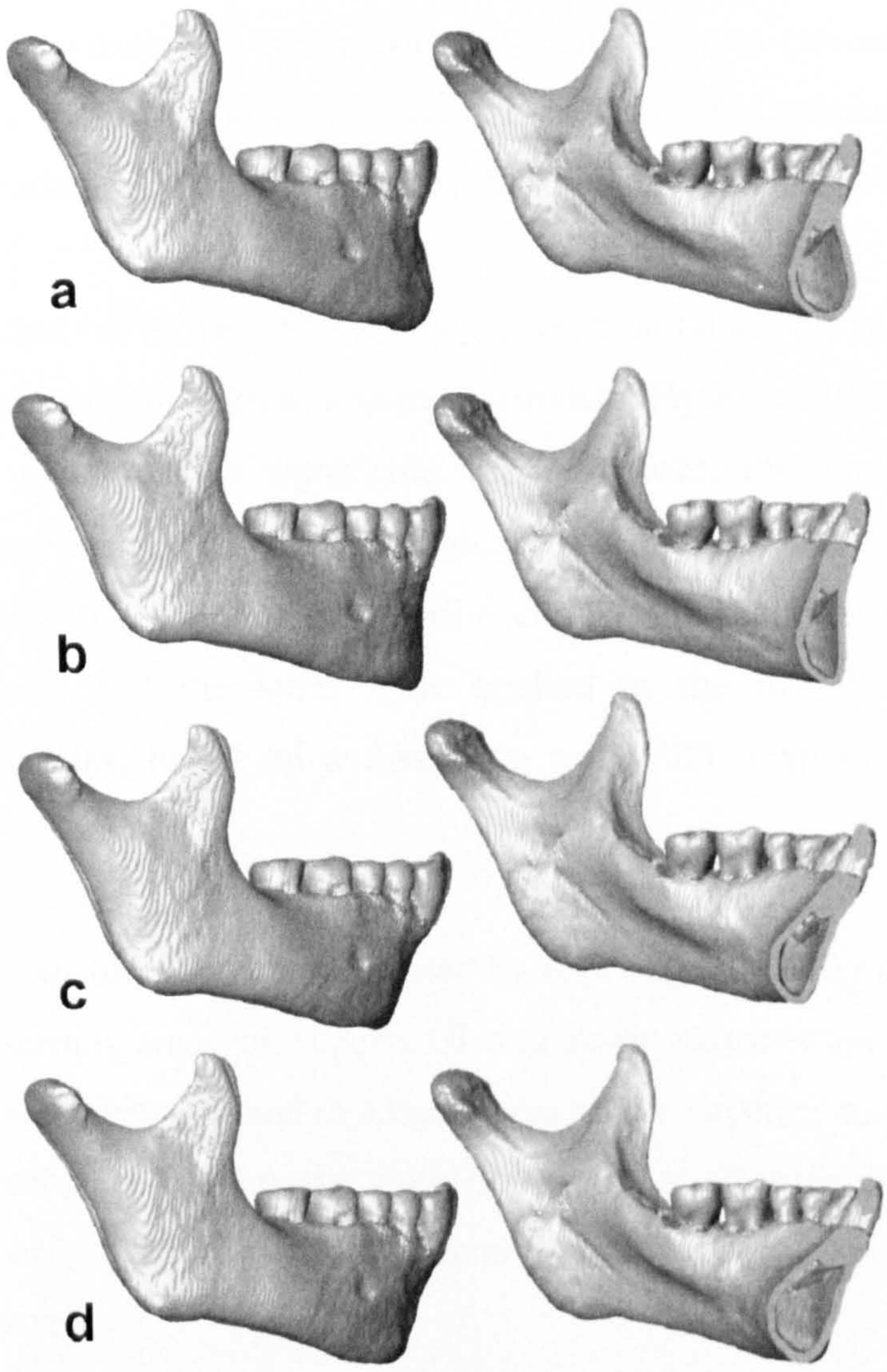

Fig. 9.3. Variation in symphyseal shape between the models. Left row: complete models, right row: right halves of models removed. a) original human symphyseal shape, b) vertical symphysis without chin, c) inclined symphysis, d) Neanderthal symphyseal shape. Note that the cortical bone thickness is kept the same in all the models.

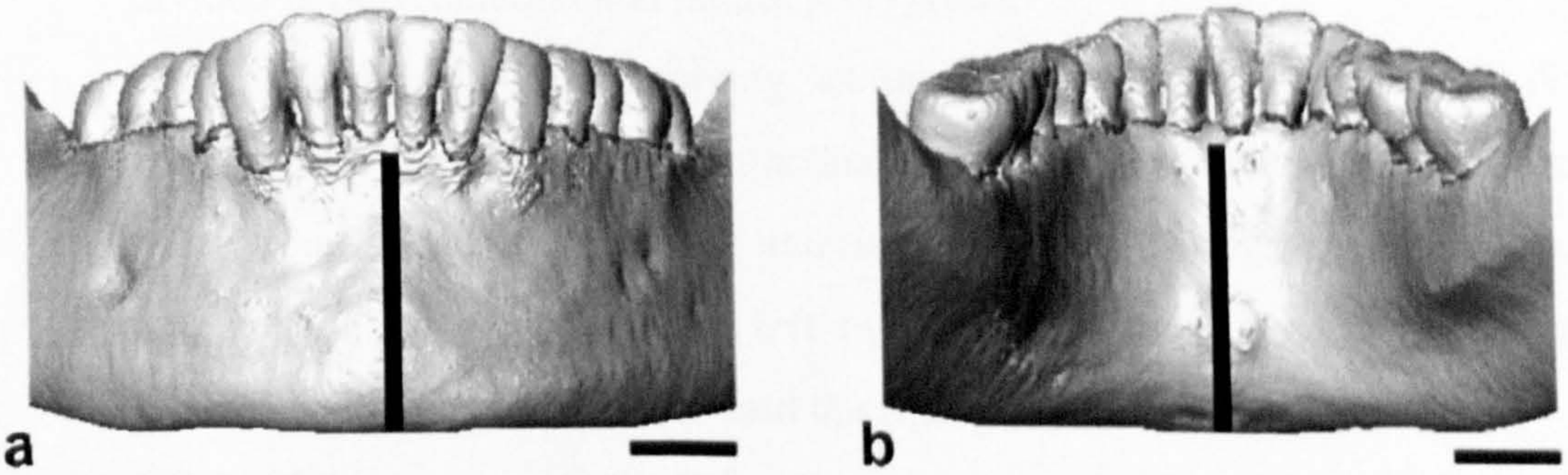

Fig. 9.4. Areas on the labial (a) and lingual symphysis (b) from which surface strain values were extracted for quantitative comparison. Each measurement area is ca. 27 x 1.5 mm in size. Scale bars = 1cm.

The final 3D volumes were exported as BMP stacks and converted into FE meshes by direct voxel conversion converted into a finite element, resulting in models with ca. 1.3 million elements. The identical material properties as used for the previous studies were then applied to the models, including PDL as an extra material.

Four load cases (**Figure 9.5**) were modelled to simulate the major load types known from experiments with non-human primates (Hylander 1984, 1985). While these loading scenarios are significant simplifications, the applied forces and constraints were defined in a physiologically reasonable manner, for example, constraints were placed on the superior condylar surfaces and the occlusal surfaces of teeth and the loads were applied to the insertion areas of the masticatory muscles, based on a dissection and a CT scan of a male human cadaver.

- LTB or wishboning was simulated by applying a laterally directed force to the insertion areas of superficial and deep masseter on both sides and constraints were applied to a linear area on the superior condylar surface in the vertical axis and to the right first molar in all three axes. The applied force was 80 N on each side, equally divided among the two portions of the masseter.
- MTB or reverse wishboning was simulated by applying a medially directed force to the insertion areas of the medial pterygoids and the inferior heads of the lateral pterygoids using the same constraints as in the wishboning case. The applied force was 80 N on each side, equally divided between medial and lateral pterygoids.
- DVS was modelled by applying an upwardly directed force of 80 N distributed equally among the attachment areas of the jaw closing muscles (superficial and deep masseter, anterior, middle and posterior temporalis and medial pterygoid) on the left ramus, while the right condyle was constrained in the vertical axis and the right first molar in all three axes.
- CB resulting from a twisting of each corpus around its anteroposterior axis was simulated by applying a medially directed force (400 N) to the occlusal surface of the first and second molars on each side and a laterally directed force (400 N to the insertion areas of the superficial masseter on

each side, while the condyles were constrained in all three axes and the tips of the medial incisors were constrained in the vertical axis.

In addition to these simplified loading regimes, physiological loading during incision and a unilateral molar bite on the right M1 was simulated (see 3.8 for the details about the muscle forces). For these load cases, the model included TMJs, which were constrained in all three axes. The occlusal plane of the right M1 was also constrained in all directions, whereas the incisors were constrained in the vertical axis only.

The maximum (ε_1) and minimum principal strains (ε_3) as well as von Mises strains (ε_v) were used in the evaluation of the models. For quantitative comparisons of the results, strain values were extracted from vertical linear areas through the midsagittal section on the labial and lingual surfaces of the symphysis, each ca. 27 x 1.5 mm in size, ranging from slightly below the alveolar margin of the incisors to the base of the symphysis (**Fig. 9.4**).

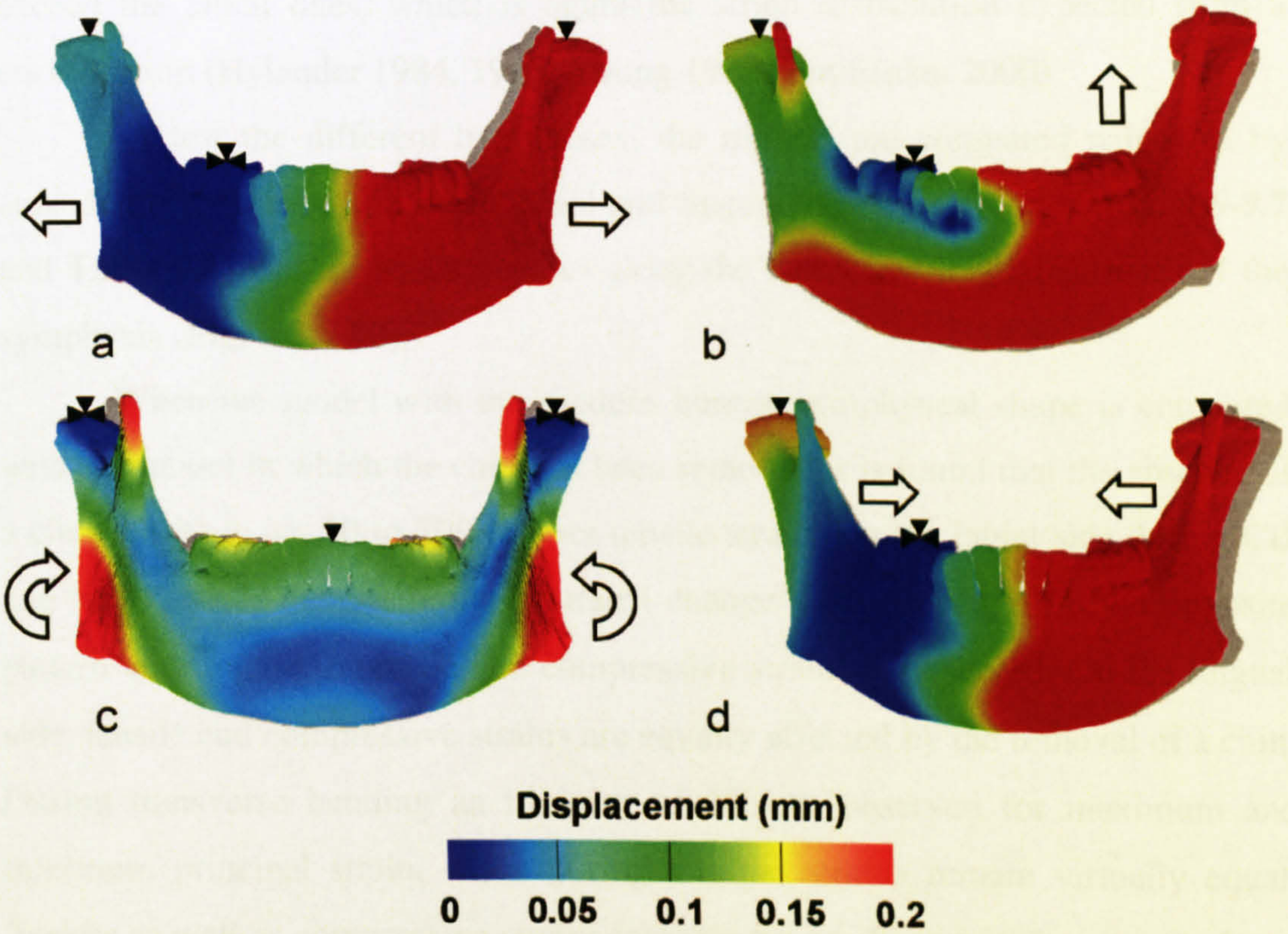

Fig. 9.5. Displacement plots for the simplified load cases with a 20:1 scale deformation. a) LTB, b) DVS, c) CB, d) MTB. The outlines of the undeformed models are shown in grey. The small black triangles indicate constrained nodes (each triangle represents a constraint in one axis), while the large arrows visualise the external forces applied to the models.

9.3. Results

Simplified load cases

The displacement plots for all simplified load cases confirm that the applied forces and constraints resulted in the expected deformations (**Fig. 9.5**). **Figure 9.6** provides an overview of the maximum and minimum principal strains at the labial and lingual sides of the symphysis and thus allows an assessment of the distribution of compressive and tensile strains in the different load cases. LTB results in dominant labial compression and lingual tension, whereas MTB causes dominant labial tension and lingual compression, which is consistent with the behaviour of a curved beam (Hylander 1984, 1985, Young 1989, van Eijden 2000). In CB and DVS compressive and tensile strains on the two sides of the symphysis have relatively equal magnitudes, suggesting that these load cases are free from transverse bending.

Figure 9.7 shows the mean von Mises strains on the labial and lingual side of the symphysis of each model. In each loading scenario the lingual strains exceed the labial ones, which is again the strain distribution expected from a curved beam (Hylander 1984, 1985, Young 1989, van Eijden 2000).

To test the different hypotheses, the models are compared pair-wise by considering differences in mean labial and lingual strain magnitudes (**Fig. 9.6-9.7** and **Table 9.1**) and the strain profiles along the labial and lingual surfaces of the symphysis (**Fig. 9.8-9.10**).

When the model with the modern human symphyseal shape is compared with the model in which the chin has been removed it is found that the absence of a chin results in ca. 20 to 30% higher tensile strains on the labial side during CB and MTB, while the compressive strains change little. During LTB the opposite pattern with regard to tensile and compressive strains is observed. On the lingual side, tensile and compressive strains are equally affected by the removal of a chin. During transverse bending an increase of 10% is observed for maximum and minimum principal strain, while during CB the strains remain virtually equal. Tensile as well as compressive strains increase by ca. 30 and 10% respectively on the labial side and ca. 10% on the lingual side during DVS.

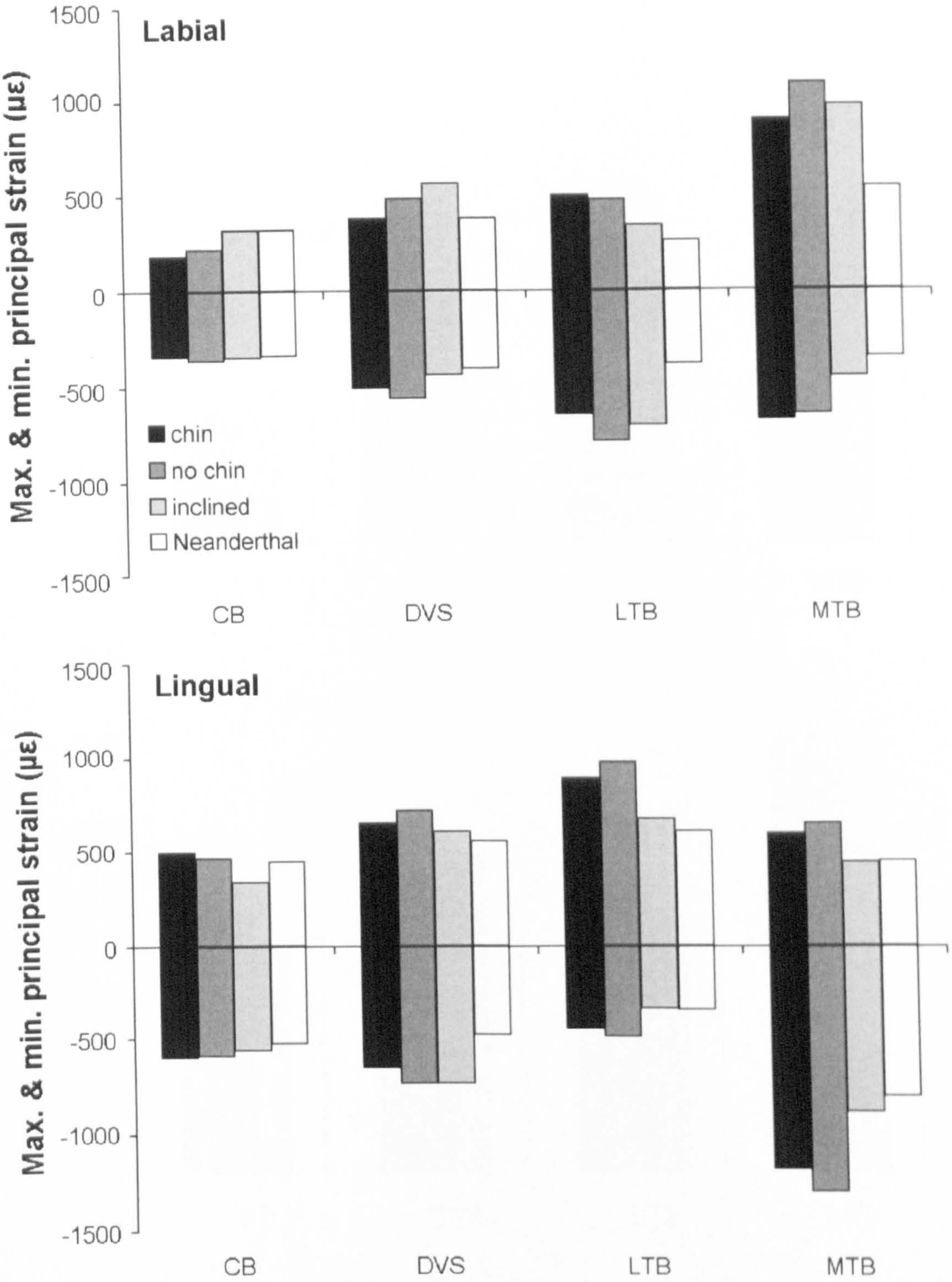

Fig. 9.6. Maximum and minimum principal strains at the labial and lingual surfaces of the symphysis during the simplified load cases. The difference between maximum and minimum principal strain values for each model and load case represents the maximum shear strain ($\gamma_{max} = \varepsilon_1 - \varepsilon_3$). See **Fig. 9.3** for an illustration of the different symphyseal shapes.

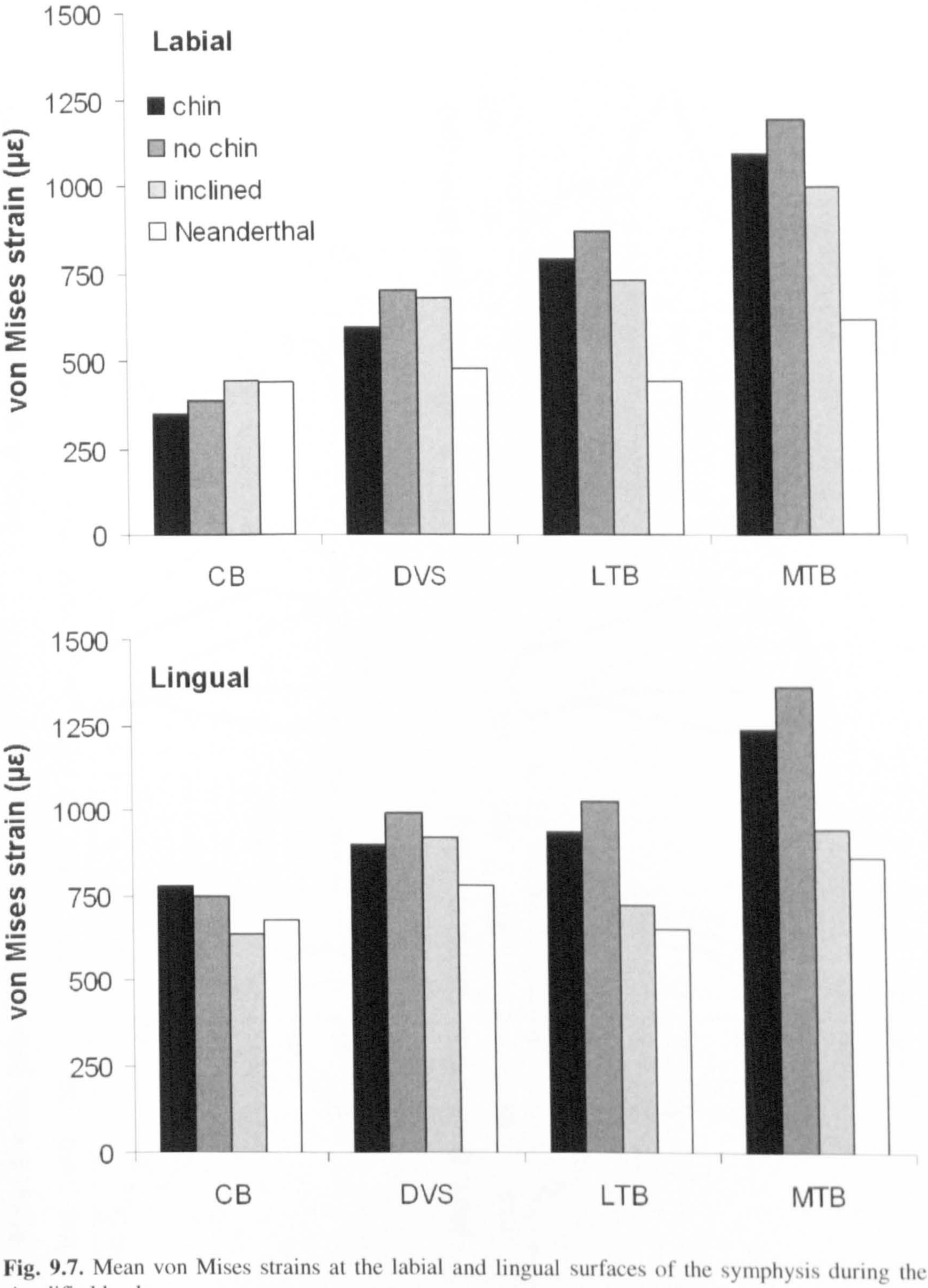

Fig. 9.7. Mean von Mises strains at the labial and lingual surfaces of the symphysis during the simplified load cases.

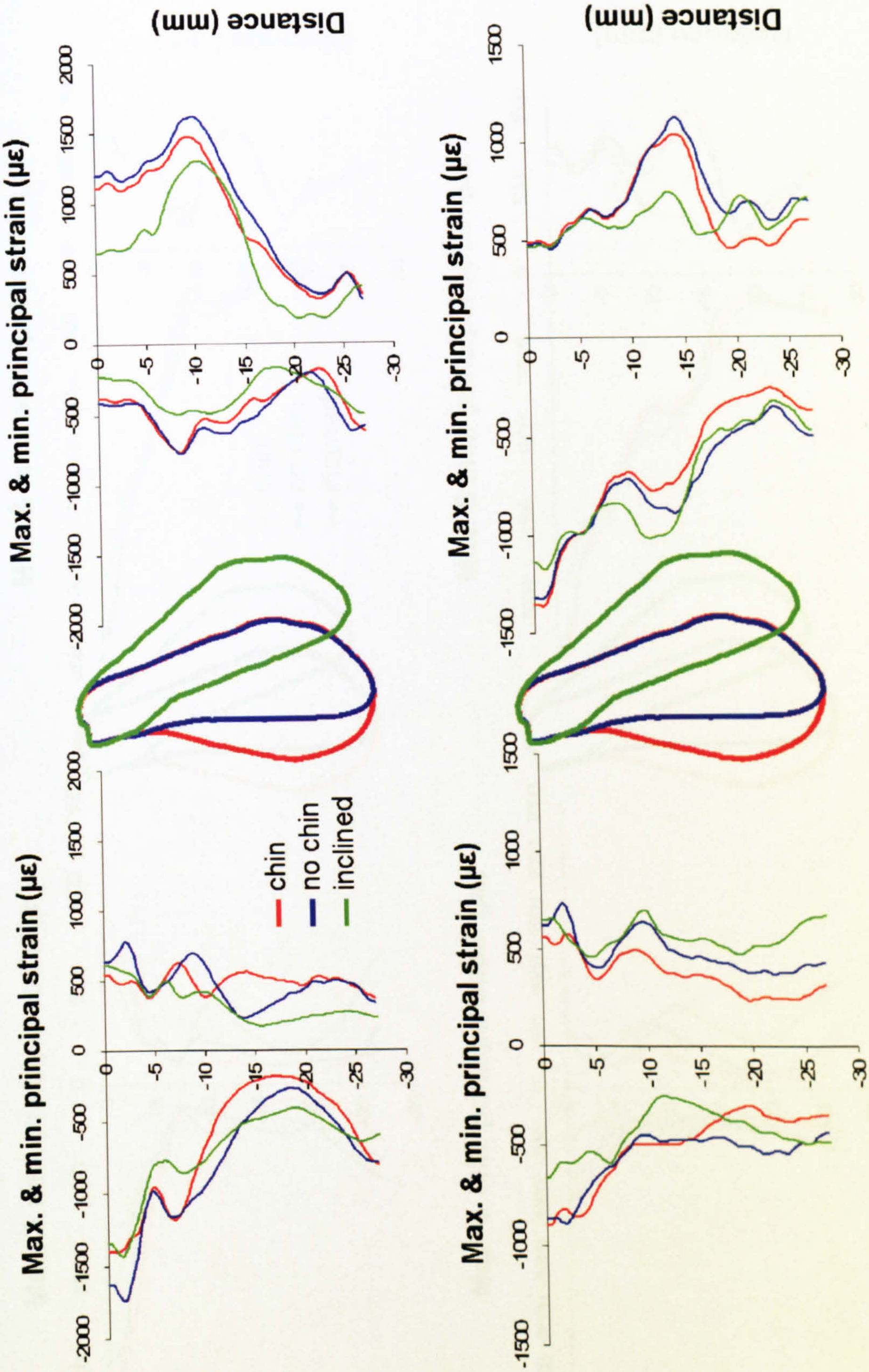

Fig. 9.8. Vertical strain profiles for maximum and minimum principal strains on the labial and lingual surfaces of the symphysis. The location of each value on the surfaces is indicated by the symphyseal cross-sectional outlines in corresponding colours. These are scaled so that the vertical symphyseal outlines match the profile distance. At the top: LTB, at the bottom: DVS. The strain profiles for MTB, which are not shown here, have the same pattern as for LTB, but mirrored and with higher overall magnitudes.

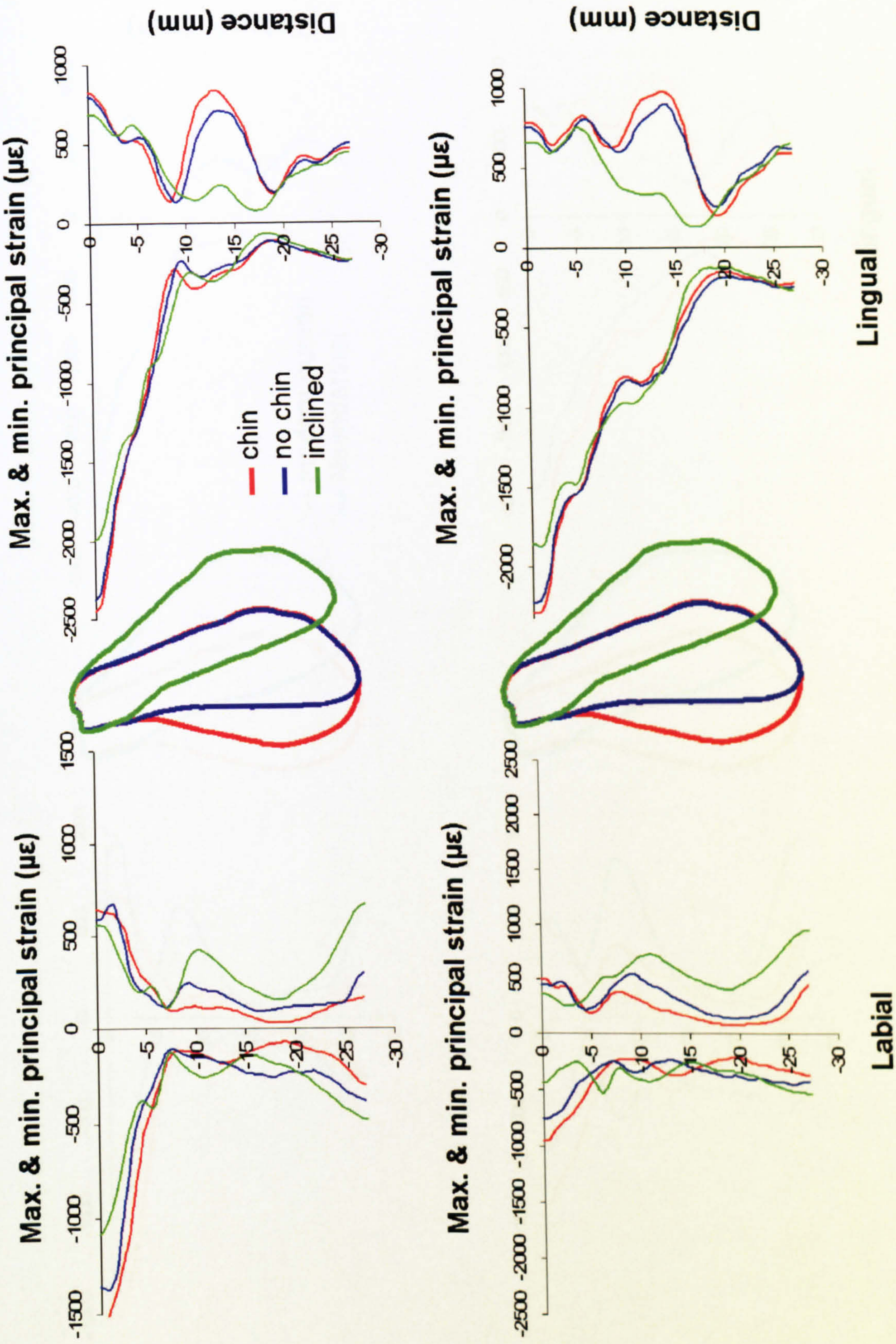

Fig. 9.9. Strain profiles for maximum and minimum principal strains on the labial and lingual surfaces of the symphysis. At the top: CB, at the bottom: molar bite. For more details see legend of **Fig. 9.8.**

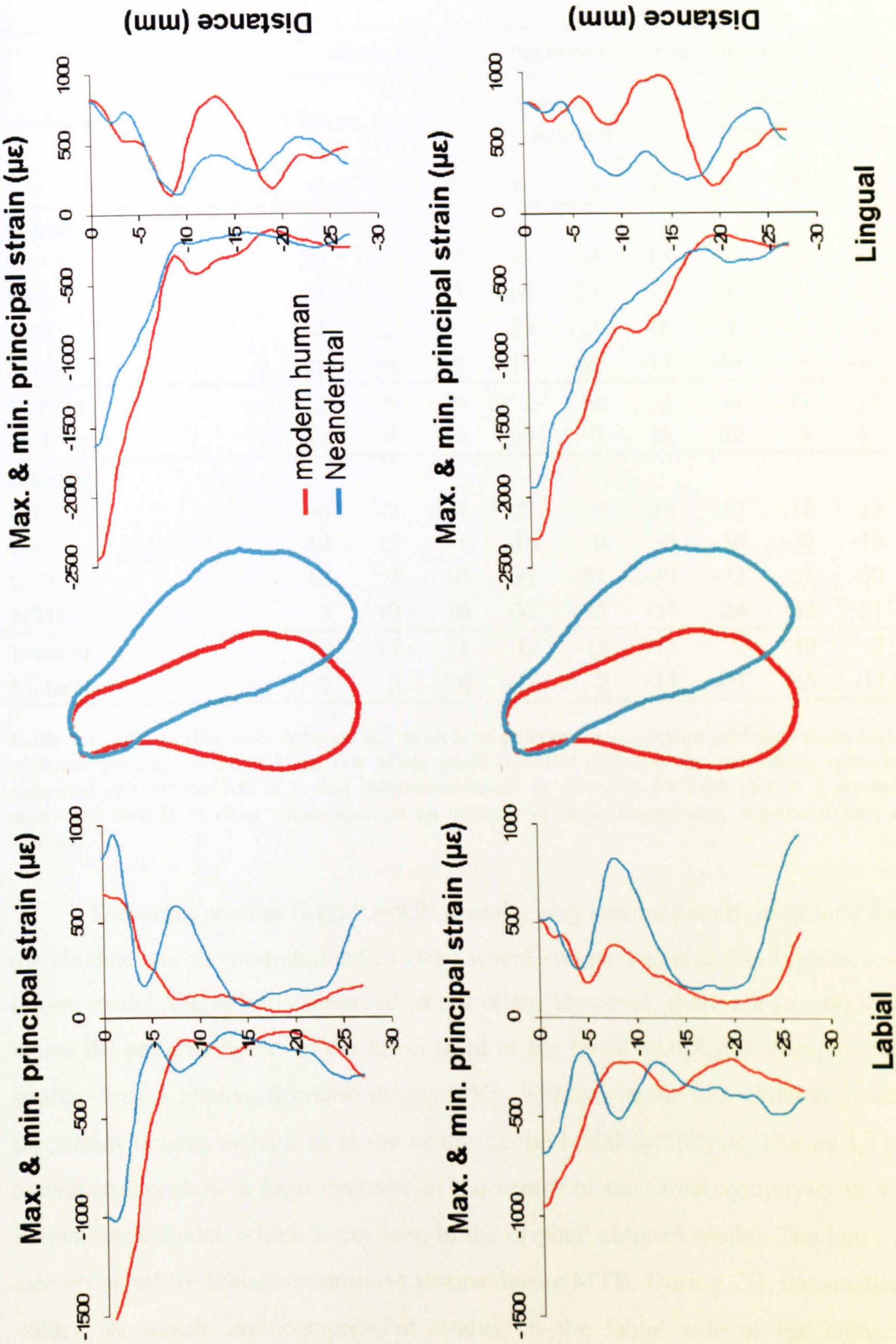

Fig. 9.10. Strain profiles for maximum and minimum principal strains on the labial and lingual surfaces of the symphysis. The symphyseal cross-sectional outlines in corresponding colours are scaled so that they match the profile distance. At the top: CB, at the bottom: molar bite.

Load cases	Strain differences between the models in percent								
	Chin vs. no chin			Vertical vs. inclined			Modern vs. Neanderthal		
	ε_1	ε_3	ε_v	ε_1	ε_3	ε_v	ε_1	ε_3	ε_v
Labial									
CB	20	6	10	48	-4	15	80	-1	25
DVS	29	10	17	16	-21	-3	0	-20	-20
LTB	-4	22	10	-29	-11	-16	-48	-40	-44
MTB	22	-5	9	-11	-30	-17	-40	-48	-44
Incision	22	-5	9	2	-16	-3	-4	-17	-11
Molar bite	40	4	16	65	-3	28	82	4	32
Lingual									
CB	-6	-2	-4	-27	-5	-15	-10	-12	-13
DVS	10	13	11	-16	0	-8	-16	-26	-13
LTB	10	9	10	-31	-31	-30	-32	-23	-30
MTB	9	10	10	-32	-32	-31	-24	-32	-31
Incision	10	11	11	-12	-19	-15	0	-10	-7
Molar bite	-2	3	0	-28	-7	-14	-21	-15	-17

Table 9.1. Strain differences between the models in percent for maximum principal strain (ε_1), minimum principal strain (ε_3) and von Mises strain (ε_v). For each pair the percentage value is computed as ((a-b)/a)*100 (a = first mentioned model in the table for each pair, b = second mentioned model). Positive values indicate an increase in strain magnitudes, negative values a decrease.

The strain profiles (**Fig. 9.8-9.9**) reveal a very similar pattern in general for the chinned and the non-chinned models: where strains are relatively high or low in one model, the same is observed in the other. However, there are two regions where the patterns differ. In the lower third of the labial symphysis, compressive strains show a relative decrease during DVS, whereas in the non-chinned model the strains remain as high as at the centre of the labial symphysis. During LTB, tensile strains show a local decrease at the centre of the labial symphysis in the non-chinned model, which is not seen in the original chinned model. The latter is also observed for labial compressive strains during MTB. During CB, the smallest values for tensile and compressive strains on the labial side of the chinned symphysis are found at the most anteriorly projecting part of the *mentum osseum*. This decrease in strains is not observed in the non-chinned symphysis.

The lingual rotation of the non-chinned symphysis by 20° results in much lower strains during transverse bending. Labially, tensile strains decreases by ca.

30% and compressive strains by ca. 10% during LTB and vice versa during MTB. Lingually, tensile as well as compressive strains are reduced by ca. 30% during both transverse bending regimes. During CB, a marked increase of labial tensile strains by 48% is found, but also a reduction of compressive strains of 27% on the lingual side. During DVS, one principal strain increases, while the other decreases or does not change. This is observed labially and lingually. The von Mises strains remain therefore relatively constant: They decrease only slightly by 4 and 8% labially and lingually.

Despite these differences in magnitude, the overall pattern of variation is similar between the vertical and the inclined symphysis. In some regions, however, the inclined symphysis shows a pronounced local decrease in strains compared to the vertical symphysis model: a reduction of tensile strains at the centre of the lingual symphysis during CB and DVS, and a reduction of compressive strains at the centre of the labial symphysis during DVS. During LTB the inclination of the symphysis results in a pronounced decrease in tensile strains in the lingual alveolar region and the lower half of the labial symphysis, and a decrease of compressive strains at the same locations during MTB.

When the model with the Neanderthal symphysis is compared with the original modern human model, a pronounced decrease in strain magnitudes is found during transverse bending. Labially, compressive and tensile strains are reduced by ca. 40 to 50% and lingually by ca. 20 to 30%. During DVS, the principal strains decrease by 16 to 26% apart from the tensile strains on the labial side, which remain the same. In CB lingual compressive and tensile strains are also lower (by ca. 10%) in the Neanderthal symphysis. However, on the labial side the tensile strains show a very pronounced increase of 80%.

The strain profiles (**Fig. 9.10**) differ more between the Neanderthal symphysis and modern human symphysis than between the other models, but some of these differences are very similar to the ones found between the vertical non-chinned symphysis and the inclined symphysis. So, the Neanderthal symphysis behaves similarly to the inclined symphysis under loading, whereas the modern human symphysis behaves similarly to the non-chinned vertical symphysis. These differences are 1) a pronounced local decrease in tensile strains at the centre of the lingual Neanderthal symphysis during CB, which is the point of maximum labio-lingual thickness, 2) a marked decrease of tensile strains at the

same location during DVS, 3) a pronounced decrease in tensile strain magnitudes at the lingual alveolar region during LTB (and of compressive strains during MTB), 4) an increase in labial tensile strain magnitudes at the lower border of the alveolar region and 5) at the base of the symphysis during CB, 6) an increase in tensile strain magnitudes at the labial base of the symphysis during DVS. In addition, compressive strains are markedly reduced in the upper half of the lingual Neanderthal symphysis during DVS and tensile strains are particularly reduced at the centre of the labial Neanderthal symphysis during LTB (compressive strains during MTB).

Incision and molar bite

Figures 9.11 and **9.12** show the magnitudes of maximum and minimum principal strains and von Mises strains for the two simulated biting tasks. Labially, compressive strains reach higher magnitudes than tensile ones. Lingually, the pattern is reversed. This indicates that reverse wishboning occurred, which results in labial compression and lingual tension. In addition, the displacements and strain profiles indicate that in the simulated molar bite DVS and CB occur and during the incision load some degree of sagittal bending. The pattern of strain differences between the models for the two biting tasks is similar to the general pattern found for the simplified load cases.

The removal of the chin leads to an increase in labial tensile strains of ca. 20% and 40% during the simulated incision and the molar bite respectively, whereas the compressive strains remain constant. On the lingual side neither compressive nor tensile strains are affected by the removal of the chin during the molar bite, but an increase of ca. 10% of compressive and tensile strains is observed during incision. The strain profiles reveal that the observed differences are due to an overall increase in strain magnitudes in the non-chinned symphysis, while the spatial pattern of strain variation is very similar between the two models.

The inclination of the symphysis results in 16 and 19% lower compressive strain magnitudes on the labial and lingual sides respectively during incision relative to the model with a vertical symphysis, while the tensile strains only decrease on the lingual side (by 12%). During a molar bite, however, the differences are more pronounced. Labially, the tensile strains increase by 65% and

lingually they decrease by almost 30%, whereas the compressive strains are hardly affected. The strain profiles show that this large increase in tensile strains during the simulated molar bite occurs in the lower two thirds of the labial side and at the centre of the lingual side. These differences in the strain patterns are similar to the ones observed during CB and DVS.

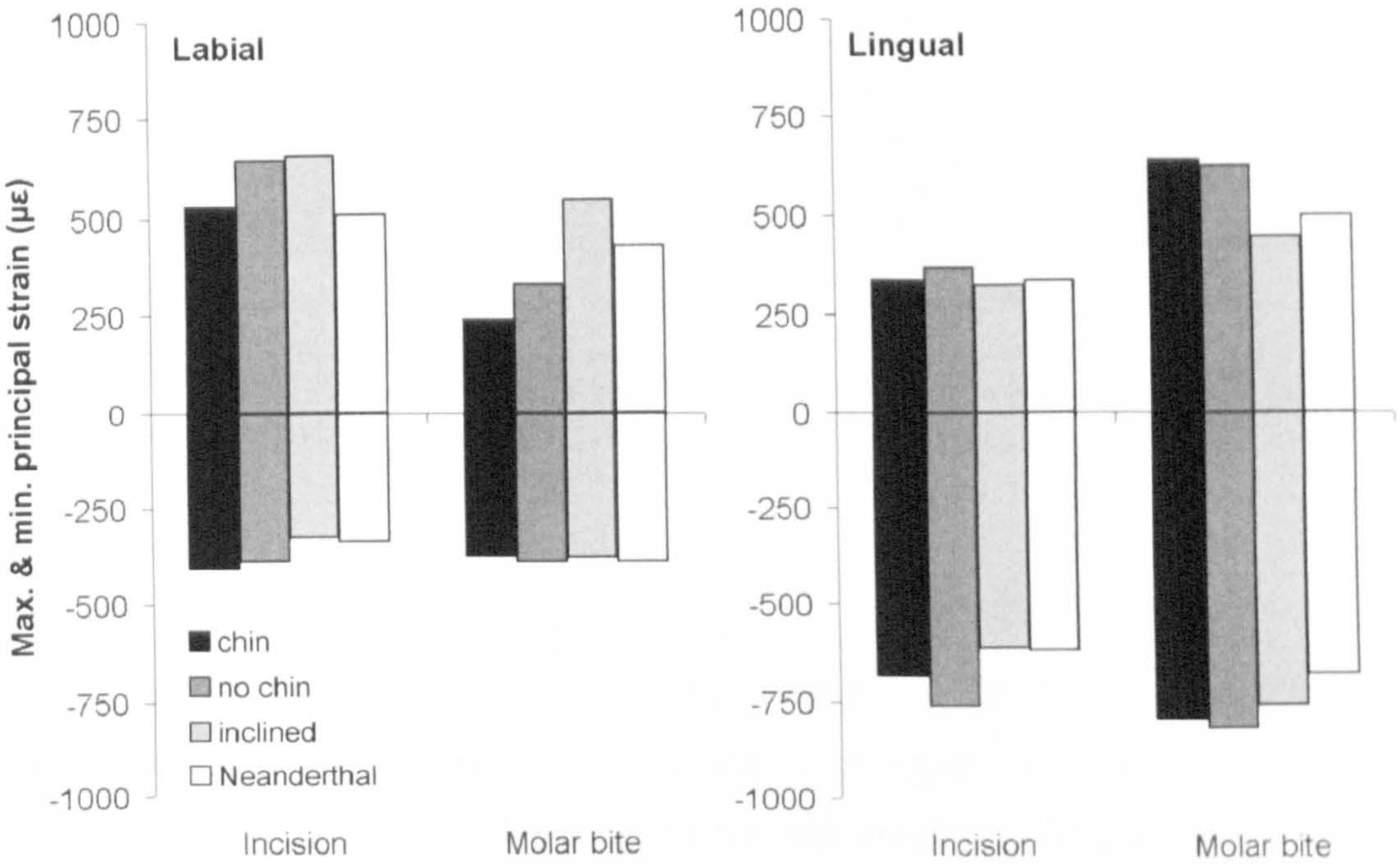

Fig. 9.11. Maximum and minimum principal strains on the labial and lingual surfaces of the symphysis during a simulated incision and molar bite. The difference between maximum and minimum principal strain values for each model and load case represents the maximum shear strain.

When the modern human is compared with the Neanderthal symphysis, principal strain magnitudes are by 6 to 17% lower in the Neanderthal symphysis labially and lingually during incision, but during the molar bite the labial tensile strains are dramatically higher in the Neanderthal symphysis (by 82%), while the lingual strains are reduced by ca. 15 and 20% for compressive and tensile strains respectively. The strain profiles for the unilateral molar bite indicate that the dramatic reduction of labial tensile strains occurs primarily at the bottom of the alveolar region and the base of the symphysis, and this is very similar to the differences observed during CB. The reduction of tensile strains on the lingual side occurs mainly at the centre of the lingual symphysis, where the maximum labio-lingual thickness is reached. This also very similar to the pattern seen in CB and DVS.

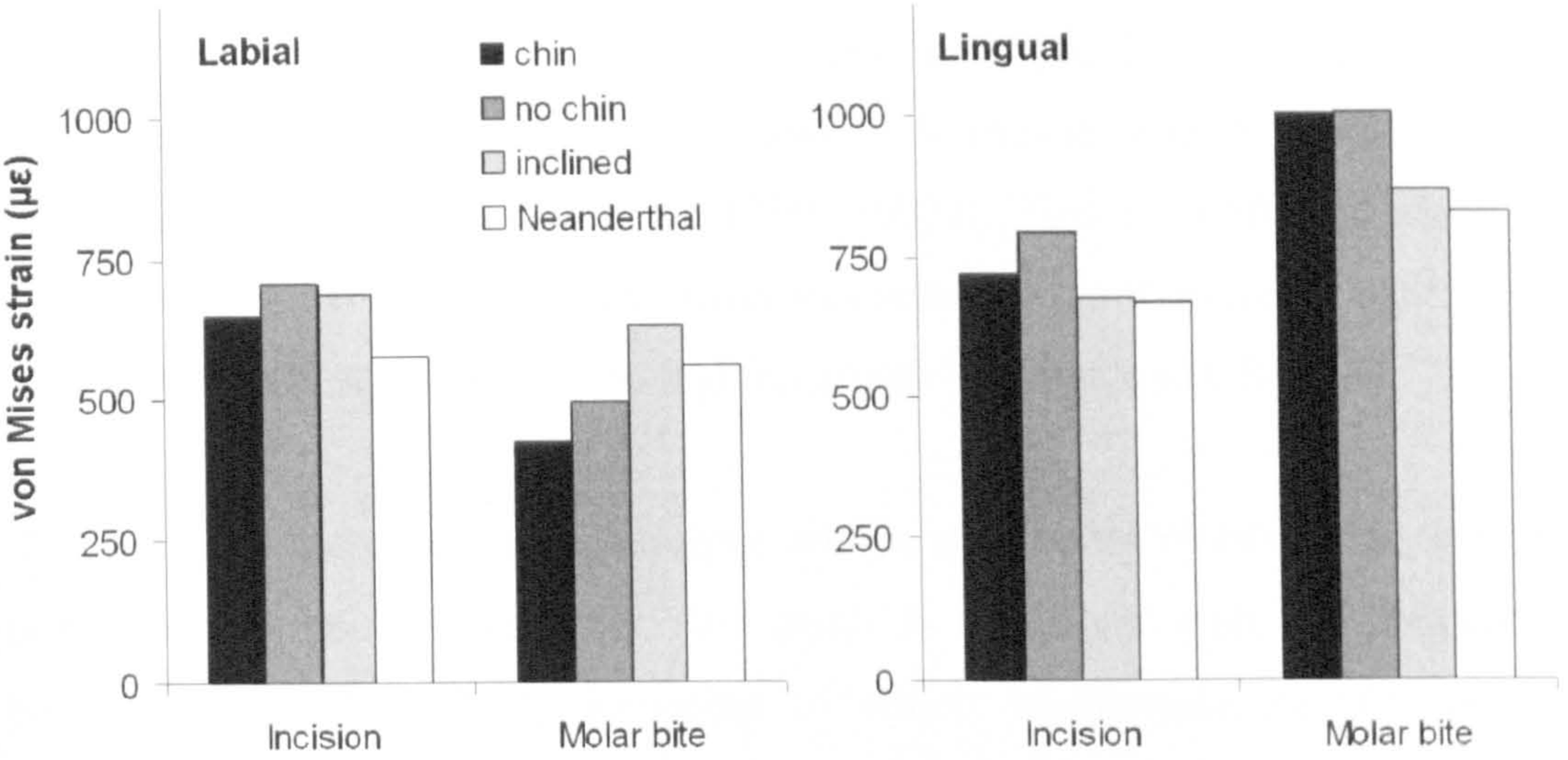

Fig. 9.12. Von Mises strains on the labial and lingual surfaces of the symphysis during a simulated incision and molar bite.

9.4. Discussion and conclusions

The results of this study show that changes in symphyseal shape have a profound effect on the strain magnitudes and spatial distributions, even if variables like symphyseal height, cross-sectional area and cortical bone thickness are kept constant. The predictions based on the hypotheses described at the beginning are mainly confirmed by the results:

1) The presence of a chin, as compared to a vertical symphysis without chin, should lead to better resistance to CB, transverse bending (LTB and MTB) and DVS (Hylander 1984, 1985). This is confirmed since in all load cases, the symphysis with a chin better resists loads than the non-chinned vertical symphysis, as shown by lower labial and lingual strains.
2) A vertically orientated symphysis should show a better resistance to CB, but a weaker resistance to transverse bending (LTB and MTB) than an inclined symphysis (Hylander 1984, Daegling 1990, Ravosa 1991, Daegling 2001). This is mostly confirmed by the results since during CB, the labial tensile strains are much lower in the vertical symphysis compared to the inclined symphysis, but tensile strains on the lingual side also show a pronounced local increase. During transverse bending the vertical symphysis shows considerably higher strains than the inclined symphysis.

3) When a modern human symphysis is compared with a Neanderthal symphysis without a chin the CB-resistance should be equal between the two and the resistance to wishboning should be reduced in the modern human symphysis (Daegling 1990, 1993a). This is confirmed since the modern human symphysis shows less resistance to transverse bending, but relatively equal or in some regions greater resistance to CB.

In all load cases, the symphysis with a chin better resists loads than the non-chinned vertical symphysis. This result is consistent with the predictions based on Hylander (1984) according to which an increase in labio-lingual thickness of the symphysis should improve the resistance to CB and transverse bending and a concentration of bone in the inferior part of the symphysis should lead to better resistance to CB and DVS. Both of these features are associated with the presence of a chin and might therefore be responsible for the observed decrease in-strains. Since cortical thickness was kept constant during this study, the effect of concentration of bone at the lower aspect of the symphysis was not studied in the strict sense, rather the effect of increasing the cross-sectional area of the inferior part of the symphysis was investigated. As expected, the most pronounced decrease in strains in the chinned model is found in the lower half of the symphysis, where the cross-sectional area is increased, and especially at the most anteriorly projecting part of the chin, where the labio-lingual thickness of the symphysis reaches its maximum.

The rotation of the non-chinned vertical symphysis by 20° proves very effective in improving the resistance to transverse bending, labially and even more so lingually. This confirms the prediction by previous authors (Hylander 1984, Daegling 1990, Ravosa 1991, Daegling 2001) that an inclined symphysis is better at resisting transverse bending than a vertical one. Since in this study cortical thickness and cross-sectional area were kept constant between the two models, the decrease in strains can be attributed solely to the difference in the orientation of the symphysis. During CB and DVS the inclination of the symphysis does not result in a better load resistance. The values for von Mises strain during DVS are very similar in the vertical and the inclined symphysis. This is consistent with Hylander's (1984) finding that the resistance to DVS is mainly dependent on the cross-sectional area of the symphysis, which was kept constant between the two

models. During CB, the labial tensile strains are much lower in the vertical symphysis, but tensile strains on the lingual side also show a pronounced local increase at the centre of the symphysis. Thus, the prediction that a vertical symphysis is better in resisting CB than an inclined one (Hylander 1984, Daegling 1990, Ravosa 1991, Daegling 2001) can in general be confirmed, but the overall decrease in strains is achieved at the expense of a local increase of tensile strain on the lingual side of the symphysis, which would require morphological adaptations, for example, a local increase in cortical bone thickness.

The comparison between the modern human and the Neanderthal symphyses yields marked strain differences for DVS and both transverse bending loads. During these load cases, the Neanderthal symphyseal shape results in clearly lower strains labially as well as lingually, whereas during CB, the lingual strains are similar between the two models and labial strains are higher in the Neanderthal symphysis. The improved resistance to DVS in the Neanderthal symphysis might be simply due to the ca. 8% larger cross-sectional area of this symphysis compared to the modern human one, since DVS-resistance mainly depends on cross-sectional area (Hylander 1984). The finding that the modern human compared to the Neanderthal symphysis is clearly less effective in resisting transverse bending, but equally or more resistant to CB, when labial strains are considered, confirms Daegling's (1990, 1993a) hypothesis.

Dobson and Trinkaus (2002) also found a trend towards less resistance to transverse bending during the later Pleistocene, but did not find a significant difference between Neanderthals and early modern humans regarding transverse bending resistance. As such, they could not fully confirm Daegling's (1990, 1993a) hypothesis. The present study did not include symphyses of early modern humans and it is therefore possible that the observed strain differences between the anatomically modern human and the Neanderthal symphysis would be smaller if an early anatomically modern human mandible had been tested. Nonetheless, the application of FEA in this study allowed a test of the direct mechanical effects of different symphyseal shapes, whereas Dobson and Trinkaus (2002) could only estimate the resistance of symphyseal cross-sections based on measurements.

In addition, the use of two hypothetical symphyseal shapes in this study yielded results that are worth further consideration. Daegling (1990, 1993a) suggested that the presence of a chin reduces tensile strains at the base of the

symphysis during CB, which is advantageous since bone is weaker under tension than under compression. This can be confirmed by comparing the strain profiles of the chinned and the non-chinned models. If, however, the chin evolved to buttress the symphysis against CB, this conflicts with the finding that the presence of a chin has the smallest effect during CB. The chin is more effective in reducing the strains in DVS and transverse bending. Thus, it seems that the increase in labio-lingual thickness and cross-sectional area associated with the presence of a chin does not have such a large effect in CB as in the other load cases. However, the effect of the concentration of bone at the symphyseal base and thus an increase in bone mass by increasing the cortical thickness, has not been examined here. Studies of the internal morphology of the human symphysis have shown that the highest cortical bone thickness is found at the lower lingual aspect of the symphysis and labially at the mental protuberance (Fukase 2007, Fukase & Suwa 2008). Following Hylander (1984), such a concentration of bone should improve resistance to CB and DVS. Therefore, it is likely that the presence of a chin combined with a concentration of cortical bone at the lower aspect of the symphysis buttresses the human symphysis very effectively against CB and DVS, but not against CB specifically.

Unfortunately, published experimental data do not clearly indicate which symphyseal load case is predominant during human masticatory function. In cercopithecine primates, it is wishboning that causes the highest strains at the symphysis during the powerstroke of mastication, followed by DVS (Hylander 1985). EMG data from humans are very different from those of cercopithecine primates (Møller 1966, Hylander & Johnson 1994) and if wishboning or reverse wishboning occurs in humans, it is unlikely to have a large effect in the relatively short and wide human mandible because of the shorter moment arms associated with wishboning and the less sharp curvature at the symphysis (Daegling 1990, 1993a, Hylander & Johnson 1994).

That transverse bending resistance has become less important for the human symphysis is supported by the results of our comparison between the vertical and inclined symphyses. Since the inclined symphysis proves very effective in resisting transverse bending, it is difficult to imagine, how a more vertically orientated symphysis could evolve during human evolution if transverse bending remained the predominant symphyseal load type. A vertical symphysis is,

however, not disadvantageous in resisting CB or DVS. Together with the fact that the emergence of the chin is highly correlated with an increasingly vertical symphysis during the later Pleistocene (Dobson & Trinkaus 2002) this provides further support for Daegling's (1990, 1993a) hypothesis. It also shows that the evolution of the chin should not be seen in isolation but in the context of an increasingly vertical symphysis, since it is likely that these two aspects of modern human symphyseal morphology are, from a mechanical point of view, closely interconnected.

To date, the change in symphyseal orientation during human evolution has not been as much discussed as the emergence of the chin. Given the evidence from this study, it is possible that a vertical symphysis evolved because it provided better resistance to altered masticatory loads like an increase in the relative importance of CB, or because other factors like the reduction of maxillary prognathism or developmental constraints favoured the development of a more vertical symphysis in the absence of selection for strong transverse bending resistance. Our results cannot provide a clear answer to this question. If CB became relatively more important during human evolution, a vertical symphysis would have decreased overall tensile strains, but at the expense of locally increased strains on the lingual side of the symphysis.

Although the theoretical division of masticatory loading into simple load cases is very useful for understanding of the mechanisms of functional adaptation in the symphysis, there is the risk of oversimplification, since the overlap of these loads during masticatory function might result in more complex strain patterns. The deformations during our incision and molar bite simulations represent a mixture of CB, DVS and transverse bending, but interestingly CB is the predominant load type of the simulated molar bite. As in the CB simulations, the modern human symphysis shows better resistance than the Neanderthal one, since the tensile strains on the labial side are very much reduced. The comparison of strain magnitudes and patterns between the other models shows that this is primarily the result of the vertical orientation of the modern human symphysis.

In general, the results of this study confirm prior mechanical hypotheses about the modern human as well as symphyseal morphology in general and show that the use of FEA can be very useful for testing such hypotheses, since the effects of specific loads and morphological features can be studied if confounding

variables are carefully controlled. Future FEA studies could also explore the mechanical significance of sexual dimorphism in human chin morphology. It is possible that the different chin forms of males and females are the result of sexual selection since sexual dimorphism in chin morphology is closely related to facial attractiveness (Barber 1995) and/or caused by the direct influence of sex hormones on mandibular growth as known from animal experiments (Moutier et al. 1992, Fujita et al. 2001, Fujita et al. 2004), but this is difficult to test. Alternatively, sexual dimorphism in chin morphology could reflect mechanical adaptations to different masticatory forces in males and females resulting, for example, from differences in mandibular dimensions and muscle force magnitudes, which can be studied with FEA (Daegling 1993a).

However, for a full understanding of the evolution of human symphyseal morphology, it will be necessary to obtain more data on masticatory function in modern humans and apes and to create more realistic models. In addition, which mechanical parameters are most relevant for assessing how well a bone resists loads needs to be clarified, for example, tensile or compressive stresses and strains, von Mises stress or strain energy density. In this study, special attention was drawn to the increase and decrease of tensile strains, since bone is weaker under tension than under compression and the reduction of tension has been used as a major argument for the evolution of the human chin (DuBrul & Sicher 1954, Daegling 1990, 1993a). However, there is no consensus in the biomechanical literature yet that the morphology of bones is indeed optimised to this criterion. Better understanding of what parameters are important would provide a better basis for comparative FEA studies in future.

Chapter 10: Variation of load resistance in mandibles of late *Homo*

10.1. Introduction

Since the Middle Pleistocene human mandibular morphology has changed considerably. In general, there has been a trend towards reduced overall size and robusticity as well as to smaller tooth dimensions, especially with regard to the postcanine dentition (Brace 1979, Franciscus & Trinkaus 1995, Wolpoff 1999, Nicholson & Harvati 2006). This gracilisation is visible not only in the lineage leading towards anatomically modern humans, but also within Neanderthals (Franciscus & Trinkaus 1995).

Several authors have suggested that this morphological change is the result of new food preparation techniques (e.g. cutting, pounding, grinding and especially cooking) developed since the Middle Pleistocene (Brace 1979, Franciscus & Trinkaus 1995, Wolpoff 1999). Microwear analyses have shown that there is a trend towards a less abrasive and softer diet since the Middle Pleistocene, most probably due to food processing (Pérez-Pérez et al. 2003). Such advances in food preparation techniques certainly improved the digestibility of the food and made food softer and smaller in particle size, so that less occlusal force and fewer chewing cycles were required for food breakdown (Lucas & Luke 1984, Lieberman et al. 2004a). It is possible that this reduction of masticatory loads had an impact on mandibular morphology in two ways: 1) by reducing the selection pressure for maintaining a large dentition and robust mandibular morphology (Brace 1979), 2) by reducing strains in the bone that stimulate craniofacial growth (Lieberman et al. 2004a).

The latter is supported by animal experiments which have shown that softer and more processed food does indeed lead to a reduction of strains in the skull and to reduced craniofacial growth resulting in smaller skulls of different shape when compared to individuals raised on hard, unprocessed food (Beecher et al. 1983, Kiliaridis et al. 1985, Engström et al. 1986, Lieberman et al. 2004a). Similar changes in craniofacial morphology have been reported from human populations that developed new techniques of food processing, for example, due to the introduction of agriculture or the industrialisation (Carlson 1976, Carlson & van Gerven 1977, Corruccini 1984, 1990, Varrela 1992). Based on this evidence it is likely that a part of the variation in mandibular morphology in late *Homo* can be

explained by adaptations to more processed and soft food. This is not an hypothesis that can be fully tested due to the lack of data and the fact that direct experiments are not possible, but the prediction can be made that if there was an adaptation to reduced masticatory loads, resistance to masticatory load should have decreased over time, and this can be tested with FEA.

However, when Neanderthal morphology is considered, the picture becomes more complex. Although a gracilisation trend including a reduction in postcanine tooth size is also observed in Neanderthals (Stefan & Trinkaus 1998b), the reduction in tooth size does not apply to their incisors, which remained large (Brace 1979). Some authors have therefore suggested a specific selective force acting on the Neanderthal anterior dentition that is not related to food processing but to the manipulation of non-edible objects (Brace 1967, Brose & Wolpoff 1971, Wolpoff 1975, Brace 1979). The relatively large incisors together with their shovel-shape and typically high degree of wear compared to the postcanine dentition as well as the high prevalence of degenerative changes in the TMJs of Neanderthals have been regarded as evidence that Neanderthals used their front teeth regularly for such non-food processing purposes (Stewart 1959, Brace 1962, Coon 1962, Brace et al. 1981, Smith 1983, Trinkaus 1983, Smith & Paquette 1989). This idea provided the basis for the "anterior dental loading hypothesis" (ADLH), which suggests that the typical Neanderthal craniofacial morphology can be partly explained as an adaptation to regular heavy anterior dental loads that resulted from the use of the front teeth as a tool (Smith 1983, Rak 1986, Demes 1987, Trinkaus 1987, Spencer & Demes 1993).

Previous studies that have tried to test the ADLH focused on bite force production capability and efficiency of Neanderthals (Antón 1990, Spencer & Demes 1993, Antón 1994, O'Connor et al. 2005). If Neanderthals are specifically adapted to regular high anterior dental loads as the ADLH posits, then they should have been able to produce higher bite forces on the anterior dentition than modern humans and should have been more efficient in doing so. However, studies that tested this prediction yielded contradictory results (Antón 1990, Spencer & Demes 1993, Antón 1994, O'Connor et al. 2005). Spencer and Demes (1993) evaluated the position of the masticatory muscles relative to the TMJ and concluded that Neanderthals had increased ability to produce large anterior bite forces compared to anatomically modern humans. Antón (1990, 1994), on the

contrary, estimated smaller bite forces in Neanderthals than in modern humans. The most recent 3D modelling study by O'Connor and colleagues (2005) suggests that Neanderthals and modern humans were equally able to produce anterior bite forces. The differences in bite force production that O'Connor and co-workers (2005) found were between large robust individuals and small gracile individuals rather than between anatomically modern humans and Neanderthals.

However, all of the studies that have tried to test the ADLH to date have only considered the production of bite forces. So far, differences in load resistance between modern humans and Neanderthals have not been explored, although such differences are also likely to be of importance in testing the ADLH. This study will apply FEA to simulate masticatory loads in mandibles of *H. heidelbergensis*, Neanderthal and anatomically modern humans and evaluate differences in load resistance between them. The aim is to test the predictions of the ADLH as well as predictions that arise from the hypothesis that the overall gracilisation trend in late *Homo* is the result of reduced masticatory loads.

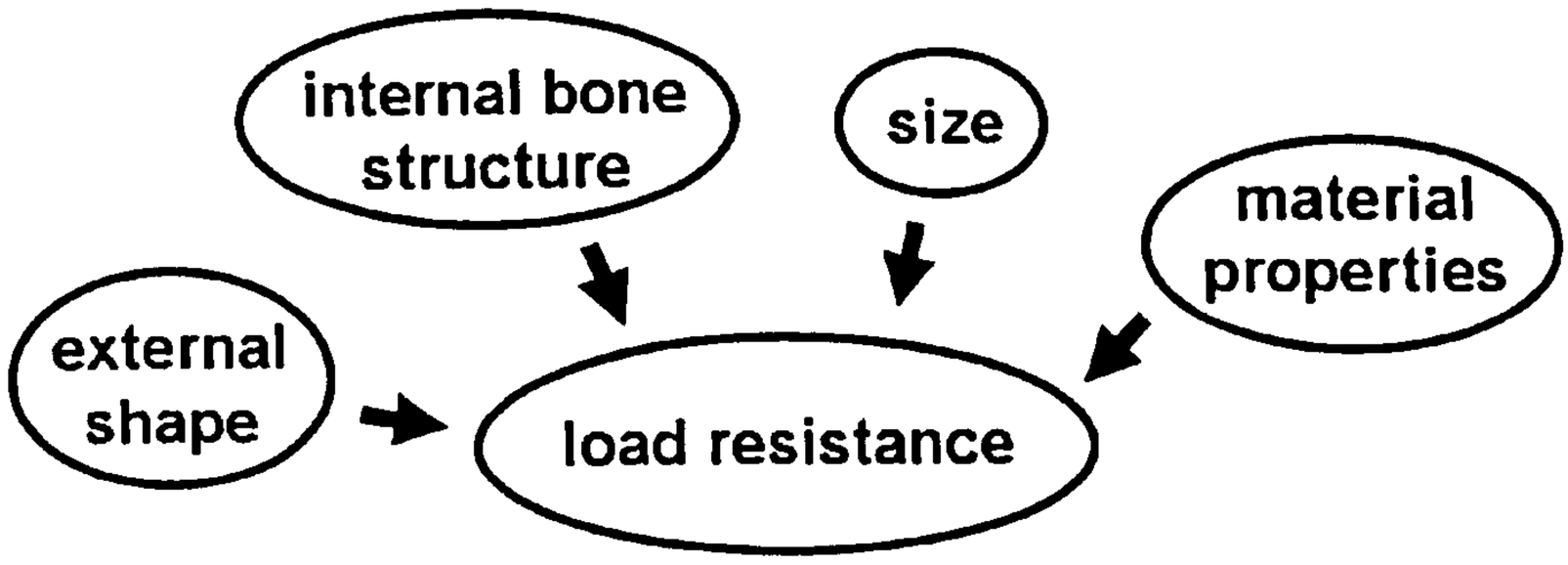

Fig. 10.1. Factors that potentially have an impact on the load resistance of a bone. In this study primarily the effects of size and cortical bone thickness (as one aspect of internal bone structure) are investigated.

Furthermore, by controlling variables, the potential causes of differences in load resistance will be explored. **Figure 10.1** illustrates which factors are likely to have a major effect on the load resistance of a mandible. The exact material properties of bone tissue of extinct taxa are unknown and thus the effect of this variable cannot be explored here. The other aspects of mandibular morphology can however be studied in well preserved specimens. In this study, especially the effect of size and cortical bone thickness, one aspect of the internal bone structure, will be investigated. The following predictions will be tested:

1) If Neanderthals are specifically adapted to resist high loads on the incisors, strains should be lower in Neanderthal mandibles than in other mandibles

of late *Homo* when incision is simulated and these differences should be larger than during molar loading.

2) If late *Homo* mandibles have become adapted to lower masticatory loads due to advances in food processing, load resistance should have decreased over time. Strains resulting from masticatory loads should therefore be highest in the most recent specimens and decrease with increasing age of the specimens.

3) If size and cortical bone thickness cause differences in load resistance and thus strains, then controlling these factors should decrease the variation in strain magnitudes. The more important the factor is for load resistance, the greater should be the effect on the strain variation when it is controlled.

10.2. Material and Methods

The sample consisted of 7 mandibles of modern and fossil humans. **Table 10.1** provides some information about the specimens. More details about the specimens and their respective CT scans can be found in Chapter 3. Three of these mandibles (Régourdou 1, H-A 001, H-A 002) have already been used for the studies described in the previous chapters and thus FE models of these specimens were already available.

The remaining models were created by applying the same methodology as described before, using thresholding and manual segmentation tools in Amira. Fragmentary specimens were reconstructed by mirror-imaging and manual closure of small cracks (more details under 3.5). After the initial segmentation and additional reconstruction of the fossil specimens, a layer of PDL was added to the models by drawing a thin line around each tooth root in the CT slices and simplified models of the TMJs were attached to the condylar surfaces. In the next step those datasets that consisted of anisotropic voxels (Mauer 1, Krapina 59, ANAT 800) were converted into isotropic datasets. In order to control for cortical thickness, one additional model was created for each specimen, in which the cortical bone had an equal thickness of 1.7-1.9 mm.

The final 3D volume datasets were exported as BMP image stacks and converted into finite element meshes by direct voxel conversion. **Table 10.2** lists the resulting element number and element size for each model. The material properties assigned to the models were identical to the ones for all previous analyses. After assigning the material properties and defining the muscle

attachment areas and muscle vector orientations, the following loading scenarios were modelled (see 3.8 for details about the muscle forces): 1) incision with modern human muscle forces applied to all specimens, 2) incision with estimated muscle forces based on bony proxies for the fossil specimens, 3) bite on the right M1 with modern human forces for all specimens, 4) bite on the right M1 with estimated muscle forces for the fossil specimens. For the incision simulation, the models were constrained in the axis vertical to the occlusal plane at the incisors and for the molar bite in all axes at the occlusal surface of the respective molar. For both load cases the blocks representing the TMJs were constrained in all three axes at their upper corners (see Chapter 5).

Specimen	Taxon	Estimated age
ANAT 800	*H. sapiens*	modern
H-A 001	*H. sapiens*	modern
H-A 002	*H. sapiens*	modern
Skhūl 5	*H. sapiens*	100-130 ka (Stringer et al. 1989, Grün et al. 2005)
Régourdou 1	*H. neanderthalensis*	65-75 ka (Bonifay 1964, Vandermeersch 1965)
Krapina 59	*H. neanderthalensis*	120-140 ka (Rink et al. 1995)
Mauer 1	*H. heidelbergensis*	640-735 ka (Hambach 1996)

Table 10.1. Mandibular specimens included in this FEA. More information about the specimens is given in sections 3.2 and 3.3.

The resulting deformations in the models were quantified using von Mises strain (ε_v). Differences in strain patterns and magnitudes were then evaluated by comparing the colour-coded contour plots and strain values from 123 selected locations on the bone surfaces. These locations represent landmark and semilandmark positions that were applicable to all mandibles, after they were all orientated so that the occlusal plane was horizontal. Examples of these positions are: the tip of the coronoid, the most inferior point on the corpus below the right M1, the point half way between the former point and the alveolar margin of the right M1 on the buccal surface. **Figure 10.2** shows the positions of these points on

one of the mandibles. The extracted strain values were used to calculate the mean strain magnitudes and standard deviations. In order to compare the interindividual variation in strain magnitudes between different analyses, the standard deviations were divided by the overall mean for each analysis, so that the variation could be compared despite differences in magnitudes between the analyses.

Specimen	Number of elements		Element size in mm
	Orginal models	Equal cortical thickness models	
ANAT 800	492995	418967	0.488
H-A 001	2138871	1575227	0.300
H-A 002	3333138	3055907	0.240
Skhūl 5	753880	564580	0.488
Régourdou 1	2037088	1597548	0.350
Krapina 59	4852796	3691602	0.295
Mauer 1	1426412	913633	0.437

Table 10.2. Finite element numbers and element sizes of the models.

In order to test the effect of size on the variation of strain magnitudes, the strain values were scaled following the methodology of Dumont et al. (2009). These authors showed that von Mises stress in FE models of different size can be compared when they are scaled according to the cube root of their volume squared, which approximates their surface areas. For this purpose, the volume of each mandible, including bone, teeth and PDL, but excluding the blocks representing the TMJs, was measured in Amira and the mean volume for all specimens was calculated (67.76 cm^3 for the original models, 47.3 cm^3 for the equal cortical thickness models). The scaling factor for each model was then calculated as (model volume)$^{2/3}$ divided by (mean volume)$^{2/3}$. Finally, these scaling factors (**Table 10.3**) were multiplied with the von Mises strain values.

Specimen	Original models		Equal cortical thickness models	
	Volume in cm^3	Scaling factor	Volume in cm^3	Scaling factor
ANAT 800	49.61	0.81	41.00	0.72
H-A 001	50.24	0.82	35.03	0.64
H-A 002	38.16	0.68	34.33	0.64
Skhūl 5	72.58	1.05	48.55	0.80
Régourdou 1	69.33	1.02	50.39	0.82
Krapina 59	91.51	1.22	61.78	0.94
Mauer 1	102.86	1.32	60.06	0.92

Table 10.3. Volumes of the models excluding the TMJ blocks and calculated scaling factors for scaling the strain magnitudes to the mean volume of the specimens.

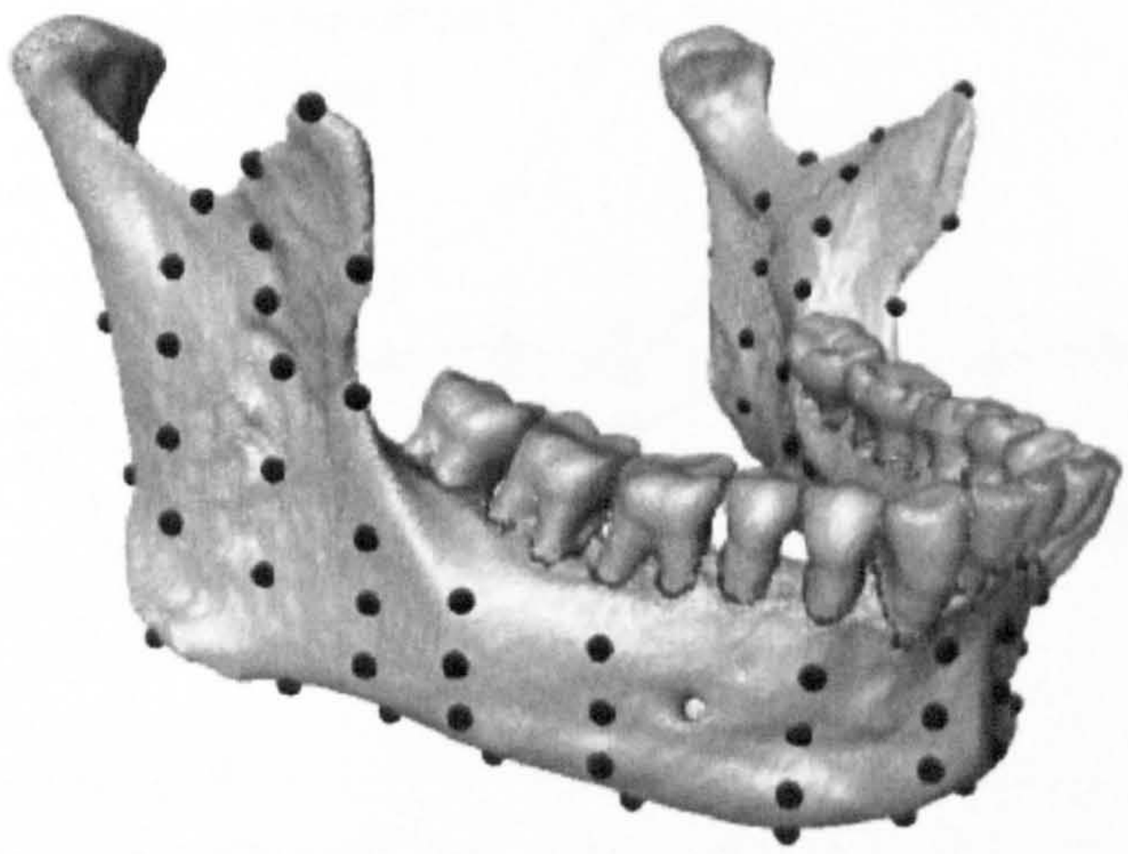

Fig. 10.2. Landmark and semilandmark positions on the bone surface used for the extraction of strains values.

10.3. Results

Figure 10.3 shows the von Mises strain magnitudes for incision with identical modern human muscle forces applied to all specimens. The highest strains are found in the modern human specimens, especially in the anterior corpus. One modern human specimen (H-A 002) also shows high strains in the left posterior corpus and ramus, which is most probably due to differences in muscle force orientations between the left and right side (see Chapter 5). The strains in the two Neanderthal specimens are at the bottom of the modern human

range or below. At almost all locations the early Neanderthal Krapina 59 shows lower strains than the Neanderthal Régourdou 1. Even lower strains are found in the *H. heidelbergensis* mandible Mauer 1. The lowest strains in the mandibular corpus are, however, found in the early anatomically modern specimen Skhūl 5.

Fig. 10.4 shows the strain values for incision, when the Neanderthals and the *H. heidelbergensis* are loaded with muscle force magnitudes that have been estimated based on their anatomy. These higher muscle forces result in higher strain values in the respective specimens, so that they are now within the modern human range or in the case of the Mauer mandible on the lower border of this range.

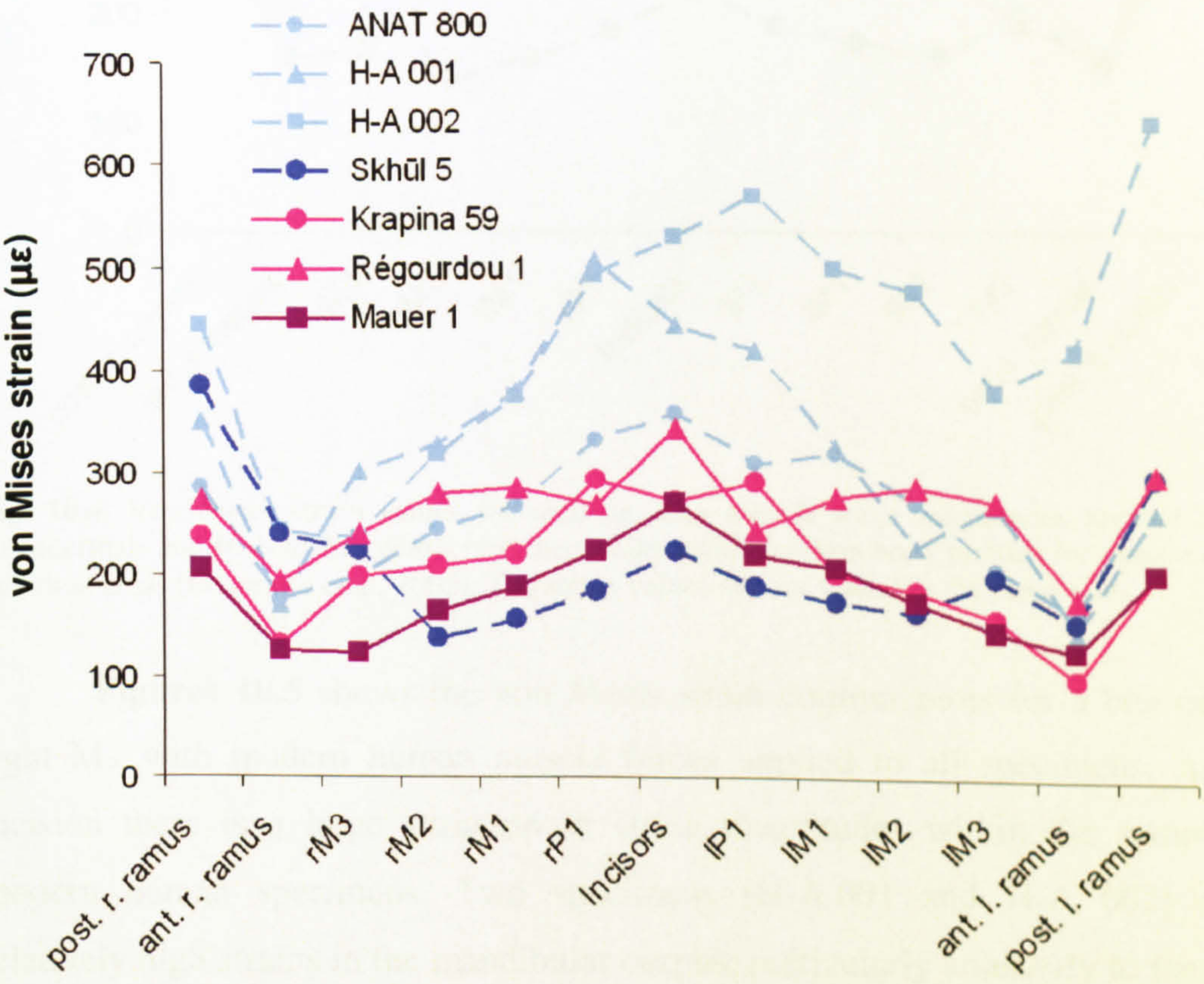

Fig. 10.3. Von Mises strain values for incision with identical modern human muscle force magnitudes applied to all specimens. The strain values of the modern human specimens are shown in light blue, which also applies to all following graphs in this chapter. The strain values are not scaled to the same size.

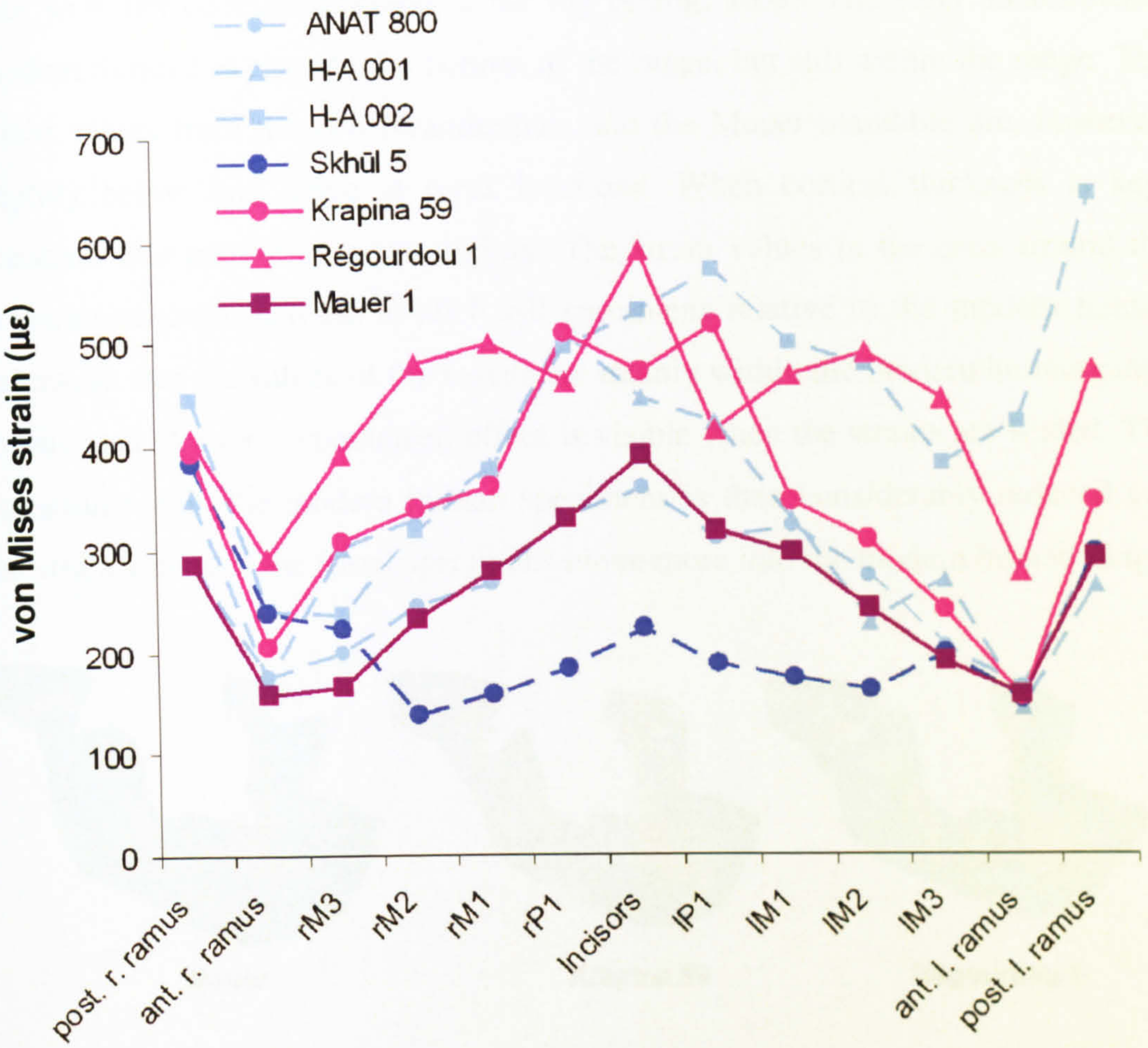

Fig. 10.4. Von Mises strain values for incision. The muscle force magnitudes applied to the Neanderthals and *H. heidelbergensis* have been calculated based on bony proxies for muscle cross-sectional areas (O'Connor et al. 2005). The strain values are not scaled to the same size.

Figures 10.5 shows the von Mises strain contour plots for a bite on the right M1 with modern human muscle forces applied to all specimens. As for incision there is a large variation in strain magnitudes within the sample of modern human specimens. Two specimens (H-A 001 and H-A 002) show relatively high strains in the mandibular corpus, particularly anteriorly to the right M1. In addition, one of these specimens (H-A 002) exhibits very high strains over the posterior half of the balancing side corpus. The third modern human specimen (ANAT 800) and the early anatomically modern specimen Skhūl 5 show similarly high strains only directly around the biting tooth and in some small areas of the rami. The two Neanderthals and the Mauer mandible show the lowest strains: compared to the other specimens, high strains only occur directly below the constrained M1.

The large variation of strain magnitudes is also clearly visible in the extracted strain values from the original analyses, in which cortical thickness and

size were not controlled (graph at the top of **Fig. 10.6**). The early anatomically modern Skhūl 5 is close to the bottom of the range, but still within the range. The strain values from the two Neanderthals and the Mauer mandible are, however, slightly below this range at most locations. When cortical thickness is kept constant, this pattern changes slightly. The strain values in the area around the constrained tooth increase in all fossil specimens relative to the modern human values, so that the values of the fossils are mainly within the modern human range in this area. A more pronounced effect is visible when the strains are scaled. The variation within the modern human specimens is then considerably reduced and the strain values of the fossil specimens move more into the modern human range.

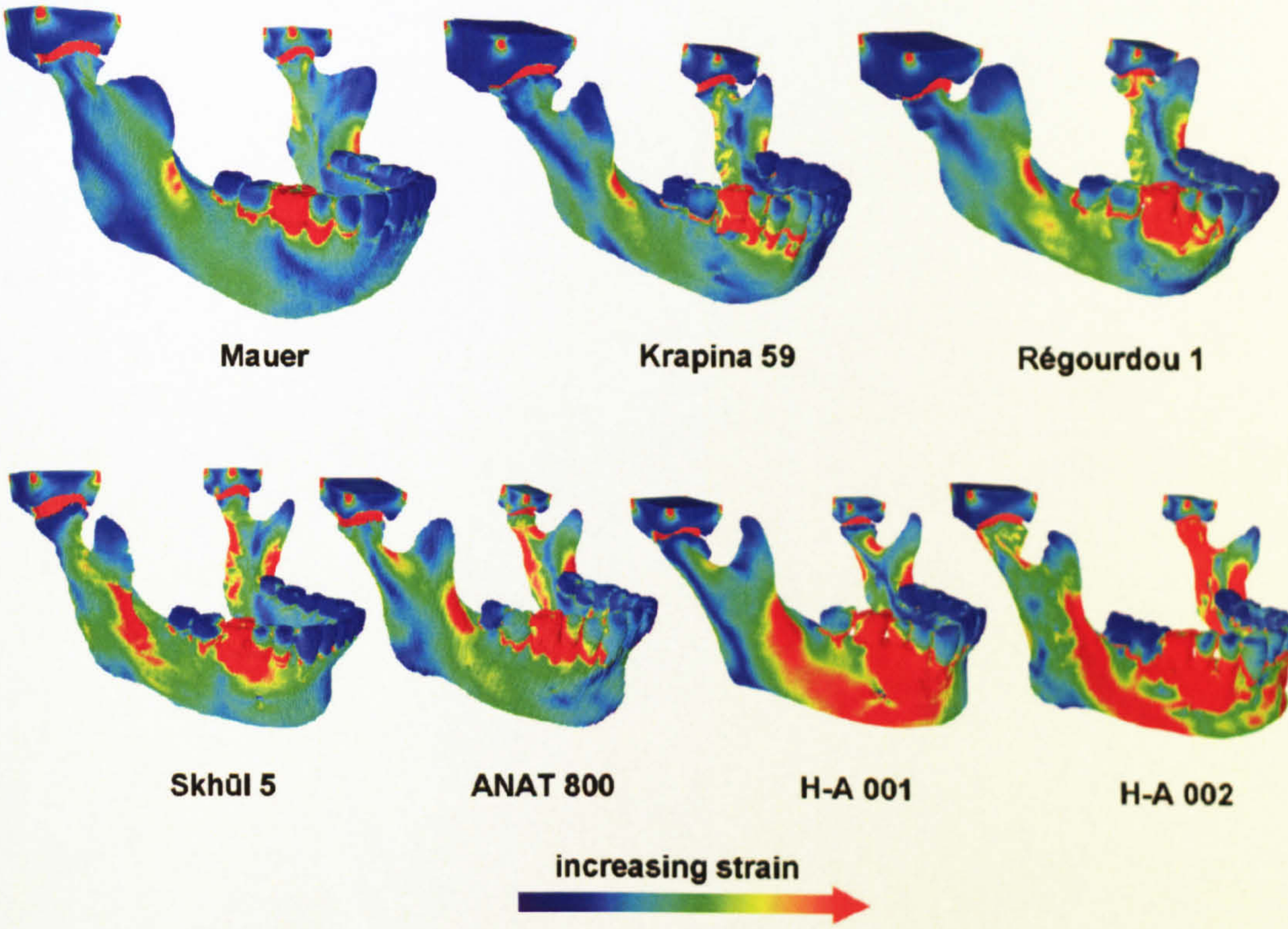

Fig. 10.5. Von Mises strain contour plots for a bite on the right M1. Identical modern human muscle force magnitudes have been applied to all specimens.

The use of estimated muscle forces based on bony proxies for the Neanderthals and *H. heidelbergensis* yields very similar strain differences overall to those observed above, where the same muscle forces were applied as to the modern human specimens. However, there is, in general, a slightly larger area of overlap with the modern human strain values (**Fig. 10.7**). Controlling cortical thickness and size results in the same effects, but this time, more strain values

from the Mauer mandible and the two Neanderthals fall into the centre of the modern range.

A summary of the differences in strain magnitudes between the specimens and how controlling cortical thickness changes the variation of strain magnitudes is provided by **Table 10.4**. It shows that the variation in strain magnitudes is always larger during molar biting than during incision. In addition, it confirms that controlling cortical thickness and even more so controlling size reduces the variation in strains between the specimens.

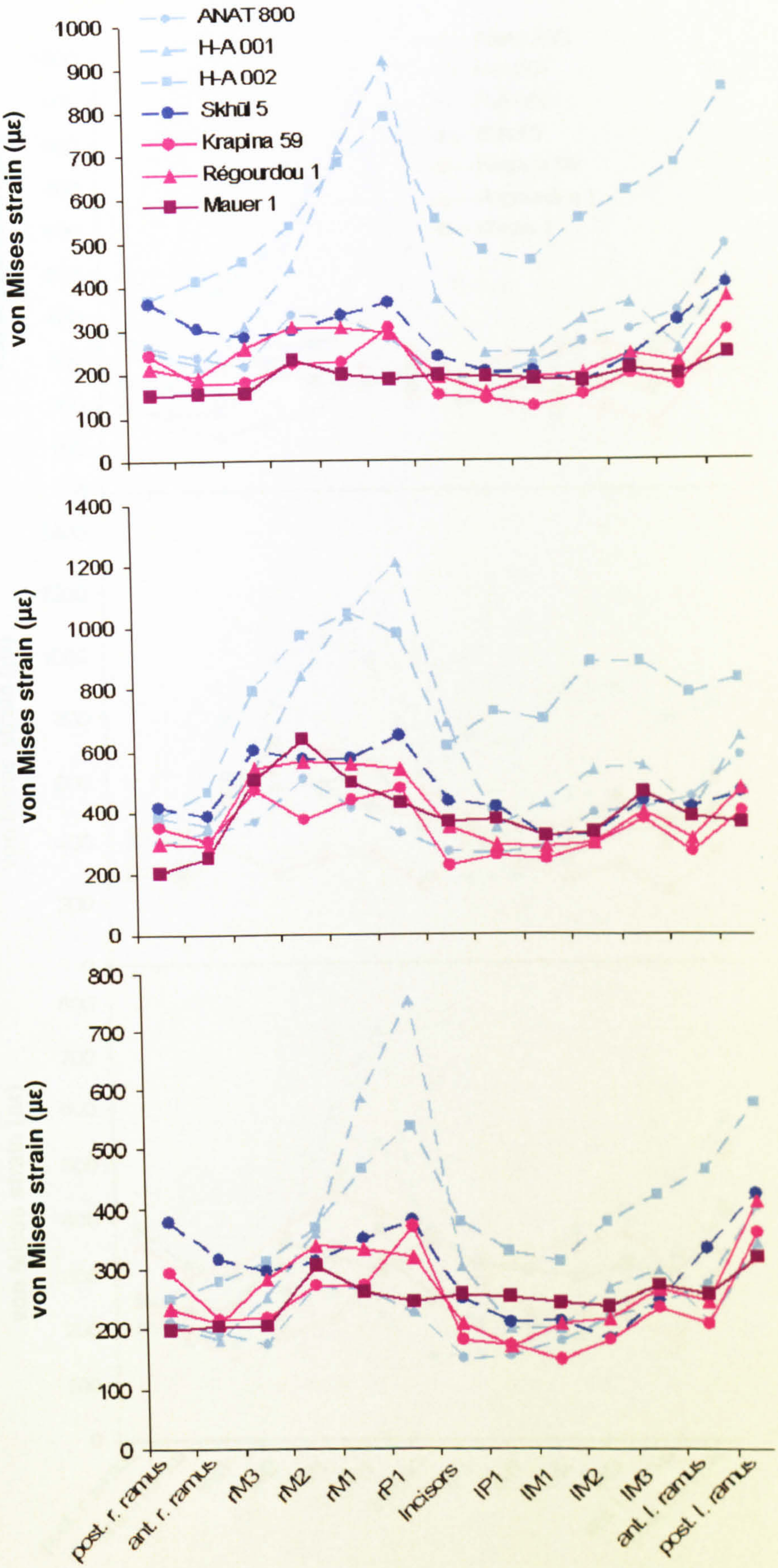

Fig. 10.6. Von Mises strain values for a bite on the right M1. From top to bottom: original models, models with equal cortical bone thickness, original models with strains scaled to mean volume. Identical modern human muscle force magnitudes were applied to all specimens.

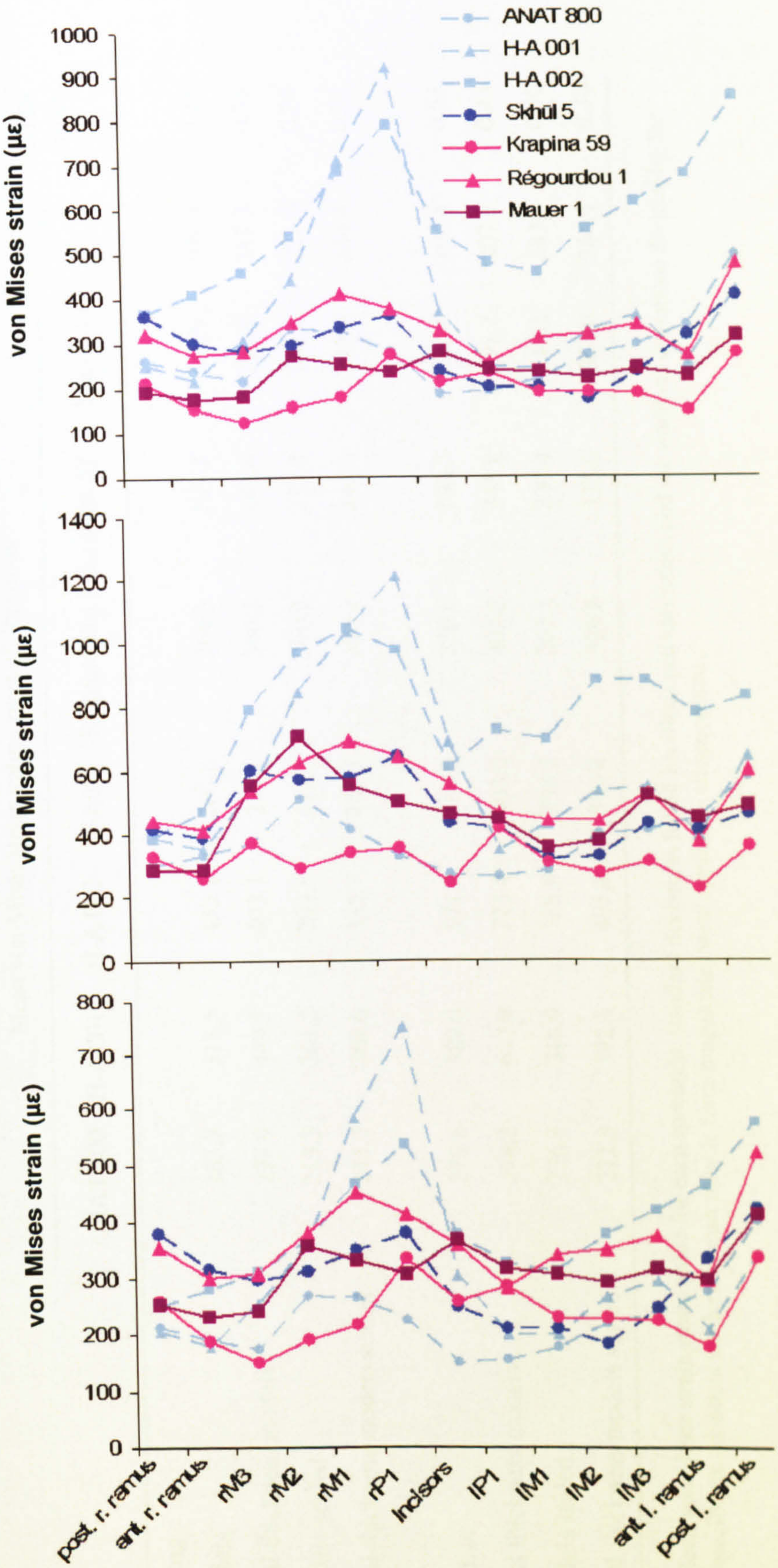

Fig. 10.7. Von Mises strain values for a bite on the right M1. From top to bottom: original models, models with equal cortical bone thickness, original models with strains scaled to mean volume. The muscle force magnitudes applied to the Neanderthal and *H. heidelbergensis* have been calculated based on bony proxies for muscle cross-sectional areas (O'Connor et al. 2005).

Analyses	Mean von Mises strain values over all locations							STD	STD/ Mean
	ANAT 800	H-A 001	H-A 002	Skhūl 5	Régourdou 1	Krapina 59	Mauer 1		
Incisal loading									
Original models	263.3	318.5	433.1	208.8	264.5	207.2	182.9	109.3	0.41
Equal cortical thickness models	297.9	449.5	493.7	251.1	360.2	281.6	296.9	347.3	0.35
Original models scaled	213.3	261.2	294.5	219.3	290.9	252.8	241.4	253.3	0.29
Equal cortical thickness models scaled	241.3	368.6	335.7	263.7	396.2	343.6	392.0	334.4	0.29
Molar bite									
Original models	279.6	389.0	571.7	284.0	239.6	196.3	188.8	163.8	0.53
Equal cortical thickness models	378.2	612.9	773.4	463.0	402.2	345.8	395.7	207.7	0.43
Original models scaled	226.5	318.9	388.8	298.2	263.5	239.4	249.2	283.5	0.36
Equal cortical thickness models scaled	272.3	392.3	495.0	370.4	329.8	325.0	364.0	364.1	0.34

Table 10.4. Mean von Mises strain strain value for each specimen, standard deviations for all locations and specimens and the standard deviations divided by the means for all specimens. Identical modern human muscle force magnitudes were applied to all specimens.

10.4. Discussion and Conclusions

The simulation of incision and biting on the right M1 results in very different strains between the specimens even when identical muscle forces are applied to them. The largest differences can be observed in the anterior half of the corpus. Here, the highest values are found in the modern human specimens. The strains in the fossils are at the bottom of or below the modern human range. Controlling cortical thickness has an effect on the results by increasing the overlap of strain values in the fossil specimens with the modern human range of strain values. However, the largest effect is however achieved when size is controlled. The variation of strain values is then considerably reduced and the strain values of the fossil specimens move into the modern human range.

The ADLH predicts that Neanderthals are better adapted to anterior dental loads and should thus show lower strain magnitudes during simulated incision than other mandibles of late *Homo*. The strains in the anterior corpus of the two studied Neanderthals are indeed lower compared to the modern human specimens, especially in the anterior corpus, when modern human muscle force magnitudes are applied. However, even lower corpus strains are measured in the *H. heidelbergensis* specimen Mauer 1 and the early anatomically modern mandible Skhūl 5. In addition, the differences in load resistance between the Neanderthal and modern human specimens disappear, when the Neanderthal mandibles are loaded with "Neanderthal muscle force magnitudes" instead of modern human ones (**Fig. 10.4**). Finally, the strain differences between the groups are not larger than during molar biting.

So, at least with regard to the mandible, it can be stated that there is no evidence that Neanderthals are specifically adapted to better resist anterior dental loading than *H. heidelbergensis* or modern humans. Instead, they seem to better resist masticatory loads in general compared to the studied modern human mandibles and are thus similar to the *H. heidelbergensis* specimen Mauer 1 and the early anatomically modern human Skhūl 5. In other words, the differences in strain magnitudes lie between all studied fossil specimens on the one hand and the modern mandibles on the other, not between Neanderthal and non-Neanderthal specimens. Therefore, the resistance to anterior dental loading in the studied specimens seems to rather depend on the general robusticity including size and bone thickness of each mandible instead of the presence or absence of

Neanderthal morphology. These results are similar to the results of the 3D rigid-body modelling study of O'Connor and colleagues (2005), which also suggest a dichotomy between robust and gracile specimens instead of Neanderthals vs. modern humans with regard to bite force production.

Beyond the investigation of specific mechanical adaptation in Neanderthals, this study aimed to check whether or not there is a general trend towards less resistance to masticatory loads through time. If advances in food processing led to a reduction of masticatory loads to which the mandibles adapted, there should be an increase in strains with decreasing age of the specimens. Although the sample size used here is too small to test this prediction statistically, the results confirm such a trend overall. The highest strains are found in the modern human specimens, whereas the lowest strains are found in the *H. heidelbergensis* mandible. Interestingly, there is also a difference between the two Neanderthals in the sample. The early Neanderthal specimen Krapina 59 shows lower strains overall than the classic Neanderthal Régourdou 1. The picture becomes more complex however, when Skhūl 5 is considered. As expected, it lies at the bottom of the modern human range during a molar bite, but that it shows lower strains than the Neanderthals during incision is rather surprising and deserves further investigation.

In general, the results of this study support the hypothesis that there was a trend towards an adaptation to reduced masticatory loads since the Middle Pleistocene. This decrease in load resistance is certainly the result of a combination of morphological changes, but two morphological variables have been explicitly tested here. As the results show, the differences in cortical bone thickness explain some part of the variation in strain magnitudes. This is not surprising, given the large differences in cortical bone thickness between the modern human and the fossil specimens (**Fig. 10.8**) and the fact that the cortical thickness is known to be critical in resisting bending, since during bending strains increase with the distance from the neutral axis and are thus highest in the cortical shell. However, a larger part of the variation seems to be due to the size differences between the specimens, which have been quantified here as the differences in volume$^{2/3}$. If the strains are scaled based on the mean volume$^{2/3}$ of the specimens, the differences between the modern human and the fossil mandibles disappear.

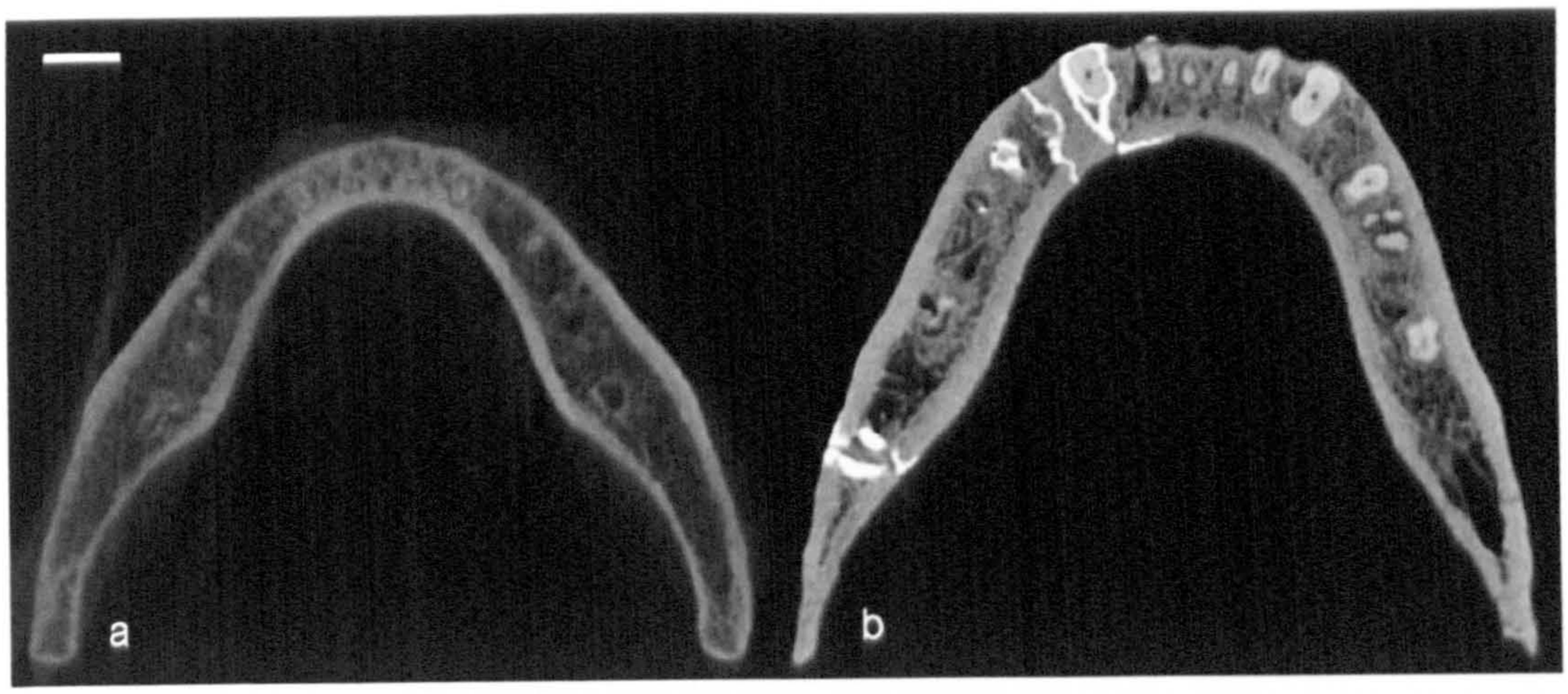

Fig. 10.8. Transverse CT slices through the mid-corpus of the modern human mandible H-A 001 (a) and the Neanderthal specimen Krapina 59 (b). Note the difference in size and cortical thickness. Scale bar = 1 cm.

Thus, the dichotomy between large, robust and small, gracile individuals that was found by O'Connor and co-workers (2005) regarding force production seems also to be true for the resistance to loads. In addition, experiments and measurements of human populations have shown that reduction of masticatory loads due to the consumption of more processed soft food leads to a decrease in mandibular dimensions or skull dimensions in general (Carlson 1976, Carlson & van Gerven 1977, Corruccini 1984, 1990, Varrela 1992). It seems that size is the major variable that changes when masticatory loads decrease. However, it is also the most easily measured variable. External shape, internal bone geometry or the mechanical properties of bones are more difficult to measure and far fewer data are therefore available to evaluate how they are related to changes in masticatory loads.

The application of FEA to test the effect of each variable and thus to evaluate their relative importance is certainly a promising approach, but how to best control certain variables is not always straightforward. One example is the question which muscle forces are to be applied to specimens in comparative studies. In this study, two approaches have been used. First, identical muscle force magnitudes based on estimates of modern human forces were applied to all specimens to allow a direct comparison, but this leads to artificially low muscle forces in the case of the fossil specimens. Therefore, the fossil specimens were also loaded with muscle forces estimated based on bony proxies. However, the use of bony proxies for the calculation of the physiological cross-sectional area (PCSA) and thus the maximum force of a muscle can only be a very crude

estimate. So, both approaches raise methodological problems, but it is advisable to apply both in order to evaluate the robusticity of the results.

Another variable that can affect the comparability of the strains between specimens is model resolution. As has been discussed in Chapter 4, a low spatial resolution and image blurriness can result in inaccurate model geometry, for example, an overestimation of cortical bone thickness. The CT scans used for this study are quite variable regarding their spatial and contrast resolution (see 3.4) so that some part of the variation in strain magnitudes is certainly due to differences in scan resolution. However, the largest variation in scan resolution is found within the modern human sample, which suggests that the differences between the modern human and the fossil strain values are real. In addition, potential overestimations of cortical thickness due to low scan resolution were controlled by creating models with equal cortical bone thickness. It is reassuring that the strain differences in these models were very similar to the ones in the original models. So, it seems that the error introduced by differences in scan resolution is relatively small, but, ideally, future comparative FEA studies should try to use CT scans obtained from the same scanner and identical setting in order to achieve maximum comparability.

Finally, the comparability of the results, at least for testing the ADLH, could be significantly improved by including anatomically modern human specimens from prehistoric and extant hunter-gatherer populations instead of specimens from modern agricultural or industrialised societies, since differences in diet, food processing techniques and overall robusticity as potential confounding variables should be controlled as much as possible. The Near Eastern early anatomically modern specimens from Skūhl and Qafzeh are especially interesting in this context, since they were not only associated with Mousterian artefacts, which are similar to the tools attributed to Neanderthals (Garrod & Bate 1937), but also show the same macro- and microwear pattern as Neanderthals (P. Smith 1976, Pérez-Pérez et al. 2003). Future FEA studies could investigate how these not only compare with Neanderthals but also with Upper Palaeolithic populations.

In order to study adaptation to reduced masticatory load resulting from new ways of food processing, it would be interesting study a sample from a population, in which a relatively abrupt change of food processing techniques

occurred, for example, during the introduction of agriculture or industrialisation. Thus geographic as well as genetic variation could be kept small and differences in load resistance are likely to reflect adaptations to the new diet. Additionally, it would be most interesting to include subadult specimens in order to study adaptations to reduced loads during ontogeny.

Probably the most important result of this study is that it shows how large the intraspecific variation in strain distributions and magnitudes can be. This stresses the need to increase sample sizes in FEA studies. Most FEA studies, even comparative ones (Wroe et al. 2007, Wroe 2008, Strait et al. 2009), have modelled only one specimen per taxon. This is mainly due to the fact that the creation and loading of an FE model is a time-consuming task. However, the morphological variation within species is thus completely ignored. Faster model creation methods, like direct voxel conversion, allow to increase sample sizes and will in future also allow the application of statistical methods to quantify differences in load resistance.

Chapter 11: Conclusions

In this study, finite element analysis (FEA) was used to investigate the mechanical significance of anatomically modern human and Neanderthal mandibular morphology. First, the FE modelling approach was successfully validated and the importance of different input variables was assessed in a series of sensitivity studies (Chapters 4 and 5). Second, masticatory loads were simulated in FE models of anatomically modern human, Neanderthal and *H. heidelbergensis* mandibles in order to investigate the mechanical significance of specific aspects of human mandibular morphology or to compare the load resistance of whole mandibles (Chapter 6 to 10).

11.1. Review of key findings

The FE modelling approach (the combination of mesh type and material properties) applied here had not been validated before. It was therefore necessary to compare the FEA results with strain measurements from an *in vitro* experiment, in which a dry human mandible was loaded in a simple, controlled way (Chapter 4). The comparison between the numerical predictions and the experimental results yielded a very good correspondence between the two and, additionally, the effects of scan and model resolution as well as different ways of modelling the trabecular bone tissue were evaluated. From a methodological point of view, this study was interesting, because it applied a novel strain measurement technique, digital speckle pattern interferometry (DSPI) for measuring bone strains in the *in vitro* experiment. It has been shown that this full-field strain measurement technique provides reliable results even for complex and curved bone surfaces and that it offers several advantages for the validation of FE models compared to strain gauges.

The subsequent sensitivity study (Chapter 5) showed how sensitive FEA results are to changes in input variables and that varying some input variables has a larger effect than varying others. These results confirm that it is absolutely crucial to apply the correct loads and constraints and that it is also desirable to include soft tissue elements like periodontal ligament (PDL) and the cartilaginous parts of the temporomandibular joints (TMJs). Although the modelling of masticatory loads could not be validated against *in vivo* data, since those are lacking from human mandibles, it has been shown that some of the combinations

of input variables yield strain distributions that are consistent with general findings from animal experiments and theoretical predictions. Those combinations that showed the highest consistency were used in the following analyses (Chapter 6 to 10).

When this approach was applied to model several masticatory loads in two models with altered internal morphology (i.e. one model had an equal cortical bone thickness, the other was completely filled with bone material) the peak strain maps showed a high correspondence with the distribution of cortical bone in the real mandible (Chapter 6). This finding supports the idea that the distribution of cortical bone in the mandible is related to the distribution of masticatory strains (Demes et al. 1984, Daegling 1989, Daegling & Grine 1991, Daegling 2002, Fukase 2007, Fukase & Suwa 2008). One example is the strain difference found between the buccal and lingual sides of the posterior corpus, which corresponds to the uneven distribution of cortical bone in the same area (Demes et al. 1984). These findings also indicate that the modelling approach used here is realistic enough to predict major aspects of mandibular morphology, since it is unlikely that this remarkable correspondence is the result of pure chance. This kind of comparison between peak strain maps in models with hypothetical internal morphology and the distribution of cortical bone might be thus considered as a potential validation method if *in vivo* strain data are missing.

The same approach was also applied to study the relationship between the presence or absence of a retromolar space, the shape of the anterior ramus and the distribution of cortical bone within the ramus (Chapter 7). First, a significant relationship between these three variables was determined in a morphometric study. Then, the effects on the strain distribution of changing ramus shape and of creating/removing a "retromolar space" by adding or removing teeth were investigated with FEA, using models without variation in cortical bone thickness. It was shown that the presence or absence of a space between the ramus and the most posterior molar did not have an effect on the strain distribution in the ramus, but changing the shape of the anterior ramus did in an expected manner. It is hypothesised that the cortical thickness distribution within the anterior ramus depends on ramus shape, which itself is influenced by the spatial demands of the molar dentition.

The subsequent study showed that superior ramus morphology can be linked to the orientation of the temporalis' lines of action (Chapter 8). Deleting temporalis portions resulted in strain distributions that were partly expected based on the results of animal experiments (Avis 1959, Moss & Meehan 1970). This can be related to the typical differences in superior ramus morphology between anatomically modern humans and Neanderthals (Rak 1998, Rak et al. 2002). The results support the idea that these morphological differences might be related to differences in the orientation of temporalis fibres or different activations of the individual temporalis portions during masticatory function, but further studies are necessary to confirm this relationship.

In addition to those two aspects of ramus morphology, the mechanical significance of symphyseal morphology was studied (Chapter 9). Anatomically modern human symphyseal morphology is unique with regard to the vertical orientation of the symphysis and the presence of a chin. By altering the shape of the symphysis in a human mandible, it was shown that the modern human morphology is advantageous for resisting coronal bending in the vertical plane, but disadvantageous for resisting transverse bending. In general, the results support Daegling's (1990, 1993a) hypothesis, which states that the modern human chin evolved because of a reduction of transverse bending and relative increase in coronal bending during human evolution. Thus, the results are rather different to those of recent FEA studies (Ichim et al. 2006a, 2006b), which did not find a relationship between the presence of a chin and resistance to masticatory loads.

Finally, FEA of several mandibles of anatomically modern humans, Neanderthals and *H. heidelbergensis* were conducted (Chapter 10) in order to test two more general hypotheses about mechanical adaptations in late *Homo*: 1) the so-called anterior dental loading hypothesis (ADLH), which posits that many aspects of Neanderthal craniofacial morphology are adaptations to frequent high loads on the anterior dentition (Smith 1983, Rak 1986, Demes 1987, Trinkaus 1987, Spencer & Demes 1993), 2) the hypothesis that advances in food processing since the Middle Pleistocene have reduced masticatory loads to which the face adapted and thus became less resistant to masticatory loads (Brace 1979, Franciscus & Trinkaus 1995, Wolpoff 1999). The results could not confirm that Neanderthal mandibles are specifically good in resisting anterior dental loads, but rather that they are good at resisting masticatory loads in general compared to

modern humans. However, the results are consistent with the food processing hypothesis as they confirm a trend to less resistance to masticatory loads through time. Although it is not here possible to test the relationship of this decrease in load resistance with advances in food processing, it is most likely that changes in food processing played a major role, as animal experiments and observations in human populations suggest (Carlson 1976, Carlson & van Gerven 1977, Beecher et al. 1983, Corruccini 1984, Kiliaridis et al. 1985, Engström et al. 1986, Corruccini 1990, Varrela 1992, Lieberman et al. 2004a). By controlling variables, it could be shown that the decrease in load resistance is primarily due to a decrease in size and to a lesser degree to a decrease in cortical bone thickness. However, the results also stress the need for a larger sample size for such comparative studies, since even in the small sample used here, large variations in load resistance were observed within the modern human specimens.

11.2. Implications for future research

This study has applied a number of new approaches, which are very promising for future research on human craniofacial evolution and development. In addition, some analyses have been limited by the currently available techniques, so that they could not fully answer certain questions. With advances in computing power and the further development of existing software applications, future studies will be able to explore these questions further.

The successful validation presented here (Chapter 4) suggests that the full-field strain measurement technique of DSPI should be used in future validation studies, if the DSPI equipment is available. Unlike strain gauges, which measure strains only at single points, DSPI provides a measurement of the strain distribution over the whole measured surface. Here, the measured strain distributions were compared with the FEA results only by visual comparison of the contour maps and by plotting strain profiles. Future studies could, however, take into account all points on the measured surface and quantify the match between numerical predictions and experimental results in a more sophisticated way using multivariate statistics.

In addition, the use of models with hypothetical morphologies has proven to be very useful for testing mechanical hypotheses. By altering features, for example, by landmark-based warping, while keeping the rest of the morphology

constant, it was possible to investigate the mechanical significance of single features. The control of gross aspects of morphology like size and cortical bone thickness allowed their relative importance for variations in load resistance to be studied. This approach of virtually manipulating morphology is very promising for future studies in functional morphology since it allows causal analyses that can complement and test the functional predictions of statistical analyses. It is particularly useful for palaeoanthropology, because experiments are not possible in the case of fossil taxa and often difficult in extant humans and non-human primates for ethical reasons. This study is the first that has applied such an approach to fossil hominins and it will certainly inspire future studies in this area.

The use of models with hypothetical morphologies proved especially useful in studying the relationship between strain distributions and internal bone geometry. As described above, a high correspondence between the two was found. It will be interesting to see whether the addition of more load cases (e.g. biting on the third molars or biting on large objects with resulting differences in muscle orientations) results in an even better match. Further, when the external shape is altered, it is possible to investigate the relationship between shape and internal bone structure, which is also a very promising approach for future studies.

To understand how the shapes of bones adapt to functional loads will be a major challenge for future research. It is known that the shapes of bones relate to diverse functions, not only to load resistance, for example, to protect organs, allow certain movements or provide mechanically advantageous attachments for muscles, and that some aspects of bone shape are the non-functional consequence of developmental or phylogenetic constraints. The internal morphology (i.e. cortical bone thickness and geometry of the trabecular network) of bones, on the other hand, is most probably mainly determined by their roles as load-bearing structures, but the relationship between functional load and internal bone geometry is still not straightforward (Currey 2002, Cunningham & Black 2009). Understanding the relationship between functional loads and outer bone shape is therefore even more difficult, if so many other factors play a role. Since bone modelling, which determines the gross shapes of adult bones, occurs during development, future studies should focus more on subadult individuals if they want to investigate how bone shape adapts to mechanical loads and ideally this research should be accompanied by analyses of bone resorption and deposition in

real specimens, either using histological sections or scanning electron microscopy of bone surfaces. Some pioneering work using this approach has been done on macaque crania (Kupczik et al. 2009). In future, this approach will hopefully also be applied to humans.

Another aim of future FEA studies should be to increase sample sizes. As the results presented in Chapter 10 indicate, there can be a large variation between individuals of the same species. Since comparative FEA studies have to date been limited to typically just one specimen per species (Wroe et al. 2007, Wroe 2008, Strait et al. 2009), intraspecific variations in strain magnitudes and distributions have not been considered. However, in order to study differences in load resistance between, for example, two species, it is necessary to quantify this variation.

If sample sizes get larger, it will be also possible to use geometric morphometrics (GMM) in order to warp models into statistically defined target forms, for example, means of populations, extremes of variation or regressions of form on biomechanically or ecologically interesting variables. The first studies that have combined FEA and GMM in such a way yielded promising results (Pierce et al. 2008, O'Higgins et al. 2009). In addition, the combination of GMM and FEA could provide a new tool for quantifying and evaluating FEA results, since deformations occurring during loading can be also treated as form changes. This latter, post-FEA application of GMM and associated statistical tools is currently being explored. Especially sensitivity studies and comparative studies based on large sample sizes could benefit from this new approach.

Future FEA studies should also try to simulate physiological loading more accurately. The necessary data can partly be provided by additional experimental data or, especially in the case of fossil taxa, where no experiments are possible, from multi-body dynamic analyses (MDA). MDA models are becoming increasingly sophisticated and by including optimisation algorithms allow us to make predictions about muscle activation patterns for different masticatory tasks (Langenbach et al. 2006, Curtis et al. in press). These resulting muscle forces can then be directly imported into FEA software and thus applied to an FE model. Applying loads in this way has two major advantages: 1) The forces are by default in equilibrium, so that artefacts caused by constraints are negligible. 2) The automatic force export from an MDA allows fast creation of additional load cases,

for example, changes in muscle forces at different sizes of gape or during the break down of food with different mechanical properties, so that the forces acting on the skull during mastication can be simulated more comprehensively.

The long-term aim should be to combine rigid-body (MDA) and deformation (FEA) models in a single software application. Such a combined MDA-FEA model of the human masticatory apparatus has been developed recently, but the only deformable part of this model was the soft tissues of the TMJ (Koolstra & van Eijden 2005, 2006, Koolstra & Tanaka 2009). In future, such combined models could also include FE models of the bone. With advances in computing power this should be feasible soon.

Finally, in order to investigate mechanical adaptations during development FEA needs to be combined with bone modelling algorithms, since the evaluation of stresses and strains in a static form can only provide very limited information (see discussion in Chapter 8). If the FE model adapts to applied loads, form-function relationships can be studied directly. Some pioneering work using this approach has been done on a sauropod cranium using a simple block as a start form, which iteratively adapts to the applied loads by removal of low strain areas (Witzel & Preuschoft 2005). By applying a bone modelling algorithm to subadult individuals, it would be possible to study the mechanical adaptation of bone form during development. Currently, such a bone modelling algorithm is integrated in the FEA software VOX-FE. However, there is no consensus about the mechanical stimulus that modulates the modelling of bone, like stress or strain magnitudes, strain gradients or strain frequency (see 2.1). The next step should, therefore, be to compare the results of different algorithms with the form changes observed in experiments. Some of the data presented here (particularly in Chapter 8) provide a good basis for such future modelling studies.

Glossary

ADLH – Anterior dental loading hypothesis (Smith 1983, Rak 1986, Demes 1987, Trinkaus 1987, Spencer & Demes 1993)

Balancing side – Non-chewing side, the side contralateral to the chewing or biting side

Bone modelling – The gross shape changes of a bone by resorption and deposition on its endosteal and periosteal surfaces during development (Currey 2002)

Bone remodelling – Deposition and resorption involving only a small packet of bone, the basic multicellular unit (BMU) and affecting principally all surfaces, including vascular cavities. Typically, the amount of bone is unchanged by this process; new bone merely replaces old bone (Currey 2002).

Boundary conditions – Loads and constraints applied to a finite element model

Cancellous bone material – The solid bone of which the individual trabeculae consist (Currey 2002)

Cancellous bone tissue – The whole trabecular structure, including the holes between the trabeculae (Currey 2002)

CB – Coronal bending in the vertical plane

Constraint – Region of immobility in a finite element model

CT – Computed tomography

DSPI – Digital speckle pattern interferometry, a full-field optical strain measurement technique

DVS – Dorsoventral shear

EMG – Electromyography

FEA – Finite element analysis

GMM – Geometric morphometrics

HMH – Half-maximum height protocol

Isotropic – Referring to material properties: having the same properties in all directions, referring to voxel dimensions: having the same dimensions in all directions

Landmarks – Points of correspondence, matching within and between populations. Biologically, they are discrete, homologous anatomical loci (Zelditch et al. 2004).

LTB – Lateral transverse bending

Maximum principal strain (ε_1) – The most tensile strain at a point in a strained object. By convention maximum principal strain values are positive. Its axis is perpendicular to the axis of the minimum principal strain.

Maximum shear strain (γ_{max}) – The difference between maximum and minimum principal strain at a point, defined as $\varepsilon_1 - \varepsilon_3$. The axis is midway between the maximum and minimum principal strain axes (inclined at 45° to the principal strain axes)

MDA – Multibody dynamic analysis

Minimum principal strain (ε_3) – The most compressive strain at a point in a strained object. By convention minimum principal strain values are negative. Its axis is perpendicular to the axis of the maximum principal strain.

MRI – Magnetic resonance imaging

MTB – Medial transverse bending

Neutral axis – The line of zero fibre stress in any given section of an object subject to bending (Young 1989)

Orthotropic - When the material properties differ in each of three perpendicular directions

PCSA – Physiological cross-sectional area of a muscle, which is the total cross-sectional area of all muscle fibres at a specific length

PDL – Periodontal ligament

Poisson's ratio (v) – When an object is, for example, tensed in one direction, it contracts in another (Poisson effect). The Poisson's ratio is the lateral strain divided by axial strain, thus representing how much the sides of a material will contract as it is tensed (or, conversely, how the material will expand as it is compressed).

Powerstroke – Forceful contact of food between the occlusal surfaces of the upper and lower teeth. It is one of the three basic strokes during a chewing cycle. The other two are the opening and the closing strokes (Hylander 1992).

Robusticity – General term that refers to the strength of a bone as reflected by its size, shape and cortical thickness.

Second moment of area (I) – Or second moment of inertia, a measurement, which reflects the resistance of a beam to bending. It is the moment of

inertia of an area with respect to an axis, which is the sum of the products obtained by multiplying each element of the area by the square of its distance from the respective axis (Young 1989).

Semilandmarks – Points on a geometric feature (curve, edge or surface) defined by their positions on that feature (e.g. at 50% of the length of the curve, Zelditch et al. 2004).

STD – Standard deviation

Strain (ε) – Quantifies the deformation in an object under load. Strain is defined as the change in length divided by the original length ($\Delta L/L$). In biomechanics it is usually measured in microstrain (με).

Stress (σ) – Is a measure for the internal forces in the loaded bone resulting from a deformation (Currey 2002) and is defined as force per unit area (F/A).

Thin-plate splines - Interpolation functions, which can be used to warp a reference and a target shape. Thin-plate splines are analogous to bending of a thin metal sheet in which bending energy is minimised, resulting in a deformation that is as smooth as possible (Zelditch et al. 2004).

TMJ – Temporomandibular joint

Von Mises strain (ε_v) – Also called equivalent strain, a function of all principal strains (ε_1, ε_2, ε_3), which can be used to predict failure in a ductile material under load

Working side – Chewing or biting side

Young's modulus of elasticity (E) – Describes the elasticity of a material. It is defined as stress/strain in the linear region of the stress-strain curve (Fig. 1.3). The higher the value is, the stiffer is the material.

References

Ahlgren, J. (1966). Mechanism of mastication: a quantitative cinematographic and electromyographic study of masticatory movements in children, with special reference to occlusion of the teeth. *Acta Odontol Scand* **24 (Suppl. 44)**: 1-109.

An, K. N., Takahashi, K., Harrigan, T. P. & Chao, E. Y. (1984). Determination of muscle orientations and moment arms. *J Biomech Eng* **106**: 280-282.

Andersen, K. L., Pedersen, E. H. & Melsen, B. (1991). Material parameters and stress profiles within the periodontal ligament. *Am J Orthod Dentofacial Orthop* **99**: 427-440.

Antón, S. C. (1990). Neandertals and the anterior dental loading hypothesis: a biomechanical evaluation of bite force production. *Kroeber Anthropol Soc Pap* **71-72**: 67-76.

Antón, S. C. (1994). Mechanical and other perspectives on Neandertal craniofacial morphology. In Corruccini, R. S. & Ciochon, R. L. (eds.): *Integrative Paths to the Past: Palaeoanthropological Advances in Honor of F. Clark Howell.* Englewood Cliffs: Prentice Hall, pp. 677-695.

Archbold, E., Burch, J. M. & Ennos, A. E. (1970). Recording of in-plane surface displacement by double-exposure speckle photography. *Opt Acta* **17**: 883-898.

Archbold, E., Burch, J. M., Ennos, A. E. & Taylor, P. A. (1969). Visual observation of surface vibration nodal patterns. *Nature* **222**: 263-265.

Archbold, E. & Ennos, A. E. (1968). Observation of surface vibration modes by stroboscopic hologram interferometry. *Nature* **217**: 942-943.

Arendts, F. J. & Sigolotto, C. (1989). Standardabmessungen, Elastizitätskennwerte und Festigkeitsverhalten des Human-Unterkiefers, ein Beitrag zur Darstellung der Biomechanik der Unterkiefer - Teil I. *Biomed Tech (Berl)* **34**: 248-255.

Arendts, F. J. & Sigolotto, C. (1990). Mechanische Kennwerte des Human-Unterkiefers und Untersuchung zum "in-vivo"-Verhalten des kompakten Knochengewebes, ein Beitrag zur Darstellung der Biomechanik des Unterkiefers - Teil II. *Biomed Tech (Berl)* **35**: 123-130.

Arensburg, B. & Belfer-Cohen, A. (1998). Sapiens and Neandertals: rethinking the Levantine Middle Paleolithic hominids. In Akazawa, T., Aoki, K. & Bar-Yosef, O. (eds.): *Neanderthals and Modern Humans in Western Asia.* New York: Plenum, pp. 311–322.

Ascenzi, A. & Segre, A. G. (1971). A new Neandertal child mandible from an Upper Pleistocene site in southern Italy. *Nature* **233**: 280-283.

Ashman, R. B., Cowin, S. C., van Buskirk, W. C. & Rice, J. C. (1984). A continuous wave technique for the measurement of the elastic properties of cortical bone. *J Biomech* **17**: 349-361.

Ashman, R. B. & van Buskirk, W. C. (1987). The elastic properties of a human mandible. *Adv Dent Res* **1**: 64-67.

Avis, V. (1959). The relation of the temporal muscle to the form of the coronoid process. *Am J Phys Anthropol* **17**: 99-104.

Avis, V. (1961). The significance of the angle of the mandible: an experimental and comparative study. *Am J Phys Anthropol* **19**: 55-61.

Bailey, S. E. & Hublin, J.-J. (2005). Who made the early Aurignacian? A reconsideration of the Brassempouy dental remains. *Bull Mém Soc Anthropol Paris* **17**: 115-121.

Bailey, S. E. & Hublin, J.-J. (2006). Dental remains from the Grotte du Renne at Arcy-sur-Cure (Yonne). *J Hum Evol* **50**: 485-508.

Baragar, F. A. & Osborn, J. W. (1984). A model relating patterns of human jaw movement to biomechanical constraints. *J Biomech* **17**: 757-767.

Barak, M. M., Currey, J. D., Weiner, S. & Shahar, R. (2009). Are tensile and compressive Young's moduli of compact bone different? *Journal of the Mechanical Behavior of Biomedical Materials* **2**: 51-60.

Barber, N. (1995). The evolutionary psychology of physical attractiveness: sexual selection and human morphology. *Ethology and Sociobiology* **16**: 395-424.

Basara, A. (2007). *Evaluation of High Pressure Components of Fuel Injection Systems Using Speckle Interferometry*. Dr-Ing Thesis. University of Erlangen-Nürnberg, Erlangen.

Bassett, C. A. (1965). Electrical effects in bone. *Sci Am* **213**: 18-25.

Bastir, M. (2008). A systems-model for the morphological analysis of integration and modularity in human craniofacial evolution. *JASs* **86**: 37-58.

Bastir, M., O'Higgins, P. & Rosas, A. (2007). Facial ontogeny in Neanderthals and modern humans. *Proc Biol Sci* **274**: 1125–1132.

Bastir, M., Rosas, A. & Kuroe, K. (2004). Petrosal orientation and mandibular ramus breadth: evidence for an integrated petroso-mandibular developmental unit. *Am J Phys Anthropol* **123**: 340-350.

Bastir, M., Rosas, A., Lieberman, D. E. & O'Higgins, P. (2008). Middle cranial fossa anatomy and the origin of modern humans. *Anat Rec* **291**: 130-140.

Baxter, B. S. & Sorenson, J. A. (1981). Factors affecting the measurement of size and CT number in computed tomography. *Invest Radiol* **16**: 337-341.

Beaupré, G. S. & Carter, D. R. (1992). Finite element analysis in biomechanics. In Biewener, A. A. (ed.): *Biomechanics: Structures and Systems*. Oxford: Oxford University Press, pp. 149-173.

Beecher, R. M., Corruccini, R. S. & Freeman, M. (1983). Craniofacial correlates of dietary consistency in a nonhuman primate. *J Craniofac Genet Dev Biol* **3**: 193-202.

Beek, M., Aarnts, M. P., Koolstra, J. H., Feilzer, A. J. & van Eijden, T. M. (2001). Dynamic properties of the human temporomandibular joint disc. *J Dent Res* **80**: 876-880.

Beek, M., Koolstra, J. H., van Ruijven, L. J. & van Eijden, T. M. (2000). Three-dimensional finite element analysis of the human temporomandibular joint disc. *J Biomech* **33**: 307-316.

Bennell, K. L., Malcolm, S. A., Khan, K. M., Thomas, S. A., Reid, S. J., Brukner, P. D., Ebeling, P. R. & Wark, J. D. (1997). Bone mass and bone turnover in power athletes, endurance athletes, and controls: a 12-month longitudinal study. *Bone* **20**: 477-484.

Biggerstaff, R. H. (1977). The biology of the human chin. In Dahlberg, A. A. & Graber, T. M. (eds.): *Orofacial Growth and Development*. The Hague: Mouton, pp. 70-87.

Biggerstaff, R. H. & Mazaheri, M. (1968). Oral manifestations of the Ellis-van Creveld syndrome. *J Amer dent Ass* **77**: 1090-1095.

Björk, A. & Skieller, V. (1983). Normal and abnormal growth of the mandible. A synthesis of longitudinal cephalometric implant studies over a period of 25 years. *Eur J Orthod* **5**: 1-46.

Blanksma, N. G. & van Eijden, T. M. (1990). Electromyographic heterogeneity in the human temporalis muscle. *J Dent Res* **69**: 1686-1690.

Blanksma, N. G. & van Eijden, T. M. (1995). Electromyographic heterogeneity in the human temporalis and masseter muscles during static biting, open/close excursions, and chewing. *J Dent Res* **74**: 1318-1327.

Blanksma, N. G., van Eijden, T. M., van Ruijven, L. J. & Weijs, W. A. (1997). Electromyographic heterogeneity in the human temporalis and masseter muscles during dynamic tasks guided by visual feedback. *J Dent Res* **76**: 542-551.

Blanksma, N. G., van Eijden, T. M. & Weijs, W. A. (1992). Electromyographic heterogeneity in the human masseter muscle. *J Dent Res* **71**: 47-52.

Blechschmidt, E. (1973). Die Entstehung des Unterkiefers. *J Orofac Orthop* **34**: 337-358.

Blechschmidt, E. & Freeman, B. (2004). *The Ontogenetic Basis of Human Anatomy: A Biodynamic Approach to Development from Conception to Birth*. Murrieta: Pacific Distributing.

Bocherens, H., Billiou, D., Mariotti, A., Toussaint, M., Patou-Mathis, M., Bonjean, D. & Otte, M. (2001). New isotopic evidence for dietary habits of Neandertals from Belgium. *J Hum Evol* **40**: 497-505.

Bocherens, H., Drucker, D. G., Billiou, D., Patou-Mathis, M. & Vandermeersch, B. (2005). Isotopic evidence for diet and subsistence pattern of the Saint-Césaire I Neanderthal: review and use of a multi-source mixing model. *J Hum Evol* **49**: 71-87.

Bolk, L. (1924). *Die Entstehung des Menschenkinnes. Ein Beitrag zur Entwicklungsgeschichte des Unterkiefers*. Amsterdam: Koninklijke Akademie van Wetenschappen te Amsterdam.

Bonifay, E. (1964). La grotte de Régourdou (Montignac, Dordogne). Stratigraphie et industrie lithique moustérienne. *L'Anthropologie* **68**: 49-64.

Bookstein, F. (1989). Principal warps: thin-plate splines and the decomposition of deformation. *IEEE Transactions on Pattern Analysis and Machine Intelligence* **11**: 567-585.

Bookstein, F., Schäfer, K., Prossinger, H., Seidler, H., Fieder, M., Stringer, C., Weber, G. W., Arsuaga, J. L., Slice, D. E., Rohlf, F. J., Recheis, W.,

Mariam, A. J. & Marcus, L. F. (1999). Comparing frontal cranial profiles in archaic and modern *Homo* by morphometric analysis. *Anat Rec* **257**: 217-224.

Bouvier, M. (1989). The biology and composition of bone. In Cowin, S. C. (ed.): *Bone Mechanics*. Boca Raton: CRC Press, pp. 1-13.

Brace, C. L. (1962). Cultural factors in the evolution of the human dentition. In Montagu, M. F. A. (ed.): *Culture and the Evolution of Man*. New York: Oxford University Press, pp. 343-354.

Brace, C. L. (1964a). The fate of the "Classic" Neanderthals: A consideration of hominid catastrophism. *Curr Anthropol* **5**: 3-43.

Brace, C. L. (1964b). The probable mutation effect. *The American Naturalist* **98**: 453-455.

Brace, C. L. (1967). Environment, tooth form, and size in the Pleistocene. *J Dent Res* **46**: 809-816.

Brace, C. L. (1975). Comment on "Did La Ferrassie I use his teeth as a tool?" *Curr Anthropol* **16**: 396-397.

Brace, C. L. (1977). Occlusion to the anthropological eye. In McNamara, J. A. (ed.): *The Biology of Occlusal Development*. Ann Arbor, Michigan: Center for Human Growth and Development, pp. 179-209.

Brace, C. L. (1979). Krapina, "Classic" Neanderthals, and the evolution of the European face. *J Hum Evol* **8**: 527-550.

Brace, C. L., Ryan, A. S. & Smith, B. H. (1981). Comment on: "Tooth wear in La Ferrassie man". *Curr Anthropol* **22**: 426-430.

Bräuer, G. (1984). A craniological approach to the origin of anatomically modern *Homo sapiens* in Africa and implications for the appearance of modern Europeans. In Smith, F. H. & Spencer, F. (eds.): *The Origins of Modern Humans: A World Survey of the Fossil Evidence*. New York: Alan R. Liss, pp. 327-410.

Brose, D. S. & Wolpoff, M. H. (1971). Early Upper Paleolithic man and late Middle Paleolithic tools. *Am Anthropol* **73**: 1156-1194.

Buchanan, C. R. & Preece, M. A. (1992). Hormonal control of bone growth. In Hall, B. K. (ed.): *Bone: Volume 6. Bone Growth*. Boca Raton: CRC Press, pp. 53-89.

Burdi, A. R. & Spyropoulos, M. N. (1978). Prenatal growth patterns of the human mandible and masseter muscle complex. *Am J Orthod* **74**: 380-387.

Burr, D. B., Martin, R. B., Schaffler, M. B. & Radin, E. L. (1985). Bone remodeling in response to *in vivo* fatigue microdamage. *J Biomech* **18**: 189-200.

Buzug, T. M. (2008). *Computed Tomography: From Photon Statistics to Modern Cone-Beam CT*. Heidelberg: Springer.

Calderale, P. M., Rossetto, M. & Pezzoli, M. (1986). Biomechanical analysis of coupling between mandible and removable partial dentures. In Bergmann, G., Kolbert, R. & Rohlmann, A. (eds.): *Biomechanics: Basic and Applied Research*. Dordrecht: Martinus Nijhoff, pp. 745-750.

Carlson, D. S. (1976). Temporal variation in prehistoric Nubian crania. *Am J Phys Anthropol* **45**: 467-484.

Carlson, D. S. & van Gerven, D. P. (1977). Masticatory function and post-Pleistocene evolution in Nubia. *Am J Phys Anthropol* **46**: 495-506.

Carter, D. R. (1984). Mechanical loading histories and cortical bone remodeling. *Calcif Tissue Int* **36 (Suppl. 1)**: 19-24.

Carter, D. R., Fyhrie, D. P. & Whalen, R. T. (1987). Trabecular bone density and loading history: regulation of connective tissue biology by mechanical energy. *J Biomech* **20**: 785-794.

Cattaneo, P. M., Dalstra, M. & Melsen, B. (2005). The finite element method: a tool to study orthodontic tooth movement. *J Dent Res* **84**: 428-433.

Cattaneo, P. M., Dalstra, M. & Melsen, B. (2009). Strains in periodontal ligament and alveolar bone associated with orthodontic tooth movement analyzed by finite element. *Orthod Craniofac Res* **12**: 120-128.

Chen, J., Akyuz, U., Xu, L. & Pidaparti, R. M. (1998). Stress analysis of the human temporomandibular joint. *Med Eng Phys* **20**: 565-572.

Chen, X. & Chen, H. (1998). The influence of alveolar structures on the torsional strain field in a gorilla corporeal cross-section. *J Hum Evol* **35**: 611-633.

Chevalier, Y., Pahr, D., Allmer, H., Charlebois, M. & Zysset, P. (2007). Validation of a voxel-based FE method for prediction of the uniaxial apparent modulus of human trabecular bone using macroscopic mechanical tests and nanoindentation. *J Biomech* **40**: 3333-3340.

Choi, A. H., Ben-Nissan, B. & Conway, R. C. (2005). Three-dimensional modelling and finite element analysis of the human mandible during clenching. *Aust Dent J* **50**: 42-48.

Coleman, M. N. & Colbert, M. W. (2007). Technical note: CT thresholding protocols for taking measurements on three-dimensional models. *Am J Phys Anthropol* **133**: 723-725.

Compston, J. E. (2001). Sex steroids and bone. *Physiol Rev* **81**: 419-447.

Condemi, S. (1991). Some considerations concerning Neandertal features and the presence of Neandertals in the Near East. *Riv Antropol (Roma)* **69**: 27-38.

Coon, C. S. (1962). *The Origin of Races*. New York: Knopf.

Coqueugniot, H. (2000). La position du foramen mentonnier chez l'enfant: révision ontogénétique et phylogénétique. *Bull Mém Soc Anthropol Paris* **12**: 227-246.

Coqueugniot, H. & Minugh-Purvis, N. (2003). Ontogenetic patterning and phylogenetic significance of mental foramen number and position in the evolution of upper Pleistocene *Homo sapiens*. In Thompson, J. T., Krovitz, G. E. & Nelson, A. J. (eds.): *Patterns of Growth and Development in the Genus Homo*. Cambridge: Cambridge University Press, pp. 343-360.

Corruccini, R. S. (1984). An epidemiologic transition in dental occlusion in world populations. *Am J Orthod* **86**: 419-426.

Corruccini, R. S. (1990). Australian aboriginal tooth succession, interproximal attrition, and Begg's theory. *Am J Orthod Dentofacial Orthop* **97**: 349-357.

Cowin, S. C. (1984). Mechanical modeling of the stress adaptation process in bone. *Calcif Tissue Int* **36 (Suppl. 1)**: 98-103.

Crompton, A. W. (1995). Masticatory function in nonmammalian cynodonts and early mammals. In Thomason, J. J. (ed.): *Functional Morphology in Vertebrate Paleontology*. Cambridge: Cambridge University Press, pp. 55–75.

Culmann, K. (1864-1966). *Die graphische Statik*. Zürich: Meyer & Zeller.

Cunningham, C. A. & Black, S. M. (2009). Anticipating bipedalism: trabecular organization in the newborn ilium. *J Anat* **214**: 817-29.

Currey, J. D. (1968). The adaptation of bones to stress. *J Theor Biol* **20**: 91-106.

Currey, J. D. (1984). *The Mechanical Adaptations of Bones*. Princeton: Princeton University Press.

Currey, J. D. (2002). *Bones: Structure and Mechanics*. Princeton: Princeton University Press.

Curtis, N., Jones, M. E., Evans, S. E., Shi, J., O'Higgins, P. & Fagan, M. J. (in press). Predicting muscle activation patterns from motion and anatomy: modelling the skull of Sphenodon (Diapsida: Rhynchocephalia). *J R Soc Interface*.

Curtis, N., Kupczik, K., O'Higgins, P., Moazen, M. & Fagan, M. J. (2008). Predicting skull loading: applying multibody dynamics analysis to a macaque skull. *Anat Rec* **291**: 491-501.

Cybulski, J. S. (1974). Tooth wear and material culture: precontact patterns in the Tsimshian area, British Columbia. *Syesis* **7**: 31-35.

Czarnetzki, A., Jakob, T. & Pusch, C. M. (2003). Palaeopathological and variant conditions of the *Homo heidelbergensis* type specimen (Mauer, Germany). *J Hum Evol* **44**: 479-495.

Daegling, D. J. (1989). Biomechanics of cross-sectional size and shape in the hominoid mandibular corpus. *Am J Phys Anthropol* **80**: 91-106.

Daegling, D. J. (1990). *Geometry and Biomechanics of Hominoid Mandibles*. PhD Thesis. State University of New York at Stony Brook.

Daegling, D. J. (1993a). Functional morphology of the human chin. *Evol Anthropol* **1**: 170-177.

Daegling, D. J. (1993b). The relationship of *in vivo* bone strain to mandibular corpus morphology in *Macaca fascicularis*. *J Hum Evol* **25**: 247-269.

Daegling, D. J. (2001). Biomechanical scaling of the hominoid mandibular symphysis. *J Morphol* **250**: 12-23.

Daegling, D. J. (2002). Bone geometry in cercopithecoid mandibles. *Arch Oral Biol* **47**: 315-325.

Daegling, D. J. & Grine, F. E. (1991). Compact bone distribution and biomechanics of early hominid mandibles. *Am J Phys Anthropol* **86**: 321-339.

Daegling, D. J. & Hotzman, J. L. (2003). Functional significance of cortical bone distribution in anthropoid mandibles: an *in vitro* assessment of bone strain under combined loads. *Am J Phys Anthropol* **122**: 38-50.

Daegling, D. J. & Hylander, W. L. (1994). Strain distribution in the human mandible. *Am J Phys Anthropol* **S18**: 75.

Daegling, D. J. & Hylander, W. L. (1998). Biomechanics of torsion in the human mandible. *Am J Phys Anthropol* **105**: 73-87.

Daegling, D. J. & Hylander, W. L. (2000). Experimental observation, theoretical models, and biomechanical inference in the study of mandibular form. *Am J Phys Anthropol* **112**: 541-551.

Daegling, D. J., Ravosa, M. J., Johnson, K. R. & Hylander, W. L. (1992). Influence of teeth, alveoli, and periodontal ligaments on torsional rigidity in human mandibles. *Am J Phys Anthropol* **89**: 59-72.

Dar, F. H., Meakin, J. R. & Aspden, R. M. (2002). Statistical methods in finite element analysis. *J Biomech* **35**: 1155-1161.

Darwin, C. (1859). *On the Origin of Species by Means of Natural Selection, or the Preservation of Favoured Races in the Struggle for Life*. London: John Murray.

de Lumley, M. A. (1973). *Anténéandertaliens et Néandertaliens du Bassin Méditerranéen Occidental Européen: Cova Negra, Le Lazaret, Bañolas, Grotte du Prince, Carigüela, Hortus, Agut, Macassargues, La Masque, Rigabe, La Crouzade, Les Peyrards, Bau de l'Aubesier*. Marseille: Éditions du Laboratoire de paléontologie humaine et de préhistoire, Université de Provence.

Dean, D., Hublin, J. J., Holloway, R. & Ziegler, R. (1998). On the phylogenetic position of the pre-Neandertal specimen from Reilingen, Germany. *J Hum Evol* **34**: 485-508.

Debénath, A. & Jelinek, A. (1998). Nouvelles fouilles à La Quina (Charente): Résultats préliminaires. *Gallia Préhistoire* **40**: 29-74.

Dechow, P. C., Nail, G. A., Schwartz-Dabney, C. L. & Ashman, R. B. (1993). Elastic properties of human supraorbital and mandibular bone. *Am J Phys Anthropol* **90**: 291-306.

Dechow, P. C., Schwartz-Dabney, C. L. & Asman, R. B. (1992). Elastic properties of the human mandibular corpus. In Goldstein, S. A. & Carlson, D. S. (eds.): *Bone Biodynamics in Orthodontic and Orthopedic Treatment*. Ann Arbor: University of Michigan, pp. 299-314.

Demes, B. (1987). Another look at an old face: biomechanics of the Neandertal facial skeleton reconsidered. *J Hum Evol* **16**: 297-303.

Demes, B. & Creel, N. (1988). Bite force, diet, and cranial morphology of fossil hominids. *J Hum Evol* **17**: 657-670.

Demes, B., Jungers, W. L. & Walker, C. (2000). Cortical bone distribution in the femoral neck of strepsirhine primates. *J Hum Evol* **39**: 367-379.

Demes, B., Preuschoft, H. & Wolff, J. E. A. (1984). Stress-strength relationships in the mandibles of hominoids. In Chivers, D. J., Wood, B. A. &

Bilsborough, A. (eds.): *Food Acquisition and Processing in Primates.* New York: Plenum, pp. 369-390.

Dobson, S. D. & Trinkaus, E. (2002). Cross-sectional geometry and morphology of the mandibular symphysis in Middle and Late Pleistocene *Homo*. *J Hum Evol* **43**: 67-87.

Dorow, C., Krstin, N. & Sander, F.-G. (2003). Determination of the mechanical properties of the periodontal ligament in a uniaxial tensional experiment. *J Orofac Orthop* **64**: 100-107.

DuBrul, L. E. & Sicher, H. (1954). *The Adaptive Chin*. Springfield: Charles C. Thomas.

DuChesne, A., Unnewehr, M., Schmidt, P. F., Sotonyi, P., Brinkmann, B., Piffko, J., Fischer, G. & Bajanowski, T. (2003). Deformation characteristics of the human mandible in low impact experiments. *Int J Legal Med* **117**: 257-62.

Dumont, E. R., Grosse, I. R. & Slater, G. J. (2009). Requirements for comparing the performance of finite element models of biological structures. *J Theor Biol* **256**: 96-103.

Dumont, E. R., Piccirillo, J. & Grosse, I. R. (2005). Finite-element analysis of biting behavior and bone stress in the facial skeletons of bats. *Anat Rec A Discov Mol Cell Evol Biol* **283**: 319-30.

Engström, C., Kiliaridis, S. & Thilander, B. (1986). The relationship between masticatory function and craniofacial morphology. II A histological study in the growing rat fed a soft diet. *Eur J Orthod* **8**: 271-279.

Enlow, D. H. (1992). The Condyle and Facial Growth. In Sarnat, B. G. & Laskin, D. M. (eds.): *The Temporomandibular Joint: A Biological Basis for Clinical Practice*. Philadelphia: W.B. Saunders Co., pp. 48-59.

Enlow, D. H. & Hans, M. G. (1996). *Essentials of Facial Growth*. Philadelphia: Saunders.

Enlow, D. H. & Harris, D. B. (1964). A study of the postnatal growth of the human mandible. *Am J Orthod* **50**: 25-50.

Enlow, D. H., Moyers, R. E. & Merow, W. W. (1982). *Handbook of Facial Growth*. Philadelphia: W. B. Saunders.

Eubanks, B. A., Cann, C. E. & Brant-Zawadzki, M. (1985). CT measurement of the diameter of spinal and other bony canals: effects of section angle and thickness. *Radiology* **157**: 243-246.

Fagan, M. J. (1992). *Finite Element Analysis*. Harlow: Longman Scientific & Technical.

Fagan, M. J., Curtis, N., Dobson, C. A., Karunanayake, J. H., Kupczik, K., Moazen, M., Page, L., Phillips, R. & O'Higgins, P. (2007). Voxel-based finite element analysis: working directly with microCT scan data. *J Morphol* **268**: 1071.

Fajardo, R. J., Ryan, T. M. & Kappelman, J. (2002). Assessing the accuracy of high-resolution X-ray computed tomography of primate trabecular bone by comparisons with histological sections. *Am J Phys Anthropol* **118**: 1-10.

Field, C., Li, Q., Li, W. & Swain, M. (2008). Influence of tooth removal on mandibular bone response to mastication. *Arch Oral Biol* **53**: 1129-1137.

Franciscus, R. G. & Trinkaus, E. (1988). The Neandertal nose. *Am J Phys Anthropol* **75**: 209-210.

Franciscus, R. G. & Trinkaus, E. (1995). Determinants of retromolar space presence in Pleistocene *Homo* mandibles. *J Hum Evol* **28**: 577-595.

Frayer, D. W. (1977). Metric dental change in the European Upper Paleolithic and Mesolithic. *Am J Phys Anthropol* **46**: 109-120.

Frost, H. M. (1964). *The Laws of Bone Structure*. Springfield: Charles C. Thomas.

Frost, H. M. (1973). *Bone Modeling and Skeletal Modeling Errors*. Springfield: Charles C. Thomas.

Frost, H. M. (1983). The skeletal intermediary organization. *Metab Bone Dis Relat Res* **4**: 281-290.

Frost, H. M. (1987). Bone "mass" and the "mechanostat": a proposal. *Anat Rec* **219**: 1-9.

Frost, H. M. (2003). Bone's mechanostat: a 2003 update. *Anat Rec A Discov Mol Cell Evol Biol* **275**: 1081-1101.

Fujita, T., Kawata, T., Tokimasa, C. & Tanne, K. (2001). Influence of oestrogen and androgen on modelling of the mandibular condylar bone in ovariectomized and orchiectomized growing mice. *Arch Oral Biol* **46**: 57-65.

Fujita, T., Ohtani, J., Shigekawa, M., Kawata, T., Kaku, M., Kohno, S., Tsutsui, K., Tenjo, K., Motokawa, M., Tohma, Y. & Tanne, K. (2004). Effects of sex hormone disturbances on craniofacial growth in newborn mice. *J Dent Res* **83**: 250-254.

Fukase, H. (2007). Functional significance of bone distribution in the human mandibular symphysis. *Anthrop Sci* **115**: 55-62.

Fukase, H. & Suwa, G. (2008). Growth-related changes in prehistoric Jomon and modern Japanese mandibles with emphasis on cortical bone distribution. *Am J Phys Anthropol* **136**: 441-454.

Fukazawa, H. & Sakamoto, T. (1982). A morphological study on the growth and development of the rat mandible after biresection of the jaw closing muscles. *J Jpn Orthodont Soc* **41**: 521-530.

Fyhrie, D. P. & Carter, D. R. (1986). A unifying principle relating stress to trabecular bone morphology. *J Orthop Res* **4**: 304-317.

Garrod, D. A. E. & Bate, D. M. A. (1937). *The Stone Age of Mount Carmel: Excavations at the Wady el-Mughara*. Oxford: Clarendon Press.

Giesen, E. B., Ding, M., Dalstra, M. & van Eijden, T. M. (2001). Mechanical properties of cancellous bone in the human mandibular condyle are anisotropic. *J Biomech* **34**: 799-803.

Gingerich, P. D. (1971). Functional significance of mandibular translation in vertebrate jaw mechanics. *Postilla* **152**: 1-10.

Goodship, A. E., Lanyon, L. E. & McFie, H. (1979). Functional adaptation of bone to increased stress. An experimental study. *J Bone Joint Surg Am* **61**: 539-546.

Goret-Nicaise, M. (1981). Influence des insertions de muscles masticateurs sur la structure mandibulaire du nouveau-né. *Bull Assoc Anat (Nancy)* **65**: 287-296.

Goret-Nicaise, M. & Dhem, A. (1984). The mandibular body of the human fetus. Histologic analysis of the basilar part. *Anat Embryol (Berl)* **169**: 231-236.

Gorjanović-Kramberger, D. (1906). Der diluviale Mensch von Krapina in Kroatien: Ein Beitrag zur Paläoanthropologie. In Walkhoff, O. (ed.): *Studien über die Entwicklungsmechanik des Primatenskelletes, Volume II.* Wiesbaden: Kreidel, pp. 59-277.

Gorlin, R. J. & Pindborg, J. P. (1964). *Syndromes of the Head and Neck.* New York: McGraw-Hill.

Goto, T. K., Langenbach, G. E. J., Korioth, T. W. P., Hagiwara, M., Tonndorf, M. L. & Hannam, A. G. (1995). Functional movements of putative jaw muscle insertions. *Anat Rec* **242**: 278-288.

Gray, H., Standring, S., Ellis, H. & Berkovitz, B. K. B. (2005). *Gray's anatomy: The Anatomical Basis of Clinical Practice*. Edinburgh: Elsevier Churchill Livingstone.

Greaves, W. S. (1978). The jaw lever system in ungulates: a new model. *J Zool* **184**: 271-285.

Gröning, F., Liu, J., Fagan, M. J. & O'Higgins, P. (2009). Validating a voxel-based finite element model of a human mandible using digital speckle pattern interferometry. *J Biomech* **42**: 1224-1229.

Gross, T. S., Edwards, J. L., McLeod, K. J. & Rubin, C. T. (1997). Strain gradients correlate with sites of periosteal bone formation. *J Bone Miner Res* **12**: 982-988.

Grumme, T., Kluge, W., Kretzschmar, K. & Roesler, A. (1998). *Zerebrale und spinale Computertomographie*. Berlin: Blackwell.

Grün, R. & Stringer, C. (2000). Tabun revisited: revised ESR chronology and new ESR and U-series analyses of dental material from Tabun C1. *J Hum Evol* **39**: 601-612.

Grün, R., Stringer, C., McDermott, F., Nathan, R., Porat, N., Robertson, S., Taylor, L., Mortimer, G., Eggins, S. & McCulloch, M. (2005). U-series and ESR analyses of bones and teeth relating to the human burials from Skhul. *J Hum Evol* **49**: 316-334.

Grün, R. & Stringer, C. B. (1991). Electron spin resonance dating and the evolution of modern humans. *Archaeometry* **33**: 153-199.

Gupta, K. K., Knoell, A. C. & Grenoble, D. E. (1973). Mathematical modeling and structural analysis of the mandible. *Biomater Med Devices Artif Organs* **1**: 469-479.

Hambach, U. (1996). Paläo- und gesteinsmagnetische Untersuchungen im Quartär der Grube Grafenrain: Fundplatz des *Homo erectus heidelbergensis*. *Mannheimer Geschichtsblätter* **1**: 41-46.

Hannam, A. G. & Wood, W. W. (1989). Relationships between the size and spatial morphology of human masseter and medial pterygoid muscles, the craniofacial skeleton, and jaw biomechanics. *Am J Phys Anthropol* **80**: 429-45.

Hans, M. G., Enlow, D. H. & Noachtar, R. (1995). Age-related differences in mandibular ramus growth: a histologic study. *Angle Orthod* **65**: 335-340.

Hansson, T., Oberg, T., Carlsson, G. E. & Kopp, S. (1977). Thickness of the soft tissue layers and the articular disk in the temporomandibular joint. *Acta Odontol Scand* **35**: 77-83.

Hara, T., Tanck, E., Homminga, J. & Huiskes, R. (2002). The influence of microcomputed tomography threshold variations on the assessment of structural and mechanical trabecular bone properties. *Bone* **31**: 107-109.

Harrigan, T. P. & Hamilton, J. J. (1992). An analytical and numerical study of the stability of bone remodelling theories: dependence on microstructural stimulus. *J Biomech* **25**: 477-488.

Hart, R. T., Davy, D. T. & Heiple, K. G. (1984). Mathematical modeling and numerical solutions for functionally dependent bone remodeling. *Calcif Tissue Int* **36 (Suppl. 1)**: 104-109.

Hart, R. T., Hennebel, V. V., Thongpreda, N., Van Buskirk, W. C. & Anderson, R. C. (1992). Modeling the biomechanics of the mandible: a three-dimensional finite element study. *J Biomech* **25**: 261-286.

Hart, R. T. & Thongpreda, N. (1988). A finite element based study of the biomechanics of the mandible. In Harris, G. & Walker, C. (eds.): *Proc. International Conference of the IEEE Engineering in Medicine and Biology Society*. New York: IEEE, pp. 1886-1887.

Harvati, K., Frost, S. R. & McNulty, K. P. (2004). Neanderthal taxonomy reconsidered: implications of 3D primate models of intra- and interspecific differences. *Proc Natl Acad Sci U S A* **101**: 1147-1152.

Haskell, B., Day, M. & Tetz, J. (1986). Computer-aided modeling in the assessment of the biomechanical determinants of diverse skeletal patterns. *Am J Orthod* **89**: 363-382.

Heim, J.-L. (1976). *Les Hommes Fossiles de La Ferrassie. Tome I. Le Gisement, les Squelettes Adultes.* Paris: CNRS.

Hems, T. & Tillmann, B. (2000). Tendon entheses of the human masticatory muscles. *Anat Embryol (Berl)* **202**: 201-208.

Herring, S. W. (1993). Epigenetic and functional influences on skull growth. In Hanken, J. & Hall, B. K. (eds.): *The Skull: Volume 1. Development.* Chicago: University of Chicago Press, pp. 153-206.

Hert, J., Sklenská, A. & Lisková, M. (1971). Reaction of bone to mechanical stimuli 5. Effect of intermittent stress on the rabbit tibia after resection of the peripheral nerves. *Folia Morphol* **19**: 378-387.

Hirschberg, J. (2005). *Simulations of Mechanical Adaptation and Their Relationship to Stress Bearing in Skeletal Tissue.* PhD Thesis. University of Western Australia, Perth.

Hodgskinson, R. & Currey, J. D. (1992). Young's modulus, density and material properties in cancellous bone over a large density range. *Journal of Materials Science: Materials in Medicine* **3**: 377-381.

Howell, F. C. (1951). The place of Neanderthal man in human evolution. *Am J Phys Anthropol* **9**: 379-416.

Howell, F. C. (1960). European and northwest African Middle Pleistocene hominids. *Curr Anthropol* **1**: 195-232.

Howells, W. W. (1974). Neandertal man: facts and figures. In Tuttle, R. H. (ed.): *Paleoanthropology: Morphology and Paleoecology*. The Hague: Mouton, pp. 389-407.

Hrdlička, A. (1911). Human dentition and teeth from the evolutionary and racial standpoint. *Dom. Dental J.* **21**: 1–15.

Hublin, J.-J. (1998). Climatic changes, paleography, and the evolution of the Neanderthals. In Akazawa, T., Aoki, K. & Bar-Yosef, O. (eds.): *Neanderthals and Modern Humans in Western Asia.* New York: Plenum, pp. 295-310.

Hublin, J.-J., Trinkaus, E. & Stefan, V. H. (1998). The Mousterian human remains from Zafarraya (Andalucia, Spain). *Am J Phys Anthropol* **S26**: 122-123.

Huiskes, R. (2000). If bone is the answer, then what is the question? *J Anat* **197**: 145-156.

Huiskes, R. & Nunamaker, D. (1984). Local stresses and bone adaption around orthopedic implants. *Calcif Tissue Int* **36 (Suppl. 1)**: 110-117.

Huiskes, R., Weinans, H., Grootenboer, H. J., Dalstra, M., Fudala, B. & Slooff, T. J. (1987). Adaptive bone-remodeling theory applied to prosthetic-design analysis. *J Biomech* **20**: 1135-50.

Hung, Y. Y., Rowlands, R. E. & Daniel, I. M. (1975). Speckle-shearing interferometric technique: a full-field strain gauge. *Appl Optic* **14**: 618-622.

Hylander, W. L. (1975). The human mandible: lever or link? *Am J Phys Anthropol* **43**: 227-242.

Hylander, W. L. (1977). The adaptive significance of Eskimo craniofacial morphology. In Dahlberg, A. A. & Graber, T. M. (eds.): *Orofacial Growth and Development*. The Hague: Mouton, pp. 129-169.

Hylander, W. L. (1978). Incisal bite force direction in humans and the functional significance of mammalian mandibular translation. *Am J Phys Anthropol* **48**: 1-7.

Hylander, W. L. (1979a). Experimental analysis of temporomandibular joint reaction force in macaques. *Am J Phys Anthropol* **51**: 433-456.

Hylander, W. L. (1979b). Mandibular function in *Galago crassicaudatus* and *Macaca fascicularis*: an *in vivo* approach to stress analysis of the mandible. *J Morphol* **159**: 253-296.

Hylander, W. L. (1984). Stress and strain in the mandibular symphysis of primates: a test of competing hypotheses. *Am J Phys Anthropol* **64**: 1-46.

Hylander, W. L. (1985). Mandibular function and biomechanical stress and scaling. *Am Zool* **25**: 315-330.

Hylander, W. L. (1992). Functional anatomy. In Sarnat, B. G. & Laskin, D. M. (eds.): *The Temporomandibular Joint: A Biological Basis for Clinical Practice*. Philadelphia: W.B. Saunders, pp. 60-92.

Hylander, W. L. & Crompton, A. W. (1986). Jaw movements and patterns of mandibular bone strain during mastication in the monkey *Macaca fascicularis*. *Arch Oral Biol* **31**: 841-848.

Hylander, W. L. & Johnson, K. R. (1994). Jaw muscle function and wishboning of the mandible during mastication in macaques and baboons. *Am J Phys Anthropol* **94**: 523-547.

Hylander, W. L., Johnson, K. R. & Crompton, A. W. (1987). Loading patterns and jaw movements during mastication in *Macaca fascicularis*: a bone-strain, electromyographic, and cineradiographic analysis. *Am J Phys Anthropol* **72**: 287-314.

Hylander, W. L., Ravosa, M. J., Ross, C. F. & Johnson, K. R. (1998). Mandibular corpus strain in primates: further evidence for a functional link between symphyseal fusion and jaw-adductor muscle force. *Am J Phys Anthropol* **107**: 257-271.

Ichim, I., Kieser, J. & Swain, M. (2007a). Tongue contractions during speech may have led to the development of the bony geometry of the chin following the evolution of human language: A mechanobiological hypothesis for the development of the human chin. *Med Hypotheses* **69**: 20-24.

Ichim, I., Kieser, J. A. & Swain, M. V. (2007b). Functional significance of strain distribution in the human mandible under masticatory load: numerical predictions. *Arch Oral Biol* **52**: 465-473.

Ichim, I., Swain, M. & Kieser, J. A. (2006a). Mandibular biomechanics and development of the human chin. *J Dent Res* **85**: 638-642.

Ichim, I., Swain, M. V. & Kieser, J. A. (2006b). Mandibular stiffness in humans: numerical predictions. *J Biomech* **39**: 1903-1913.

Iseri, H. & Solow, B. (2000). Change in the width of the mandibular body from 6 to 23 years of age: an implant study. *Eur J Orthod* **22**: 229-238.

Jansen, M. (1920). *On Bone Formation: Its Relation to Tension and Pressure*. London: Longmans.

Jaworski, Z. F., Liskova-Kiar, M. & Uhthoff, H. K. (1980). Effect of long-term immobilisation on the pattern of bone loss in older dogs. *J Bone Joint Surg Br* **62-B**: 104-110.

Jones, H. H., Priest, J. D., Hayes, W. C., Tichenor, C. C. & Nagel, D. A. (1977). Humeral hypertrophy in response to exercise. *J Bone Joint Surg Am* **59**: 204-208.

Jones, M. L., Hickman, J., Middleton, J., Knox, J. & Volp, C. (2001). A validated finite element method study of orthodontic tooth movement in the human subject. *J Orthod* **28**: 29-38.

Jones, R. & Butters, J. N. (1975). Some observations on the direct comparison of the geometry of two objects using speckle pattern interferometric contouring. *J Phys E Sci Instrum* **8**: 231-234.

Jones, R. & Wykes, C. (1989). *Holographic and Speckle Interferometry: A Discussion of the Theory, Practice and Application of the Techniques.* Cambridge: Cambridge University Press.

Kessler, O., Lacatusu, E., Sommers, M. B., Mayr, E. & Bottlang, M. (2006). Malrotation in total knee arthroplasty: effect on tibial cortex strain captured by laser-based strain acquisition. *Clin Biomech* **21**: 603-609.

Kikuchi, M., Lu, C. H., Sebata, M. & Yamamoto, Y. (1978). The mandibular development of the rat after the denervation of the masseteric nerve. *Bull Tokyo Dent Coll* **19**: 75-86.

Kiliaridis, S. (1995). Masticatory muscle influence on craniofacial growth. *Acta Odontol Scand* **53**: 196-202.

Kiliaridis, S., Engström, C. & Thilander, B. (1985). The relationship between masticatory function and craniofacial morphology: I. A cephalometric longitudinal analysis in the growing rat fed a soft diet. *Eur J Orthod* **7**: 273-283.

Kiliaridis, S., Mejersjo, C. & Thilander, B. (1989). Muscle function and craniofacial morphology: a clinical study in patients with myotonic dystrophy. *Eur J Orthod* **11**: 131-138.

Klein, R. G. (1994). Southern Africa before the Iron Age. In Corrucini, R. S. & Ciochon, R. L. (eds.): *Integrative Paths to the Past: Paleoanthropological Advances in Honour of F. Clark Howell.* Englewood Cliffs: Prentice-Hall, pp. 471-519.

Klein, R. G. (1999). *The Human Career: Human Biological and Cultural Origins.* Chicago: University of Chicago Press.

Knoell, A. C. (1977). A mathematical model of an *in vitro* human mandible. *J Biomech* **10**: 159-166.

Kober, C., Erdmann, B., Hellmich, C., Sader, R. & Zeilhofer, H. F. (2006a). Consideration of anisotropic elasticity minimizes volumetric rather than shear deformation in human mandible. *Comput Methods Biomech Biomed Engin* **9**: 91-101.

Kober, C., Erdmann, B., Lang, J., Sader, R. & Zeilhofer, H. F. (2004). Sensitivity of the temporomandibular joint capsule for the structural behaviour of the human mandible. *Biomed Tech (Berl)* **49 (Suppl. 2)**: 372-373.

Kober, C., Stübinger, S., Hellmich, C., Radtke, T., Sader, R. & Zeilhofer, H.-F. (2006b). Finite element simulation of the human mandible: the influence of the PDL on its structural behaviour. *Int Poster J Dent Oral Med* **8**: Poster 334.

Koby, F. E. (1956). Une incisive néandertalienne trouvé en Suisse. *Verh Naturf Gesellsch Basel* **67**: 1-15.

Koehler, P. R., Anderson, R. E. & Baxter, B. (1979). The effect of computed tomography viewer controls on anatomical measurements. *Radiology* **130**: 189-194.

Koolstra, J. H. & Tanaka, E. (2009). Tensile stress patterns predicted in the articular disc of the human temporomandibular joint. *J Anat* **215**: 411-416.

Koolstra, J. H. & van Eijden, T. M. (1992). Application and validation of a three-dimensional mathematical model of the human masticatory system *in vivo*. *J Biomech* **25**: 175-187.

Koolstra, J. H. & van Eijden, T. M. (1995). Biomechanical analysis of jaw-closing movements. *J Dent Res* **74**: 1564-1570.

Koolstra, J. H. & van Eijden, T. M. (1996). Influence of the dynamical properties of the human masticatory muscles on jaw closing movements. *Eur J Morphol* **34**: 11-18.

Koolstra, J. H. & van Eijden, T. M. (1997). Dynamics of the human masticatory muscles during a jaw open-close movement. *J Biomech* **30**: 883-889.

Koolstra, J. H. & van Eijden, T. M. (2001). A method to predict muscle control in the kinematically and mechanically indeterminate human masticatory system. *J Biomech* **34**: 1179-1188.

Koolstra, J. H. & van Eijden, T. M. (2005). Combined finite-element and rigid-body analysis of human jaw joint dynamics. *J Biomech* **38**: 2431-2439.

Koolstra, J. H. & van Eijden, T. M. (2006). Prediction of volumetric strain in the human temporomandibular joint cartilage during jaw movement. *J Anat* **209**: 369-380.

Koolstra, J. H., van Eijden, T. M., van Spronsen, P. H., Weijs, W. A. & Valk, J. (1990). Computer-assisted estimation of lines of action of human masticatory muscles reconstructed *in vivo* by means of magnetic resonance imaging of parallel sections. *Arch Oral Biol* **35**: 549-556.

Koolstra, J. H., van Eijden, T. M. & Weijs, W. A. (1989). An iterative procedure to estimate muscle lines of action *in vivo*. *J Biomech* **22**: 911-920.

Koolstra, J. H., van Eijden, T. M., Weijs, W. A. & Naeije, M. (1988). A three-dimensional mathematical model of the human masticatory system predicting maximum possible bite forces. *J Biomech* **21**: 563-576.

Korioth, T. W. & Hannam, A. G. (1994a). Deformation of the human mandible during simulated tooth clenching. *J Dent Res* **73**: 56-66.

Korioth, T. W. & Hannam, A. G. (1994b). Mandibular forces during simulated tooth clenching. *J Orofac Pain* **8**: 178-89.

Korioth, T. W., Romilly, D. P. & Hannam, A. G. (1992). Three-dimensional finite element stress analysis of the dentate human mandible. *Am J Phys Anthropol* **88**: 69-96.

Krarup, S., Darvann, T. A., Larsen, P., Marsh, J. L. & Kreiborg, S. (2005). Three-dimensional analysis of mandibular growth and tooth eruption. *J Anat* **207**: 669-682.

Kupczik, K., Dobson, C. A., Crompton, R. H., Phillips, R., Oxnard, C. E., Fagan, M. J. & O'Higgins, P. (2009). Masticatory loading and bone adaptation in the supraorbital torus of developing macaques. *Am J Phys Anthropol* **139**: 193-203.

Kupczik, K., Dobson, C. A., Fagan, M. J., Crompton, R. H., Oxnard, C. E. & O'Higgins, P. (2007). Assessing mechanical function of the zygomatic region in macaques: validation and sensitivity testing of finite element models. *J Anat* **210**: 41-53.

Lalueza-Fox, C. & Frayer, D. W. (1997). Non-dietary marks in the anterior dentition of the Krapina Neanderthals. *International Journal of Osteoarchaeology* **7**: 133-149.

Lam, Y. M., Pearson, O. M. & Smith, C. M. (1996). Chin morphology and sexual dimorphism in the fossil hominid mandible sample from Klasies River Mouth. *Am J Phys Anthropol* **100**: 545-557.

Langenbach, G. E., Zhang, F., Herring, S. W., van Eijden, T. M. & Hannam, A. G. (2006). Dynamic mechanics in the pig mandibular symphysis. *J Anat* **209**: 69-78.

Lanyon, L. E., Goodship, A. E., Pye, C. J. & MacFie, J. H. (1982). Mechanically adaptive bone remodelling. *J Biomech* **15**: 141-154.

Lanyon, L. E. & Rubin, C. T. (1984). Static vs dynamic loads as an influence on bone remodelling. *J Biomech* **17**: 897-905.

Lanyon, L. E. & Rubin, C. T. (1985). Functional adaptation in skeletal structures. In Hildebrand, M., Bramble, D. M., Liem, K. F. & Wake, D. B. (eds.): *Functional Vertebrate Morphology*. Cambridge: Harvard University Press, pp. 1-25.

Larsen, C. S. (1985). Dental modifications and tool use in the western Great Basin. *Am J Phys Anthropol* **67**: 393-402.

Lazarus, F. & Verroust, A. (1998). Three-dimensional metamorphosis: a survey. *The Visual Computer* **14**: 373-389.

Lee, S. K., Kim, Y. S., Oh, H. S., Yang, K. H., Kim, E. C. & Chi, J. G. (2001). Prenatal development of the human mandible. *Anat Rec* **263**: 314-325.

Leendertz, J. A. (1970). Interferometric displacement measurement on scattering surfaces utilizing speckle effect. *J Phys E Sci Instrum* **3**: 214-218.

Lieberman, D. E. (1995). Testing hypotheses about recent human evolution from skulls: integrating morphology, function, development, and phylogeny. *Curr Anthropol* **36**: 159-197.

Lieberman, D. E. (1996). How and why humans grow thin skulls: experimental evidence for systemic cortical robusticity. *Am J Phys Anthropol* **101**: 217-236.

Lieberman, D. E. & Crompton, A. W. (1998). Responses of bone to stress: constraints on symmorphosis. In Weibel, E. R., Taylor, C. R. & Bolis, L. (eds.): *Principles of Animal Design: The Optimization and Symmorphosis Debate*. Cambridge: Cambridge University Press, pp. 78-86.

Lieberman, D. E., Krovitz, G. E., Yates, F. W., Devlin, M. & St Claire, M. (2004a). Effects of food processing on masticatory strain and craniofacial growth in a retrognathic face. *J Hum Evol* **46**: 655-677.

Lieberman, D. E., McBratney, B. M. & Krovitz, G. (2002). The evolution and development of cranial form in *Homo sapiens*. *Proc Natl Acad Sci U S A* **99**: 1134-1139.

Lieberman, D. E., Polk, J. D. & Demes, B. (2004b). Predicting long bone loading from cross-sectional geometry. *Am J Phys Anthropol* **123**: 156-171.

Liu, Z. J. & Herring, S. W. (2000). Masticatory strains on osseous and ligamentous components of the temporomandibular joint in miniature pigs. *J Orofac Pain* **14**: 265-278.

Lovejoy, C. O., Meindl, R. S., Ohman, J. C., Heiple, K. G. & White, T. D. (2002). The Maka femur and its bearing on the antiquity of human walking: applying contemporary concepts of morphogenesis to the human fossil record. *Am J Phys Anthropol* **119**: 97-133.

Lucas, P. W. & Luke, D. A. (1984). Chewing it over - basic principles of food breakdown. In Chivers, D. J., Wood, B. A. & Bilsborough, A. (eds.): *Food Acquisition and Processing in Primates*. New York: Plenum, pp. 283-302.

MacCurdy, G. G. (1915). Interglacial man from Ehringsdorf near Weimar. *Am Anthropol* **17**: 139-142.

Macho, G. A. & Spears, I. R. (1999). Effects of loading on the biomechanical behavior of molars of *Homo*, *Pan*, and *Pongo*. *Am J Phys Anthropol* **109**: 211-227.

Mallick, R. & Frank, N. (2002). A new technique for precise uranium-series dating of travertine micro-samples. *Geochim Cosmochim Acta* **66**: 4261-4272.

Marinescu, R., Daegling, D. J. & Rapoff, A. J. (2005). Finite-element modeling of the anthropoid mandible: the effects of altered boundary conditions. *Anat Rec A Discov Mol Cell Evol Biol* **283A**: 300-309.

Marks, L., Teng, S., Årtun, J. & Herring, S. (1997). Reaction strains on the condylar neck during mastication and maximum muscle stimulation in different condylar positions: an experimental study in the miniature pig. *J Dent Res* **76**: 1412-1420.

Martin, H. (1923). *L'Homme Fossile de La Quina*. Paris: Librairie Octave Doin.

Martin, H. (1926). Mâchoire humaine trouvée dans la station de La Quina. *L'Homme Préhistorique* **13**: 3-21.

Martin, R. B. & Burr, D. B. (1982). A hypothetical mechanism for the stimulation of osteonal remodelling by fatigue damage. *J Biomech* **15**: 137-139.

Maureille, B., Vandermeersch, B., Rougier, H. & Houët, F. (2001). Les dents inférieures du Néandertalien Regourdou 1 (site de Regourdou, commune de Montignac, Dordogne): analyses métriques et comparatives. *Paléo* **13**: 183-200.

Mazurier, A., Volpato, V. & Macchiarelli, R. (2006). Improved noninvasive microstructural analysis of fossil tissues by means of SR-microtomography. *Applied Physics A: Materials Science & Processing* **83**: 229-233.

McCown, T. D. & Keith, A. (1939). *The Stone Age of Mount Carmel: The Fossil Remains from the Levalloiso-Mousterian*. Oxford: Clarendon Press.

McDevitt, W. E. (1989). *Functional Anatomy of the Masticatory System*. London: Wright.

McNamara, L. M. & Prendergast, P. J. (2007). Bone remodelling algorithms incorporating both strain and microdamage stimuli. *J Biomech* **40**: 1381-1391.

Merbs, C. F. (1983). *Patterns of activity-induced pathology in a Canadian Inuit population*. Ottawa: National Museums of Canada.

Mercier, N. (1992). *Apports des méthodes radionucléaires de datation à l'étude du peuplement de l'Europe et du Proche-Orient au cours du Pléistocène moyen et supérieur*. PhD Thesis. Université de Bordeaux I.

Mercier, N. & Valladas, H. (2003). Reassessment of TL age estimates of burnt flints from the Paleolithic site of Tabun Cave, Israel. *J Hum Evol* **45**: 401-409.

Meyer, C., Kahn, J. L., Boutemi, P. & Wilk, A. (2002). Photoelastic analysis of bone deformation in the region of the mandibular condyle during mastication. *J Craniomaxillofac Surg* **30**: 160-169.

Milner, G. R. & Larsen, C. S. (1991). Teeth as artifacts of human behavior: intentional mutilation and accidental modification. In Kelley, A. & Larsen, C. S. (eds.): *Advances in Dental Anthropology*. New York: Wiley-Liss, pp. 357-378.

Minugh-Purvis, N. & Lewandowski, J. (1992). Functional anatomy, ontogeny, and behavioural implications of coronoid process morphology in Upper Pleistocene hominines. *Am J Phys Anthropol* **S14**: 124-125.

Misch, C. E., Qu, Z. & Bidez, M. W. (1999). Mechanical properties of trabecular bone in the human mandible: implications for dental implant treatment planning and surgical placement. *J Oral Maxillofac Surg* **57**: 700-706.

Møller, E. (1966). The chewing apparatus. An electromyographic study of the action of the muscles of mastication and its correlation to facial morphology. *Acta Physiol Scand Suppl* **280**: 1-229.

Möller, K. (2005). *Morphologische Veränderungen an der sich entwickelnden Mandibula des Menschen*. Dr. med. Thesis. Friedrich-Schiller-Universität Jena.

Molnar, S. (1972). Tooth wear and culture: a survey of tooth functions among some prehistoric populations. *Curr Anthropol* **13**: 511-526.

Molnar, S., Hildebolt, C., Molnar, I. M., Radovčić, J. & Gravier, M. (1993). Hominid enamel thickness: I. The Krapina Neandertals. *Am J Phys Anthropol* **92**: 131-138.

Mongini, F., Calderale, P. M. & Barberi, G. (1979). Relationship between structure and the stress pattern in the human mandible. *J Dent Res* **58**: 2334-2337.

Mongini, F., Preti, G., Calderale, P. M. & Barberi, G. (1981). Experimental strain analysis on the mandibular condyle under various conditions. *Med Biol Eng Comput* **19**: 521-523.

Moore, W. J. (1959). *The Influence of Muscle Function on the Growth of the Rat Skull*. PhD Thesis. University of Birmingham.

Moore, W. J. (1973). An experimental study of the functional components of growth in the rat mandible. *Acta Anat (Basel)* **85**: 378-85.

Morey, E. R. & Baylink, D. J. (1978). Inhibition of bone formation during space flight. *Science* **201**: 1138-1141.

Mori, S. & Burr, D. B. (1993). Increased intracortical remodeling following fatigue damage. *Bone* **14**: 103-109.

Moss, M. L. (1962). The functional matrix. In Kraus, B. S. & Reidel, R. A. (eds.): *Vistas in Orthodontics*. Philadelphia: Lea & Febiger, pp. 85-98.

Moss, M. L. (1969). The differential roles of periosteal and capsular functional matrices in oro-facial growth. *Rep Congr Eur Orthod Soc*: 193-205.

Moss, M. L. & Meehan, M. A. (1970). Functional cranial analysis of the coronoid process in the rat. *Acta Anat (Basel)* **77**: 11-24.

Moss, M. L. & Rankow, R. M. (1968). The role of the functional matrix in mandibular growth. *Angle Orthod* **38**: 95-103.

Moss, M. L. & Salentijn, L. (1969). The primary role of functional matrices in facial growth. *Am J Orthod* **55**: 566-577.

Mounier, A., Marchal, F. & Condemi, S. (2009). Is *Homo heidelbergensis* a distinct species? New insight on the Mauer mandible. *J Hum Evol* **56**: 219-246.

Moutier, R., Signore, P. & Nosten-Bertrand, M. (1992). Mandible shape analysis in a testicular feminization (Tfm) strain of mice. *J Hered* **83**: 235-7.

Murray, G. M., Phanachet, I. & Klineberg, I. J. (1999). Electromyographic evidence for functional heterogeneity in the inferior head of the human lateral pterygoid muscle: a preliminary multi-unit study. *Clin Neurophysiol* **110**: 944-950.

Nelson, G. J. (1986). *Three Dimensional Computer Modeling of the Human Mandibular Biomechanics*. MSc Thesis. University of British Columbia, Vancouver.

Nicholson, E. & Harvati, K. (2006). Quantitative analysis of human mandibular shape using three-dimensional geometric morphometrics. *Am J Phys Anthropol* **131**: 368-383.

O'Connor, C. F., Franciscus, R. G. & Holton, N. E. (2005). Bite force production capability and efficiency in Neandertals and modern humans. *Am J Phys Anthropol* **127**: 129-151.

O'Connor, J. A., Lanyon, L. E. & MacFie, H. (1982). The influence of strain rate on adaptive bone remodelling. *J Biomech* **15**: 767-781.

O'Higgins, P., Cobb, S. N., Fitton, L. C., Gröning, F., Phillips, R. & Fagan, M. J. (2009). Facial mechanics in early hominins: a study combining geometric morphometrics and finite element analysis. *Am J Phys Anthropol* **S48**: 201-202.

Ödman, C. & Kiliaridis, S. (1996). Masticatory muscle activity in myotonic dystrophy patients. *J Oral Rehabil* **23**: 5-10.

Ohman, J. C., Krochta, T. J., Lovejoy, C. O., Mensforth, R. P. & Latimer, B. (1997). Cortical bone distribution in the femoral neck of hominoids: implications for the locomotion of *Australopithecus afarensis*. *Am J Phys Anthropol* **104**: 117-131.

Olejniczak, A. J., Smith, T. M., Feeney, R. N., Macchiarelli, R., Mazurier, A., Bondioli, L., Rosas, A., Fortea, J., de la Rasilla, M., Garcia-Tabernero, A., Radovčić, J., Skinner, M. M., Toussaint, M. & Hublin, J. J. (2008). Dental tissue proportions and enamel thickness in Neandertal and modern human molars. *J Hum Evol* **55**: 12-23.

Osborn, J. W. (1995). Biomechanical implications of lateral pterygoid contribution to biting and jaw opening in humans. *Arch Oral Biol* **40**: 1099-1108.

Osborn, J. W. (1996). Features of human jaw design which maximize the bite force. *J Biomech* **29**: 589-595.

Osborn, J. W. & Baragar, F. A. (1985). Predicted pattern of human muscle activity during clenching derived from a computer assisted model: symmetric vertical bite forces. *J Biomech* **18**: 599-612.

Oxnard, C. E., Lannigan, F. & O'Higgins, P. (1994). The mechanism of bone adaptation: tension and resorption in the human incus. In Odgaard, A. & Weinans, H. (eds.): *Bone Structure and Remodelling*. Singapore: World Scientific, pp. 105-125.

Patte, E. (1959). *La Dentition des Néandertaliens*. Paris: Masson.

Patte, E. (1960). Découverte d'un Néandertalien dans la Vienne. *L'Anthropologie* **64**: 512-517.

Pérez-Pérez, A., Espurz, V., Bermúdez de Castro, J. M., de Lumley, M. A. & Turbón, D. (2003). Non-occlusal dental microwear variability in a sample of Middle and Late Pleistocene human populations from Europe and the Near East. *J Hum Evol* **44**: 497-513.

Pierce, S. E., Angielczyk, K. D. & Rayfield, E. J. (2008). Patterns of morphospace occupation and mechanical performance in extant crocodilian skulls: a combined geometric morphometric and finite element modeling approach. *J Morphol* **269**: 840-864.

Piperno, M. & Scichilone, G., eds. (1991). *The Circeo 1 Neanderthal Skull: Studies and Documentation*. Rome: Istituto Poligrafico e Zecca Della Stato.

Piveteau, J. (1964). La grotte de Régourdou (Dordogne). Paléontologie Humaine. *Ann Paléont* **50**: 155-194.

Ponce de León, M. S. & Zollikofer, C. P. E. (2001). Neanderthal cranial ontogeny and its implications for late hominid diversity. *Nature* **412**: 534-8.

Poppe, M., Bourauel, C. & Jager, A. (2002). Determination of the elasticity parameters of the human periodontal ligament and the location of the center of resistance of single-rooted teeth a study of autopsy specimens and their conversion into finite element models. *J Orofac Orthop* **63**: 358-370.

Pratt, L. W. (1943). Experimental masseterectomy in the laboratory rat. *J Mammal* **24**: 204-211.

Prendergast, P. J. & Taylor, D. (1994). Prediction of bone adaptation using damage accumulation. *J Biomech* **27**: 1067-1076.

Preuschoft, H. & Witzel, U. (2004). A biomechanical approach to craniofacial shape in primates, using FESA. *Ann Anat* **186**: 397-404.

Pruim, G. J., de Jongh, H. J. & ten Bosch, J. J. (1980). Forces acting on the mandible during bilateral static bite at different bite force levels. *J Biomech* **13**: 755-763.

Puech, P.-F. (1979). The diet of early man: evidence from abrasion of teeth and tools. *Curr Anthropol* **20**: 590-592.

Puech, P.-F. (1981). Tooth wear in La Ferrassie man. *Curr Anthropol* **22**: 424-425.

Pycraft, W. P., Elliot Smith, G., Yearsley, M., Carter, J. T., Smith, R. A., Hopwood, A. T., Bate, D. M. A. & Swinton, W. E. (1928). *Rhodesian Man and Associated Remains*. London: British Museum (Natural History).

Quam, R., Bailey, S. & Wood, B. (2009). Evolution of M^1 crown size and cusp proportions in the genus *Homo*. *J Anat* **214**: 655-670.

Quam, R. M. & Smith, F. H. (1998). A reassesment of the Tabun C2 mandible. In Akazawa, T., Aoki, K. & Bar-Yosef, O. (eds.): *Neanderthals and Modern Humans in Western Asia*. New York: Plenum, pp. 405-422.

Radlanski, R. J. & Klarkowski, M. C. (2001). Bone remodeling of the human mandible during prenatal development. *J Orofac Orthop* **62**: 191-201.

Radlanski, R. J., Renz, H. & Klarkowski, M. C. (2003). Prenatal development of the human mandible. 3D reconstructions, morphometry and bone remodelling pattern, sizes 12-117 mm CRL. *Anat Embryol (Berl)* **207**: 221-232.

Radlanski, R. J., van der Linden, F. P. G. M. & Ohnesorge, I. (1999). 4D-Computerized visualisation of human craniofacial skeletal growth and of the development of the dentition. *Ann Anat* **181**: 3-8.

Radovčić, J., Smith, F., Trinkaus, E. & Wolpoff, M. (1988). *The Krapina Hominids. An Illustrated Catalog of Skeletal Collection*. Zagreb: Croatian Natural History Museum.

Rak, Y. (1986). The Neanderthal: a new look at an old face. *J Hum Evol* **15**: 151-164.

Rak, Y. (1998). Does any Mousterian cave present evidence of two hominid species? In Akazawa, T., Aoki, K. & Bar-Yosef, O. (eds.): *Neanderthals and Modern Humans in Western Asia*. New York: Plenum, pp. 353-366.

Rak, Y., Ginzburg, A. & Geffen, E. (2002). Does *Homo neanderthalensis* play a role in modern human ancestry? The mandibular evidence. *Am J Phys Anthropol* **119**: 199-204.

Rak, Y. & Hylander, W. L. (2003). Neandertal facial morphology and increased jaw gap. *Am J Phys Anthropol* **S36**: 174.

Rak, Y. & Hylander, W. L. (2007). The functional significance of the retromolar space in the Neanderthal mandible. In Society, P. (ed.): *Abstracts of the Annual Meeting of the Paleoanthropology Society in Philadelphia, 27-28 March 2007*. http://www.paleoanthro.org/meeting.htm.

Ralph, J. P. (1975). Photoelastic studies in the edentulous human mandible. *J Dent* **3**: 9-14.

Ralph, J. P. & Caputo, A. A. (1975). Analysis of stress patterns in the human mandible. *J Dent Res* **54**: 814-21.

Ranly, D. M. (1988). *A Synopsis of Craniofacial Growth*. Norwalk: Appleton & Lange.

Ravosa, M. J. (1991). Structural allometry of the prosimian mandibular corpus and symphysis. *J Hum Evol* **20**: 3-20.

Rayfield, E. J. (2005). Using finite-element analysis to investigate suture morphology: a case study using large carnivorous dinosaurs. *Anat Rec A Discov Mol Cell Evol Biol* **283**: 349-65.

Rayfield, E. J. (2007). Finite element analysis and understanding the biomechanics and evolution of living and fossil organisms. *Annu Rev Earth Planet Sci* **35**: 541-576.

Rayfield, E. J., Norman, D. B., Horner, C. C., Horner, J. R., Smith, P. M., Thomason, J. J. & Upchurch, P. (2001). Cranial design and function in a large theropod dinosaur. *Nature* **409**: 1033-1037.

Rees, J. S. & Jacobsen, P. H. (1997). Elastic modulus of the periodontal ligament. *Biomaterials* **18**: 995-999.

Reina, J. M., García-Aznar, J. M., Domínguez, J. & Doblaré, M. (2006). Numerical estimation of bone density and elastic constants distribution in a human mandible. *J Biomech* **40**: 828-836.

Richards, M. P., Pettitt, P. B., Trinkaus, E., Smith, F. H., Paunović, M. & Karavanić, I. (2000). Neanderthal diet at Vindija and Neanderthal predation: the evidence from stable isotopes. *Proc Natl Acad Sci U S A* **97**: 7663-7666.

Richards, M. P., Taylor, G., Steele, T., McPherron, S. P., Soressi, M., Jaubert, J., Orschiedt, J., Mallye, J. B., Rendu, W. & Hublin, J.-J. (2008). Isotopic dietary analysis of a Neanderthal and associated fauna from the site of Jonzac (Charente-Maritime), France. *J Hum Evol* **55**: 179-185.

Richards, M. P. & Trinkaus, E. (2009). Isotopic evidence for the diets of European Neanderthals and early modern humans. *Proc Natl Acad Sci U S A* **106**: 16034-16039.

Richmond, B. G., Wright, B. W., Grosse, L., Dechow, P. C., Ross, C. F., Spencer, M. A. & Strait, D. S. (2005). Finite element analysis in functional morphology. *Anat Rec A Discov Mol Cell Evol Biol* **283A**: 259-274.

Riesenfeld, A. (1969). The adaptive mandible: an experimental study. *Acta Anat (Basel)* **72**: 246-262.

Rink, W. J., Schwarcz, H. P., Smith, F. H. & Radovčić, J. (1995). ESR ages for Krapina hominids. *Nature* **378**: 24.

Robinson, L. (1913). The story of the chin. *Knowledge* **36**: 410-420.

Robinson, M. (1946). The temporomandibular joint: theory of reflex controlled non-lever action of the mandible. *J Amer dent Ass* **33**: 1260-1271.

Roesler, H. (1981). Some historical remarks on the theory of cancellous bone structure (Wolff's law). In Cowin, S. C. (ed.): *Mechanical Properties of Bone*. New York: ASME, pp. 27-42.

Roesler, H. (1987). The history of some fundamental concepts in bone biomechanics. *J Biomech* **20**: 1025-1034.

Rosas, A. (1995). Seventeen new mandibular specimens from the Atapuerca/Ibeas Middle Pleistocene hominids sample (1985-1992). *J Hum Evol* **28**: 533-559.

Rosas, A. (2001). Occurrence of Neanderthal features in mandibles from the Atapuerca-SH site. *Am J Phys Anthropol* **114**: 74-91.

Rosas, A. & Bastir, M. (2004). Geometric morphometric analysis of allometric variation in the mandibular morphology of the hominids of Atapuerca, Sima de los Huesos site. *Anat Rec A Discov Mol Cell Evol Biol* **278**: 551-560.

Rosas, A., Martínez-Maza, C., Bastir, M., García-Tabernero, A., Lalueza-Fox, C., Huguet, R., Ortiz, J. E., Julià, R., Soler, V., de Torres, T., Martínez, E., Cañaveras, J. C., Sánchez-Moral, S., Cuezva, S., Lario, J., Santamaría, D., de la Rasilla, M. & Fortea, J. (2006). Paleobiology and comparative morphology of a late Neandertal sample from El Sidrón, Asturias, Spain. *Proc Natl Acad Sci U S A* **103**: 19266-19271.

Ross, C. F. (1993). *The Functions of the Postorbital Septum and Anthropoid Origins*. PhD Thesis. Duke University, Ann Arbor.

Ross, C. F. (2001). *In vivo* function of the craniofacial haft: the interorbital "pillar". *Am J Phys Anthropol* **116**: 108-139.

Ross, C. F. & Hylander, W. L. (1996). *In vivo* and *in vitro* bone strain in the owl monkey circumorbital region and the function of the postorbital septum. *Am J Phys Anthropol* **101**: 183-215.

Ross, C. F., Patel, B. A., Slice, D. E., Strait, D. S., Dechow, P. C., Richmond, B. G. & Spencer, M. A. (2005). Modeling masticatory muscle force in finite element analysis: sensitivity analysis using principal coordinates analysis. *Anat Rec A Discov Mol Cell Evol Biol* **283**: 288-299.

Roux, W. (1881). *Der zuchtende Kampf der Teile, oder die 'Teilauslese' im Organismus (Theorie der 'funktionellen Anpassung')*. Leipzig: Wilhelm Engelmann.

Rubin, C. T. (1984). Skeletal strain and the functional significance of bone architecture. *Calcif Tissue Int* **36 (Suppl. 1)**: 11-18.

Rubin, C. T. & Lanyon, L. E. (1987). Osteoregulatory nature of mechanical stimuli: function as a determinant for adaptive remodeling in bone. *J Orthop Res* **5**: 300-310.

Rubin, C. T., Turner, A. S., Bain, S., Mallinckrodt, C. & McLeod, K. (2001). Anabolism. Low mechanical signals strengthen long bones. *Nature* **412**: 603-4.

Ruff, C. B., Trinkaus, E., Walker, A. & Larsen, C. S. (1993). Postcranial robusticity in *Homo*. I: Temporal trends and mechanical interpretation. *Am J Phys Anthropol* **91**: 21-53.

Ruff, C. B., Walker, A. & Trinkaus, E. (1994). Postcranial robusticity in *Homo*. III: Ontogeny. *Am J Phys Anthropol* **93**: 35-54.

Ruimerman, R., Hilbers, P., van Rietbergen, B. & Huiskes, R. (2005). A theoretical framework for strain-related trabecular bone maintenance and adaptation. *J Biomech* **38**: 931-41.

Ryan, A. S. (1980). *Anterior Dental Microwear in Hominid Evolution: Comparisons with Human and Nonhuman Primates*. PhD Thesis. University of Michigan, Ann Arbor.

Scherf, H. & Tilgner, R. (2009). A new high-resolution computed tomography (CT) segmentation method for trabecular bone architectural analysis. *Am J Phys Anthropol* **140**: 39-51.

Schoetensack, O. (1908). *Der Unterkiefer des Homo heidelbergensis aus den Sanden von Mauer bei Heidelberg. Ein Beitrag zur Paläontologie des Menschen*. Leipzig: Engelmann.

Schumacher, G. H. (1961). *Funktionelle Morphologie der Kaumuskulatur*. Jena: G. Fischer.

Schwalbe, G. (1914). Über einen bei Ehringsdorf in der Nähe von Weimar gefundenen Unterkiefer des *Homo primigenius*. *Anat Anz* **47**: 337-345.

Schwarcz, H. P., Bietti, A., Buhay, W. M., Stiner, M. C., Grün, R. & Segre, A. (1991). On the reexamination of Grotta Guattari uranium-series and electron-spin-resonance dates. *Curr Anthropol* **32**: 313-316.

Schwartz-Dabney, C. L. & Dechow, P. C. (2003). Variations in cortical material properties throughout the human dentate mandible. *Am J Phys Anthropol* **120**: 252-277.

Schwartz, J. H. & Tattersall, I. (2000). The human chin revisited: what is it and who has it? *J Hum Evol* **38**: 367-409.

Sellers, W. I. & Crompton, R. H. (2004). Using sensitivity analysis to validate the predictions of a biomechanical model of bite forces. *Ann Anat* **186**: 89-95.

Sergi, S. (1962). The Neanderthal Palaeanthropi in Italy. In Howells, W. W. (ed.): *Ideas on Human Evolution: Selected Essays, 1949-1961*. Cambridge: Harvard University Press, pp. 500-506.

Sergi, S. (1974). *Il Cranio Neandertaliano del Monte Circeo (Circeo 1)*. Rome: Istituto Poligrafico e Zecca Della Stato.

Sergi, S. (1991). The Neandertal cranium of Monte Circeo (Circeo 1). In Piperno, M. & Scichilone, G. (eds.): *The Circeo 1 Neanderthal Skull: Studies and Documentation*. Rome: Istituto Poligrafico e Zecca Della Stato, pp. 23-174.

Shahar, R., Zaslansky, P., Barak, M., Friesem, A. A., Currey, J. D. & Weiner, S. (2007). Anisotropic Poisson's ratio and compression modulus of cortical bone determined by speckle interferometry. *J Biomech* **40**: 252-264.

Siffre, A. (1923). L'alimentation des hominids mousteriens et l'usure de leurs dents. *Rev. d'Anthropol* **33**: 291-293.

Sigal, I. A., Hardisty, M. R. & Whyne, C. M. (2008). Mesh-morphing algorithms for specimen-specific finite element modeling. *J Biomech* **41**: 1381-1389.

Simon, M. R. & Moss, M. L. (1973). A functional cranial analysis of human sigmoid notch form. *Acta Anat (Basel)* **85**: 133-144.

Singer, R. (1958). The Rhodesian, Florisbad and Saldanha Skulls. In von Koenigswald, G. H. R. (ed.): *Hundert Jahre Neanderthaler*. Utrecht: Kemink en Zoon, pp. 52-62.

Skerry, T. (2000). Biomechanical influences on skeletal growth and development. In O'Higgins, P. & Cohen, M. (eds.): *Development, Growth, and Evolution: Implications for the Study of the Hominid Skeleton*. San Diego: Academic Press, pp. 29-39.

Skerry, T. M. & Lanyon, L. E. (1995). Interruption of disuse by short duration walking exercise does not prevent bone loss in the sheep calcaneus. *Bone* **16**: 269-74.

Smith, D. M., McLachlan, K. R. & McCall, W. D., Jr. (1986). A numerical model of temporomandibular joint loading. *J Dent Res* **65**: 1046-1052.

Smith, F. H. (1976). *The Neandertal Remains from Krapina: A Descriptive and Comparative Study*. PhD Thesis. University of Michigan.

Smith, F. H. (1976). On anterior tooth wear at Krapina and Ochoz. *Curr Anthropol* **17**: 167-168.

Smith, F. H. (1983). Behavioral interpretations of changes in craniofacial morphology across the archaic/modern *Homo sapiens* transition. In Trinkaus, E. (ed.): *The Mousterian Legacy: Human Biocultural Change in the Upper Pleistocene*. Oxford: British Archaeological Reports, pp. 141-163.

Smith, F. H. (1984). Fossil hominids from the Upper Pleistocene of Central Europe and the origin of modern Europeans. In Smith, F. H. & Spencer, F. (eds.): *The Origins of Modern Humans: A World Survey of the Fossil Evidence*. New York: Alan R. Liss, pp. 137–209.

Smith, F. H. & Paquette, S. P. (1989). The adaptive basis of Neandertal facial form, with some thoughts on the nature of modern human origins. In Trinkaus, E. (ed.): *The Emergence of Modern Humans*. Cambridge: Cambridge University Press, pp. 181-210.

Smith, P. (1976). Dental pathology in fossil hominids: What did Neanderthals do with their teeth? *Curr Anthropol* **17**: 149-151.

Smith, P. & Zilberman, U. (1994). Thin enamel and other tooth components in Neanderthals and other hominids. *Am J Phys Anthropol* **95**: 85-87.

Smith, R. J. (1978). Mandibular biomechanics and temporomandibular joint function in primates. *Am J Phys Anthropol* **49**: 341-349.

Spencer, M. A. (1998). Force production in the primate masticatory system: electromyographic tests of biomechanical hypotheses. *J Hum Evol* **34**: 25-54.

Spencer, M. A. & Demes, B. (1993). Biomechanical analysis of masticatory system configuration in Neandertals and Inuits. *Am J Phys Anthropol* **91**: 1-20.

Sperber, G. H. (2001). *Craniofacial Development*. Hamilton: B. C. Decker.

Spoor, C. F., Zonneveld, F. W. & Macho, G. A. (1993). Linear measurements of cortical bone and dental enamel by computed tomography: applications and problems. *Am J Phys Anthropol* **91**: 469-484.

Spoor, F., Jeffery, N. & Zonneveld, F. (2000). Imaging skeletal growth and evolution. In O'Higgins, P. & Cohen, M. (eds.): *Development, Growth, and Evolution: Implications for the Study of the Hominid Skeleton*. San Diego: Academic Press, pp. 123-161.

Spoor, F., O'Higgins, P., Dean, C. & Lieberman, D. E. (1999). Anterior sphenoid in modern humans. *Nature* **397**: 572.

Standlee, J. P., Caputo, A. A. & Ralph, J. P. (1977). Stress trajectories within the mandible under occlusal loads. *J Dent Res* **56**: 1297-1302.

Standlee, J. P., Caputo, A. A. & Ralph, J. P. (1981). The condyle as a stress-distributing component of the temporomandibular joint. *J Oral Rehabil* **8**: 391-400.

Stefan, V. H. & Trinkaus, E. (1998a). Discrete trait and dental morphometric affinities of the Tabun 2 mandible. *J Hum Evol* **34**: 443-468.

Stefan, V. H. & Trinkaus, E. (1998b). La Quina 9 and Neandertal mandibular variability. *Bull Mém Soc Anthropol Paris* **10**: 293-324.

Stewart, T. D. (1959). Restoration and study of the Shanidar I Neanderthal skeleton in Baghdad. *Yearb Am Phil Soc* **1958**: 274-278.

Strait, D. S., Richmond, B. G., Spencer, M. A., Ross, C. F., Dechow, P. C. & Wood, B. A. (2007). Masticatory biomechanics and its relevance to early hominid phylogeny: An examination of palatal thickness using finite-element analysis. *J Hum Evol* **52**: 585-599.

Strait, D. S., Wang, Q., Dechow, P. C., Ross, C. F., Richmond, B. G., Spencer, M. A. & Patel, B. A. (2005). Modeling elastic properties in finite element analysis: How much precision is needed to produce an accurate model? *Anat Rec A Discov Mol Cell Evol Biol* **283A**: 275-287.

Strait, D. S., Weber, G. W., Neubauer, S., Chalk, J., Richmond, B. G., Lucas, P. W., Spencer, M. A., Schrein, C., Dechow, P. C., Ross, C. F., Grosse, I. R., Wright, B. W., Constantino, P., Wood, B. A., Lawn, B., Hylander, W. L., Wang, Q., Byron, C., Slice, D. E. & Smith, A. L. (2009). The feeding biomechanics and dietary ecology of *Australopithecus africanus*. *Proc Natl Acad Sci U S A* **106**: 2124-2129.

Stringer, C. B., Grün, R., Schwarcz, H. P. & Goldberg, P. (1989). ESR dates for the hominid burial site of Es Skhul in Israel. *Nature* **338**: 756-758.

Stringer, C. B., Hublin, J. J. & Vandermeersch, B. (1984). The origin of anatomically modern humans in Western Europe. In Smith, F. H. & Spencer, F. (eds.): *The Origins of Modern Humans: A World Survey of the Fossil Evidence*. New York: Alan R. Liss, pp. 51-135.

Su, M., Samala, P. R., Jiang, H. H., Liu, S., Yang, L. & Yokota, H. (2005). Measurement of bone strain using electronic speckle pattern interferometry. *J Holography Speckle* **2**: 34-39.

Sverdlova, N. S. & Witzel, U. (in press). Principles of determination and verification of muscle forces in the human musculoskeletal system: Muscle forces to minimise bending stress. *J Biomech.*

Tafforeau, P. & Smith, T. M. (2008). Nondestructive imaging of hominoid dental microstructure using phase contrast X-ray synchrotron microtomography. *J Hum Evol* **54**: 272-278.

Tanaka, E., Tanne, K. & Sakuda, M. (1994). A three-dimensional finite element model of the mandible including the TMJ and its application to stress analysis in the TMJ during clenching. *Med Eng Phys* **16**: 316-322.

Tanne, K., Lu, Y. C., Tanaka, E. & Sakuda, M. (1993). Biomechanical changes of the mandible from orthopaedic chin cup force studied in a three-dimensional finite element model. *Eur J Orthod* **15**: 527-533.

Tanne, K., Sakuda, M. & Burstone, C. J. (1987). Three-dimensional finite element analysis for stress in the periodontal tissue by orthodontic forces. *Am J Orthod Dentofacial Orthop* **92**: 499-505.

Tanne, K., Tanaka, E. & Sakuda, M. (1991). The elastic modulus of the temporomandibular joint disc from adult dogs. *J Dent Res* **70**: 1545-1548.

Tattersall, I. (1973). Cranial anatomy of Archeolemurinae (Lemuroidea, Primates). *Anthropol Paper Am Mus Nat Hist* **52**: 1-110.

Thomason, J. J., Grovum, L. E., Deswysen, A. G. & Bignell, W. W. (2001). *In vivo* surface strain and stereology of the frontal and maxillary bones of sheep: implications for the structural design of the mammalian skull. *Anat Rec* **264**: 325-338.

Thompson, J. L. & Illerhaus, B. (1998). A new reconstruction of the Le Moustier 1 skull and investigation of internal structures using 3-D-μCT data. *J Hum Evol* **35**: 647-665.

Throckmorton, G. S. (1985). Quantitative calculations of temporomandibular joint reaction forces II. The importance of the direction of the jaw muscle forces. *J Biomech* **18**: 453-461.

Throckmorton, G. S. & Dechow, P. C. (1994). *In vitro* strain measurements in the condylar process of the human mandible. *Arch Oral Biol* **39**: 853-867.

Thurn, P. & Bücheler, E. (1992). Computertomographie. In Thurn, P. & Bücheler, E. (eds.): *Einführung in die radiologische Diagnostik*. Stuttgart: Thieme, pp. 35-40.

Tillier, A.-M. (1988). A propos de sequences phylétique et ontogénétique chez les neanderthaliens. In Trinkaus, E. (ed.): *L'Homme de Néandertal. Volume 3. L'Anatomie*. Liège: Eraul, pp. 125-135.

Trainor, P. G., McLachlan, K. R. & McCall, W. D. (1995). Modelling of forces in the human masticatory system with optimization of the angulations of the joint loads. *J Biomech* **28**: 829-843.

Triepel, H. (1922). Über gestaltliche Beziehungen zwischen Struktur und Organform. *Z Anat Enwicklungsgesch* **63**: 608-623.

Trinkaus, E. (1983). *The Shanidar Neandertals*. New York: Academic Press.

Trinkaus, E. (1984). Western Asia. In Smith, F. H. & Spencer, F. (eds.): *The Origins of Modern Humans: A World Survey of the Fossil Evidence*. New York: Alan R. Liss, pp. 251-293.

Trinkaus, E. (1987). The Neandertal face: evolutionary and functional perspectives on a recent hominid face. *J Hum Evol* **16**: 429-443.

Trinkaus, E. (1997). Appendicular robusticity and the paleobiology of modern human emergence. *Proc Natl Acad Sci U S A* **94**: 13367-13373.

Trinkaus, E., Churchill, S. E. & Ruff, C. B. (1994). Postcranial robusticity in *Homo*. II: Humeral bilateral asymmetry and bone plasticity. *Am J Phys Anthropol* **93**: 1-34.

Tsubota, K. & Adachi, T. (2005). Spatial and temporal regulation of cancellous bone structure: characterization of a rate equation of trabecular surface remodeling. *Med Eng Phys* **27**: 305-311.

Tsubota, K., Suzuki, Y., Yamada, T., Hojo, M., Makinouchi, A. & Adachi, T. (2009). Computer simulation of trabecular remodeling in human proximal femur using large-scale voxel FE models: Approach to understanding Wolff's law. *J Biomech* **42**: 1088-1094.

Tyrer, J. R., Heras-Palou, C. & Slater, T. (1995). Three-dimensional human femoral strain analysis using ESPI. *Optic Laser Eng* **23**: 291-303.

Uhthoff, H. K. & Jaworski, Z. F. (1978). Bone loss in response to long-term immobilisation. *J Bone Joint Surg Br* **60-B**: 420-429.

Ullrich, C. G., Binet, E. F., Sanecki, M. G. & Kieffer, S. A. (1980). Quantitative assessment of the lumbar spinal canal by computed tomography. *Radiology* **134**: 137-143.

Umemura, Y., Ishiko, T., Yamauchi, T., Kurono, M. & Mashiko, S. (1997). Five jumps per day increase bone mass and breaking force in rats. *J Bone Miner Res* **12**: 1480-1485.

Ungar, P. S., Fennell, K. J., Gordon, K. & Trinkaus, E. (1997). Neandertal incisor beveling. *J Hum Evol* **32**: 407-421.

van Eijden, T. M. (2000). Biomechanics of the mandible. *Crit Rev Oral Biol Med* **11**: 123-136.

van Eijden, T. M., Koolstra, J. H. & Brugman, P. (1995). Architecture of the human pterygoid muscles. *J Dent Res* **74**: 1489-1495.

van Eijden, T. M., Koolstra, J. H. & Brugman, P. (1996). Three-dimensional structure of the human temporalis muscle. *Anat Rec* **246**: 565-572.

van Eijden, T. M., Korfage, J. A. M. & Brugman, P. (1997). Architecture of the human jaw-closing and jaw-opening muscles. *Anat Rec* **248**: 464-474.

van Rietbergen, B., Huiskes, R., Eckstein, F. & Ruegsegger, P. (2003). Trabecular bone tissue strains in the healthy and osteoporotic human femur. *J Bone Miner Res* **18**: 1781-1788.

van Rietbergen, B., Weinans, H., Huiskes, R. & Polman, B. J. W. (1996). Computational strategies for iterative solutions of large FEM applications employing voxel data. *Int J Numer Meth Eng* **39**: 2743-2767.

van Ruijven, L. J., Mulder, L. & van Eijden, T. M. G. J. (2007). Variations in mineralization affect the stress and strain distributions in cortical and trabecular bone. *J Biomech* **40**: 1211-1218.

van Spronsen, P. H., Koolstra, J. H., van Ginkel, F. C., Weijs, W. A., Valk, J. & Prahl-Andersen, B. (1997). Relationships between the orientation and moment arms of the human jaw muscles and normal craniofacial morphology. *Eur J Orthod* **19**: 313-328.

van Spronsen, P. H., Weijs, W. A., Valk, J., Prahl-Andersen, B. & van Ginkel, F. C. (1989). Comparison of jaw-muscle bite-force cross-sections obtained by means of magnetic resonance imaging and high-resolution CT scanning. *J Dent Res* **68**: 1765-1770.

Vandermeersch, B. (1965). Position stratigraphique et chronologique des restes humains du paléolithique moyen du sud-ouest de la France. *Ann Paléont* **51**: 69-126.

Varrela, J. (1992). Dimensional variation of craniofacial structures in relation to changing masticatory-functional demands. *Eur J Orthod* **14**: 31-36.

Verhulp, E., van Rietbergen, B. & Huiskes, R. (2006). Comparison of micro-level and continuum-level voxel models of the proximal femur. *J Biomech* **39**: 2951-2957.

Verhulp, E., van Rietbergen, B. & Huiskes, R. (2008). Load distribution in the healthy and osteoporotic human proximal femur during a fall to the side. *Bone* **42**: 30-35.

Verna, C. (2006). *The Neandertal Remains from la Quina (Charente)*. PhD Thesis. University of Bordeaux 1.

Vitti, M. & Basmajian, J. V. (1977). Integrated actions of masticatory muscles: simultaneous EMG from eight intramuscular electrodes. *Anat Rec* **187**: 173-189.

Vlček, E. (1993). *Fossile Menschenfunde von Weimar-Ehringsdorf*. Stuttgart: Theiss.

Vollmer, D., Bourauel, C., Maier, K. & Jager, A. (1999). Determination of the centre of resistance in an upper human canine and idealized tooth model. *Eur J Orthod* **21**: 633-648.

Vollmer, D., Meyer, U., Joos, U., Vegh, A. & Piffko, J. (2000). Experimental and finite element study of a human mandible. *J Craniomaxillofac Surg* **28**: 91-96.

Vrba, E. S. (1982). Biostratigraphy and chronology, based particularly on Bovidae, of southern African hominid-associated assemblages: Makapansgat, Sterkfontein, Taung, Kromdraai, Swartkrans; also Elandsfontein (Saldanha), Broken Hill (Kabwe) and Cave of Hearths. In de Lumley, M. A. (ed.): *L'Homo erectus et la Place de l'Homme de Tautavel parmi les Hominidés Fossiles. I. Congrès International de Paléontologic Humaine, Nice 16-21 octobre 1982*. Paris: Institut de paléontologie humaine, pp. 707-752.

Walkhoff, O. (1904). Die menschliche Sprache in ihrer Bedeutung für die funktionelle Gestalt des Unterkiefers. *Anat Anz* **24**: 129-139.

Wallace, J. A. (1975). Did La Ferrassie I use his teeth as a tool? *Curr Anthropol* **16**: 393-396.

Washburn, S. L. (1947). The relation of the temporal muscle to the form of the skull. *Anat Rec* **99**: 239-248.

Weaver, T. D. (2009). The meaning of neandertal skeletal morphology. *Proc Natl Acad Sci U S A* **106**: 16028-16033.

Wegener, O. H. (1992). *Ganzkörpercomputertomographie*. Berlin: Blackwell.

Weidenreich, F. (1936). The mandibles of *Sinanthropus pekinensis*: A comparative study. *Palaeontologia Sinica Series* **D 7**: 1-162.

Weijs, W. A. (1989). The functional significance of morphological variation of the human mandible and masticatory muscles. *Acta Morphol Neerl Scand* **27**: 149-162.

Weijs, W. A. & Hillen, B. (1985). Physiological cross-section of the human jaw muscles. *Acta Anat (Basel)* **121**: 31-35.

Weijs, W. A. & Hillen, B. (1986). Correlations between the cross-sectional area of the jaw muscles and craniofacial size and shape. *Am J Phys Anthropol* **70**: 423-431.

Weinans, H., Huiskes, R. & Grootenboer, H. J. (1992). The behavior of adaptive bone-remodeling simulation models. *J Biomech* **25**: 1425-41.

White, T. D. (1977). *The Anterior Mandibular Corpus of Early African Hominidae: Functional Significance of Shape and Size*. PhD Thesis. University of Michigan, Ann Arbor.

Williams, S. H., Vinyard, C. J., Wall, C. E. & Hylander, W. L. (2009). Mandibular corpus bone strain in goats and alpacas: Implications for understanding the biomechanics of mandibular form in selenodont artiodactyls. *J Anat* **214**: 65-78.

Witzel, U. (2006). Virtual synthesis of the skull in Neanderthals by FESS. In Alfred-Wegner-Stiftung (ed.): *150 Years of Neanderthal Discoveries, Early Europeans - Continuity & Discontinuity, July 21st – 26th, 2006 in Bonn, Germany*. Berlin: Selbstverlag der GeoUnion Alfred-Wegner-Stiftung, pp. 141.

Witzel, U. (2007). Eine neue Methode zur virtuellen Schädelsynthese am Beispiel Camarasaurus. *Hallesches Jahrbuch für Geowissenschaften* **23**: 73-78.

Witzel, U. & Preuschoft, H. (2005). Finite-element model construction for the virtual synthesis of the skulls in vertebrates: case study of Diplodocus. *Anat Rec A Discov Mol Cell Evol Biol* **283A**: 391-401.

Wolff, J. (1892). *Das Gesetz der Transformation der Knochen*. Berlin: Hirschwald.

Wolpoff, M. H. (1971). *Metric Trends in Hominid Dental Evolution*. Cleveland: Case Western Reserve University Press.

Wolpoff, M. H. (1975). Comment on: "Did La Ferrassie I use his teeth as a tool?" *Curr Anthropol* **16**: 393-399.

Wolpoff, M. H. (1979). The Krapina dental remains. *Am J Phys Anthropol* **50**: 67-114.

Wolpoff, M. H. (1999). *Paleoanthropology*. Boston: McGraw-Hill.

Wolpoff, M. H. & Frayer, D. W. (2005). Unique ramus anatomy for Neandertals? *Am J Phys Anthropol* **128**: 245-251.

Wolpoff, M. H., Smith, F. H., Malez, M., Radovcic, J. & Rukavina, D. (1981). Upper Pleistocene human remains from Vindija Cave. *Am J Phys Anthropol* **54**: 499-545.

Woodward, A. S. (1921). A new cave man from Rhodesia, South Africa. *Nature* **108**: 371-372.

Wroe, S. (2008). Cranial mechanics compared in extinct marsupial and extant African lions using a finite-element approach. *J Zool* **274**: 332-339.

Wroe, S., Clausen, P., McHenry, C., Moreno, K. & Cunningham, E. (2007). Computer simulation of feeding behaviour in the thylacine and dingo as a novel test for convergence and niche overlap. *Proc Biol Sci* **274**: 2819-2828.

Wronski, T. J., Morey-Holton, E. R., Doty, S. B., Maese, A. C. & Walsh, C. C. (1987). Histomorphometric analysis of rat skeleton following spaceflight. *Am J Physiol* **252**: R252-255.

Wykes, C. (1977). DE-correlation effects in speckle pattern interferometry I. *Opt Acta* **24**: 517.

Yang, L. & Ettemeyer, A. (2003). Strain measurement by three-dimensional electronic speckle pattern interferometry: potentials, limitations, and applications. *Opt Eng* **42**: 1257-1266.

Yang, L. & Yokota, H. (2007). Recent developments of speckle pattern interferometer for bone strain measurement. In Gdoutos, E. E. (ed.): *Experimental Analysis of Nano and Engineering Materials and Structures*. Dordrecht: Springer, pp. 581-582.

Yang, L., Zhang, P., Liu, S., Samala, P. R., Su, M. & Yokota, H. (2007). Measurement of strain distributions in mouse femora with 3D-digital speckle pattern interferometry. *Optic Laser Eng* **45**: 843-851.

Yeni, Y. N., Christopherson, G. T., Dong, X. N., Kim, D. G. & Fyhrie, D. P. (2005). Effect of microcomputed tomography voxel size on the finite element model accuracy for human cancellous bone. *J Biomech Eng* **127**: 1-8.

Yonemitsu, I., Muramoto, T. & Soma, K. (2007). The influence of masseter activity on rat mandibular growth. *Arch Oral Biol* **52**: 487-493.

Young, W. C. (1989). *Roark's Formulas for Stress and Strain*. New York: McGraw-Hill.

Zanoteli, E., Yamashita, H. K., Suzuki, H., Oliveira, A. S. & Gabbai, A. A. (2002). Temporomandibular joint and masticatory muscle involvement in myotonic dystrophy: a study by magnetic resonance imaging. *Oral Surg Oral Med Oral Pathol Oral Radiol Endod* **94**: 262-271.

Zaslansky, P., Currey, J. D., Friesem, A. A. & Weiner, S. (2005). Phase shifting speckle interferometry for determination of strain and Young's modulus of mineralized biological materials: a study of tooth dentin compression in water. *J Biomed Optic* **10**: 024020 1-13.

Zelditch, M. L., Swiderski, D. L., Sheets, H. D. & Fink, W. L. (2004). *Geometric Morphometrics for Biologists: A Primer*. Boston: Elsevier Academic Press.

Zhang, D., Arola, D. D. & Rouland, J. A. (2001). Evaluating the elastic modulus of bone using electronic speckle pattern interferometry. *Experimental Techniques* **25**: 32-34.

Zienkiewicz, O. C., Taylor, R. L. & Zhu, J. Z. (2005). *The Finite Element Method: Its Basis and Fundamentals*. Amsterdam: Elsevier Butterworth-Heinemann.

Zollikofer, C. P. E. & Ponce de León, M. S. (2005). *Virtual Reconstruction: A Primer in Computer-Assisted Paleontology and Biomedicine*. Hoboken: Wiley & Sons.

Zollikofer, C. P. E., Ponce de León, M. S., Martin, R. D. & Stucki, P. (1995). Neanderthal computer skulls. *Nature* **375**: 283-285.

Zou, Y., Diao, H., Peng, X. & Tiziani, H. (1992). Geometry for contouring by electronic speckle pattern interferometry based on shifting illumination beams. *Appl Optic* **31**: 6616-6621.